GROWTH INHIBITORY DIOXONAPHTHOIMIDAZOLIUMS RELATED TO YM155: SYNTHESIS AND MECHANISTIC INVESTIGATIONS

HO SI HAN SHERMAN

(B.Sc (Pharm.) (Hons.), NUS)

A THESIS SUBMITTED

FOR THE DEGREE OF DOCTOR OF PHILOSOPHY

DEPARTMENT OF PHARMACY

NATIONAL UNIVERSITY OF SINGAPORE

2015

DECLARATION

I hereby declare that the thesis is my original work and it has been written by me in its entirely. I have duly acknowledged all the sources of information which have been used in the thesis.

The thesis has also not been submitted for any degree in any university previously.

_____

Ho Si Han Sherman

23 July 2015

Table of Contents

Acknowledgments

Conferences

1. 1st GSK-ICES-Novartis-RSC Symposium in Organic and Bioorganic Chemistry

   April 13, 2015; Biopolis, Singapore

   Oral presentation: Structure-Activity Relationship studies on YM155 as chemotherapeutic agents for treatment of RCC and NSCLC

2. ARPS 2015 + AAPS-NUS 10th PharmSci@Asia Symposium

   April 8-9, 2015; NUS, Singapore

   Oral presentation: Structure-Activity Relationship studies on YM155 as chemotherapeutic agents for treatment of RCC and NSCLC *[Awarded Best Podium Presentation]*

3. ICBS 2014

   3rd Annual Conference of the International Chemical Biology Society

   November 17-19, 2014; Hotel Intercontinental, San Francisco, USA

   Poster presentation: Structure-Activity Relationship studies on YM155 as chemotherapeutic agents for treatment of RCC and NSCLC

4. AAPS 2014

   Annual Meeting and Exposition of the American Association of Pharmaceutical Scientists

   November 2-6, 2014; San Diego Convention Center, San Diego, USA

   Poster presentation: YM155 and its analog AB-1 cause apoptosis in RCC and NSCLC by disrupting the NF-κB signaling pathway *[Awarded a Travelship by the Drug Development and Discovery Interface Section, AAPS]*

5. Humboldt Kolleg International Symposium on Environment and Health in the 21st Century

   September 22, 2014; Center for Life Sciences, NUS, Singapore

   Poster presentation: YM155 and its analog AB-1 cause apoptosis in RCC and NSCLC by disrupting the NF-κB signaling pathway

6. ARPS 2014

   Annual Pharmacy Research Symposium (Department of Pharmacy, NUS, Singapore)

April 9, 2014; Biopolis, Singapore

Oral presentation: YM155 and its analog AB-1 cause apoptosis in RCC and NSCLC by disrupting the NF-κB signaling pathway *[Awarded the First Prize for Postgraduate Abstract Presentation Contest (Pharmaceutical Sciences Category)]*

7. ITB-NUS Pharmacy Scientific Symposium 2013: Updates in Pharmaceutical Sciences

   November 12, 2013; University Hall, NUS, Singapore

   Poster presentation: Investigations of dioxonaphthoimidazolium analogs based on YM155 as chemotherapeutics for renal cell carcinoma

8. AIMECS 2013

   9th AFMC International Medicinal Chemistry Symposium

   October 15-18, 2013; Grand Hotel, Taipei, Taiwan

   Oral presentation: Investigations of dioxonaphthoimidazolium analogs based on YM155 as chemotherapeutics for renal cell carcinoma

9. APRS 2013

   Annual Pharmacy Research Symposium (Department of Pharmacy, NUS, Singapore)

   April 4, 2013; Kent Ridge Guild House, NUS, Singapore

10. Yong Loo Lin School of Medicine 3rd Annual Graduate Scientific Congress 2013

    January 30th, 2013; NUHS, Singapore

    Poster presentation: SAR studies on YM155 as a chemotherapeutic agent in the treatment of renal cell carcinoma

11. AAPS-NUS 7th PharmSci@Asia Symposium

    June 6-7, 2012; Kent Ridge Guild House, NUS, Singapore

    Poster presentation: Modification approaches on Terameprocol, an NDGA derivative, as chemotherapeutic agents for pancreatic cancer *[Awarded Best Poster Prize]*

Publications

1. Ho, S. S. H., Go, M. L. Restraining the central linker in terameprocol results in constrained analogs with improved growth inhibitory activity. *Bioorg Med Chem Lett*, **2013**. 23(22): 6127-6133.

2. Ho, S. S. H., Sim, M. Y., Yee, W. L. S., Yang, T. M., Yuen, J. S. P., Go, M. L. Antiproliferative, DNA intercalation and redox cycling activities of dioxonaphtho[2,3-d]imidazolium analogs of sepantronium bromide (YM155): A structure-activity relationship study. *Eur J Med Chem,* **2015.** 104: 42-56.

3. Ho, S. S. H., Ali, A. B., Go, M. L. Dioxonaphthoimidazoliums AB1 and YM155 disrupt phosphorylation of p50 in the NF-κB pathway. *Manuscript submitted to Oncotarget.*

4. Ho, S. S. H., Ng, Y. C., Lam, K. K., Chan, W. K., Go, M. L. Dioxonaphtho[2,3-d]imidazolium analogs as novel rogue stem cell clearing agents. *Manuscript in preparation.*

Summary

YM155 is a dioxonaphthoimidazolium analog with potent growth inhibitory activities on a variety of cancer cell lines. Although initially reported as a suppressor of survivin, its specificity has been queried with concerns raised over its purported DNA damaging activity. The purpose of this thesis was to investigate the hypothesis that a detailed understanding of the mode of action of YM155 would promote the development of dioxonaphthoimidazolium analogs as a promising class of anti-cancer therapeutics. To this end, we investigated the hitherto unreported structure-activity relationships (SAR) of YM155 with regards to growth inhibition, DNA intercalation and redox cycling using a library of synthesized YM155 analogs. This was followed by investigations on the mechanism of action with emphasis placed on the NF-κB pathway and the induction of apoptosis.

With regards to growth inhibition, two salient points have emerged. First, the intact dioxonaphthoimidazolium scaffold was essential for potent growth inhibitory activity. Second, the pyrazin-2'-ylmethyl and 2'-methoxyethyl side chains served to fine-tune activity. Two promising analogs **AB1** (IC_{50} 17 – 44 nM) and **AB7** (IC_{50} 8.6 – 29 nM) were identified which had comparable or slightly more potent activity than YM155 (IC_{50} 14 – 54 nM) on the renal cell carcinoma (RCC786-0, RCC4/VA) and non-small cell lung carcinoma (H1299, H1666) cell lines. Potency against malignant cells was approximately 10 times greater than on non-malignant fibroblast IMR-90 cells. SAR for DNA intercalation and redox cycling showed limited overlaps with that for growth inhibition and together with the delayed increase in γH2AX, a DNA damage marker, it is concluded that DNA damage was unlikely to contribute in a significant capacity to the mechanism of action of the dioxonaphthoimidazoliums

As survivin is regulated by the NF-κB pathway, the effects of YM155 and **AB1** on this pathway were investigated. A key finding was that YM155 and **AB1** inhibited phosphorylation of the p50 subunit of NF-κB and reduced reporter activity in malignant cells. Disruption of NFkB signaling would lead to apoptosis with upregulation of cleaved caspases 3/7 and downregulation of antiapoptotic proteins survivin, Mcl1 and Bcl-xl.

Reports of YM155 as a potential therapeutic agent for the eradication of rogue stem cells in differentiated tissues inspired a SAR study on two embryonal carcinoma (NCCIT, NTERA-2) cell lines employed as surrogates of embryonic stem cells. YM155 and analogs displayed greater potency on these cells as compared to malignant cells. Selectivity ratios which exceeded 100-fold were highly favorable. A subset of analogs including YM155 were then tested and found to be as potent on embryonic stem cell line H9 and an induced pluripotent stem cell line HCT-8 3.11. YM155, **AB1** and **AB7** reduced mRNA and protein levels expression of a pluripotency-related gene Sox2 in NCCIT, H9 and HCT-8 3.11. Phosphorylation of p50 was also inhibited, suggesting a putative role for NF-κB in maintaining pluripotency and viability of stem cells.

In conclusion, dioxonaphthoimidazolium analogs hold promise as anticancer agents for renal and non-small cell lung carcinomas, as well as stem cell clearing agents for the prevention of teratomas.

(492 words)

List of Tables

List of Figures

translocates to the nucleus where it acts as a transcription factor and upregulates the transcription of genes that encode the growth factors VEGF, PDGF and TGF-α among others. (C): When the VHL gene undergoes a mutation, deletion or methylation event, the defective pVHL is unable to interact with E3 ubiquitin ligase to give a functional complex. Ubiquination of HIF-α decreases, leading to its accumulation and subsequent upregulation of growth factors even in normoxic conditions.

Figure 3.2. The EGFR pathway. Binding of EGF to EGFR leads to receptor dimerization and phosphorylation of cytoplasmic domains. At least three pathways lie downstream. Grb-2 recruitment sets off a phosphorylation cascade through the Ras-Raf-MEK-ERK pathway. Transcription factor STAT3 is directly activated by EGFR dimers, and localizes in the nucleus where it upregulate its target genes. Activated EGFR also directly activates PI3K, which phosphorylates PIP2 to PIP3. PIP3 binds to Akt, and together with phosphorylation by mTORC2 and PDPK1, activates the latter. The three downstream pathways subsequently contribute to cell proliferation and prevention of apoptosis by different mechanisms.

Figure 3.3. Summary of growth inhibitory structure-activity relationships of YM155

Figure 4.1. Representative dose response curves for the displacement of ThO by YM155 and doxorubicin.

Figure 4.2. Representative redox cycling dose response plot of YM155 and naphthoquinone (NQ) on the phenol red-HRP assay.

Figure 4.3. Generation of free radicals in RCC786-0 and H1299 cells at different concentrations of test compounds as determined by the fold change in H_2DCF fluorescence.

Figure 4.4. Levels of cleaved caspase 3 and γH2AX after 6, 12, 24 72 h treatment of RCC786-0 or H1299 with YM155, **AB1** or **AB7**. Concentrations used were 50 nM (YM155), 37.5 nM (AB1) and 30 nM (AB7) on 786-0 cells, and 37.5 nM (YM155, AB1), and 30 nM (AB7) on H1299 cells. The p19 fragment of cleaved caspase 3 is the precursor of p17. GAPDH was used as loading control.

Figure 5.1. Members of the NF-κB family of transcription factors. Members contain a Rel homology domain (RHD) that is required for binding to the consensus sequence GGGPNNPyPyCC (where P is A/G, Py is C/T, and N is any base) on DNA. Only p65, RelB and c-Rel contain transactivation domains (TAD) which are necessary for upregulating NF-κB controlled genes. p52 and p50 are synthesized as the larger p100 and p105 precursor proteins. The ankyrin repeats are cleaved from the C-terminal to give p52 and p50.

Figure 5.2. Activation of the NF-κB pathway. (A) In the canonical pathway, activation of the IKK complex leads to phosphorylation of IκB and its eventual proteosomal degradation. p65 is released, dimerizes with p50 and translocates to the nucleus, where it upregulates the transcription of genes with antiapoptotic and anti-inflammatory functions. (B) In the non-canonical pathway, NIK activation is followed by activation of an IKKα homodimer which then phosphorylates p100 and release of p52 upon p100 cleavage. p52 heterodimerizes with RelB, translocates to the nucleus and upregulates genes responsible for lymphoid organogenesis and B-cell development. (C) The atypical pathway is triggered by DNA damage which activates p38 and CK2 sequentially, leading to phosphorylation of IκB in an IKK independent manner. The subsequent steps converge with the canonical pathway.

Figure 5.3. Evaluation of YM155, **AB1**, **A4-1** and **B2-4** on cell viability, cytotoxicity and caspases 3 and 7 activation using the multiplex Apotox-Glo™ assay. Compounds were incubated with RCC786-0 cells for 48h at concentrations ranging from 0.2x to 5x IC$_{50}$ on RCC786-0. Y axis on left hand side monitors % viability while the right hand side axis monitors fold change in cytotoxicity or normalized caspase activation compared to untreated control cells. Normalized caspase activation is the caspase activity per viable cell.

Figure 5.4. Evaluation of YM155, **AB1**, **A4-1** and **B2-4** on cell viability, cytotoxicity and caspases 3 and 7 activation using the multiplex Apotox-Glo™ assay. Compounds were incubated with H1299 cells for 48h at concentrations ranging from 0.2x to 5x IC$_{50}$ on H1299.

Figure 5.11. (A) Silencing of p50 and p65 leads to loss of cell viability in both RCC786-0 and H1299 cells. Error bars represent the standard deviations of three separate experiments. * $p < 0.05$; ** $p < 0.01$; *** $p < 0.001$ (Tukey post-hoc test of respective populations of siRNA-treated groups vs control). (B) Western blotting showing successful silencing of p50 and p65 in H1299 and RCC786-0 cells 72 h post-transfection. p105 is the precursor form of p50 and is cleaved to give the latter. All siRNA were used at 50 nM for Western blotting. Negative control cells were treated with empty Lipofectamine 3000. Non-targeting siRNA treated cells were treated with siRNA not specific to any known sequences. GAPDH was used as loading control.

Figure 5.12. YM155 and **AB1** caused losses in the binding of p65 and p50 to the consensus NF-κB response elements. Cells were treated with 0.5x, 1x or 2x growth inhibitory IC_{50} of YM155 or **AB1** for 48 h, nuclear lysates were prepared and tested as described in text. Error bars represent the standard deviations of three separate experiments. Significant statistical difference from vehicle control is indicated as follows: * $p < 0.05$; ** $p < 0.01$; *** $p < 0.001$ (Tukey post-hoc test of respective populations of treated groups vs control).

Figure 5.13. YM155 and **AB1** induced losses in binding of p65 and p50 to the consensus NF-κB response element DNA sequence. Cells were treated with 0.5x, 1x or 2x growth inhibitory IC_{50} of YM155 or **AB1** for 48 h in the presence of 25 ng/mL TNF-α. Error bars represent the standard deviations of three separate experiments. Significant statistical difference from vehicle control is indicated as follows: * $p < 0.05$; ** $p < 0.01$; *** $p < 0.001$ (Tukey post-hoc test of respective populations of treated groups vs control).

Figure 5.14. Levels of IκBα, NF-κB subunits p50 (p105), p65 and their respective phosphorylated forms (p.p50, p.p65) after 6, 24, 48, 72 h treatment of RCC786-0 or H1299 with YM155 or **AB1.** Concentrations used were 50 nM (YM155) or 37.5 nM (**AB1**) on 786-0 cells, and 37.5 nM (YM155, AB1) on H1299 cells. GAPDH was used as a loading control.

asterisk (*) when p<0.05, two asterisks (**) when p<0.01 and three asterisks (***) when p<0.001 (Tukey post-hoc test of respective populations of treated groups vs control).

Figure 6.4. Expression levels of Oct4 mRNA following 12 or 24 h of treatment with YM155, **AB1** or **AB7** quantified by qRT-PCR. Bars represent the fold-change of cDNA normalized against GAPDH in the same sample. Error bars represent the standard deviations of three separate experiments. Significant statistical difference from vehicle control is represented by an asterisk (*) when p<0.05, two asterisks (**) when p<0.01 and three asterisks (***) when p<0.001 (Tukey post-hoc test of respective populations of treated groups vs control).

Figure 6.5. Expression levels of Nanog mRNA following 12 or 24 h of treatment with YM155, **AB1** or **AB7** quantified by qRT-PCR. Bars represent the fold-change of cDNA normalized against GAPDH in the same sample. Error bars represent the standard deviations of three separate experiments. Significant statistical difference from vehicle control is represented by an asterisk (*) when p<0.05, two asterisks (**) when p<0.01 and three asterisks (***) when p<0.001 (Tukey post-hoc test of respective populations of treated groups vs control).

Figure 6.6. Expression levels of p50 mRNA following 12 or 24 h of treatment with YM155, **AB1** or **AB7** quantified by qRT-PCR. Bars represent the fold-change of cDNA normalized against GAPDH in the same sample. Error bars represent the standard deviations of three separate experiments. Significant statistical difference from vehicle control is represented by an asterisk (*) when p<0.05, two asterisks (**) when p<0.01 and three asterisks (***) when p<0.001 (Tukey post-hoc test of respective populations of treated groups vs control).

Figure 6.7. Cleaved caspase 3, survivin, Sox2 and NF-κB subunits p50, p65, p105 and their phosphorylated forms (p.p50, p.p65) levels in NCCIT, HCT-8 and HCT-8 3.11 after treatment with YM155 and **AB1** for 48 h. GAPDH was used as loading control.

Figure 7.1. Summary of growth inhibitory structure-activity relationships of YM155

List of Schemes

Scheme 2.1. Reagents and conditions: (a) R_1-amines, EtOH, rt, 18 h; (b) acetic anhydride, conc. H_2SO_4, rt, 1.5 h; (c) R_2-amines, toluene, 45°C, 4 h; (d) 48% HBr (aq), EtOH + EtOAc, 45°C, 4 h to rt, overnight.

Scheme 2.2. Reagents and conditions: (a) 2-aminopyrazine, Pd(dba)$_2$, BINAP, t-BuOK, toluene, 60°C, 5 h; (b) 48% HBr (aq), EtOH + EtOAc, 45°C, 4 h to rt, overnight.

Scheme 2.3. Reagents and conditions: (a) pyrazin-2-ylmethylamine, triethylamine; (b) acetic anhydride, conc. H_2SO_4; (c) 2-methoxyethylamine, toluene; (d) 48% HBr (aq), EtOH + EtOAc, 45°C, 4 h to rt, overnight.

Scheme 2.4. Reagents and conditions: (a) 2-methoxyethyl bromide, KOH, DMSO, rt, 1.5 h; (b) 2-bromomethylpyrazine, CH_3CN, 80°C, 24 h.

Scheme 2.5. Reagents and conditions: (a) pyrazin-2-carbaldehyde, Et$_3$SiH, TFA, DCM, 0°C, 1 h; (b) 2-methoxyethyl bromide, KOH, DMSO, rt, 1.5 h; (c) MeMgBr, dry toluene, DCM, 0ºC, 30 min; (d) 2-methoxyethyl bromide, 0ºC → 40ºC, 24 h; (d) 2-bromomethylpyrazine, KOH, DMSO, rt, 30 min.

Scheme 2.6. Reagents and conditions: (a) NH_3 in MeOH, EtOH, 35°C, 3 h; (b) Acetic anhydride, conc. H_2SO_4, rt, 1.5 h; (c) 2-methoxyethylamine/pyrazin-2-ylmethylamine, triethylamine, toluene + EtOh, 45°C, 1h; (d) 48% HBr (aq), 2 drops of 2M NaOH(aq), EtOH, 50°C, 1 h.

List of Abbreviations

Bcl-2, B-cell lymphoma 2
Bcl-xl, B-cell lymphoma-extra large
BAX, Bcl-2 associated X protein
BAK, Bcl-2 homologous antagonist/killer
CAIX, carbonic anhydrase 9
ccRCC, clear cell renal cell carcinoma
CK2, casein kinase 2
CPC, chromosomal passenger complex
CR, complete response
CREB, cAMP response element-binding protein
DNA, deoxyribonucleic acid
EGF, epidermal growth factor
EGFR, epidermal growth factor receptor
ELISA, enzyme-linked immunosorbent assay
ERK, extracellular signal-regulated kinase
FID, fluorescent intercalator displacement (assay)
FITC, fluorescein isothiocyanate
GLUT-4, glucose transporter-4
Grb2, growth receptor binding protein-2
HBXIP, hepatitis B X-interacting protein
HCC, hepatocellular carcinoma
HRE, hypoxia response element
HRP, horseradish peroxidase
IGF1R, insulin-like growth factor-1 receptor
LTB, lymphotoxin B
LTBR, lymphotoxin B receptor
MAPK, mitogen activated protein kinase
Mcl1, myeloid cell leukemia 1
MEK, mitogen/extracellular signal-regulated kinase
mTOR, mammalian target of rapamycin
mTORC2, mammalian target of rapamycin complex 2
NEMO, NF-κB essential modulator
NF-κB, nuclear factor kappa light chain enhancer of activated B cells
NIK, NF-κB inducing kinase
IκBα, nuclear factor of kappa light chain enhancer of activated B cells inhibitor, alpha
IKK, IκB kinase
ILF3/NF110, interleukin enhancer-binding factor 3/nuclear factor 110
NQ, naphthoquinone
NSCLC, non-small cell lung carcinoma
OCT, organic cation transporter
OR, overall response
OS, overall survival

p-ERK, phosphorylated extracellular signal-regulated kinase
p-STAT3, phosphorylated signal transducer and activator of transcription 3
PAX2, paired box gene 2
PDGF, platelet-derived growth factor
PDPK1, 3-phosphoinositide dependent protein kinase 1
PFS, progression free survival
PI, propidium iodide
PI3K, phosphoinositide 3 kinase
PIP2, phosphatidylinositol-4,5-bisphosphate
PIP3, phosphatidylinositol-3,4,5-trisphosphate
pKAP1, phosphorylated KRAB associated protein 1
PR, partial response
PS, phosphatidylserine
Raf, rapidly accelerated fibrosarcoma
Ras, rat sarcoma
RANKL, receptor activator of nuclear factor kappa-B ligand
RCC, renal cell carcinoma
RHD, Rel homology domain
RNA, ribonucleic acid
ROS, reactive oxygen species
RTK, receptor tyrosine kinase
SAR, structure-activity relationship
siRNA, silencing RNA
SLC, solute carrier
Smac/DIABLO,
ThO, thiazole orange
TGF-α, transforming growth factor-α
TNF-α, tumor necrosis factor-α
TNFR, tumor necrosis factor receptor
TRAF2, TNF receptor-associated factor 2
VEGF, vasculoendothelial growth factor
γH2AX, phosphorylated histone H2AX

Chapter 1: Introduction

1.1. Survivin as an anticancer target

The 16.5 kDa protein survivin is the smallest member of the family of Inhibitor of Apoptosis (IAP) proteins.[1] IAP proteins are characterized by the presence of at least one ~ 70 amino acid-long baculovirus IAP repeat (BIR) domain and the ability to inhibit apoptosis. By this criteria, eight IAPs have been identified and they include c-IAP1, c-IAP2 and XIAP.[2, 3] The BIRs are the sites to which executioner caspases are bound and inhibited. These interactions are well studied for XIAP[4-6] and may apply to other IAP proteins (including survivin) as well.[7, 8] Notwithstanding, the precise mechanism by which survivin suppresses apoptosis is still poorly understood and conflicting reports abound. One study proposes that survivin does not directly inhibit caspase 3.[9] Others have reported that survivin inhibits caspases indirectly by interacting with intermediate proteins like Smac/DIABLO. The pro-apoptotic Smac/DIABLO binds XIAP, thus preventing it from inhibiting apoptosis.[6, 10-12] By sequestering Smac/DIABLO from XIAP, survivin effectively frees XIAP for binding to pro-caspases, thus blocking their conversion to the activated states. Yet another possibility is that survivin requires the cofactor hepatitis B X-interacting protein (HBXIP) to bind pro-caspase 9 before it can prevent apoptosis via the intrinsic pathway.[13] Survivin also regulates cell division, a property that is not shared by other IAP proteins. It forms part of the chromosomal passenger complex (CPC) which includes aurora B kinase, inner centromere protein (INCENP) and borealin.[14, 15] The CPC oversees the proper alignment of chromosomes to the mitotic spindle during cell division. Survivin also promotes the proper assembly of the mitotic spindle and cytokinesis. Knockdown of survivin expression resulted in cells that fail to divide in a proper manner and thus succumb to mitotic catastrophe and cell death.[16] Taken together, survivin has a unique bifunctional role as an inhibitor of apoptosis and regulator of cell division.

Given its important roles in cellular dynamics, it comes as no surprise that survivin is over-expressed in a plethora of cancers, including melanoma[17], gastric cancer[18], lymphoma[19-21], NSCLC[22] and RCC.[23, 24] High survivin expression correlates with metastatic spread, tumor invasiveness and poor prognosis arising from chemoresistance.[1, 25] Because survivin is rarely expressed in terminally differentiated adult tissues and is among the most tumor specific of all gene products, there is considerable interest in its potential as a target for anti-cancer therapy.[26-29]

YM155   FL118   Terameprocol   5-Deazaflavin analog
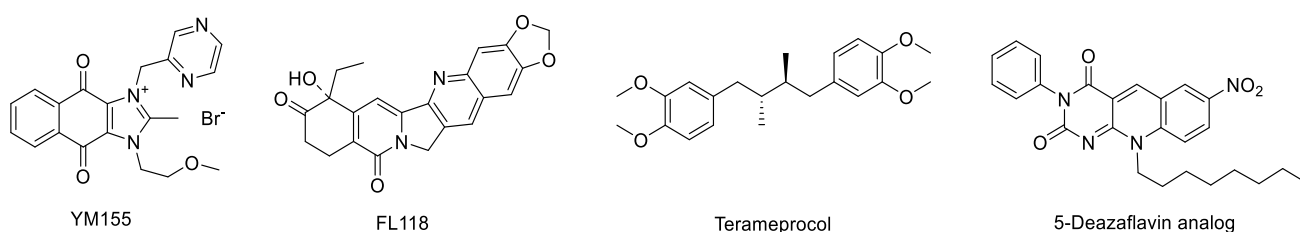
Figure 1.1. Small molecules with anticancer activities reportedly linked to suppression or inhibition of survivin.

Despite its potential as an anticancer target, few small molecule inhibitors of survivin have been reported to date. The more widely cited members are listed in Figure 1.1. The dioxonaphthoimidazolium YM155 is arguably the most widely investigated survivin suppressant to date. It was discovered in 2010 by Astellas Pharma, a Japanese pharmaceutical company during a high-throughput screen for survivin suppressants in a gene promoter assay.[1] YM155 will be discussed in greater detail in Section 1.2. Like YM155, FL118 was discovered in a high-throughput screen for suppressors of survivin.[30, 31] FL118 downregulates the expression of survivin, two other IAP proteins (XIAP, c-IAP2) and Mcl1, an anti-apoptotic member of the Bcl-2 family of proteins. Terameprocol is a synthetic lignan derivative of nordihydroguaiaretic acid found in extracts of the creosote bush.[32] It downregulates survivin by inhibiting the function of the transcription factor specificity protein 1 (Sp1).[33] YM155, terameprocol and FL118 are transcriptional inhibitors of survivin gene expression and do not directly interact with the survivin

protein. This raises the question as to whether these compounds suppress survivin solely by inhibiting its gene expression or if they have other protein targets that lie upstream from survivin and whose interception would also result in the suppression of survivin.

Unlike the aforementioned compounds, the 5-deazaflavin analog is unique in that it directly interferes with the interaction between survivin and the pro-apoptotic Smac/DIABLO.[11] Consequently, Smac/DIABLO is free to bind to XIAP, hence preventing it from binding and inhibiting caspases.

1.2. YM155: A potent anticancer agent

YM155 is a potent survivin suppressor. It downregulates survivin expression in prostate cancer PC3 cells at nanomolar concentrations and has potent growth inhibitory activities on a variety of refractory prostate cancer and melanoma cell lines, besides suppressing the growth of tumor-bearing xenografts in mice when delivered via subcutaneous pumps.[34]

Subsequent studies affirm the potent growth inhibitory activity of YM155 on a wide panel of malignant cell lines.[35] These include cells derived from solid tumors (non-small cell lung cancer (NSCLC), small cell lung cancer, renal cancer, colorectal cancer, breast cancer), hemapoietic malignancies (lymphomas, leukemias) and brain malignancies (gliomas). Overall, the mean concentration for 50% inhibition of cell growth (GI_{50}) was less than 16 nM. Cell lines with or without an intact p53 gene were equally susceptible to YM155, suggesting limited involvement of p53 in the mechanism of action.

Following its promising *in vitro* results, YM155 was evaluated in phase I and phase II clinical trials. It was reported to achieve a 5.4% overall response rate in stage III/IV non-small cell lung cancer (NSCLC) patients with another 37.8% of patients attaining a stable disease state .[36] In

patients with stage III/IV melanoma, the overall response rate was only 3.4%.[37] YM155 also

produced a 6.2% partial response rate in patients with taxane-pretreated prostate cancer.[38]

More recently, YM155 and docetaxel were used in combination for the treatment of stage IV

triple-negative breast cancer[39] and stage III/IV melanoma[40]. In both cases, YM155 did not

confer any significant benefit when combined with docetaxel. The modest response rates

notwithstanding, YM155 was well tolerated in the clinical trials and was associated with only

rare incidences of high-grade toxicities.

Many factors could have accounted for the modest response rates of YM155 in the clinical trials.

For one, the majority of patients involved in the trials had highly resistant tumors that failed to

respond to prior chemotherapy. The other reason may be that the mechanistic basis for the

anticancer activity of YM155 has yet to be fully understood. YM155 may thus be suited for

certain cancers only or should be used in combination, rather than a single drug. In addition,

YM155 is positively charged and this physicochemical characteristic might affect its ability to

penetrate tumors and malignant cells.

1.3.   Mode of action of YM155

YM155 intercepts the binding of various transcription factors to the survivin promoter. One of

these is the interleukin enhancer-binding factor 3 (ILF3), or more specifically its nuclear factor

110 (NF110) isoform.[41, 42] YM155 blocks ILF3 from binding to the survivin promoter by

interfering with the association of ILF3 and p54^{nrb}.[42] YM155 also interferes with the binding of

the transcription factor Sp1 to the survivin promoter region (-149 to -71).[43] The survivin gene is

activated by other transcription factors as well, such as nuclear factor-kappa B (NF-κB)[44, 45] and

signal transducer and activator of transcription 3 (STAT3).[46] In view of its exceptionally potent

activity as a survivin suppressant, it is tempting to speculate that YM155 acts on other

transcription factors apart from ILF3 and Sp1.
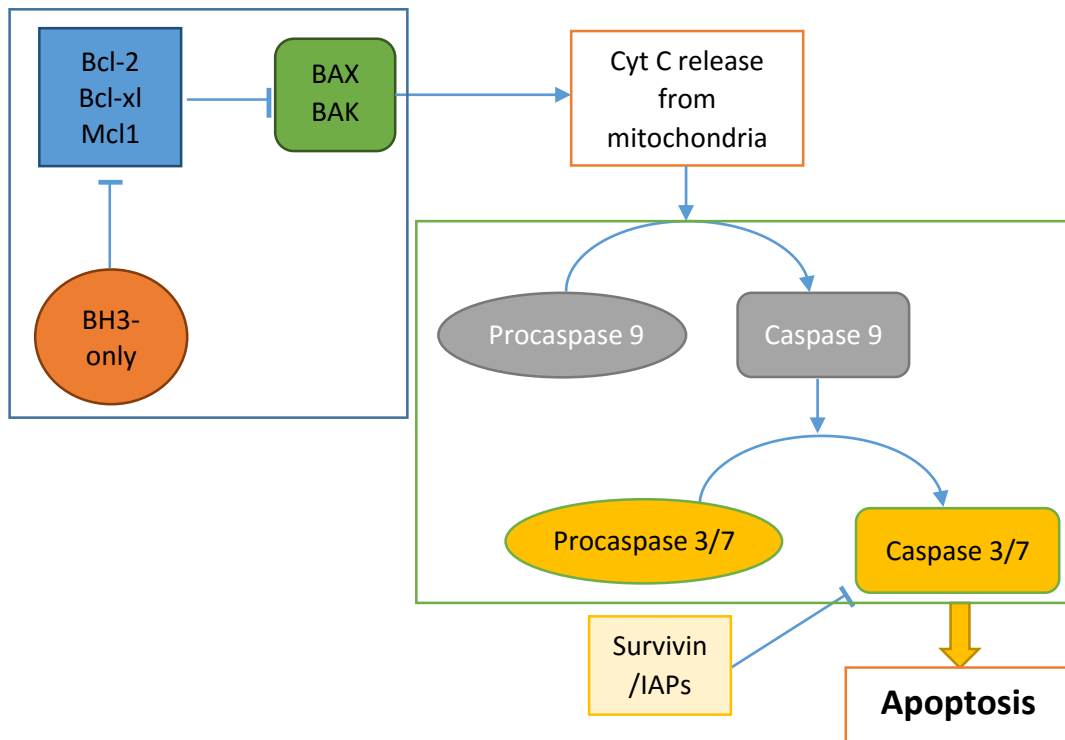
Figure 1.2. Schematic diagram of the interactions between Bcl-2 family (boxed in blue), caspases (boxed in orange) and the IAP family including survivin. Upon apoptotic stimuli, BH3-only members such as Noxa Puma, Bid, Bad, which possess only a BH3 (Bcl-2 homology 3) domain sequester anti-apoptotic Bcl-2, Bcl-xl and Mcl1 which are bound to BAX and BAK. This releases the latter pro-apoptotic proteins which oligomerize and open pores in the mitochondrial outer membrane. Subsequent release of cytochrome C activates caspase 9, which in turn cleaves and activates caspases 3 and 7, the effectors of apoptosis. Survivin and the other IAPs (inhibitors of apoptosis) bind to and inhibit caspase function.

Reports in recent literature support an alternative view that the suppression of survivin gene transcription is not the sole means by which YM155 induces cell death. A widely cited target of YM155 is Mcl1, a member of Bcl-2 family of proteins.[47-49] Mcl1, like Bcl-2 and Bcl-xl are anti-apoptotic proteins. They serve to bind to the pro-apoptotic members of the same family, BAX

and BAK, preventing the latter from oligomerization and forming pores on the outer mitochondrial membrane, which is an essential step in the intrinsic apoptotic pathway.[47, 48] The pores permeabilize the mitochondrial membrane and cause cytochrome c to be released from the intermembrane space. This is turn leads to the formation of the apoptosome and activation of the caspase cascade, which begins with the stepwise activation of initiator caspases (such as caspase 9) followed by executioner caspases 3 and 7. In a detailed study, Tang et al demonstrated that downregulation of Mcl1 by YM155 occurred at the transcriptional level and was independent of survivin expression and caspase activity.[49] The downregulation of Mcl1 by YM155 has been usefully exploited by combining it with BH3-only peptidomimetics ABT-263 and ABT-737.[49, 50] ABT-263 and ABT-737 inhibit Bcl-2 and Bcl-xl and cause apoptosis in cancer cells. However, cells with high Mcl1 expression bypass this inhibition by compensating for the functions of Bcl-2 and Bcl-xl, thus reducing the apoptotic effects of ABT-263 and ABT-737. On the other hand, when YM155 was used together with these compounds, the concurrent downregulation of Mcl1 synergized with the inhibition of Bcl-2 and Bcl-xl to restore apoptotic cell death.

YM155 has been reported to downregulate EGFR in pancreatic cancer cell lines, leading to the suppression of downstream proteins PI3K, p-ERK and p-STAT3.[51] It also downregulates XIAP.[50, 52] Dohi et al noted that XIAP forms a complex with survivin which protects XIAP from ubiquitination and proteasomal degradation.[53] The concurrent downregulation of survivin and XIAP by YM155 would result in synergistic inhibition of apoptosis. A transcriptome analysis of Wilms' tumor cells treated with YM155 revealed down-regulation of several other genes besides survivin as well as the up-regulation of the pro-apoptotic genes caspase 9 and Smac/DIABLO. That study also highlighted tumor necrosis factor receptor 1 (TNFR1) signaling as one of the most significant pathways affected by YM155.[54]

A widely cited claim for YM155 is its ability to induce a DNA damage response.[55] Here, the authors subjected YM155 and another dioxonaphthoimidazolium analog (NSC80467) to the COMPARE analysis against two DNA damaging agents (chromomycin A3, bisantrene) and a DNA directed inhibitor of transcription (actinomycin D). Briefly, this analysis involved elucidating the GI_{50} values for the above agents on the NCI-60 panel of 60 malignant cell lines representing a large variety of cancer types. The GI_{50} values for YM155 and NSC80467 were then correlated with those of the three reference compounds. It was found that the growth inhibitory profiles of the two dioxonaphthoimidazoliums were strongly and positively correlated to that of the three DNA targeting agents. YM155 and NSC80467 were then shown to preferentially inhibit DNA synthesis over RNA and protein synthesis. Subsequently, they demonstrated that YM155 and NSC80467 effectively stimulated the phosphorylation of the histone H2AX and the transcriptional repressor KAP1 at concentrations lower than that required to reduce survivin levels. Phosphorylated H2AX (γH2AX) and phosphorylated KAP1 (pKAP1) are biomarkers for DNA double stranded breaks, and their appearance at concentrations of YM155 that did not induce a decline in survivin levels was taken to signify that survivin suppression was secondary to the DNA damage response.

A separate study by Winter et al showed that YM155 induced a dose dependent increase in γH2AX and pKAP1.[56] It also interfered with topological changes in plasmid DNA caused in vitro by topoisomerase treatment. In this regard, YM155 behaved like ethidium bromide, an intercalator of DNA. Furthermore, YM155 did not inhibit topoisomerase I or interfered with DNA replication. The authors concluded that YM155 has the features of a DNA intercalator. They noted that chloroquine, another DNA intercalator also inhibited DNA replication and induced phosphorylation of H2AX.

The proposition that YM155 intercalates with DNA is consistent with its structural features. The positively charged planar scaffold of YM155 would strongly promote DNA intercalation. A point to note is that YM155 is also a quinone and this moiety is an established pharmacophore for redox cycling.[57] It is conceivable that free radicals generated during the quinone to semiquinone interconversion could initiate DNA strand breaks and trigger the DNA damage response as proposed by Glaros et al.[55] If YM155 is indeed a DNA damaging agent, this would call into question its relatively low toxicity profile as reported in clinical trials. Anticancer drugs that act by inducing DNA damage are unlikely to act selectively on cancer cells and would elicit severe side effects. Doxorubicin and irinotecan are such examples. Interestingly, Cheng et al reported that the silencing of survivin with siRNAs resulted in elevated levels in γH2AX.[52] This raises the question as to whether the increases in γH2AX are due to YM155-induced DNA damage or is an outcome of survivin suppression. Furthermore, work by Véquaud et al. suggested that DNA damage was a consequence of autophagy which was in turn a consequence from an unknown mechanism of action of YM155 on the NF-κB pathway. From the foregoing discussion, it is clear that important unknowns remain with regard to the interaction of YM155 and DNA and its significance to the mode of action of YM155.

Table 1.1. Summary table of research investigating the mechanisms of action of YM155.

Research Group	Year	Mechanism
Nakahara et al.[34]	2007	- ↓ survivin
Nakamura et al.[41]	2012	- Blocks ILF3 binding to survivin promoter
Yamauchi et al.[42]	2012	- Blocks ILF3-p54^{nrb} association
Cheng et al.[43]	2012	- Blocks Sp1 binding to survivin promoter
Na et al.[51]	2012	- ↓ EGFR, PI3K, p-ERK, p-STAT3 and XIAP
Glaros et al.[55]	2012	- Damages DNA - ↑ γH2AX, pKAP1
Tao et al.[54]	2012	- Affects TNFR1 signaling
Winter et al.[56]	2015	- Intercalates and damages DNA
Cheng et al.[52]	2015	- Induces autophagy - ↑ LC3-II (autophagy marker)

Véquaud et al.[58]	2015	- ↑ LC3-II
		- NF-κB pathway implicated in autophagy and DNA damage

1.4. Uptake of YM155 into cancer cells

Another aspect of YM155 that has received considerable attention is its uptake by malignant cells. The charged state of YM155 would hamper its diffusion into cells. Thus physiological transporters may be involved in its uptake into cells. Early investigations on the cellular uptake of YM155 showed that the mechanisms by which YM155 gained access into cancer cells and hepatocytes were distinctly different.[59-61] The organic cation transporter OCT1 played a key role in uptake into hepatocytes but not into cancer cells. The implication was that a yet to be identified transporter(s) was involved and this was indeed proven by Winter et al when they reported the involvement of a relatively uncharacterized transporter, the solute carrier family member 35F2 (SLC35F2), in the uptake of YM155 into cancer cells.[56] SLC35F2 was upregulated in several cancers and in the absence of SLC35F2, growth inhibition by YM155 was greatly attenuated. Additionally, SLC35F2 expression and YM155 sensitivity were correlated across a panel of cancer cell lines. The authors noted that YM155 retained some growth inhibitory activity on SLC35F2 knockout cells, suggesting that OCT still had a role in the uptake of YM155. Taken together, the mechanism by which YM155 gains access into cancer cells is clearly as important as its binding targets in defining the mechanistic basis of its mode of action.

1.5. YM155 inhibits teratoma formation

Survivin is found in abundance in primary tumors but rarely expressed in terminally differentiated cells. It is however present in fetal tissues, actively dividing tissues such as those of hematopoietic lineage, and in stem cells of embryonic and mesenchymal origin.[26, 62-66] Its presence in undifferentiated stem cells is traced to the need for stem cells to maintain low

mutation frequencies in order to ensure the genomic integrity of subsequent generations of somatic cells. Consequently, stem cells preferentially succumb to cell death under genotoxic stress rather than resorting to DNA repair. To achieve this end, stem cells express a large number of pro-apoptotic genes and relatively fewer anti-apoptotic genes compared to their differentiated counterparts. The abundance of pro-apoptotic genes would mean that the survival and self-renewal of stem cells are critically dependent on the few resident anti-apoptotic genes, including survivin. This was illustrated by Guvenc et al where glioma stem cells lost viability when protein interactions of survivin were inhibited.[67]

In 2013, Lee et al showed that nanomolar concentrations of YM155 induced apoptosis in human pluripotent stem cells.[68] This effect was attributed to the suppression of survivin and was proposed as a viable means of eliminating remnant rogue undifferentiated stem cells which would otherwise transform into teratomas or teratocarcinomas. Teratoma formation would seriously undermine the safety of stem cell-based therapies.[69, 70] There has been growing interest in the use of small molecules like YM155 to eliminate remaining undifferentiated pluripotent cells from differentiated populations destined for regenerative therapies. Ideally, these compounds should selectively eliminate undifferentiated stem cells without affecting lineage specific differentiation or functionality of differentiated cells.

1.6. Hypothesis

YM155 is a dioxonaphthoimidazolium analog with exceptionally potent growth inhibitory activity on a variety of cancer cell lines. In spite of its potent activity and good safety profile, it has failed to perform to expectations in clinical trials. One of the reasons for its poor showing may stem from gaps in our understanding of the mechanistic basis of its cell killing effects. YM155 is commonly cited as a survivin suppressant but recent findings have questioned if this is the sole and main effect of the drug. The likelihood of DNA as a target of YM155 has been proposed by

10

several investigators and in its wake, caution has been advised with regards to its clinical deployment. There is also limited information on structure-activity correlations with regard to YM155.

Against this backdrop, it is hypothesized that a detailed understanding of selected aspects of the mode of action of YM155 will promote the development of dioxonaphthoimidazolium analogs as potent anti-cancer therapeutics.

To this end, the focus will be on DNA and the NF-κB signaling pathway as putative targets of YM155. A focused library of functionalized dioxonaphthoimidazoliums will be synthesized and structure-activity relationships (SAR) elucidated for growth inhibitory activity on malignant cells and stem cells, DNA binding and redox cycling. These studies will (i) provide insight into the structural requirements for activity, (ii) support a reasoned approach towards the design of more potent analogs and (iii) validate DNA as a preferred target of the scaffold.

With regards to the NF-κB pathway, it is known that survivin overexpression is a biological sequela of NF-κB activation in several malignancies. Hence, YM155 may conceivably disrupt the pathway at one or more points to add on to the suppression of survivin.

Chapter 2: Design and synthesis of YM155 analogs

2.1. The dioxonaphthoimidazolium analog YM155

The structure of YM155 comprises the fused tricyclic dioxonaphthoimidazolium core and the

substituents attached to the core. The tricyclic ring consists of a central quinone (B) flanked by a

benzene ring (A) and positively charged imidazolium (C) (Figure 2.1). The substituents are

found exclusively on the imidazolium ring. The positively charged state and embedded quinone

in YM155 are not commonly present in drugs. Drug candidates which are positively charged are

normally deemed to have suboptimal permeability and may be overly dependent on specific

transporters for uptake into cells. The quinone is an acknowledged PAIN (Pan-Assay

Interference compound) because of its potential for redox cycling.[71] Notwithstanding, YM155

complies with the Rule-of-Five mnemonic which predicts candidates with good oral absorption

profiles. It has a cLog P that is less than 5, fewer than 5 hydrogen bond donor (HBD) and 10

hydrogen bond acceptor (HBA) groups and a molecular weight that does not exceed 500 Da.
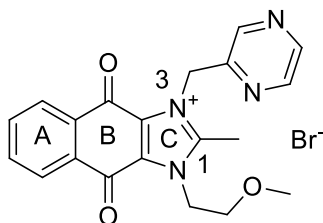
Figure 2.1. Molecular structure of YM155. The positive charge is delocalized between N^1 and

N^3.

There are limited references to the structure-activity relationship (SAR) of YM155 despite

detailed description of more than 250 related analogs in the original patent .[72] There, growth

inhibitory activities (IC_{50}) were determined on HelaS3 and melanoma A375 cells but the results

were reported as "1 µM or less" for the entire series, without details on structure-activity trends.

In a report that predated the patent by almost a decade, a dioxonaphthoimidazole **1** (Figure 2.2)

was found to be cytotoxic with a mean IC_{50} of 2.3 µM on tumor cell lines of the NCI panel.[73] Its

good activity raises the question as to whether the positive charge on the YM155 scaffold was a

necessary feature. Furthermore, two intermediates (**2**, **3**) involved in the synthesis of **1** and

related compounds were equally active, which adds to the uncertainty over the role of the

dioxonaphthoimidazolium scaffold for growth inhibition.

2: R_1= 3',5'-OMe; R_2 = -NHEt

3: R_1= 2'-F; R_2 = -Cl
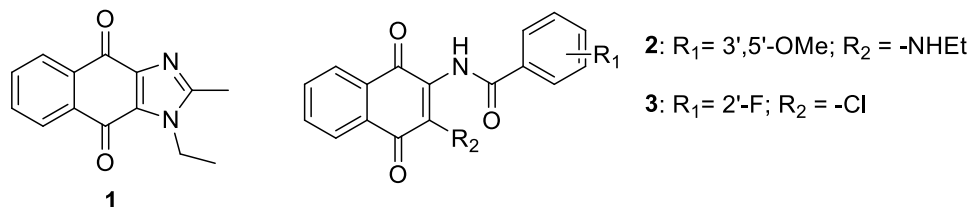
Figure 2.2. Naphtho[2,3-d]imidazole-4,9-dione **1** and intermediates (**2,3**) with anticancer activity

on NCI cancer cell lines.

Another report highlighted the growth inhibitory property of functionalized imidazoliums (Figure

2.3).[74, 75] Two hits IBN-1 and IBN-9 were identified, with IC_{50} values of 100 µM and 120 µM

respectively on a hepatocellular carcinoma (HCC) cell line. Although much less potent than

YM155, they were reported to down-regulate survivin. Further optimization yielded a more

potent analog (IBN-65, $IC_{50} \approx 5$ µM on a panel of HCC cell lines) which also suppressed

survivin. This again raises the question as to whether the intact dioxonaphthoimidazolium

scaffold of YM155 is required for growth inhibition and survivin suppression.

IBN-1   IBN-9   IBN-65
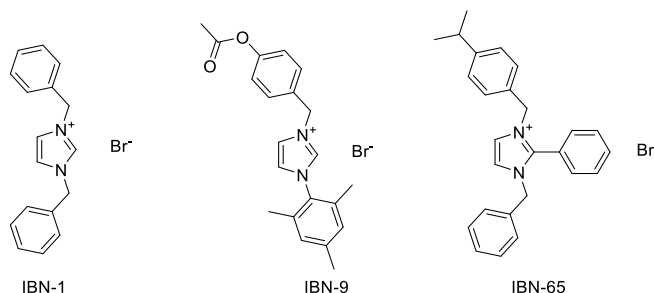
Figure 2.3. Imidazolium derivatives with anticancer properties and ability to downregulate

survivin.

2.2.   Objective

The objective of this chapter is to design and synthesize a series of dioxonaphthoimidazolium analogs in order to address the research gap that exists in the understanding of the SAR of YM155. To achieve this end, a focused library comprising 53 compounds were designed and synthesized. The compounds were organized into four series. Series A compounds focused on modifications to the pyrazin-2'-ylmethyl side chain located at N^3 of YM155 with no change to the 2'-methoxyethyl side chain at N^1. Conversely, series B compounds dealt with modifications to the N^1 2'-methoxyethyl side chain while retaining the N^3 pyrazin-2'-ylmethyl side chain. Series C consisted of compounds modified at the core dioxonaphthoimidazolium scaffold. Series AB was conceived after the evaluation of the preceding series and sought to validate the SAR gleaned from series A and B by combining promising substituents identified from these series onto a common scaffold. Hence, its designation as "series AB".

2.3.   Rationale for design of compounds

2.3.1.   Series A

The 22 compounds in series A are shown in Figure 2.4. They are subdivided into **A1-X** to **A6-X** subgroups base on the nature of the N^3 side chain. **A1-1** to **A1-3** replaces the polar pyrazine ring on YM155 with non-polar rings such as phenyl (**A1-1**), cyclohexyl (**A1-2**) and thienyl (**A1-3**). These replacements serve to elucidate the importance of retaining a polar heteroaromatic ring at N^3.

Attempts were made to introduce azoles (pyrrole, N-methylpyrrole, imidazole) in place of pyrazine at N^3. Only the imidazol-4'-ylmethyl analog **A2-1** was successfully synthesized. The imidazole ring of **A2-1** is electron rich (π-excessive) unlike pyrazine which is electron poor (π-deficient). The azomethine N in imidazole is also more basic (pKa $\approx$ 7) than those present in

pyrazine and would be protonated at physiological pH. Thus, greater polarity would be expected

for **A2-1**.

SERIES A

R groups are as follows:

A1-1[a]	**A3-2**[a]	**A3-7**[a]	**A6-2**[a]	**A6-7**[a]
A1-2	**A3-3**[a]	**A3-8**	**A6-3**[a]	**A6-8**[a]
A1-3[a]	**A3-4**[a]	**A4-1**[a]	**A6-4**[a]	
A2-1	**A3-5**[a]	**A5-1**	**A6-5**[a]	
A3-1[a]	**A3-6**[a]	**A6-1**[a]	**A6-6**	
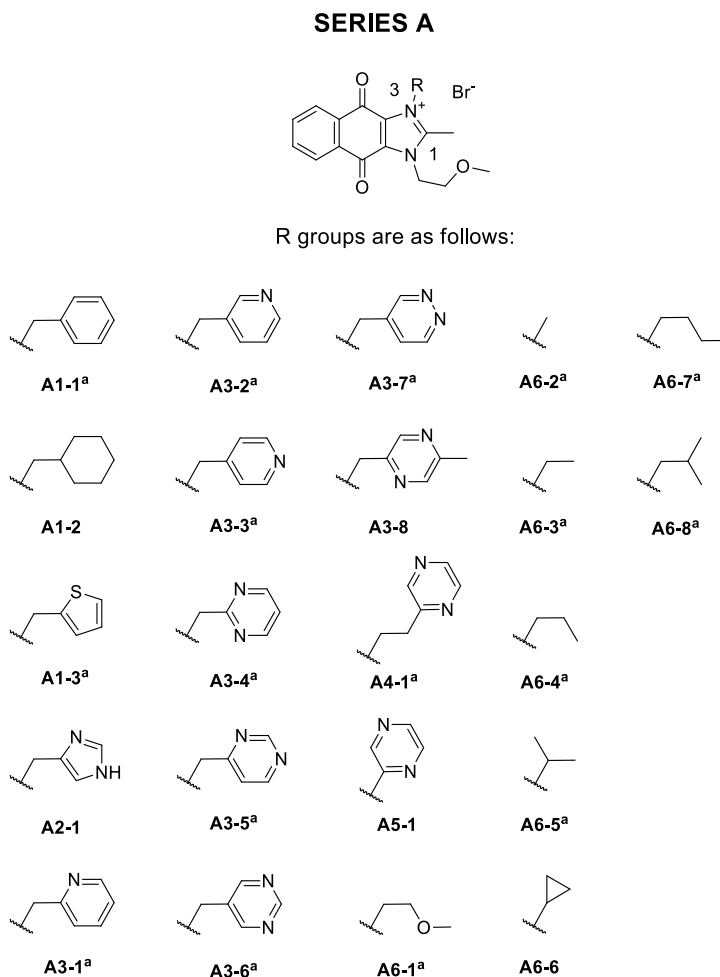
Figure 2.4. Series A analogs. [a] Compounds have been reported in SciFinder

In the **A3-X** subgroup, the pyrazine ring was replaced by an assortment of azines. **A3-1, A3-2, A3-3** are regioisomeric pyridinylmethyls, in which the azomethine N is ortho, meta or para. These compounds would determine if the location of the azomethine N in pyridine is an important determinant of activity. **A3-4, A3-5, A3-6** are regioisomeric pyrimidinylmethyls in which the azomethine nitrogens are positioned at ortho (**A3-4**), ortho-para (**A3-5**) or meta (**A3-6**) positions. Like the pyridinylmethyls, they serve to report on the importance of positional isomerism in the pyrimidinylmethyl side chain. **A3-7** is pyridazin-4'-ylmethyl. The pyridazin-3'-

ylmethyl regioisomer could not be prepared because the starting material was not available. **A3-8** is essentially YM155 with a para-methyl attached to the pyrazine ring. It was synthesized after **A3-3**, **A3-5** and **A3-7** were found to have greater growth inhibitory properties than their regioisomers. Since they have in common an azomethine nitrogen at the para position of the azine, **A3-8** was designed to query the effect of "blocking" putative interactions at that position.

A4-1 and **A5-1** are homologs of YM155 in which the methylene spacer linking the pyrazine ring to N^3 is either extended to ethyl or removed altogether. Lastly, the **A6-X** subgroup examines the impact of removing the pyrazinylmethyl moiety. In **A6-1**, it is replaced by methoxyethyl, thus yielding an N^1, N^3-symmetrically substituted analog. In **A6-2** to **A6-8**, it is replaced by a series of homologous alkyl substituents (methyl to n-butyl), branched analogs (isopropyl, isobutyl) and cyclopropyl.

2.3.2. Series B

There are 15 compounds in series B (Figure 2.5) and they are organized into four subgroups **B1-X** to **B4-X**. In **B1-X**, the terminal methoxy of the N^1 methoxyethyl side chain was removed to give the hydroxyl (**B1-1**), incorporated into a tetrahydrofuran ring (**B1-2**) or extended to its ethyl homolog (**B1-3**). The additional hydrogen bonding group in **B1-1** will increase polarity whereas homologation/cyclization will increase lipophilicity and steric bulk.

B2-X is the largest subgroup with 8 members and they serve to investigate the effects of replacing the 2'-methoxyethyl side chain with the same alkyl residues explored in series A. Also included is the cyclopentyl side chain (**B2-8**) which has no series A counterpart. Aromatic side chains are introduced in **B3-1** and **B3-2** in lieu of the methoxyethyl group. **B3-2** is analogous to **A6-1** in that both compounds are symmetrically substituted at N^1 and N^3. **B3-2** is symmetrically substituted with pyrazine-2'-ylmethyl moieties. In **B4-1** and **B4-2**, the 2'-methoxyethyl is

replaced by a basic N',N'-dimethylaminoethyl or N',N'-diethylaminoethyl side chain which would

be protonated at pH 7. Consequently, increased polarity would be expected for these

compounds.

SERIES B

R groups are as follows:

B1-1	B2-1	B2-5	B3-1
B1-2	B2-2	B2-6	B3-2
B1-3	B2-3	B2-7	B4-1
	B2-4	B2-8	B4-2
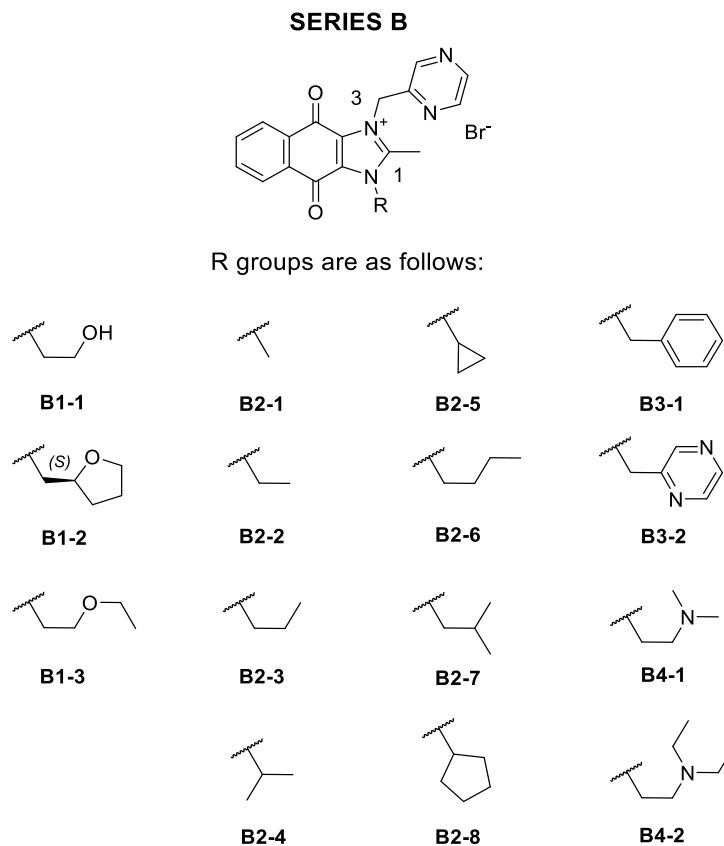
Figure 2.5. Series B analogs. **B3-2** has been reported in SciFinder

2.3.3. Series C

The series C compounds were designed to probe the importance of the intact

dioxonaphthoimidazolium scaffold for activity (Figure 2.6). **C1-1** which features an extension of

the C^2 methyl is an exception. In **C1-2**, the scaffold is reduced to a dihydrobenzo[d]imidazolium

by the removal of the distal benzene ring. Two methyl groups were introduced at C^5 and C^6 of

the quinone ring to reduce the reactivity of these positions to Michael addition by nucleophiles.

In **C2-X,** the quinone is removed from the scaffold to give the benzoimidazolium **C2-1** and

imidazolium **C2-2** or replaced to give the imidazoquinoxalinium **C2-3**. **C2-2** is structurally similar to the IBN compounds which have been reported to be survivin suppressants.[79,80] The central pyrazine ring of **C2-3** is deemed an appropriate isostere of the quinone because the azomethine nitrogens are hydrogen bond acceptors like the quinone carbonyls.
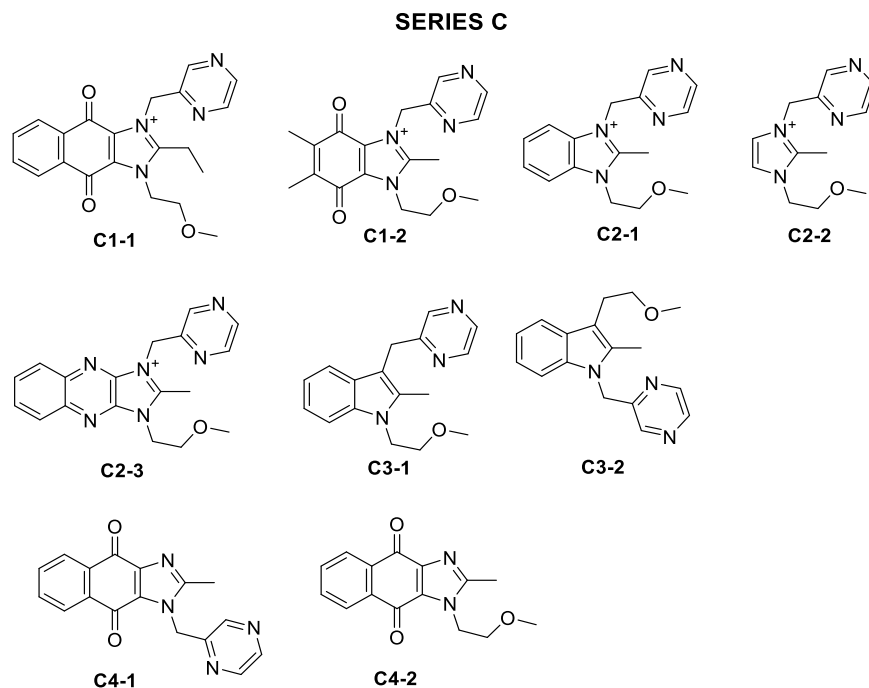
SERIES C

Figure 2.6. Series C analogs. **C1-1, C1-2, C2-1, C2-2** and **C2-3** were synthesized as bromides. **C4-1** and **C4-2** have been reported in Scifinder.

The indoles **C3-1** and **C3-2** were designed in attempts to scaffold hop. They can also be viewed as a modification of **C2-1** in which the charged benzoimidazolium is replaced by an uncharged indole. **C4-1** and **C4-2** are analogs of compound **1** (Figure 2.1) and would report on the importance of retaining the positive charge on the scaffold. Without the charged centre, only one of the two side chains of YM155 can be introduced to the scaffold and this was done in turn for **C4-1** and **C4-2**. **C4-1** and **C4-2** should also be compared to **B2-1** and **A6-2** respectively as they are essentially the N^3-demethylated analogs of these compounds. These comparisons will clearly illustrate the importance of retaining a positive charge on the scaffold.

18

Lastly, two other analogs were considered (Figure 2.7). Denoted **C5-1** and **C5-2**, these are pyrrolo[2,3-b]naphthoquinone analogs of YM155 where one of the imidazolium nitrogens is replaced by a carbon. These analogs would complement **C4-1** and **C4-2** with regard to the importance of the positive charge. Unfortunately, they were not synthetically accessible and were dropped from the final library.
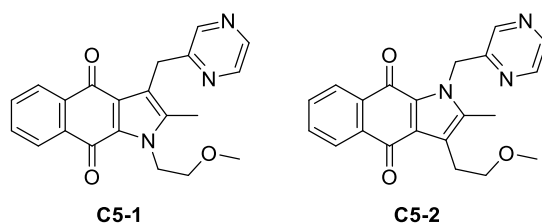
Figure 2.7. Analogs **C5-1** and **C5-2.**

2.3.4. Series AB
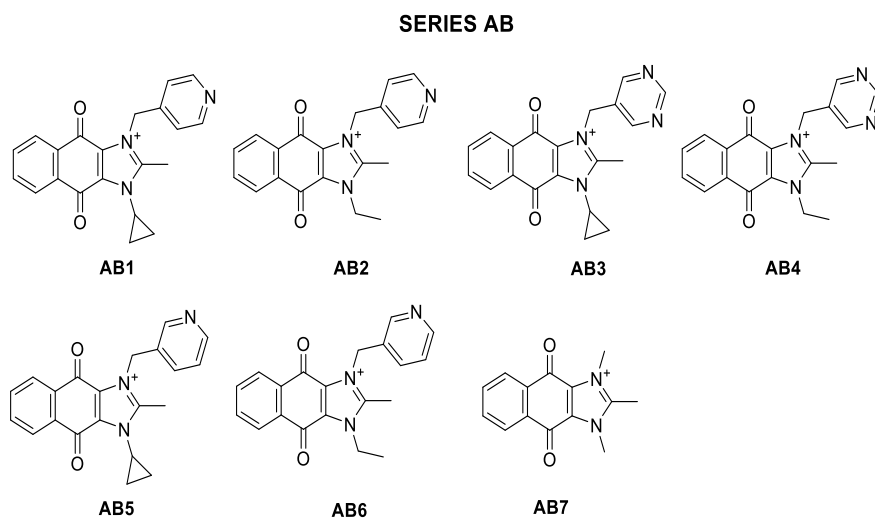
Figure 2.8. Series AB analogs. Compounds were synthesized as bromides. **AB7** has been reported in Scifinder.

Series AB compounds are planned after assessing the growth inhibitory activities of series A and B on clear cell renal cell carcinoma (ccRCC) and non-small cell lung carcinoma (NSCLC) cell lines. **A3-3, B2-2** and **B2-5** were found to be the most potent members in their respective series. Thus, the N^3 (pyridine-4'-ylmethyl, **A3-3**) and N^1 (ethyl, **B2-2**; cyclopropyl, **B2-5**) side chains are introduced simultaneously to the dioxonaphthoimidazolium scaffold in the anticipation that it will result in compounds of comparable or superior activity to YM155. The resulting compounds are **AB1** and **AB2** (Figure 2.8). To validate the preceding approach, less optimal substituents identified in series A such as pyrimidin-5'-ylmethyl, pyridine-3'-ylmethyl and methyl are also introduced at N^3. In **AB3** – **AB6**, N^1 is ethyl or cyclopropyl. Special mention should be made of **AB7** because it is substituted with methyl groups at both N^1 and N^3. Consequently, it is the most minimally substituted YM155 analog investigated here. **AB7** was conceived after observing the good growth inhibitory properties of **A6-2** (N^3-methyl) and **B2-1** (N^1-methyl).

The detailed SAR and growth inhibitory activities of the series A, B, C and AB compounds are discussed in Chapter 3.

2.4.   Chemistry

2.4.1. Synthesis of series A, B and AB

The synthesis of compounds in series A, B and AB followed the general method described in the literature.[72] As shown in Scheme 2.1, nucleophilic displacement of chlorine in 2,3-dichloro-1,4-naphthoquinone was effected by a primary amine in the presence of triethylamine to yield compounds **4-15**. The amino nitrogen was then acetylated to give *N*-acetylamides **16-27**, followed by displacement of the second chlorine by another primary amine to give compounds **28-70**. Finally, ring closure was effected by hydrobromic acid to give the final compounds (Scheme 2.1).
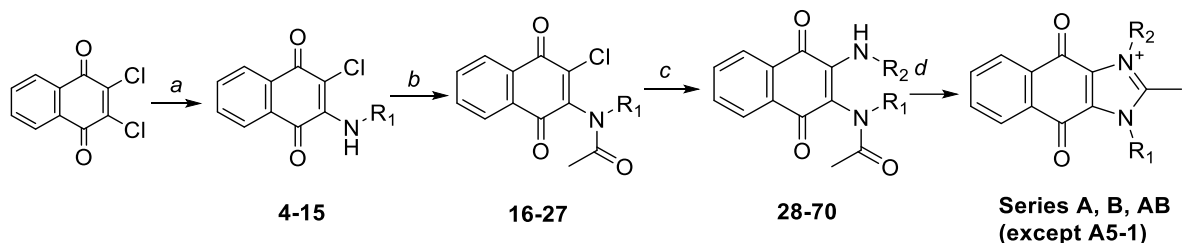
Scheme 2.1. Reagents and conditions: (a) R_1-amines, EtOH, rt, 18 h; (b) acetic anhydride, conc. H_2SO_4, rt, 1.5 h; (c) R_2-amines, toluene, 45°C, 4 h; (d) 48% HBr (aq), EtOH + EtOAc, 45°C, 4 h to rt, overnight.

A different route was applied for the synthesis of **A5-1**. The *N*-acetylamide **16** was subjected to a modified Buchwald-Hartwig coupling reaction with 2-aminopyrazine to give **71**, followed by ring closure in the presence of hydrobromic acid (Scheme 2.2).
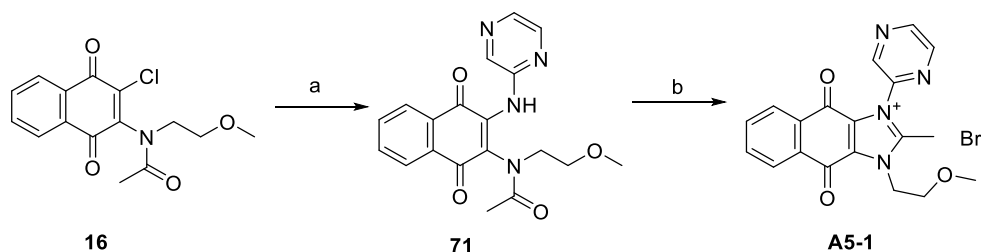
Scheme 2.2. Reagents and conditions: (a) 2-aminopyrazine, Pd(dba)$_2$, BINAP, t-BuOK, toluene, 60°C, 5 h; (b) 48% HBr (aq), EtOH + EtOAc, 45°C, 4 h to rt, overnight.

2.4.2. Synthesis of series C

Scheme 2.1 also applied to the Series C compounds **C1-1**, **C1-2** and **C2-3** with some modifications. To obtain **C1-1**, propionic anhydride was used in place of acetic anhydride for the acylation of **4.** The resulting *N*-propionate **72** was reacted with pyrazin-2-ylmethylamine to afford **73** which was then cyclized to **C1-1**. In the case of **C1-2** and **C2-3**, the same sequence of reactions were followed starting from 2,3-dichloro-5,6-dimethyl-1,4-benzoquinone and 2,3-

dichloroquinoxaline respectively, except that the initial displacement of chlorine was effected by

pyrazin-2-ylmethylamine and not 2-methoxyethylamine as shown in Scheme 2.3.
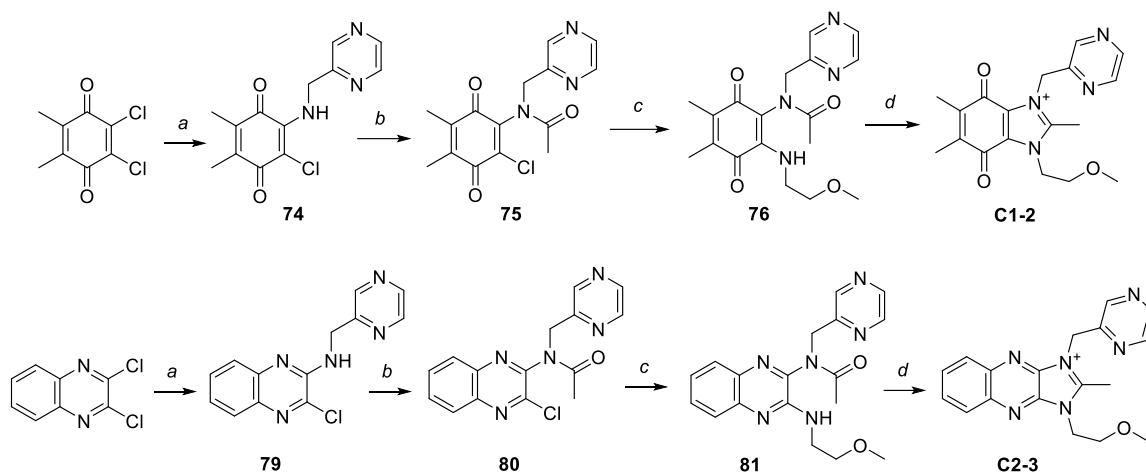
Scheme 2.3. Reagents and conditions: (a) pyrazin-2-ylmethylamine, triethylamine; (b) acetic

anhydride, conc. H_2SO_4; (c) 2-methoxyethylamine, toluene; (d) 48% HBr (aq), EtOH + EtOAc,

45°C, 4 h to rt, overnight.

The benzimidazolium **C2-1** and imidazolium **C2-2** were synthesized by *N*-alkylation with 2-

methoxyethyl bromide to give **77** and **78** respectively, followed by quaternization of the

azomethine nitrogen with 2-bromomethylpyrazine.[76, 77] Scheme 2.4 outlines the synthesis of **C2-**

1, which also applies to **C2-2.**
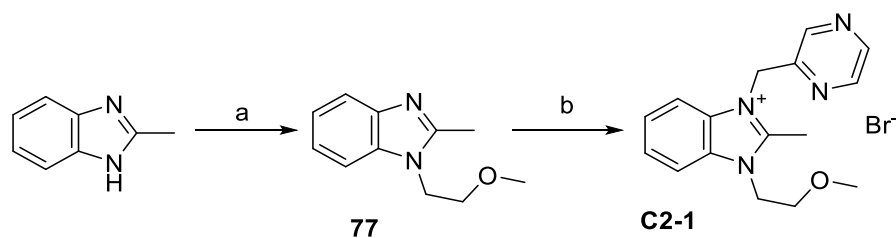
Scheme 2.4. Reagents and conditions: (a) 2-methoxyethyl bromide, KOH, DMSO, rt, 1.5 h; (b)

2-bromomethylpyrazine, CH_3CN, 80°C, 24 h.

Scheme 2.5 outlines the syntheses of the isomeric indoles **C3-1** and **C3-2**. 2-Methylindole was

reacted with pyrazin-2-carbaldehyde in the presence of triethylsilane and trifluoroacetic acid to

give **82**[78] which was then N-alkylated in the presence of KOH in DMSO to afford **C3-1**.[79] In the

case of **C3-2**, 2-methylindole was reacted with methyl magnesium bromide at the indole

nitrogen, followed by electrophilic substitution at C^3 with 2-methoxyethyl bromide.[54] The

pyrazinylmethyl side chain was then introduced at the indole N in the usual way.[79]
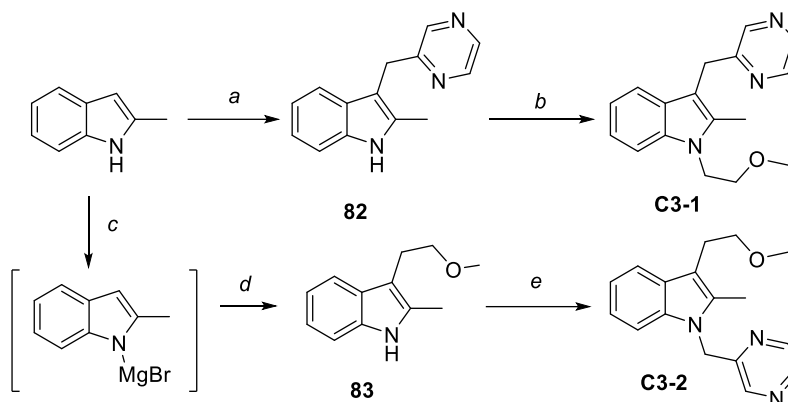
Scheme 2.5. Reagents and conditions: (a) pyrazin-2-carbaldehyde, Et₃SiH, TFA, DCM, 0°C, 1

h; (b) 2-methoxyethyl bromide, KOH, DMSO, rt, 1.5 h; (c) MeMgBr, dry toluene, DCM, 0°C, 30

min; (d) 2-methoxyethyl bromide, 0°C → 40°C, 24 h; (d) 2-bromomethylpyrazine, KOH, DMSO,

rt, 30 min.

The synthesis of **C4-1** and **C4-2** was adapted from Scheme 2.1. Nucleophilic displacement of

chlorine in 2,3-dichloro-1,4-naphthoquinone with concentrated ammonia gave **84**, followed by

acetylation by acetic anhydride to give **85**. Nucleophilic displacement of the second chlorine by

2-methoxyethylamine or pyrazin-2-ylmethylamine yielded **86** and **87** respectively. Finally, ring

closure using hydrobromic acid resulted in **C4-1** and **C4-2** respectively.
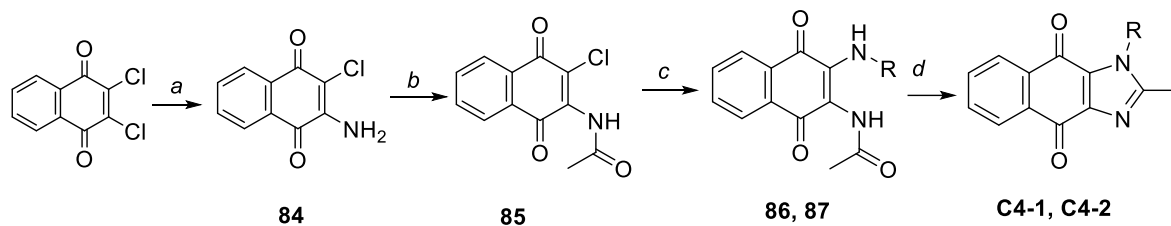
Scheme 2.6. Reagents and conditions: (a) NH_3 in MeOH, EtOH, 35°C, 3 h; (b) Acetic anhydride, conc. H_2SO_4, rt, 1.5 h; (c) 2-methoxyethylamine/pyrazin-2-ylmethylamine, triethylamine, toluene + EtOh, 45°C, 1h; (d) 48% HBr (aq), 2 drops of 2M NaOH(aq), EtOH, 50°C, 1 h.

2.5. Experimental

2.5.1. General details

Reagents (synthetic grade or better) were obtained from commercial sources and used without further purification. Reactions were monitored by thin layer chromatography using pre-coated aluminium plates (silica gel 60, F254, Merck). Compounds were purified by column chromatography on silica gel 60 (230-400 mesh, Merck).^{1}H NMR spectra (400 MHz) were recorded on a Bruker Avance 400 Ultrashield instrument (Bruker, Billerica, MA, USA), and referenced to residual solvent peaks (CDCl$_3$ at δ7.26, D$_6$-DMSO at δ2.50). ^{13}C NMR spectra (100 MHz) were recorded on the same instrument and referenced to residual solvent peaks (CDCl$_3$ at δ77.00, D$_6$-DMSO at δ39.40). Coupling constants (J) were reported in Hertz (Hz).

Nominal mass spectra were captured on an AB Sciex QTrap 2000 mass spectrometer (AB Sciex, Framingham, MA, USA) by electrospray ionization (ESI). Accurate mass information was obtained on a Bruker micrOTOFQII mass spectrometer (Bruker, Billerica, MA, USA) by ESI. Purity was determined on a reverse-phase HPLC on a Shimadzu Nexera SR HPLC system (Shimadzu Scientific Instruments, Columbia, MD, USA) with a Zorbax Eclipse XDB-C18 column (Agilent Tech. Inc., Loveland, CO) at two wavelengths: 254 and 280nm. Solvent systems used

as well as purity values are provided in Appendix 1. Purity of **C2-3** was determined by elemental

analysis (C, H, N) with the Elementar Vario Micro Cube instrument (Elementar

Analysensysteme GmbH, Hanau, Germany).

Spectral characteristics and purity data of intermediates and final compounds are reported in

Appendix 1. The synthetic details of promising analogs **AB1**, **AB7** and the intermediates leading

up to these two promising analogs are outlined in the following sections.

2.5.2.   Synthesis of 2-chloro-3-(methylamino)-1,4-naphthoquinone (**7**)

To 2,3-dichloro-1,4-naphthoquinone (0.341g, 1.50mmol) in 1.5ml of ethanol was added

methylamine (0.0465g, 1.50mmol) and triethylamine (0.227g, 2.25mmol) and the mixture stirred

at r. t. for 18h. The red precipitate formed was filtered under suction, washed with distilled water

and dried to afford (**7**) as a red solid, 91.0%. ^{1}H (CDCl$_3$) δ 8.15 (dd, 1H, J=0.9, 7.7Hz), 8.03 (dd,

1H, J=0.9, 7.7Hz), 7.72 (dt, 1H, J=1.3, 7.6Hz), 7.62 (dt, 1H, J=1.3, 7.6Hz), 6.10 (br s, 1H), 3.45

(d, 3H, J=5.6Hz); ^{13}C (CDCl$_3$) δ 180.53, 144.89, 134.94, 132.78, 132.45, 132.39, 129.74,

126.84, 126.76, 32.55.

2.5.3.   Synthesis of 2-chloro-3-cyclopropylamino-1,4-naphthoquinone (**11**)

To 2,3-dichloro-1,4-naphthoquinone (0.341g, 1.50mmol) in 1.5ml of ethanol was added

cyclopropylamine (0.0856g, 1.50mmol) and triethylamine (0.227g, 2.25mmol) and the mixture

stirred at r. t. for 18h. The red precipitate formed was filtered under suction, washed with

distilled water and dried to afford (**11**) as a red solid, 93.9%. ^{1}H (CDCl$_3$) δ 8.16 (dd, 1H, J=1.1,

7.7Hz), 8.02 (dd, 1H, J=1.1, 7.7Hz), 7.72 (dt, 1H, J=1.3, 7.6Hz), 7.62 (dt, 1H, J=1.3, 7.6Hz),

6.12 (br s, 1H), 3.34-3.28 (m, 1H), 0.97-0.92 (m, 2H), 0.78-0.73 (m, 2H); ^{13}C (CDCl$_3$) δ 180.27,

177.14, 145.07, 134.91, 132.74, 132.46, 129.75, 126.92, 126.72, 111.52, 27.43, 10.40.

2.5.4. Synthesis of *N*-(3-chloro-1,4-dioxo-1,4-dihydro-naphthalen-2-yl)-*N*-methyl-acetamide (**19**)

Two drops of concentrated sulfuric acid were added to a suspension of (**7**) (0.443g, 2.00mmol) in acetic anhydride (1.84g, 18.0mmol) and stirred for 1.5h at r. t. 10ml of distilled water was added slowly to the reaction mixture with stirring to quench excess anhydride, and extracted with EtOAc. The organic layer was washed with saturated $NaHCO_3$ solution and brine and dried over anhydrous Na_2SO_4. Purification by column (1:4 EtOAc/Hexanes) afforded (**19**) as a yellow solid, 92.6%. ^1H (CDCl$_3$) δ 8.28-8.08 (m, 2H), 7.86-7.77 (m, 2H), 3.19 (s, 3H), 1.93 (s, 3H); ^{13}C (CDCl$_3$) δ 183.10, 179.16, 177.84, 134.89, 134.77, 134.72, 134.69, 134.62, 134.16, 131.31, 127.57, 40.11, 21.76.

2.5.5. Synthesis of *N*-(3-chloro-1,4-dioxo-1,4-dihydro-naphthalen-2-yl)-*N*-cyclopropyl-acetamide (**23**)

Two drops of concentrated sulfuric acid were added to a suspension of (**11**) (0.495g, 2.0mmol) in acetic anhydride (1.84g, 18.0mmol) and stirred for 1.5h at r. t. 10ml of distilled water was added slowly to the reaction mixture with stirring to quench excess anhydride, and extracted with EtOAc. The organic layer was washed with saturated $NaHCO_3$ solution and brine and dried over anhydrous Na_2SO_4. Purification by column (1:4 EtOAc/Hexanes) afforded (**23**) as yellow plates, 89.1%. ^1H (CDCl$_3$) δ 8.20-8.12 (m, 2H), 7.84-7.74 (m, 2H), 3.27-3.17 (m, 1H), 2.43 (s, 3H), 0.98-0.68 (m, 4H); ^{13}C (CDCl$_3$) δ 178.01, 134.81, 134.66, 134.56, 134.46, 134.29, 131.40, 131.15, 127.43, 127.40, 31.31, 22.33, 8.86, 8.60.

2.5.6. Synthesis of *N*-cyclopropyl-*N*-{1,4-dioxo-3-[(pyridin-4-ylmethyl)-amino]-1,4-dihydro-naphthalen-2-yl}-acetamide (**64**)

To a suspension of (**23**) (0.955g, 3.30mmol) in 5ml of toluene was added pyridin-4-ylmethylamine (0.535g, 4.95mmol) and triethylamine (0.500mg, 4.95mmol) and stirred at 45°C

for 2h. The reaction mixture was cooled, and the precipitate was filtered under suction and washed with EtOH and distilled water to afford (**64**) as a yellow-brown solid, which was unstable and used immediately for the next step.

2.5.7. Synthesis of *N*-[1,4-dioxo-3-methylamino-1,4-dihydro-naphthalen-2-yl]-*N*-methyl-acetamide (**70**)

To a stirred suspension of (**19**) (0.400g, 1.52mmol) in 2mL of toluene was added dropwise methylamine (0.0564g, 1.82mmol) and triethylamine (0.230g, 2.28mmol). The mixture was stirred at r.t for 1h. The precipitate was filtered under suction, washed with distilled water and EtOH to afford (**70**) as red solids, 62.0%. ^{1}H (CDCl$_3$) δ 8.15 (dd, 1H, *J*=0.8, 7.7Hz), 8.08 (dd, 1H, *J*=0.8, 7.7Hz), 7.78 (dt, 1H, *J*=1.3, 7.6Hz), 7.66 (dt, 1H, *J*=1.3, 7.6Hz), 6.24 (br s, 1H), 3.13 (s, 3H), 3.11 (d, 3H, *J*=5.8Hz), 1.99 (s, 3H); ^{13}C (CDCl$_3$) δ 182.30, 179.35, 172.36, 144.11, 135.47, 132.77, 132.66, 130.14, 126.86, 126.76, 118.44, 37.50, 30.65, 21.94.

2.5.8. Synthesis of 1-cyclopropyl-2-methyl-4,9-dioxo-3-(pyridin-4-ylmethyl)-4,9-dihydro-1H-naphtho[2,3-d]imidazol-3-ium hydrogen dibromide (**AB1**)

48% Hydrobromic acid (30.0mmol) was added dropwise to a solution of crude (**64**) in a 4mL mixture of 1:1 EtOH/EtOAc and stirred at 45°C for 4h and subsequently r.t. for an additional 12h. The reaction mixture was concentrated *in vacuo* and purified by column chromatography (8:92 MeOH/CH$_2$Cl$_2$) to afford (**AB1**) as a yellow solid, 22.0%. ^{1}H (D$_6$-DMSO) δ 8.76 (d, 2H, *J*=6.4Hz), 8.23 (dd, 1H, *J*=1.1, 7.7Hz), 8.09 (dd, 1H, *J*=1.3, 7.5Hz), 8.01 (dt, 1H, *J*=1.6, 7.6Hz), 7.96 (dt, 1H, *J*=1.4, 7.5Hz), 7.72 (d, 2H, *J*=6.4Hz), 6.08 (s, 2H), 3.77-3.71 (m, 1H), 2.90 (s, 3H), 1.43-1.38 (m, 2H), 1.30-1.26 (m, 2H); ^{13}C (D$_6$-DMSO) δ 174.87, 173.50, 155.98, 147.98, 146.17, 135.58, 135.11, 132.51, 132.09, 131.24, 129.62, 127.16, 126.76, 123.23, 49.16, 29.84, 11.85, 9.00. ESI-MS: m/z 344.1 [M-Br]$^+$. High resolution MS (ESI) calcd for C$_{21}$H$_{18}$BrN$_3$O$_2$ [M-

Br]$^+$ 344.1394. Found: 344.1405. HPLC purity: system A: 99.85% (254nm), 100.00% (280nm); system B: 99.38% (254nm), 99.40% (280nm).

2.5.9. Synthesis of 1,2,3-trimethyl-4,9-dioxo-4,9-dihydro-1H-naphtho[2,3-d]imidazol-3-ium bromide (**AB7**)

48% hydrobromic acid (10.0mmol) was added dropwise to a solution of (**70**) (0.263mg, 1.0mmol) in a 1.5ml mixture of 1:1 EtOH/EtOAc and stirred at 40°C for 4h followed by r.t. for an additional 12h. The reaction mixture was concentrated *in vacuo* and purified by column chromatography (8:92 MeOH/CH$_2$Cl$_2$) to afford **AB7** as a beige solid, 21.9%. ^{1}H (D$_6$-DMSO) δ 8.18 (dd, 1H, *J*=3.3, 5.7Hz), 7.99 (dd, 1H, *J*=3.3, 5.7Hz), 4.13 (s, 6H), 2.79 (s, 3H); ^{13}C (D$_6$-DMSO) δ 175.36, 153.39, 135.60, 131.91, 130.34, 127.18, 34.37, 10.17. High resolution MS (ESI) calcd for C$_{14}$H$_{13}$BrN$_2$O$_2$ [M-Br]$^+$ 241.0972. Found 241.0967. HPLC purity: system A: 99.83% (254nm), 99.89% (280nm); system B: 99.74% (254nm), 99.74% (280nm).

2.6. Summary

53 analogs of YM155 were successfully synthesized and characterized by ^{1}H-NMR, ^{13}C-NMR and nominal mass. Of these 53, 32 compounds were not reported previously. Final compounds had acceptable purities (> 95%) when determined by reverse phase HPLC on two different solvent systems.

Chapter 3: Growth inhibitory properties and structure-activity relationship of YM155 and analogs

3.1. Objectives

This chapter describes the growth inhibitory properties of YM155 and its synthesized analogs on a panel of clear cell renal cell carcinoma (ccRCC) and non-small cell lung cancer (NSCLC) cell lines. ccRCC and NSCLC are malignances that have few therapeutic options and were thus selected for investigation. Sections 3.2 and 3.3 provide an overview of the prevalence and etiologies of ccRCC and NSCLC, as well as the therapeutic agents that are currently used in the clinics. The objectives of this chapter are to (i) elucidate SAR, (ii) determine if there are overlapping structural requirements for these disparate malignancies and (iii) evaluate the selective activity of these compounds against malignant cells as compared to the non-malignant human lung fibroblast IMR-90 cells.

3.2. Clear cell renal cell carcinoma (ccRCC)

Renal cell carcinoma (RCC) constitute about 3% of all adult malignancies and 90-95% of renal cancers worldwide.[80] It is gender related with a strong male dominance.[81] There are various histological subtypes of RCC of which the clear cell subtype (ccRCC) is the most common and synonymous with renal cell carcinoma in terms of disease management.[82, 83]

RCC is usually detected late due to the asymptomatic nature of the early stages of the disease.[84] Consequently nearly 25-30% of patients present with metastasis at the point of diagnosis.[85, 86] The prognosis is poor for these patients as surgery is not a viable option, the malignancy is highly resistant to radiotherapy and chemotherapy[87-90], and conventional chemotherapeutic agents such as vinblastine and 5-fluorouracil give dismal objective response rates ($\leq$ 10%).[89] These factors make metastatic RCC a highly lethal cancer, with a median survival of less than 13 months and a 5-year overall survival rate of less than 20%.[81, 91]

3.2.1. The von Hippel-Lindau gene and its role in ccRCC

ccRCC is characterized by a unique set of genetic aberrations, the most prominent of which is the von Hippel-Lindau (VHL) tumor-suppressor gene. In more than 60% of sporadic ccRCC cases, the VHL gene and its associated downstream pathways are implicated in tumorigenesis. This aberration is also manifested in von Hippel-Lindau disease, a rare familial disease where patients are predisposed to ccRCC in addition to other forms of cancers.[81, 92]

The VHL gene is located on the short arm of chromosome 3 at the 3p25 position and encodes its protein product pVHL.[93] pVHL is an essential part of the E3 ubiquitin ligase complex where it functions as the substrate recognition component of the hypoxia-inducible factor-α (HIF-α). HIF-α senses hypoxia in cells and the VHL-HIF-α pathway is a critical physiological response to hypoxia. HIF-α exists in three isoforms (HIF-1α, HIF-2α, HIF-3α) of which HIF-2α is most commonly cited in the context of ccRCC carcinogenesis.[94-96]

Under normal oxygen levels (normoxia), HIF-α is hydroxylated by prolyl hydroxylases and the presence of a hydroxylated proline promotes interaction with pVHL (Figure 3.1).[97, 98] Interaction and binding between HIF-α and pVHL leads to polyubiquitination and proteasomal degradation by the 26S proteasome. Conversely, hypoxic conditions inhibit the prolyl hydroxylases, inhibit hydroxylation of HIF-α, and block its interaction with pVHL.[99] Consequently, HIF-α levels are stabilized and dimerizes with HIF-β to give an active transcription factor complex which binds to its cognate hypoxia response element (HRE).[98] This promotes the transcription of downstream target genes, many of which encode cytokines and proteins that are pivotal in relieving the cell of hypoxia. These gene products include those implicated in angiogenesis (VEGF, PDGF), glucose transport (GLUT-4), pH regulation (CAIX), cell survival (IGF1R, TGF-α) and cell proliferation (c-Myc, cyclin D3, PAX2).[97, 100-104]
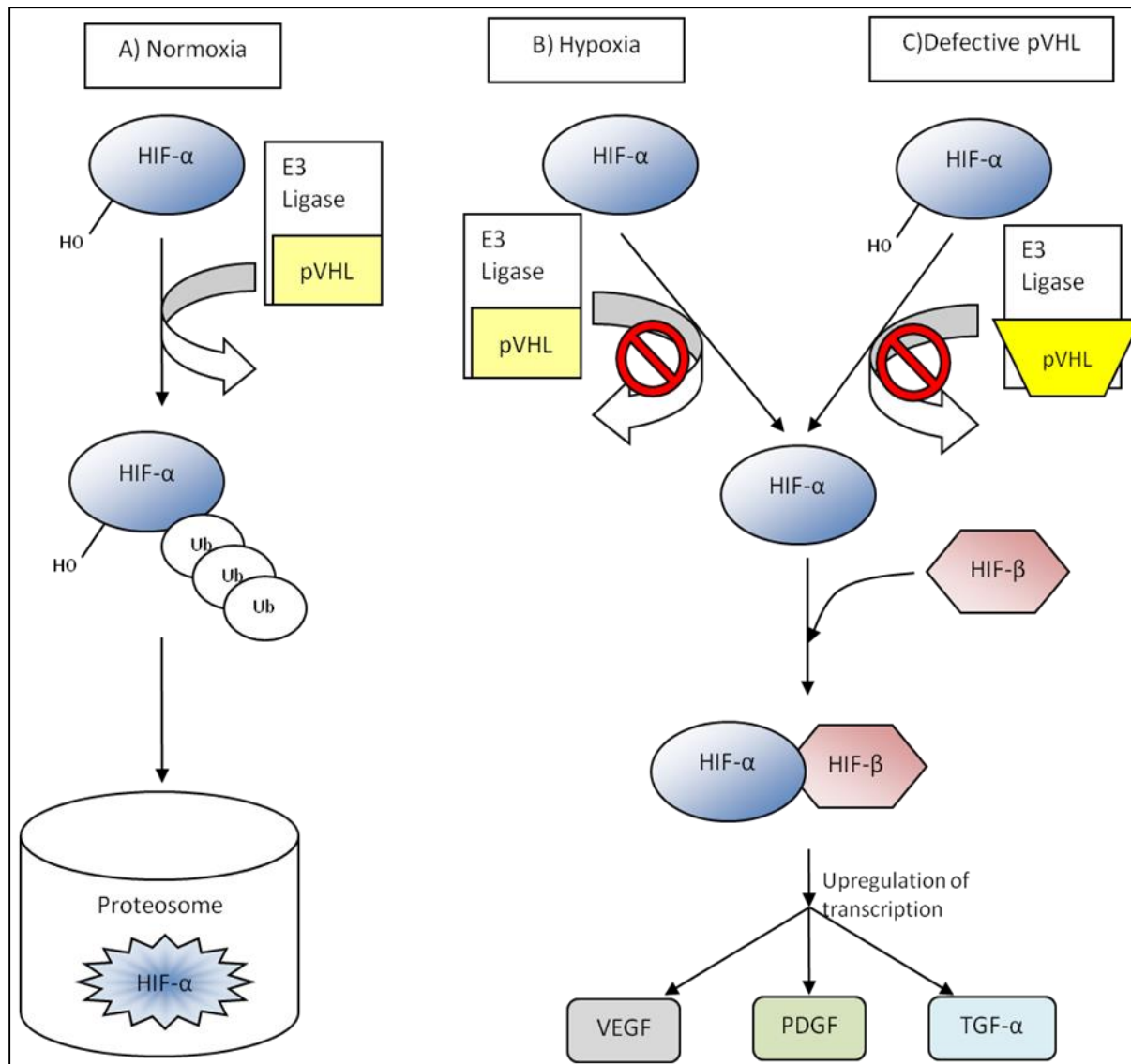
Figure 3.1. Regulation of the VHL pathway. (A): Under normal O_2 levels, HIF-1α and 2α (represented as HIF-α) are ubiquitinated by the pVHL/E3 ubiquitin ligase complex. This marks HIF-α for proteosomal-mediated degradation. (B): Under low O_2 level, the pVHL/E3 ubiquitin ligase is unable to ubiquitinate HIF-α, allowing it to dimerize with HIF-β. The resulting complex translocates to the nucleus where it acts as a transcription factor and upregulates the transcription of genes that encode the growth factors VEGF, PDGF and TGF-α among others. (C): When the VHL gene undergoes a mutation, deletion or methylation event, the defective pVHL is unable to interact with E3 ubiquitin ligase to give a functional complex. Ubiquination of

HIF-α decreases, leading to its accumulation and subsequent upregulation of growth factors even in normoxic conditions.

In sporadic ccRCC or familial VHL disease, the VHL alleles are defective or absent. Consequently, the interaction between VHL and HIF-α is prevented and HIF-α levels remain high regardless of oxygen status. This leads to the upregulation of the target genes of HIF-α, many of which promote the growth and proliferation of cancer cells. The cytokines VEGF and PDGF which are involved in angiogenesis and neovascularization of tumors are important in this regard. VEGF plays a critical role in the early stages of angiogenesis where it signals endothelial cells to proliferate and form new vasculature.[105] PDGF is implicated in the late stages of angiogenesis where it promotes the maturation of new vasculature.[106] Indeed, ccRCC tumors are highly vascularized due to the upregulation of these angiogenesis-promoting cytokines.[107-109]

The VHL-HIF-α pathway is linked to other oncogenic pathways such as the mammalian Target of Rapamycin (mTOR) and nuclear factor-kappa B (NF-κB). mTOR is a significant regulator of cell growth and proliferation and is upregulated in ccRCC.[110, 111] It upregulates HIF-α and promotes HIF-α-regulated protein expression.[96, 112] mTOR is in fact a valid target in ccRCC and mTOR inhibitors are currently used as targeted therapies for ccRCC. The NF-κB pathway is widely known for regulating immunity and inflammation.[113-115] However, many of its target genes promote cell growth and proliferation and are thus implicated in cancer.[116, 117] A more detailed discussion on the NF-κB pathway will follow in Chapter 5, but it should be noted that HIF-α expression is upregulated by NF-κB.[118] There are currently no therapies targeted against the NF-κB pathway.

3.2.2. Current targeted chemotherapeutics for RCC

The current paradigm in chemotherapy is the use of targeted therapies which are small molecules or protein-based drugs capable of directly inhibiting a particular errant pathway that is involved in oncogenesis. Many targeted therapies are used clinically, for example small molecules kinase inhibitors like imatinib and antibodies such as bevacizumab. They have revolutionized the treatment of those cancers which respond particularly well to such treatment modalities.

Before the development of targeted therapies, RCC was treated by immunotherapy using cytokines such as interferon-α (IFN-α) and interleukin-2 (IL-2). IFN-α increases the immunogenicity of the tumor whereas IL-2 recruits natural killer and activated T cells to directly kill cancer cells.[119, 120] A meta-analysis of IFN-α showed that overall response rates were less than 12% and overall survival of patients was extended by a modest 3.8 months.[120] IL-2 performed similarly, with overall response rates of 15% and complete remission of the cancer in 4% of patients, a figure considered high in metastatic RCC. To date, IL-2 remains the only agent that is able of producing significant remissions.[120] However, its main drawbacks are the high incidence of grades III and IV toxicities[120, 121], deaths in some cases (4%), and cumbersome modes of administration and dosing schedules. Consequently, immunotherapy has largely fallen out of favour except for a small subset of RCC patients.

As noted earlier, ccRCC accounts for an overwhelming percentage of all RCC cases, such that the two are generally considered to be synonymous. A clearer understand of the link between the VHL pathway and ccRCC has been pivotal in the development of targeted therapies. A summary of the targeted therapies for RCC is shown in Table 3.1.

Table 3.1. Current targeted therapies available for RCC. Response rates and progression free survivals are from placebo-controlled studies where available. CR: complete response; PR: partial response. OR: overall response (CR+PR)

Drug	Major mechanism of action	Year of FDA approval	Response rate	Progression free survival
Bevacizumab[122]	Monoclonal antibody raised against VEGF	2009	OR: 10%	4.8 months
Sorafenib[123]	VEGFR inhibitor (RTK inhibitor)	2005	CR: 0% PR: 2%	5.5 months
Sunitinib[124, 125]		2006	CR: 0% PR: 40%	8.7 months
Pazopanib[126, 127]		2009	CR: <1% PR: 30%	9.2 months
Axitinib[128-130]		2012	OR: 32%	10.1 months
Temsirolimus[131, 132]	mTOR inhibitor	2007	CR: 0% PR: 8.6%	4.3 months
Everolimus[133, 134]		2009	CR: 0% PR: 1%	4.0 months

Despite the availability of different targeted therapies for RCC, response rates remain low and more importantly, these agents do not significantly extend progression-free survival and overall survival compared to placebo. They are also associated with serious adverse events, although these are significantly fewer compared to IL-2 or IFN-α. For example, bevacizumab and other VEGF targeting agents often lead to hypertension. Bevacizumab is itself implicated in increasing the risk of gastrointestinal bleeding and bowel perforation.[135] Liver damage has been reported with pazopanib, and fatal cardiac failure with axitinib.[136] Temsirolimus is paradoxically associated with increased mortality despite producing responses in cancer patients.[137]

Therefore, there is a clear need for novel chemotherapeutics for the treatment of RCC. Since the targeting of the mTOR and VEGF-related pathways have not led to promising anti-RCC agents, novel agents should preferably target an alternative pathway.

3.3. Non-small cell lung carcinoma (NSCLC)

Lung cancer has the highest incidence worldwide in men and ranks third in women. Overall, it accounts for 13% of all adult malignancies.[138] Yearly, an estimated 1.8 million new cases are diagnosed, most commonly among smokers.[139]

Lung cancer is a heterogeneous disease and comprises two main subtypes, non-small cell lung carcinoma (NSCLC) and small cell lung carcinoma. NSCLC accounts for 85% of all lung cancers and will be the focus of the following discussion.[140] NSCLC can be further sub-divided into adenocarcinoma, squamous cell carcinoma and large cell carcinoma, but clinical management generally does not distinguish between these NSCLC subtypes. Like RCC, nearly 70% of NSCLC patients present with late stage metastatic disease at diagnosis, due to a combination of an asymptomatic early stage and the lack of effective screening tools.[140, 141] Survival rates are optimistic for early stage disease, but late stage NSCLC has a dismal 5-15% 5-year survival rate.[139, 142]

For early stage and localized NSCLC, surgical resection and radiotherapy are treatment options but they are of limited utility in the management of patients with metastatic NSCLC where chemotherapy is the only viable option. Unfortunately, NSCLC is notorious for its resistance to chemotherapy.[143] Before a clearer understanding of the genetic aberrations fueling NSCLC emerged , the treatment of choice was platinum-doublet therapy which consisted of a platinum based drug, usually carboplatin or cisplatin, coupled with another drug that acts by a different mode of action.[144] Examples of platinum doublet regimens are combinations of carboplatin with

paclitaxel, gemcitabine or docetaxel. A meta-analysis showed that these regimens increased the overall survival by 6 months which is 1.5 months longer than untreated patients.[145]

3.3.1. The EGFR pathway in NSCLC

Among-the cell signaling pathways implicated in NSCLC, the epidermal growth factor receptor (EGFR) pathway is the most widely studied. EGFR is a transmembrane receptor tyrosine kinase, and part of the HER/ErbB family of four structurally similar RTKs – EGFR (HER1/ErbB1), HER2 (neu/ErbB2), HER3 (ErbB3) and HER4 (ErbB4).[146] EGFR is significantly overexpressed in NSCLC, and activating mutations which transform EGFR into a constitutively self-activating tyrosine kinase are found in 10-20% of patients depending on their ethnicity.[147] Incidence is lower among Caucasians but higher among east Asians.[148]

EGFR is encoded by the EGFR gene which is located on the short arm of chromosome 7 (7p11.2). The 170 kDa protein product possesses a cysteine-rich extracellular receptor domain which binds to its ligand epidermal growth factor (EGF). This extracellular domain is linked by a single alpha helix through the cell membrane to its intracellular tyrosine kinase domain which is linked to a carboxy terminal signaling domain essential for downstream signaling.[149] In the absence of ligand binding, EGFR exists as discrete monomers (Figure 3.2). Binding of EGF exposes a "dimerization arm" on the extracellular region which then dimerizes with another EGFR or heterodimerizes with other members of the HER/ErbB family, notably HER2, which lacks a receptor-binding domain and acts solely as a dimerization partner for the other three members.[150, 151] Dimerization of EGFR activates its tyrosine kinase activity resulting in the autophosphorylation of a set of 7 tyrosine residues located on the adjacent cytoplasmic domain. Cross-phosphorylation is also possible between dimerized partners.[152] Phosphorylation of the tyrosine residues leads to the recruitment of a variety of proteins such as growth receptor

binding protein-2 (Grb-2) which then transduces the signals along the downstream pathways of EGFR.[153, 154]

Figure 3.2. The EGFR pathway. Binding of EGF to EGFR leads to receptor dimerization and phosphorylation of cytoplasmic domains. At least three pathways lie downstream. Grb-2 recruitment sets off a phosphorylation cascade through the Ras-Raf-MEK-ERK pathway. Transcription factor STAT3 is directly activated by EGFR dimers, and localizes in the nucleus where it upregulate its target genes. Activated EGFR also directly activates PI3K, which phosphorylates PIP2 to PIP3. PIP3 binds to Akt, and together with phosphorylation by mTORC2 and PDPK1, activates the latter. The three downstream pathways subsequently contribute to cell proliferation and prevention of apoptosis by different mechanisms.

The Ras-Raf-MEK-ERK pathway is one of the more significant downstream pathways activated by EGFR. Grb-2 binds to the cytoplasmic domain of phosphorylated EGFR and recruits/ activates Ras.[155] Activated Ras binds to Raf and triggers a phosphorylation cascade that involves MEK, MAPK and ERK.[156] The cascade ends with the activation of transcription factors c-Myc, CREB and NF-κB (among others), which are implicated in cell growth, proliferation and prevention of apoptosis. In particular c-Myc is well recognized as a proto-oncogene and is dysregulated in many cancers.[157] The Ras-Raf-MEK-ERK pathway also tilts the balance of the Bcl-2 family of proteins towards the antiapoptotic state.[158, 159]

Besides the Ras-Raf-Mek-Erk pathway, EGFR activation also stimulates the signal transducer and activator of transcription (STAT) family of transcription factors.[160] In particular, STAT3 and STAT5 have been implicated in lung cancer.[161] STAT3 activation upregulates proteins involved in angiogenesis (VEGF), cellular migration (MMP-2, MMP-9) and prevention of apoptosis (survivin, Bcl-xl, Mcl1).[162] The PI3K-Akt pathway is also activated by EGFR. Phosphoinositide-3 kinase (PI3K) is recruited to the plasma membrane by activated EGFR dimers, in particular those containing HER3. Recruitment of PI3K leads to phosphorylation of phosphatidylinositol-4,5-bisphosphate (PIP2) to form phosphatidylinositol-3,4,5-trisphosphate (PIP3). PIP3 recruits Akt to the plasma membrane where it is activated sequentially by mTOR complex 2 (mTORC2) and 3-phosphoinositide dependent protein kinase 1 (PDPK1).[163] Upon activation, Akt prevents apoptosis by phosphorylating and promoting the degradation of crucial proteins such as BAD (a pro-death protein) and IκB kinase (IKK) which inhibits the NF-κB pathway. Akt also activates murine double minute 2 (mdm2) which inhibits p53 and upregulates pro-survival proteins Bcl-2 and Mcl1.[164]

10-20% of NSCLC patients exhibit mutations in the EGFR gene. Most mutations involve deletions, insertions or point mutations at the kinase domain, and lead to an exaggerated and

sustained response to EGF binding or constitutive activity even in the absence of a ligand.[165, 166] While the above pathways activated by EGFR are essential for proper control of cellular and tissue function in non-malignant cells, EGFR overexpression or mutation in NSCLC cause these downstream pathways to take on a more nefarious role of promoting tumorigenesis and survival of cancer cells.

3.3.2. Current targeted therapies for NSCLC

Conventional chemotherapy regimens, such as platinum doublet regimens are marginally effective in NSCLC. The prominent role of the EGFR pathway in NSCLC has resulted in targeted therapies against EGFR and its associated pathways. Although there is a sound rationale for deploying these therapies, the clinical benefits are only limited to those patients with sensitizing mutations. These are a minority (~20%) when compared to the general NSCLC population and the overall survivability remains low. Novel chemotherapeutics targeting alternative pathways are therefore in dire need, perhaps more so than in RCC. Drugs that are currently deployed against NSCLC are outlined in Table 3.2.

Gefitinib, erlotinib and afatinib are tyrosine kinase inhibitors that are selective for EGFR. Gefitinib is the drug of choice for NSCLC patients with EGFR mutations, which are highly represented in women and non-smokers. Clinical guidelines require confirmation of EGFR mutations before these drugs are used in patients. In the absence of these mutations, minimal benefit is derived from their deployment, as can be seen from the lower overall responses in non-enriched trials (Table 3.2). Unfortunately, resistance to EGFR TKIs is widely encountered in the clinical setting due to conformational changes in the kinase domain or the activation of bypass pathways that do not respond to EGFR TKIs. Afatinib is the most recent EGFR inhibitor that is used clinically. Unlike its predecessors, it covalently binds to EGFR. Recent studies support a role for afatinib in patients who have developed resistance to gefitinib and erlotinib.[167]

Table 3.2. Current targeted therapies available for treatment of RCC. Response rates and progression free survival presented are from placebo-controlled phase III studies where available. CR: complete response; PR: partial response. OR: overall response (CR+PR). Enriched refers to trials that enrol only patients with EGFR mutations.

Drug	Major mechanism of action	Year of FDA approval	Response rate	Progression free survival
Bevacizumab[168, 169]	Monoclonal antibody raised against VEGF	2006	OR: 34%	6.4 months
Ramucirumab[170]		2014	OR: 23%	4.5 months
Gefitinib[171-174]	EGFR inhibitor (RTK inhibitor)	2003	OR: 10% (w/o enrichment) OR: 43-75% (enriched)	2.2 months (w/o enrichment) PR: 5.7-9.2 months (enriched)
Erlotinib[175, 176]		2004	OR: 9% (w/o enrichment) CR: 12% PR: 58% (enriched)	2.2 months (w/o enrichment)
Afatinib[167, 177]		2013	CR: 0% PR: 11% (w/o enrichment) OR: 56% (enriched)	3.3 months (w/o enrichment) 13.6 months (enriched)

3.4. Results

3.4.1. Cell-based growth inhibitory activities of YM155 and analogs
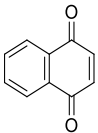
YM155 and the synthesized analogs were evaluated for their growth inhibitory effects on the clear cell renal cell carcinoma (ccRCC) cell lines (RCC786-0, RCC4/VA), the non-small cell lung carcinoma (NSCLC) cell lines (H1299, H1666) and the non-malignant human lung fibroblast IMR-90 cells. RCC786-0 and RCC4/VA are deficient in the von Hippel-Lindau (VHL) gene and reflect the genotype found in most patients with ccRCC.[97] H1299 cells are p53-null whereas H1666 cells are p53 positive, however both are EGFR wild-type. Growth inhibitory activities were determined by a colorimetric tetrazolium (MTT) assay and expressed in terms of IC_{50} which is the concentration required to reduce cell viability to 50% of levels observed in untreated cells under similar experimental conditions (Table 3.3).

Table 3.3. Growth inhibitory IC_{50} values of YM155 and synthesized analogs.

Cpd	Growth Inhibitory IC_{50}, µM [a]					Range of selectivity ratios [b]
	RCC786-0	RCC4/VA	H1299	H1666	IMR-90	
YM155	0.0535 ± 0.0068	0.0445 ± 0.0082	0.0355 ± 00012	0.0137 ± 0.0009	0.247 ± 0.037	4.6-18.0
A1-1	0.737 ± 0.140	2.83 ± 0.53	0.648 ± 0.096	0.240 ± 0.020	1.16 ± 0.07	0.4-4.8
A1-2	1.10 ± 0.16	3.39 ± 0.50	0.956 ± 0.098	0.415 ± 0.029	5.27 ± 0.96	1.6-12.7
A1-3	0.639 ± 0.060	2.74 ± 0.52	0.664 ± 0.058	0.207 ± 0.017	1.45 ± 0.05	0.5-7.0
A2-1	1.06 ± 0.20	2.42 ± 0.39	0.172 ± 0.014	0.279 ± 0.027	2.01 ± 0.11	0.8-11.7
A3-1	1.14 ± 0.03	2.36 ± 0.40	1.06 ± 0.14	0.231 ± 0.033	2.52 ± 0.11	1.1-10.9
A3-2	0.0795 ± 0.0076	0.228 ± 0.032	0.0436 ± 0.0038	0.0404 ± 0.0052	0.611 ± 0.044	2.7-15.1
A3-3	0.0267 ± 0.0050	0.0439 ± 0.0039	0.0170 ± 0.0015	0.0110 ± 0.0007	0.176 ± 0.009	4.0-16.0
A3-4	0.845 ± 0.139	2.07 ± 0.60	0.534 ± 0.031	0.152 ± 0.003	3.18 ± 0.04	1.5-20.9

Cpd	Growth Inhibitory IC$_{50}$, μM [a]					Range of selectivity ratios [b]
	RCC786-0	RCC4/VA	H1299	H1666	IMR-90	
A3-5	0.0560 ± 0.0112	0.0912 ± 0.0144	0.0191 ± 0.0024	0.00770 ± 0.00070	0.205 ± 0.014	2.2-26.6
A3-6	0.0569 ± 0.0101	0.0851 ± 0.0087	0.0431 ± 0.0065	0.0287 ± 0.0027	0.276 ± 0.027	3.2-9.6
A3-7	0.0490 ± 0.0098	0.0440 ± 0.0072	0.0175 ± 0.0015	0.0199 ± 0.0021	0.187 ± 0.012	3.8-10.7
A3-8	0.387 ± 0.075	1.09 ± 0.18	0.414 ± 0.065	0.157 ± 0.003	2.00 ± 0.13	1.8-12.7
A4-1	2.94 ± 0.41	2.50 ± 0.55	0.426 ± 0.044	0.859 ± 0.090	2.81 ± 0.52	1.0-6.6
A5-1	5.46 ± 0.60	6.09 ± 0.33	3.38 ± 0.53	8.78 ± 0.09	8.82 ± 1.21	1.0-6.6
A6-1	0.355 ± 0.061	0.781 ± 0.096	0.233 ± 0.040	0.0728 ± 0.0056	0.743 ± 0.089	1.0-10.2
A6-2	0.0593 ± 0.0022	0.0911 ± 0.0165	0.0355 ± 0.0038	0.0288 ± 0.0054	0.345 ± 0.038	3.8-12.0
A6-3	0.137 ± 0.002	0.346 ± 0.044	0.116 ± 0.003	0.073 ± 0.0035	1.23 ± 0.13	3.6-16.8
A6-4	0.167 ± 0.006	0.346 ± 0.044	0.192 ± 0.013	0.113 ± 0.018	1.72 ± 0.083	3.2-15.2
A6-5	0.892 ± 0.031	3.32 ± 0.49	0.547 ± 0.032	0.224 ± 0.02	3.89 ± 0.29	1.2-17.4
A6-6	0.112 ± 0.012	0.262 ± 0.059	0.0771 ± 0.0043	0.0559 ± 0.0111	1.16 ± 0.14	4.4-20.8
A6-7	0.236 ± 0.018	0.656 ± 0.026	0.337 ± 0.046	0.15 ± 0.027	2.64 ± 0.54	4.0-17.6
A6-8	0.31 ± 0.016	0.633 ± 0.087	0.372 ± 0.036	0.278 ± 0.056	6.79 ± 0.29	10.7-24.4
B1-1	0.302 ± 0.017	0.423 ± 0.082	0.092 ± 0.015	0.118 ± 0.017	2.48 ± 0.32	5.9-27.0
B1-2	1.84 ± 0.07	1.48 ± 0.10	1.36 ± 0.05	0.758 ± 0.121	9.89 ± 0.17	5.4-13.0
B1-3	0.0990 ± 0.0149	0.422 ± 0.070	0.181 ± 0.030	0.0377 ± 0.0045	1.43 ± 0.26	3.4-37.9
B2-1	0.0605 ± 0.0073	0.0939 ± 0.0167	0.0649 ± 0.0033	0.0415 ± 0.0081	0.582 ± 0.089	6.2-14.0
B2-2	0.0592 ± 0.0083	0.0550 ± 0.0030	0.0510 ± 0.0038	0.0349 ± 0.0020	0.480 ± 0.022	8.1-13.8
B2-3	0.0795 ± 0.0149	0.0929 ± 0.0187	0.0713 ± 0.0078	0.0405 ± 0.0033	0.565 ± 0.027	6.1-14.0

Cpd	Growth Inhibitory IC$_{50}$, µM [a]					Range of selectivity ratios [b]
	RCC786-0	RCC4/VA	H1299	H1666	IMR-90	
B2-4	0.416 ± 0.032	0.813 ± 0.051	0.300 ± 0.015	0.152 ± 0.009	1.42 ± 0.15	1.7-9.3
B2-5	0.0742 ± 0.0099	0.0455 ± 0.0089	0.0272 ± 0.0019	0.0327 ± 0.0012	0.213 ± 0.020	2.9-7.8
B2-6	0.124 ± 0.009	0.288 ± 0.036	0.0711 ± 0.0006	0.0546 ± 0.0034	1.62 ± 0.14	5.6-29.7
B2-7	0.753 ± 0.121	2.06 ± 0.22	0.632 ± 0.083	0.458 ± 0.025	7.97 ± 0.180	3.9-17.4
B2-8	2.70 ± 0.32	2.06 ± 0.32	1.06 ± 0.17	1.47 ± 0.09	6.58 ± 0.18	2.4-6.2
B3-1	2.52 ± 0,32	5.99 ± 1.36	2.66 ± 0.46	1.37 ± 0.09	5.61 ± 0.38	0.9-4.1
B3-2	1.12 ± 0.17	1.91 ± 0.34	1.35 ± 0.20	0.450 ± 0.052	3.57 ± 0.71	1.9-7.9
B4-1	2.12 ± 0.21	2.58 ± 0.30	1.31 ± 0.06	1.44 ± 0.20	7.42 ± 0.76	2.9-5.7
B4-2	1.45 ± 0.08	1.44 ± 0.26	1.94 ± 0.20	1.81 ± 0.15	3.73 ± 0.11	1.9-2.6
C1-1	0.262 ± 0.048	0.946 ± 0.083	0.567 ± 0.032	0.0960 ± 0.0127	1.90 ± 0.11	2.0-19.8
C1-2	0.394 ± 0.018	1.03 ± 0.07	0.988 ± 0.105	0.584 ± 0.097	1.36 ± 0.15	1.3-3.5
C2-1	>100	>100	>100	>100	>100	N/A
C2-2	>100	>100	>100	>100	>100	N/A
C2-3	>100	>100	>100	>100	>100	N/A
C3-1	>100	>100	>100	>100	>100	N/A
C3-2	>100	>100	>100	>100	>100	N/A
C4-1	34.1 ± 2.1	37.3 ± 0.8	24.4 ± 1.6	22.0 ± 1.5	55.4 ± 4.6	1.5-2.5
C4-2	24.2 ± 3.9	45.7 ± 2.7	44.7 ± 4.9	17.9 ± 2.0	73.0 ± 4.5	1.6-4.1
AB1	0.0336 ± 0.0026	0.0438 ± 0.0087	0.0359 ± 0.0030	0.0168 ± 0.0017	0.287 ± 0.059	6.6-17.1
AB2	0.0391 ± 0.0007	0.116 ± 0.018	0.0395 ± 0.0042	0.0298 ± 0.0032	0.310 ± 0.051	2.7-10.4
AB3	0.111 ± 0.016	0.148 ± 0.025	0.0629 ± 0.0033	0.0862 ± 0.0070	0.649 ± 0.079	4.4-10.3

Cpd	Growth Inhibitory IC$_{50}$, µM [a]					Range of selectivity ratios [b]
	RCC786-0	RCC4/VA	H1299	H1666	IMR-90	
AB4	0.0706 ± 0.0136	0.101 ± 0.005	0.0837 ± 0.0094	0.0613 ± 0.0054	0.440 ± 0.007	4.4-7.2
AB5	0.0627 ± 0.0028	0.127 ± 0.027	0.0626 ± 0.0055	0.0533 ± 0.0041	0.484 ± 0.064	3.8-9.1
AB6	0.0709 ± 0.0148	0.136 ± 0.026	0.0527 ± 0.0032	0.0355 ± 0.0049	0.475 ± 0.091	3.5-13.4
AB7	0.0286 ± 0.0016	0.0293 ± 0.0050	0.0185 ± 0.0018	0.00860 ± 0.00030	0.159 ± 0.016	5.4-18.5
NQ[c]	6.38 ± 0.13	5.51 ± 0.96	3.42 ± 0.56	9.78 ± 0.56	13.3 ± 2.0	1.4-3.9

[a] Evaluated by MTT assay, 72h incubation, 37°C, 5% CO_2. Mean ± SD for n = 3 determinations;

[b] Lowest to highest of IC$_{50\ \text{IMR-90}}$ / IC$_{50\ \text{malignant cell line}}$; [c] Naphthoquinone.

The median IC$_{50}$ values were calculated for each cell line and found to be 113 nM (H1666), 192 nM (H1299), 262 nM (RCC786-0) and 633 nM (RCC4/VA). Differences in the sensitivities to the different cell lines were small and did not exceed 6-fold. Ranking of compounds in terms of growth inhibitory potency was broadly consistent within each cell line. For example, **A5-1** had the weakest growth inhibitory activity on all four cell lines while the most potent compounds were either **A3-3** or **AB7**. This trend was also reflected in the Spearman correlation coefficients (ρ) derived from pair-wise comparisons of IC$_{50}$ values from the four cell lines. ρ values exceeding 0.85 were obtained, indicating a strong monotonic relationship among the comparators (Table 3.4). Hence the SAR deduced from one cell line should largely apply to other cell lines. In the following paragraphs, SAR is discussed with reference to growth inhibitory activities on H1666 cells.

Table 3.4. Spearman correlation matrix of ρ values derived from IC_{50} values of test compounds

on ccRCC (RCC786-0, RCC4/VA) and NSCLC (H1299, H1666) cell lines.[a]

	RCC786-0	RCC4/VA	H1299	H1666
RCC786-0	1.000	0.950	0.942	0.965
RCC4/VA	0.950	1.000	0.924	0.919
H1299	0.942	0.924	1.000	0.950
H1666	0.965	0.919	0.950	1.000

[a] Only compounds with measurable IC_{50} values were analyzed.

3.4.2. SAR of series C

Series C compounds were designed to report on the importance of the

dioxonaphthoimidazolium scaffold for activity. A key finding was that the intact scaffold was

required for potent activity. Thus, removing the distal phenyl ring or the central quinone of

YM155 to give the bicyclic analogs **C1-2** and **C2-1**, resulted in diminished activities. As a

greater loss in activity was incurred on omission of the quinone, a more critical role may be

attributed to it as compared to the distal phenyl ring. Further trimming of the bicyclic scaffold of

C1-2 or **C2-1** to give an imidazolium (**C2-2**) did not restore activity. The importance of the

quinone moiety was further underscored by the negligible activity of the imidazoquinoxalinium

C2-3 (IC_{50} > 100 µM).

C1-2
IC_{50} 580 nM

YM155
IC_{50} 14 nM

C2-1
IC_{50} >100 µM

C2-2
IC_{50} >100 µM
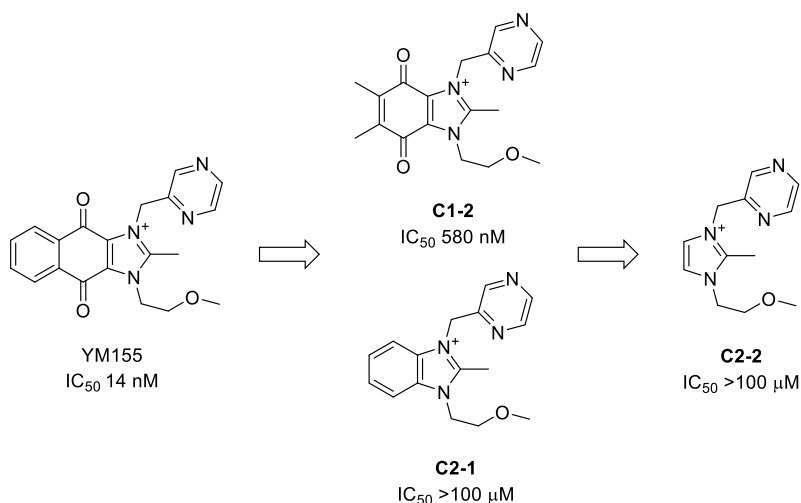
The contribution of the permanent positive charge on the scaffold to activity is best illustrated by comparisons to naphthoquinone, **C4-1** and **C4-2**. Naphthoquinone is basically YM155 without the substituted imidazolium ring. Its growth inhibitory activity (IC$_{50}$ 6.4 µM) far exceeded that of the benzimidazolium **C2-1** (IC$_{50}$ > 100 µM), clearly showing that the loss of the positively charged imidazolium ring was not as detrimental as omission of the quinone. The dioxonaphtho[2,3-d]imidazoles (**C4-1, C4-2**) which retain the quinone moiety but not the positive charge, provide added support. Both compounds had diminished potencies (IC$_{50}$ 24-34 µM) compared to their charged counterparts **A6-2** and **B2-1**. Scaffold hopping to yield indoles **C3-1** and **C3-2** which lack both the quinone and positive charge but retain the side chains was equally futile as both compounds were as inactive as the benzimidazolium **C2-1** from which they differed only in charge. Tellingly, series C analogs (**C1-2**, **C4-1**, **C4-2**) that retain the quinone moiety, even with changes made to other parts of the YM155 scaffold, were consistently more potent than those without the quinone moiety (**C2-X**, **C3-X**). It also follows that the side chains attached to N^1 and N^3 of the scaffold can be modified or even omitted without serious losses to activity.

Naphthoquinone
IC$_{50}$ 6.0 µM

C4-1
IC$_{50}$ 34 µM

C4-2
IC$_{50}$ 24 µM

C2-1
IC$_{50}$ >100 µM

A6-2
IC$_{50}$ 29 nM

B2-1
IC$_{50}$ 42 nM

C3-1
IC$_{50}$ >100 µM

C3-2
IC$_{50}$ >100 µM
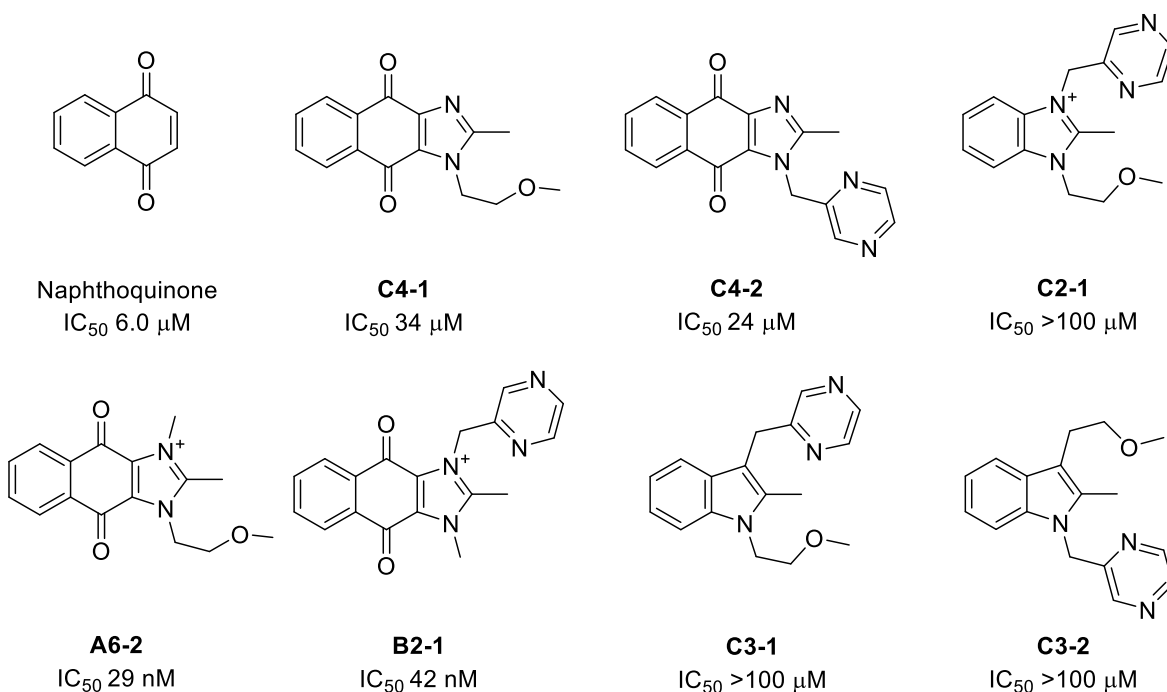
Taken together, omission of the quinone from the tricyclic scaffold had the most adverse effect on activity, followed by removal of the permanent positive charge (naphthoquinone, **C4-1, C4-2**). The least disruptive modification to the scaffold was the removal of the distal benzene ring (**C1-2**).

Mention should be made of **C1-1** which retain the tricyclic scaffold of YM155 but is modified by homologation at C^2. This modification led to a 7-fold loss in activity (**C1-1**, IC_{50} 96 nM), suggesting strict steric requirements at this position.
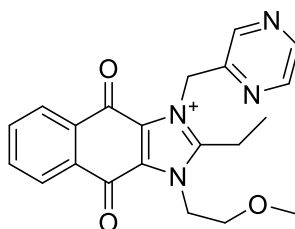
C1-1
IC_{50} 96 nM

3.4.3. SAR of series A and B

Next, the inhibitory activities of series A and B were analyzed to assess the contributions of the N^3 (pyrazin-2'-ylmethyl) and N^1 (2'-methoxyethyl) substituents to activity.

The series A compounds were designed to probe the importance of the pyrazin-2'-ylmethyl side chain at N^3 while keeping 2'-methoxyethyl at N^1. The key observations are as follows. First, the one-carbon (methylene) spacer linking the pyrazine ring to N^3 should not be lengthened or shortened. Doing so resulted in analogs (**A4-1**, IC_{50} 86 nM; **A5-1**, IC_{50} 8.8 µM) with diminished activity.
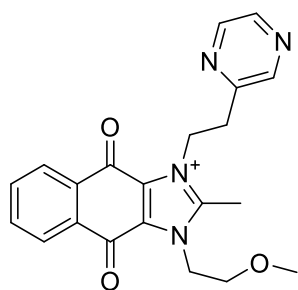
A4-1
IC$_{50}$ 86 nM
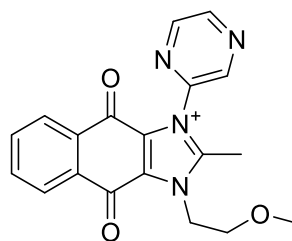
A5-1
IC$_{50}$ 8.8 µM

Second, replacing pyrazin-2'-ylmethyl with benzyl (**A1-1**, IC$_{50}$ 240 nM), cyclohexylmethyl (**A1-2**, 415 nM), thien-2'-ylmethyl (**A1-3**, IC$_{50}$ 207 nM) or imidazol-2'-ylmethyl (**A2-1**, IC$_{50}$ 279 nM) caused significant losses in activity. It may be that the azine at N^3 fulfilled a special role (H bonding) which is not met by these alternative moieties. Third, in contrast to the 2nd observation, replacing the pyrazine ring with other azines like pyridine, pyrimidine and pyridazine was generally well tolerated but only if the azomethine nitrogen was located at specific positions. The regioisomeric influence was clearly observed in the isomeric pyridinylmethyl analogs **A3-1**, **A3-2** and **A3-3.**
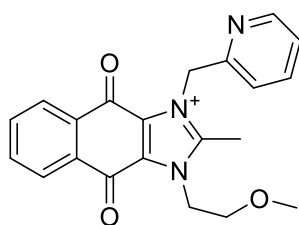
A3-1
IC$_{50}$ 230 nM
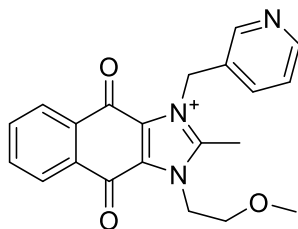
A3-2
IC$_{50}$ 40 nM
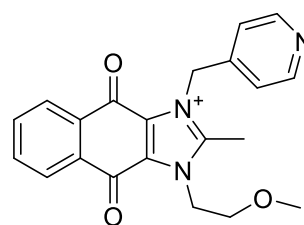
A3-3
IC$_{50}$ 11 nM

Activity improved when the azomethine nitrogen was moved from ortho (**A3-1**) to meta (**A3-2**), and likewise when it was shifted from meta (**A3-2**) to para (**A3-3**), albeit to a lesser extent. This may allude to a possible hydrogen bonding interaction that is accessible to the meta and para azomethine nitrogens but not the ortho nitrogen. The regioisomeric bias against an ortho nitrogen was again observed in **A3-4** which has a pyrimidin-2'-ylmethyl side chain at N^3. Its

48

positional isomers **A3-5** and **A3-6** which have at least one azomethine N at the meta or para position fared better. The same was true for **A3-7** which has a pyrazine-4'-ylmethyl side chain at N^3.

A3-4
IC$_{50}$ 150 nM

A3-5
IC$_{50}$ 8.0 nM

A3-6
IC$_{50}$ 29 nM

A3-7
IC$_{50}$ 20 nM
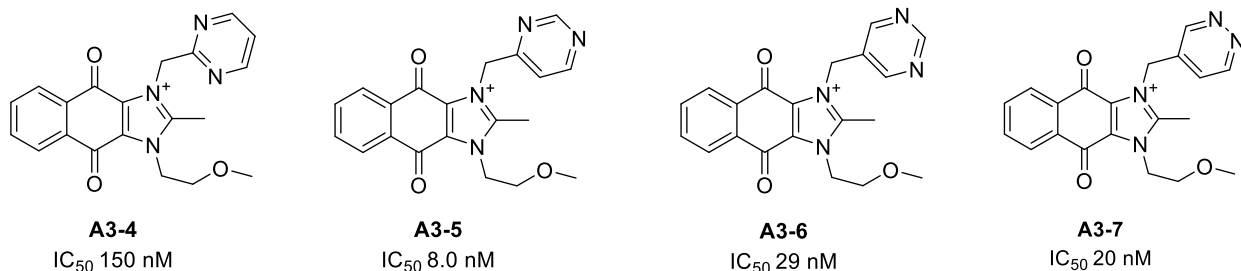
The consistent preference for azines with meta or para azomethine nitrogen as well as the requirement of maintaining a one-carbon linker between the scaffold and the ring at N^3 may reflect an optimal orientation of the side chain for a specific interaction like hydrogen bonding. When a methyl group was inserted at the para position of the pyrazine ring of YM155, activity was reduced by 10-fold (**A3-8**, IC$_{50}$ 157 nM) which implied that in the absence of a para-azomethine N, it is best to keep that position unoccupied. Lastly, replacing the pyrazinylmethyl side chain with alkyl side chains as exemplified by the **A6-X** subgroup of compounds was found to be an acceptable modification. Seven alkyl side chains were investigated and of these, methyl was the most active, followed by cyclopropyl, ethyl, propyl, n-butyl, isopropyl and isobutyl in that order. The same sequence of methyl > ethyl > propyl was observed on the other cell lines, corroborating a preference for short alkyl side chains that were not branched or cyclized. Even so, the highly ranked methyl analog **A6-2**, like the potent azinylmethyl analogs **A3-3, A3-5** and **A3-7**, were only comparable to YM155 in terms of growth inhibition.

The series B compounds were designed to report on the effects of modifying the 2'-methoxyethyl side chain at N^1 while retaining the pyrazin-2'-ylmethyl at N^3. First, it was noted that replacing 2'-methoxyethyl with 2'-hydroxyethyl resulted in an 8-fold loss in activity (**B1-1**, IC$_{50}$ 118 nM). Homologation to 2'-ethoxyethyl incurred a smaller 3-fold loss in activity (**B1-3**, IC$_{50}$

38 nM). Embedding the ether functionality in a ring (tetrahydrofuran, **B1-2**) or replacing it with a

N', N'-di-substituted aminoethyl (**B4-1**, **B4-2**) pushed IC$_{50}$ values to the micromolar range

signifying limited tolerance for bulky or charged substituents at this position. Second, replacing

2'-methoxyethyl with alkyl side chains afforded compounds with surprisingly good activity. The

side chains investigated were similar to those in series A (methyl, ethyl, propyl, butyl isopropyl,

isobutyl, cyclopropyl). Short unbranched side chains were again favored but with a different rank

order of activity (cyclopropyl > ethyl > propyl > methyl > isopropyl > isobutyl) compared to series

A. The outstanding potency of the N^1-cyclopropyl analog (**B2-5**) was evident on all cell lines

except RCC786-0, where the methyl and ethyl analogs were more active. Interestingly, **B2-8**

which has a cyclopentyl side chain at N^1 fared poorly when compared to its potent cyclopropyl

counterpart **B2-5**. Thus, the more critical requirement for alkyl substituents appears to be that of

a sterically small group at N^1, regardless of whether it is cyclized or not.
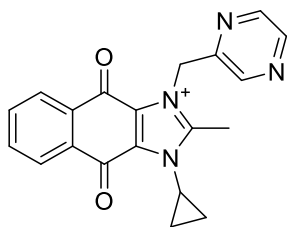
B2-5
IC$_{50}$ 33 nM
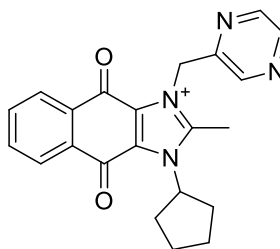
B2-8
IC$_{50}$ 1.5 μM

Lastly, replacing 2'-methoxyethyl with an aromatic ring, namely benzyl (**B3-1**) and pyrazin-2'-

ylmethyl (**B3-2**) significantly diminished activity. **B3-2** is noteworthy as it is symmetrically

substituted with pyrazinylmethyl moieties at both N^1 and N^3 and is thus comparable to **A6-1**

which is symmetrically substituted at the same positions with 2'-methoxyethyl moieties. That

A6-1 (IC$_{50}$ 73 nM) was more potent than **B3-2** (IC$_{50}$ 450 nM) lends further support to the notion

of limited tolerance for bulky substituents on the scaffold.
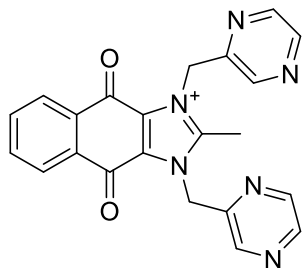
B3-2
IC$_{50}$ 450 nM
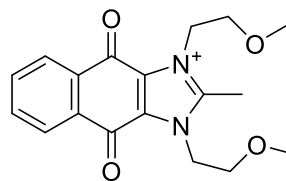
A6-1
IC$_{50}$ 73 nM

3.4.4. SAR of series AB

Having identified N^3-pyridin-4'-ylmethyl and N^1-cyclopropyl to be "optimal" substituents at their respective positions, these functionalities were then introduced to the scaffold with the expectation that it would yield more potent compounds. Less optimal substituents (pyridin-3'-ylmethyl, pyrimidin-5'-ylmethyl, methyl, ethyl) were concurrently investigated to validate this approach. In all, seven series AB analogs were synthesized, of which six were derived from permutations of pyridin-4'-ylmethyl, pyridin-3'-ylmethyl or pyrimidin-5'-ylmethyl at N^3 and ethyl or cyclopropyl at N^1. The last compound **AB7** was substituted at both N^1 and N^3 with methyl. Good activity was found in analogs that have pyridin-4'-ylmethyl at N^3 and cyclopropyl (**AB1**) or ethyl (**AB2**) at N^1. **AB1** was broadly equivalent to YM155 in terms of IC$_{50}$ while **AB2** was marginally less active than YM155, except on RCC786-0 where it was slightly more potent. Clearly, this approach of combining optimal substituents onto the scaffold did not work as well as anticipated. This is further endorsed by the disappointing activities of **AB3-AB6**.
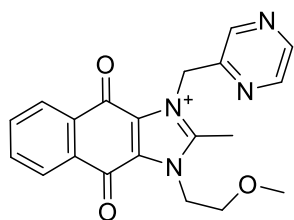
YM155
IC$_{50}$ 14 nM
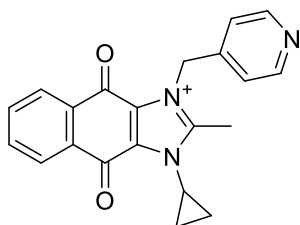
AB1
IC$_{50}$ 17 nM
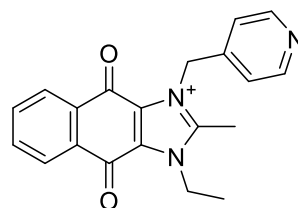
AB2
IC$_{50}$ 30 nM
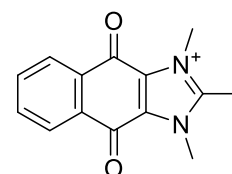
AB7
IC$_{50}$ 7 nM

An unexpected finding was that of **AB7** which was substituted with the sub-optimal methyl group

51

at N^1 and N^3. **AB7** displayed outstanding activity, exceeding YM155 by 1.5 to 2-fold and was in fact the most promising compound (IC$_{50}$ 9 – 30 nM) identified in this investigation.

| **AB3** | **AB4** | **AB5** | **AB6** |
| IC$_{50}$ 86 nM | IC$_{50}$ 61 nM | IC$_{50}$ 53 nM | IC$_{50}$ 36 nM |
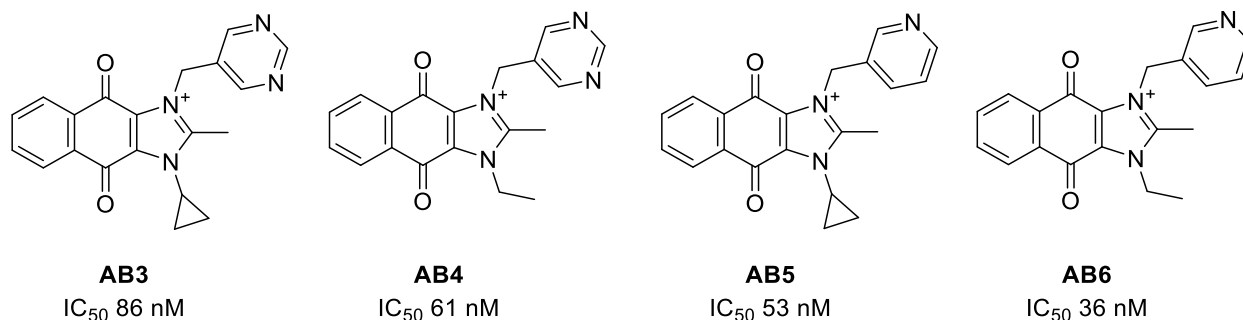
3.4.5. Selective activity against non-malignant cell lines

YM155 and the synthesized compounds were tested on non-malignant lung fibroblast IMR-90 cells to determine if they selectively affected proliferation of malignant cells. Selectivity was assessed from the four selectivity ratios derived from the IC$_{50}$ on IMR-90 cells and the IC$_{50}$ on the malignant cell line. Average ratios ranging from 1.8 to 19-fold were obtained (Table 1). The compounds were most selective for H1666, followed by H1299, RCC786-0 and finally RCC4/VA. Unfortunately, higher selectivities (as high as 38-fold) were found for compounds that had weaker growth inhibitory activities, such as **A6-6**, **A6-8, B1-1** and **B1-3**. YM155 and its potent analogs (**A3-3**, **A3-5**, **AB1**, **AB7**) had only modest selectivities that ranged from 3-19-fold.

3.5. Discussion

A key SAR finding of this chapter relates to the importance of the intact dioxonaphthoimidazolium scaffold for growth inhibition. Attempts to reduce the tricyclic scaffold to a bicyclic or monocyclic entity invariably resulted in a loss of activity. Of the various motifs on the tricyclic scaffold, the quinone was recognized as the most critical, followed by the positively charged imidazolium and lastly, the distal benzene ring.

Retention of the quinone moiety ensured a measurable growth inhibitory activity (nanomolar to micromolar IC$_{50}$), despite changes to other parts of the scaffold. This is evident from the activities of naphthoquinone, **C1-2**, **C4-1** and **C4-2**. In the absence of the quinone, steep losses in activity (IC$_{50}$ > 100 µM) were encountered, even when the tricyclic scaffold is retained. **C2-3** is a case in point.

| C1-2 | C4-1 | C4-2 | C2-3 |
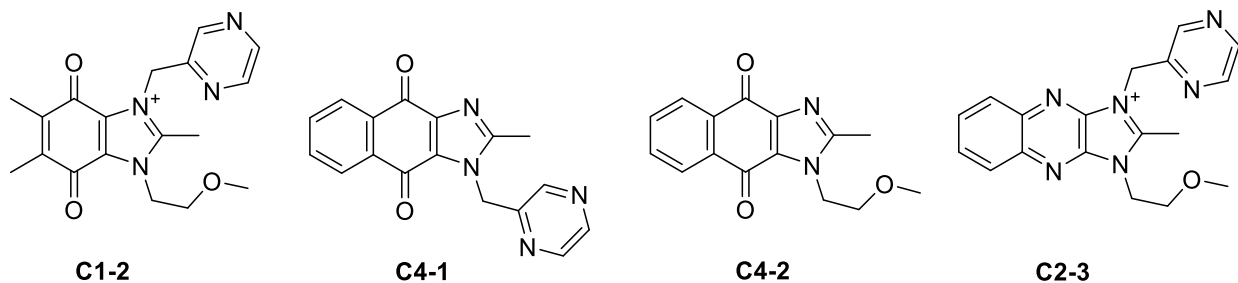
Activity was diminished to a lesser extent in the absence of a positive charge on the scaffold. The activities of **C4-1** and **C4-2** are illustrative. Both compounds differ from YM155 in lacking a substituent at N^3 and hence, a positive charge. When a methyl was inserted at N^3 of **C4-1** and **C4-2**, the positive charge was restored and with it, a rebound in activity, as seen in **B2-1** and **A6-2** respectively. It is noted that **C4-1** and **C4-2** are structurally related to the dioxonaphthoimidazole **1**, previously reported by Kuo et al.[73] Intriguingly, **1** was many times more potent than **C4-1** and **C4-2**. This would imply that alkyl substitution of the scaffold, as seen in **1**, is preferred to the more polar H bonding and sterically larger side chains found in **C4-1** and **C4-2**. Indeed, sterically compact substituents are favored on N^1, C^2 and N^3. Notably, the most potent analog identified here (**AB7**) is minimally substituted at N^1 and N^3 with methyl groups.

| C4-1 | C4-2 | B2-1 | A6-2 | 1 |
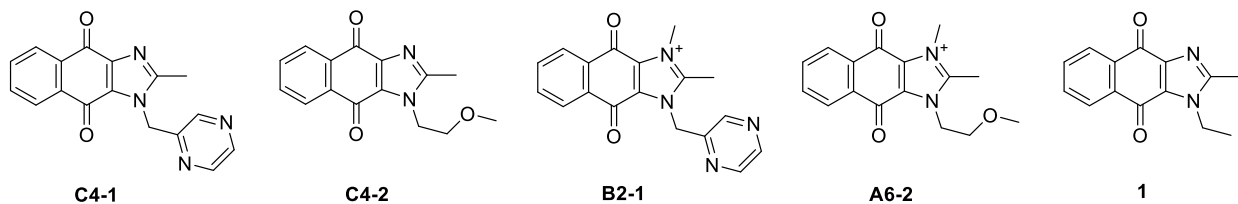
The distal phenyl ring appears to be the least important feature in the scaffold. In its absence, the resulting analog **C1-2** incurred the smallest loss in activity compared to the removal of other

rings in the scaffold. The diminished activity of **C1-2** may be related to the loss of π-π stacking on omission of the phenyl ring.

Mention should be made of the imidazolium **C2-2** whose poor activity stands in sharp contrast to that of IBN-65 which was reported to have an IC_{50} of $\approx$ 5µM on a panel of HCC cell lines.[74] The disparity is likely due to the difference in substitution on the imidazolium ring. Unlike **C2-2**, IBN-65 combines a positive charge with highly lipophilic side chains which may favor growth inhibitory activity.

C2-2   **IBN65**
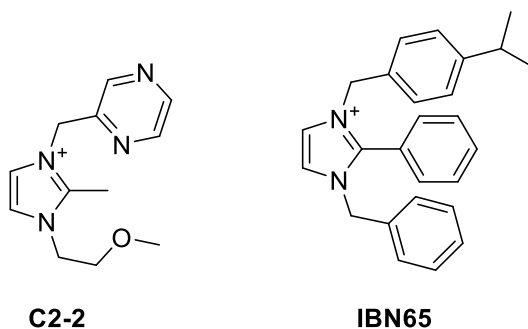
Unlike the tricyclic dioxonaphthoimidazolium scaffold which was mandatory for activity, functionalization at N^1 and N^3 served to fine-tune activity. Consequently, a greater degree of structural diversity was permitted at these positions without overt losses to activity. Notably, all series A and B analogs had determinable IC_{50} values which were within the nanomolar to low micromolar range. However, only one analog (**AB7**) was modestly more potent than YM155 although several (**AB1**, **A3-3**, **A3-7**, **B2-5**) were comparable to it. A striking SAR trend that was common to both N^1 and N^3 positions was the marked preference for short, unbranched and cyclized alkyl groups. In fact, this was the only acceptable modification of the 2'-methoxyethyl side chain at N^1. The resulting compound **B2-5** was comparable to YM155 and this raises the question as whether the 2'-methoxyethyl side chain at N^1 has any role as an H bond acceptor.

B2-5   **AB7**
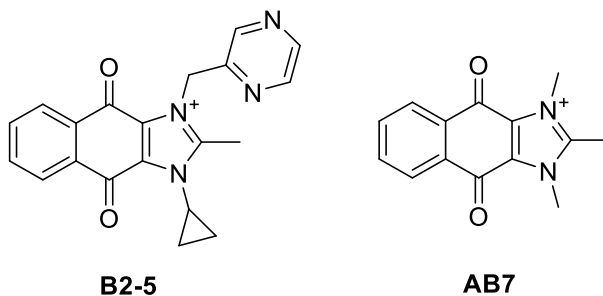
Greater leeway was permitted at the N^3 position which accepts short unbranched alkyl groups as well as isosteric modifications of the pyrazine-2'-ylmethyl side chain. A striking regioisomeric preference was observed for the latter. Notably, the pyrazine ring could be replaced by pyridine or another diazine, as long as an azomethine nitrogen was sited at the para position of the ring. The resulting analogs **A3-3**, **A3-7, AB1** bearing pyridin-4'-ylmethyl or pyridazin-4'-ylmethyl side chains were in fact equipotent or modestly more potent than YM155 on selected cell lines. Thus the SAR at N^3 indicates two disparate features that result in optimal activity, namely a short unbranched alkyl group and an extended azinylmethyl side chain with a suitably positioned azomethine N for H bonding.

With regards to selectivity, most of the potent analogs had comparable selectivities to YM155 (ca. 5-18-fold). While this is an arguably modest level of selectivity, it is noted that YM155 has an unusually low toxicity profile based on clinical trial data. Therefore, this level of selectivity may translate to an acceptable therapeutic window should any of the compounds become clinical candidates.

3.6. Conclusion

The objectives of this chapter were to (i) elucidate SAR of YM155 on RCC and NSCLC cell lines, (ii) determine if there are overlapping structure requirements for these disparate malignancies and (iii) evaluate selective activity against malignant cells. To this end, the SAR of YM155 has been established. The key findings are summarized in Figure 3.3. **A3-3**, **AB1** and

AB7 were identified as promising analogs with nanomolar growth inhibitory activities and acceptable selectivities (ca. 10-fold) on the ccRCC and NSCLC cells. In view of the close concordance in SAR trends observed across the different cell lines, a shared mode of action may be implicated for these compounds. This is despite clear differences in the common genetic aberrations between RCC and NSCLC, and it suggests that the VHL pathway for RCC and the EGFR pathway for NSCLC may not be strongly relevant to the mode of action. Conversely, this mode of action may involve particular oncogenic pathway that is prominent in both cancer types but less so than the VHL and EGFR pathways.
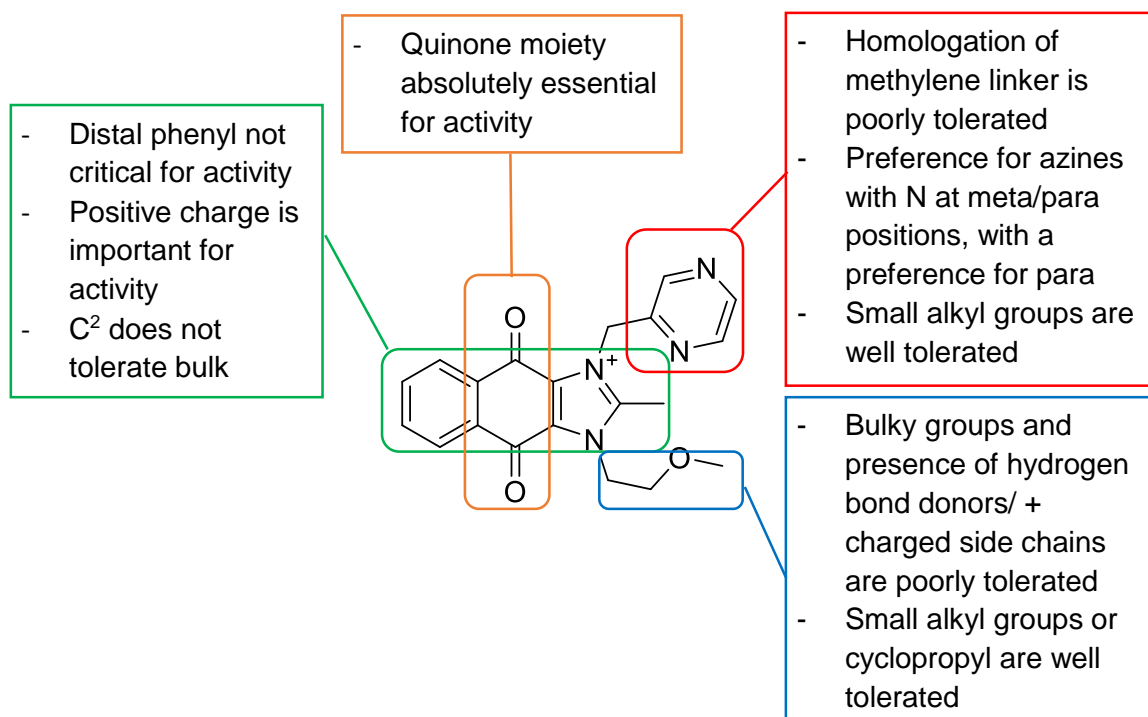
Figure 3.3. Summary of growth inhibitory structure-activity relationships of YM155

3.7. Experimental information

3.7.1. General biology

High glucose Dulbecco's Modified Eagle's Media (DMEM) and Roswell Park Memorial Institute Media 1640 (RPMI-1640) (Hyclone®, GE Healthcare, Buckinghamshire, UK) and supplemented

with 10% heat inactivated fetal bovine serum (FBS) (Hyclone®, GE Healthcare, Buckinghamshire, UK) and 0.01% w/v Penicillin-G-Streptomycin mixture (GE Healthcare, Buckinghamshire, United Kingdom). 3-(4,5-Dimethylthiazol-2-yl)-2,5-diphenyltetrazolium bromide (MTT) was purchased from Alfa Aesar, Inc. (Lancashire, United Kingdom), reconstituted in phosphate-buffered saline to 2 mg/mL and diluted with appropriate cell culture media before use.

3.7.2. Cell culture

Human clear cell renal cell carcinoma cell lines RCC786-0, RCC4/VA, non-small cell lung carcinoma cell lines H1299, H1666 and normal lung fibroblasts IMR-90 cells were obtained from American Type Culture Collection (ATCC, Rockville, MD). RCC786-0, RCC4/VA and IMR-90 cells were cultured in complete DMEM. H1299 and H1666 cells were cultured in complete RPMI-1640 and incubated at 37°C, 5% CO_2. Malignant and IMR-90 cell lines were sub-cultured at ratios of 1:6 and 1:3 respectively on reaching 90% confluence.

3.7.3. MTT assay

Cells were seeded at a density of 3.0 x 10^3 cells/well for malignant cell lines and 4.0 x 10^3 cells/well for IMR-90 in 96-well plates containing 100 μL media per well and incubated for 24 h (37°C, 5% CO_2) for cell adherence. After 24 h, media in each well was removed by aspiration and 199 μL of fresh media was added. 1 μL of test compound (prepared in DMSO stock solutions at 200-fold higher concentrations) was added to each well. The final DMSO concentration in each well was kept at 0.5% v/v. The compound-treated cells were incubated for 72 h (37°C, 5% CO_2), media was subsequently removed by aspiration and an aliquot (200 μL) of 0.5 mg/mL MTT in media was added to each well. The treated plates were incubated for 2 h (malignant cells) or 3 h (IMR-90 cells) after which the MTT containing media was removed by

aspiration and 100 µL of DMSO added to each well to dissolve the purple formazan crystals. Plates were agitated at 700 rpm, 5 min on a plate shaker before absorbance readings were read (570 nm, Tecan Infinite™ M200 Pro). Viable cells were determined from the following equation:

Percentage viability = $[(Ab_{compound} - Ab_{blank})/(Ab_{control} - Ab_{blank})]$ x 100%,

where $Ab_{compound}$ = Absorbance of compound-treated cells, $Ab_{control}$ = Absorbance of untreated/control cells and Ab_{blank} = Absorbance of DMSO.

Each test compound was assessed at 8 concentrations in at least 3 separate experiments carried out at different times. Cells were from different passage numbers and each compound was tested from 2 stock solutions. For each experiment, percentage viability was calculated using the mean absorbance value from three technical repeats at a given test concentration. The IC_{50} (the concentration of test compound required to inhibit cell growth by 50%) was determined by plotting % viability against logarithmic concentration of test compound (GraphPad Prism 5, San Diego, CA).

Chapter 4: DNA intercalating and redox cycling properties of YM155 and analogs

4.1   Introduction

The focus of this chapter is to explore the potential of YM155 and its analogs to induce a DNA damage response. Glaros et al first proposed that YM155 induced DNA damage when they noted from COMPARE analysis data that the growth inhibitory profile of   YM155 was strongly correlated to that of DNA damaging agents and a DNA directed inhibitor of transcription.[55] They proceeded to show that YM155 induced phosphorylation of H2AX and KAP1, which are biomarkers for DNA double strand breaks. When phosphorylation was observed at concentrations that were lower than that required to reduce survivin, they concluded that YM155 acted primarily by inducing DNA damage and that any effect on survivin was a secondary event caused by the general deactivation of gene expression consequent to DNA damage. Winter et al confirmed that YM155 induced the phosphorylation of H2AX and KAP1 but they proposed that this was a consequence of the ability of YM155 to intercalate DNA.[56] They noted that chloroquine inhibited DNA replication and induced phosphorylation of H2AX largely as a result of intercalation. Another archetypal DNA intercalator ethidium bromide did not directly cause DNA damage but still induced errors in DNA replication due to misreading by polymerases.[178] Acridine-based DNA intercalators such as 9-aminoacridine and quinacrine were originally thought to exert their anticancer properties by intercalation, but this was later dismissed when it was found that intercalation did not result in DNA damage in cancer cells.[179]

For an agent to induce DNA damage, it must interact reversibly or irreversibly with DNA.[180] Irreversible binding would involve alkylation of the DNA bases while reversible binding would require an initial insertion between the base pairs of the double helix (intercalation) followed by a cascade of events culminating in DNA damage. These events may involve topoisomerase-induced DNA damage as typified by campthothecins or the generation of free radicals that cause DNA strand breaks as observed in bleomycin. Structurally, YM155 is an impropable

alkylating agent as it lacks features associated with a reactive electrophilic center. On the other hand, YM155 is a likely DNA intercalator due to its planar scaffold and positively charged state. Intercalation followed by inhibition of topoisomerase can be dismissed as YM155 was not found to inhibit topoisomerase I.[56] On the other hand, free radical-induced DNA damage is probable due to the embedded quinone in YM155. The quinone is an established pharmacophore for redox cycling.[181] It accepts a single electron to give a semiquinone radical which reacts directly with DNA[182] or participates in a redox cycle of superoxide radical generation by transfer of electrons to oxygen.[183] Superoxide and its dismutation product hydrogen peroxide form hydroxyl radicals which readily initiate strand breaks when generated in the vicinity of DNA.[184]

Little is known of the structural features of YM155 that are critical for DNA binding or redox cycling. The availability of such information will provide a better understanding of the mode of action of YM155 and by extension, its potent growth inhibitory activity.

4.2 Objectives

The objective of this chapter is to investigate the DNA intercalation and redox cycling properties of YM155 and its analogs with the aim of elucidating SAR for these activities. A comparison of the structural features required for DNA intercalation/redox cycling and those for growth inhibition (Chapter 3) will provide insight as to the extent to which these properties contribute to growth inhibition.

4.3 Results

4.3.1 DNA intercalation

DNA intercalation by YM155 and analogs was examined by an *in vitro* fluorescent intercalator displacement (FID) assay that was adopted from reported procedures.[185, 186] Briefly, the dye thiazole orange (ThO) intercalates with non-specific DNA sequences in herring sperm DNA with

emission of fluorescence. When it is displaced by a competing intercalator, fluorescence is diminished. The test compound was evaluated over a range of concentrations to determine the concentration (DC_{50}) at which it reduced the basal fluorescence of ThO (10 μM) by 50%. Strong intercalators will have small DC_{50} values and vice versa. Dose response curves depicting the displacement of ThO by YM155 and doxorubicin (positive control) are provided in Figure 4.1. DNA intercalation DC_{50} values are tabulated in Table 4.1.
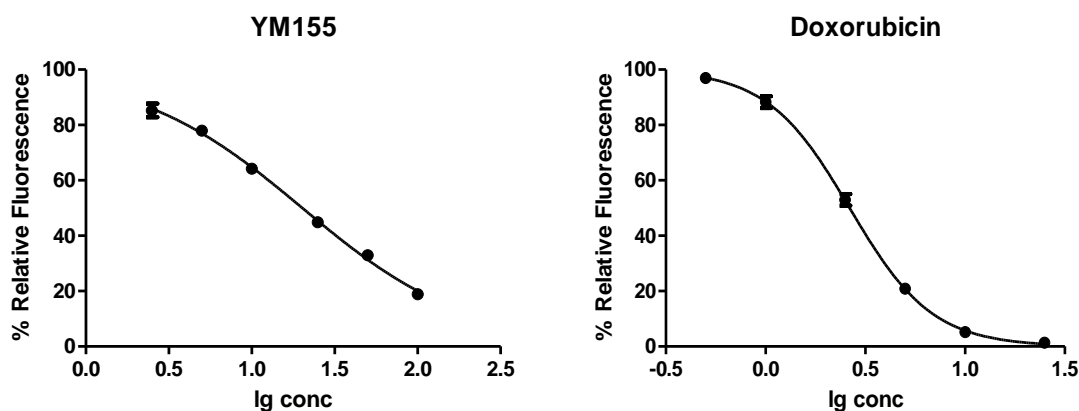
Figure 4.1. Representative dose response curves for the displacement of ThO by YM155 and doxorubicin.

Table 4.1. DNA intercalation DC_{50} and redox cycling EC_{50} values of test compounds

Compound	DC_{50} (μM)[a] for DNA intercalation	EC_{50} (μM)[b] for redox cycling
YM155	20.3 ± 3.1	1.38 ± 0.05
A1-1	27.5 ± 0.5	3.63 ± 0.71
A1-2	35.4 ± 1.4	13.0 ± 0.3
A1-3	28.6 ± 0.4	3.22 ± 0.14
A2-1	31.9 ± 1.1	6.27 ± 0.26
A3-1	28.6 ± 3.1	2.10 ± 0.24
A3-2	16.4 ± 1.3	1.91 ± 0.24
A3-3	20.0 ± 0.5	2.01 ± 0.10
A3-4	45.0 ± 3.3	1.36 ± 0.11
A3-5	25.4 ± 2.4	4.56 ± 0.13

Compound	DC$_{50}$ (µM)[a] for DNA intercalation	EC$_{50}$ (µM)[b] for redox cycling
A3-6	26.7 ± 3.4	3.09 ± 0.08
A3-7	23.0 ± 1.2	2.37 ± 0.01
A3-8	18.4 ± 1.2	2.57 ± 0.16
A4-1	44.0 ± 3.2	7.58 ± 0.20
A5-1	95.4 ± 7.5	2.96 ± 0.15
A6-1	32.3 ± 3.8	9.30 ± 0.43
A6-2	32.3 ± 1.5	5.70 ± 0.43
A6-3	40.1 ± 4.5	7.08 ± 1.18
A6-4	48.2 ± 6.0	8.47 ± 0.15
A6-5	99.0 ± 0.8	10.2 ± 0.5
A6-6	35.4 ± 4.1	6.37 ± 0.69
A6-7	44.2 ± 0.2	6.37 ± 0.69
A6-8	67.0 ± 5.8	8.75 ± 0.43
B1-1	17.7 ± 1.2	2.36 ± 0.04
B1-2	13.3 ± 0.9	3.67 ± 0.20
B1-3	20.9 ± 1.4	0.68 ± 0.00
B2-1	30.6 ± 0.8	2.94 ± 0.05
B2-2	24.0 ± 2.4	3.32 ± 0.13
B2-3	30.1 ± 1.5	2.26 ± 0.05
B2-4	56.9 ± 9.1	3.47 ± 0.45
B2-5	25.2 ± 1.6	3.92 ± 0.10
B2-6	27.9 ± 3.8	2.31 ± 0.37
B2-7	43.3 ± 2.3	5.82 ± 0.05
B2-8	78.8 ± 13.2	7.35 ± 0.06
B3-1	13.9 ± 0.7	1.85 ± 0.10
B3-2	12.0 ± 1.0	1.34 ± 0.06
B4-1	19.9 ± 4.0	1.43 ± 0.06
B4-2	15.5 ± 0.3	1.01 ± 0.04
C1-1	29.5 ± 2.6	2.00 ± 0.04
C1-2	>100	1.42 ± 0.01
C2-1	>100	>400
C2-2	>100	>400

Compound	DC_{50} (µM)[a] for DNA intercalation	EC_{50} (µM)[b] for redox cycling
C2-3	>100	>400
C3-1	>100	>400
C3-2	>100	>400
C4-1	>100	>400
C4-2	>100	>400
AB1	20.8 ± 1.3	6.10 ± 0.38
AB2	21.3 ± 3.2	3.47 ± 0.08
AB3	22.7 ± 1.6	7.61 ± 0.07
AB4	17.6 ± 1.2	3.86 ± 0.11
AB5	14.7 ± 1.5	3.48 ± 0.01
AB6	12.0 ± 0.3	2.75 ± 0.18
AB7	12.7 ± 0.5	7.55 ± 0.71
Doxorubicin	2.64 ± 0.16	195 ± 7
Naphthoquinone	>100	0.333 ± 0.008

[a] DC_{50}: Concentration required to reduce basal fluorescence of thiazole orange (10 µM) by 50%. A higher value indicates a lesser tendency to displace ThO (i.e. weaker binding affinity for DNA). Mean and SD of n=3 separate determinations. [b] EC_{50}: Concentration required to reduce oxidized phenol red absorbance to 50% of control values. Mean and SD of n=3 separate determinations.

The DC_{50} of YM155 was 20.3 µM as compared to 2.6 µM for doxorubicin. Since ThO was evaluated at a fixed concentration of 10 µM, this would imply that YM155 had half the binding affinity of ThO for DNA as compared to doxorubicin which had 4 times the DNA binding affinity of ThO. Clearly, YM155 is a significantly weaker DNA intercalator than doxorubicin.

Some interesting trends in DNA binding affinities were deduced from the DC_{50} values in Table 4.1. With regard to series C, it is striking that attempts to reduce the size of the tricyclic scaffold abolished binding affinity. Thus, the monocyclic (**C2-2**) and bicyclic (**C1-2**, **C2-1**, **C3-X**,) analogs

had DC_{50} exceeding 100 μM. This was also true of naphthoquinone and analogs that retain

modified tricyclic scaffolds (**C2-3**, **C4-X**). The only permissible modification was the extension of

the C^2 methyl to ethyl (**C1-1**) but even this minor alteration increased DC_{50} to 30 μM. These

results underscore the importance of the intact dioxonaphthoimidazolium scaffold for DNA

intercalation.

C1-2
DC_{50} >100 μM

C2-1
DC_{50} >100 μM

C2-2
DC_{50} >100 μM

C2-3
DC_{50} >100 μM

C3-1
DC_{50} >100 μM

C3-2
DC_{50} >100 μM

C4-1
DC_{50} >100 μM

C4-2
DC_{50} >100 μM
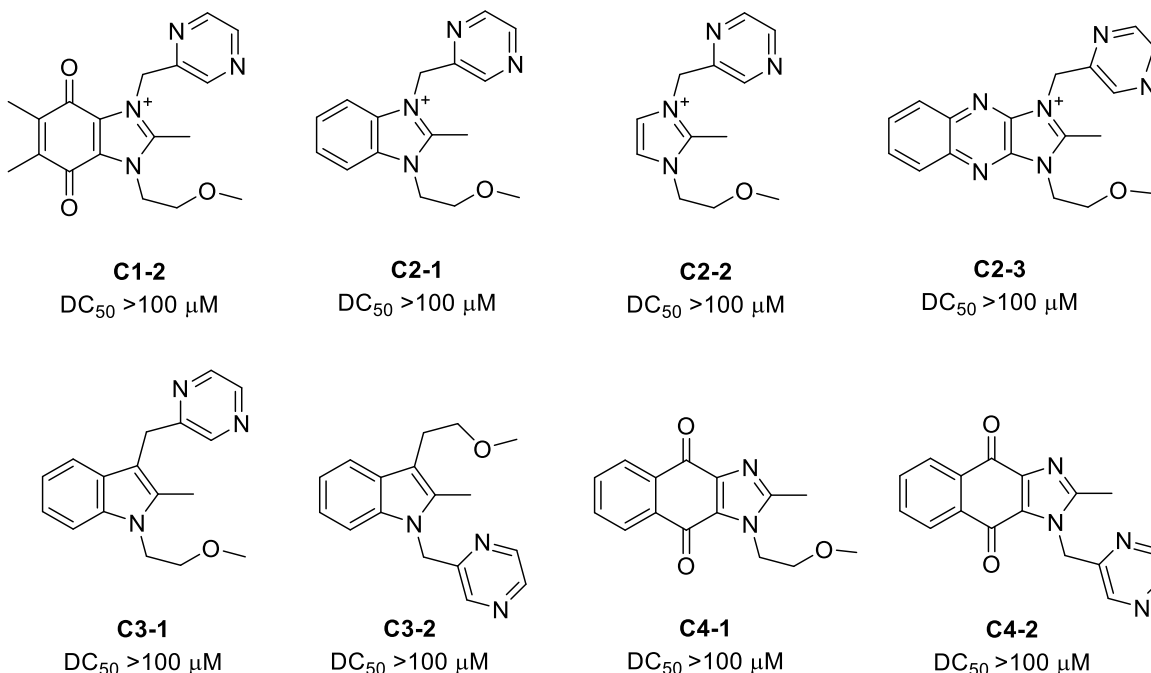
To explore functionalization at N^3, the DC_{50} values of series A compounds were analyzed. A key

observation was that modifications to the N^3 pyrazin-2'-ylmethyl side chain were poorly

tolerated. In particular, alkyl substitution at N^3 (**A6-X**) and altering the length of the methylene

spacer (**A4-1**, **A5-1**) adversely affected intercalation. Isosteric changes to the pyrazine ring gave

better, albeit modest, outcomes as seen from **A3-2** (pyridine-3'-ylmethyl, DC_{50} 16.4 μM) and **A3-

3** (pyridine-4'-ylmethyl, DC_{50} 20.0 μM). The regioisomeric bias against azines with ortho-

nitrogens was again evident for the pyridinylmethyl and pyrimidinylmethyl analogs.

YM155
DC_{50} 20 μM

A3-1
DC_{50} 29 μM

A3-2
DC_{50} 16 μM

A3-3
DC_{50} 20μM

A3-4
DC_{50} 45μM

A3-5
DC_{50} 25 μM

A3-6
DC_{50} 27 μM
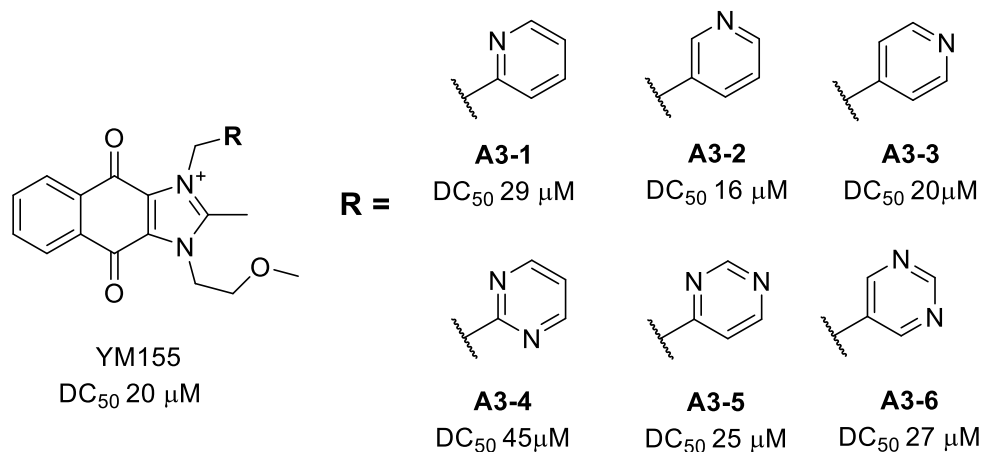
On the other hand, replacement of pyrazine with non-azines (**A1-1**, benzyl; **A1-2**, cyclohexylmethyl; **A1-3**, thien-2'-ylmethyl; **A2-1**, imidazole-5'-yl) was not favored. Methyl substitution of the pyrazine ring as in **A3-8** (5'-methylpyrazin-2-ylmethyl, DC_{50} 18.4 μM) did not adversely affect intercalation.

The role of functionalization at N^1 was deduced from series B. It is noted that 5 of the 15 series B analogs (33%) had DC_{50} values > 30 μM (arbitrarily taken to reflect poor binding), as compared to 13 of the 22 series A analogs (59%). In series B, DC_{50} values ranged from 13 μM to 79 μM (6-fold variation) whereas in series A, the variation was wider (16 – 99 μM, ca. 15-fold). Thus, there were fewer "poor" binders in series B which together with the narrower variation in DC_{50} values suggests that modifications at the N^1 position affected intercalation to a lesser extent as compared to the N^3 position. Interestingly, poor binders were highly represented among the N^1-alkyl substituted analogs (**B2-X**), as in the case of series A. Acceptable groups at N^1 included diverse cyclized entities (**B3-1**, benzyl; **B3-2**, pyrazin-2'-ylmethyl; **B1-2**, tetrahydrofurfuryl), N', N'-disubstituted aminoalkyl side chains (**B4-1**, **B4-2**), and minor modifications to the N^1 2'-methoxyethyl moiety (**B1-3**, 2'-ethoxyethyl; **B1-1**, 2'-hydroxyethyl). The binding affinities of these analogs were nearly equivalent to that of YM155.
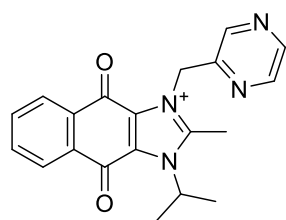
B2-4
DC$_{50}$ 57 μM
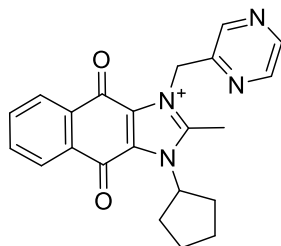
B2-8
DC$_{50}$ 79 μM
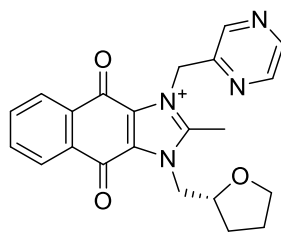
B1-2
DC$_{50}$ 13 μM
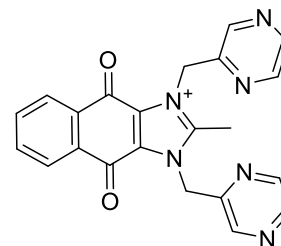
B3-2
DC$_{50}$ 12 μM

Unlike the others, series AB yielded consistently good DNA intercalators (DC$_{50}$ 12 – 23 μM). It is noted that the intercalation ability of **AB1** – **AB6** were closely aligned to that of the corresponding series A analogs. Thus, **AB1** and **AB2** which have in common a pyridin-4'-ylmethyl side chain had DC$_{50}$ values that were within the range of **A3-3** which has a similar side chain at N^3. This was again observed for **AB5**, **AB6** (compared to **A3-2**) and **AB3** (compared to **A3-6**). **AB4** was an outlier, being more potent than **A3-6**. The strong binding affinity of the N^1, N^3-dimethyl substituted **AB7** (DC$_{50}$ 13 μM) was unusual because the mono-methyl analogs, (**B2-1**, N^1-methyl, DC$_{50}$ 31 μM; **A6-2**, N3-methyl, DC$_{50}$ 32 μM) were significantly weaker intercalators.
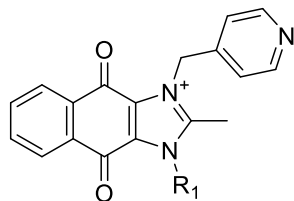
AB1: R$_1$ cyclopropyl DC$_{50}$ 21µM
AB2: R$_1$ ethyl DC$_{50}$ 21µM
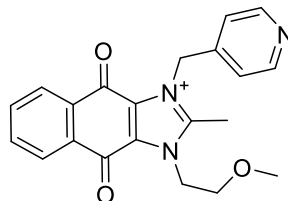
A3-3
DC$_{50}$ 20 µM
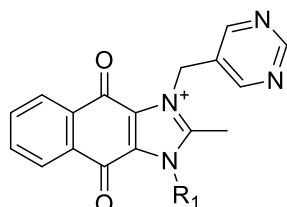
AB3: R$_1$ cyclopropyl DC$_{50}$ 23 µM
AB4: R$_1$ ethyl DC$_{50}$ 18 µM
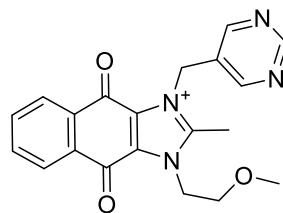
A3-6
DC$_{50}$ 27 µM
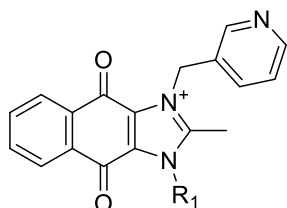
AB5: R$_1$ cyclopropyl DC$_{50}$ 15 µM
AB6: R$_1$ ethyl DC$_{50}$ 12 µM
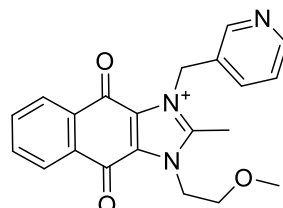
A3-2
DC$_{50}$ 16 µM

4.3.2 Redox cycling

Redox cycling by YM155 and the synthesized compounds was first investigated by an *in vitro*

assay centered on the oxidation of phenol red by hydrogen peroxide (HRP).[187, 188] In this assay,

the thiol groups of dithiothreitol are oxidized to the disulfide. The electrons released in the

process reduce the quinone to semiquinone or hydroquinone. When this reaction is reversed in

the presence of oxygen, superoxide anions are formed and these rapidly dismutate to hydrogen

peroxide which then oxidizes phenol red in the presence of horseradish peroxidase. In the

presence of a redox cycler, phenol red is continually oxidized and its absorbance at 610 nm

increases. The redox cycling propensity of the test compound is given by EC$_{50}$ which is the

concentration required to increase the absorbance of oxidized phenol red at 610 nm to half the

maximum value (Table 4.1). A strong redox cycler will have a lower EC_{50} and vice versa. Dose response plots of YM155 and naphthoquinone (positive control) are shown in Figure 4.2.
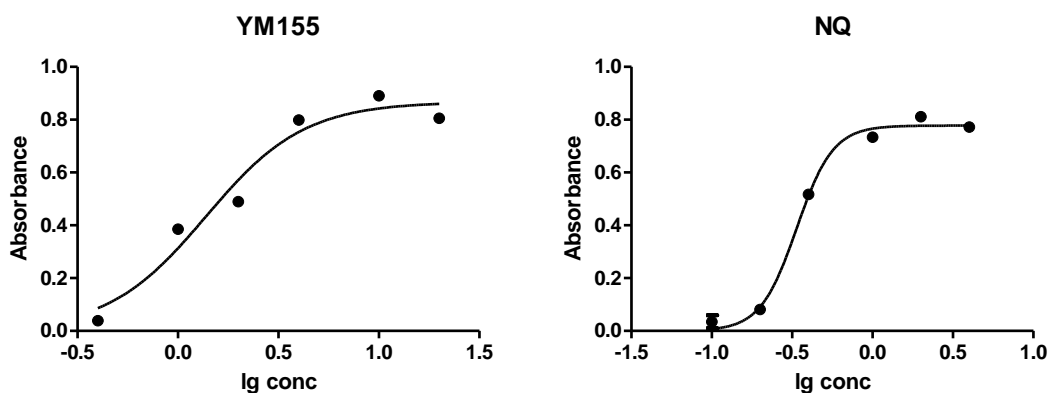
Figure 4.2. Representative redox cycling dose response plot of YM155 and naphthoquinone (NQ) on the phenol red-HRP assay.

Besides naphthoquinone, the assay was also carried out on doxorubicin. Naphthoquinone (EC_{50} 0.33 µM) was found to be a more effective redox cycler than doxorubicin (EC_{50} 195 µM). Thus a quinone presence does not always ensure redox cycling activity on this assay. Tentatively, minimal substitution around the quinone (naphthoquinone) may be preferred to embedding the quinone within a scaffold (doxorubicin). However, in spite of it having an embedded quinone, YM155 was a surprisingly good redox cycler (EC_{50} 1.4 µM), which would suggest that the substitution on the scaffold played a decisive role in influencing activity.

SAR for redox cycling was deduced for the various series. Only two of the 9 analogs in Series C were redox cyclers. They were **C1-1** (EC_{50} 2.0 µM) which is the C^2-ethyl homolog of YM155, and the positively charged bicyclic quinone **C1-2.** None of the non-quinone analogs (**C2-X**, **C3-X**) were redox cyclers but some quinone containing analogs (**C4-1**, **C4-2**) also failed to redox cycle. **C4-1** and **C4-2** are not substituted at N^3 and consequently are not positively charged. This may imply that the charged imidazolium and quinone must both be present for redox

cycling. The outstanding activity of naphthoquinone (YM155 without imidazolium) would then be anomalous. Thus, pending additional data, a reasonable conclusion would be that (i) the quinone moiety per se is not sufficient to ensure redox cycling and (ii) the intact dioxonaphthoimidazolium scaffold is not required for redox cycling.

Naphthoquinone
EC_{50} 0.33 µM

C1-2
EC_{50} 1.4 µM

C1-1
EC_{50} 2.0 µM

C4-1
EC_{50} >400 µM

C4-2
EC_{50} >400 µM
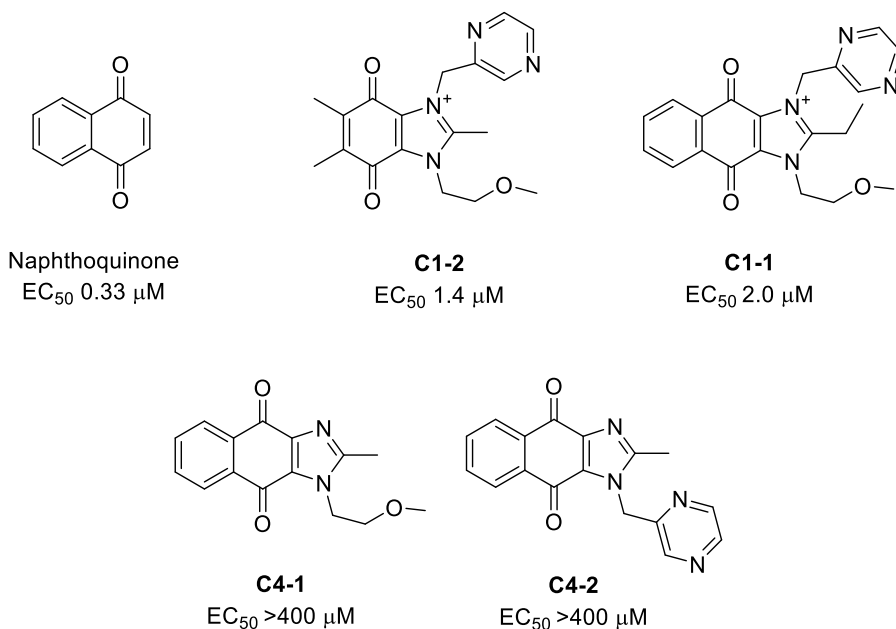
A 10-fold variation in EC_{50} values (1.4 – 13 µM) was observed in series A. Nearly 77% of the analogs had ½ the redox cycling ability of YM155 (EC_{50} > 2.8 µM, taken arbitrarily as a threshold for "weak" activity). Interestingly, these same compounds, namely N^1-alkyl analogs (**A6-X**), methylene homologs (**A4-1**, **A5-1**), and non-azinylmethyl bearing analogs (**A1-X**, **A2-1**), were also weak DNA intercalators. The azinylmethyl bearing analogs (**A3-X**) were generally better redox cyclers. The regioisomeric bias against azines with ortho-nitrogens was not consistently observed here, as seen from **A3-1** and **A3-4**.

Analysis of series B analogs showed a similar fold variation in EC_{50} values (11-fold, 0.7 – 7.4 µM) as series A, but with fewer members (47%) having half the redox cycling ability of YM155. The similarity in fold variation suggest that redox cycling is equally affected by changes at N^1 and N^3, but alterations at N^1 (i.e. series B) were better placed to yield potent compounds.

Trends in redox cycling were generally less consistent when compared to DNA intercalation where there was a clearer SAR trend. For example, variable effects were noted for analogs with N^1-alkyl groups (**B2-X**), cyclized entities (**B1-2**, **B3-X**) and bearing isosteric changes at the 2'-methoxyethyl side chain (**B1-X**). However, **B4-X** analogs were good redox cyclers.

Series AB compounds were found to be poor redox cyclers (EC_{50} 2.8 – 7.6 µM). No discernible correlation in activity could be drawn between **AB1** – **AB6** and their corresponding series A analogs. **AB7** was in fact a weak redox cycler.

Having shown that YM155 and several analogs were redox cyclers in the *in vitro* assay, the next step was to confirm these findings in a cell based assay using 2',7'-dichlorodihydrofluorescein (H_2DCF) diacetate.[189, 190] The diacetate is readily taken up into cells and hydrolyzed intracellularly by esterases to give H_2DCF. The latter is trapped within cells due to its negatively charged state. In the presence of reactive oxygen species, H_2DCF is oxidized to dichlorofluorescein which is fluorescent. When H_2DCF loaded cells are treated with a redox cycler, an increase in fluorescence would be observed.

YM155
EC_{50} 1.4 µM

A3-3
EC_{50} 2.0 µM

B1-3
EC_{50} 0.68 µM

C1-2
EC_{50} 1.4 µM

AB1
EC_{50} 6.1 µM

AB7
EC_{50} 7.6 µM
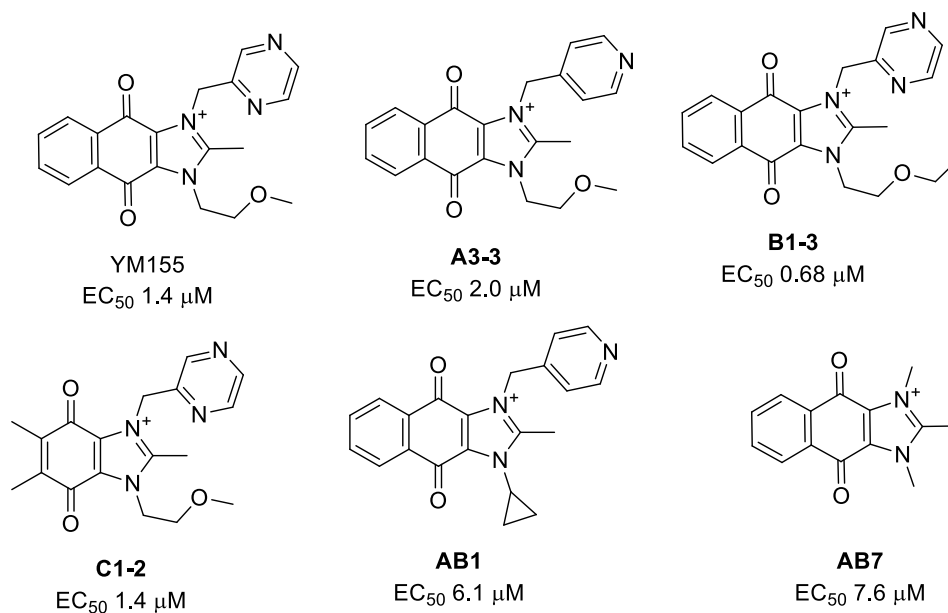
The following compounds were tested: YM155, **A3-3**, **B1-3**, **C1-2**, **AB1** and **AB7**. In terms of the

in vitro redox cycling activities, **B1-3** was the most potent (EC_{50} 0.68 µM). **C1-2** (EC_{50} 1.42 µM)

was comparable to YM155 (EC_{50} 1.38 µM) and the remaining compounds were less effective

(EC_{50} 2.0 - 7.6 µM). Naphthoquinone was included as a positive control (EC_{50} 0.33 µM). The

compounds were tested over a range of concentrations equivalent to 1x, 2x, 5x and 10x growth

inhibitory IC_{50} on RCC786-0 and H1299 cells (Table 3.1). As seen from Figure 4.3, the

compounds had similar effects on both cell lines. In each case, YM155, **A3-3**, **B1-3**, **AB1** and

AB7 did not alter the basal level of fluorescence over the entire concentration range, indicating

that at concentrations relevant to their respective IC_{50} values, these compounds did not

generate significant amounts of ROS. In contrast **C1-2** demonstrated a dose dependent

increase in fluorescence matching that of naphthoquinone at 5x IC_{50} (RCC786-0) and exceeding

it at 2x IC_{50} (H1299). Thus, among the test compounds, only **C1-2** generated significant levels of

ROS.
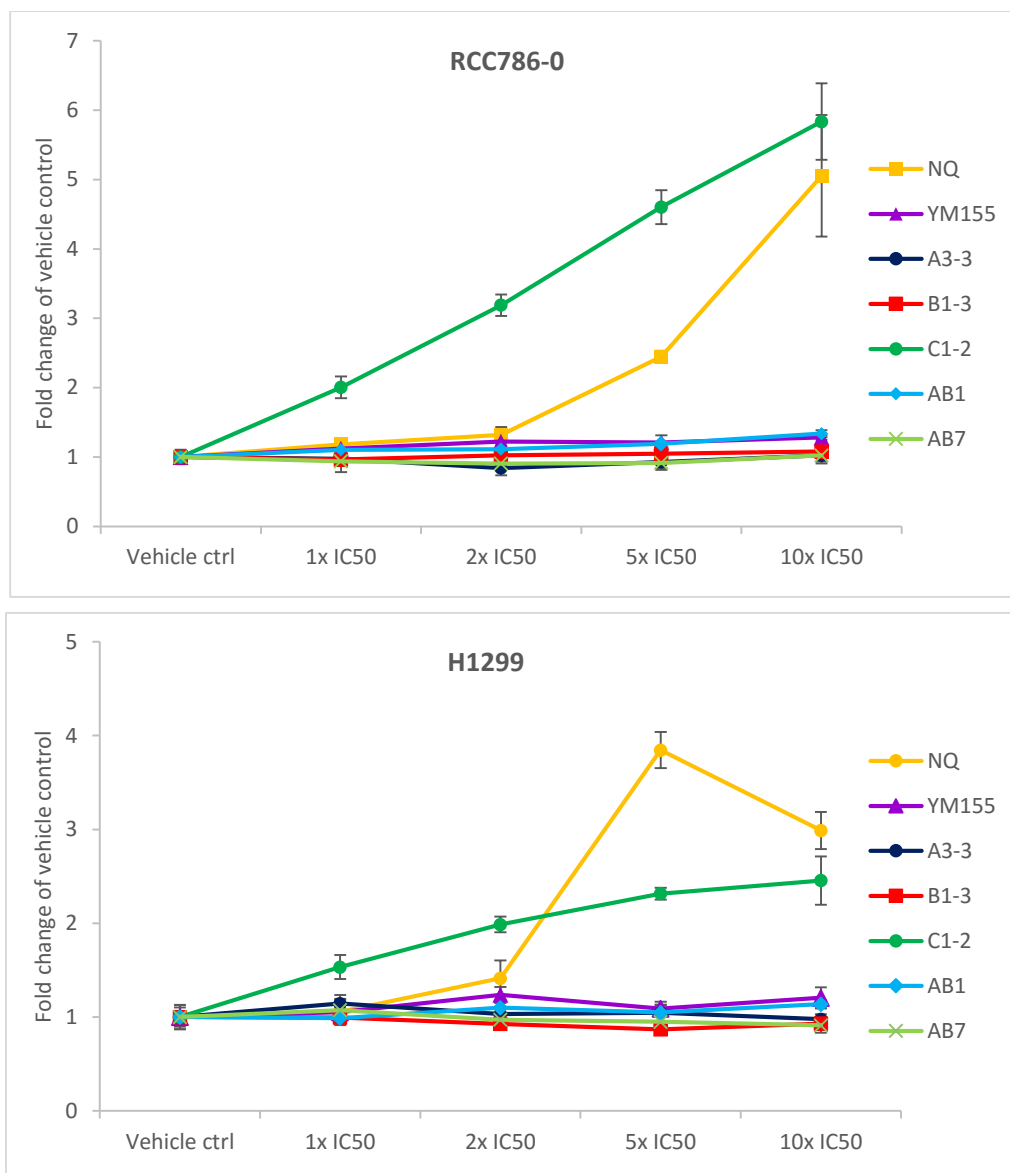
Figure 4.3. Generation of free radicals in RCC786-0 and H1299 cells at different concentrations of test compounds as determined by the fold change in H_2DCF fluorescence.

4.3.3 Correlation between growth inhibition, DNA intercalation and redox cycling

Thus far, growth inhibitory IC_{50} (4 cell lines), DNA intercalation DC_{50} and redox cycling EC_{50} values have been obtained for YM155 and its analogs. SAR has been established for these activities and some recurring trends were observed which may suggest that these activities are correlated. In order to obtain a quantitative assessment, a Spearman correlation analysis was

conducted. As seen in Table 4.2, DC_{50} and EC_{50} values were not significantly correlated to IC_{50} values on all cell lines.

Table 4.2. Spearman correlation of growth inhibitory IC_{50} on malignant cell lines, redox cycling EC_{50} values and DNA intercalation DC_{50} values.[a]

	$IC_{50 \text{ RCC786-0}}$	$IC_{50 \text{ RCC4/VA}}$	$IC_{50 \text{ H1299}}$	$IC_{50 \text{ H1666}}$
EC_{50}	-0.015	-0.02	-0.129	-0.002
DC_{50}	0.311	0.341	0.254	0.304

[a] Only compounds with measurable values were included in the analyses (47 compounds for redox cycling; 46 compounds for DNA intercalation).

4.3.4 Phosphorylation of γH2AX and evidence of apoptosis

Glaros et al have proposed that YM155 intercalates with DNA and induces DNA damage by generating ROS.[55] Evidence of DNA damage was deduced from dose dependent increases in phosphorylated histone H2AX (γH2AX) and phosphorylated KAP1 (pKAP1) which are biomarkers for double strand breaks in DNA.[191, 192] γH2AX levels also increase in response to DNA fragmentation which is a sequel of apoptosis. As such it is necessary to establish if the elevated γH2AX levels in YM155 treated cells is a consequence of DNA damage or DNA fragmentation due to apoptosis. In general, DNA damage is initiated more rapidly than apoptotic cell death. Thus, a time-based experiment in which levels of an apoptotic marker cleaved caspase 3 and γH2AX from treated cells are concurrently monitored, would be informative. If γH2AX is observed earlier than cleaved caspase 3, this would implicate DNA damage as the initiating event, but if cleaved caspase 3 precedes or appears at the same time as γH2AX, then apoptosis may be responsible for the elevated levels of γH2AX.
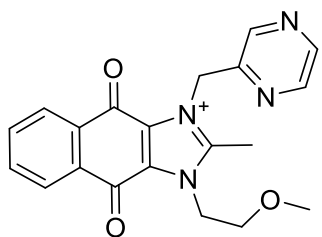
YM155
$IC_{50\ RCC786-0}$ 54 nM
$IC_{50\ H1299}$ 36 nM
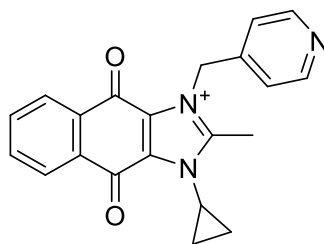
AB1
$IC_{50\ RCC786-0}$ 34 nM
$IC_{50\ H1299}$ 36 nM
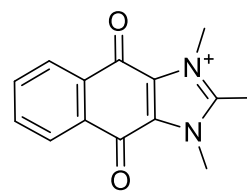
AB7
$IC_{50\ RCC786-0}$ 29 nM
$IC_{50\ H1299}$ 19 nM

RCC786-0 and H1299 cells were treated with YM155, **AB1** and **AB7** at concentrations approximating to their IC_{50} values for 6, 24, 48 and 72 h. Cell lysates were prepared and probed for cleaved caspase 3 and γH2AX by Western blotting. **AB1** (IC_{50} 34 nM) is more potent than YM155 (IC_{50} 54 nM) on RCC786-0 but comparable to it on H1299 (IC_{50} 36 nM for both). **AB7** is more potent than YM155 on both cell lines.

As seen from Figure 4.4, γH2AX and cleaved caspase 3 increased with time on both cell lines. In RCC786-0, γH2AX was detected at 24h in YM155 treated cells and 48 h in **AB1** and **AB7**-treated cells. Cleaved caspase 3 was observed to increase in tandem with γH2AX. In H1299 cells, both γH2AX and cleaved caspase 3 were concurrently detected at 48h (YM155, **AB1, AB7**).
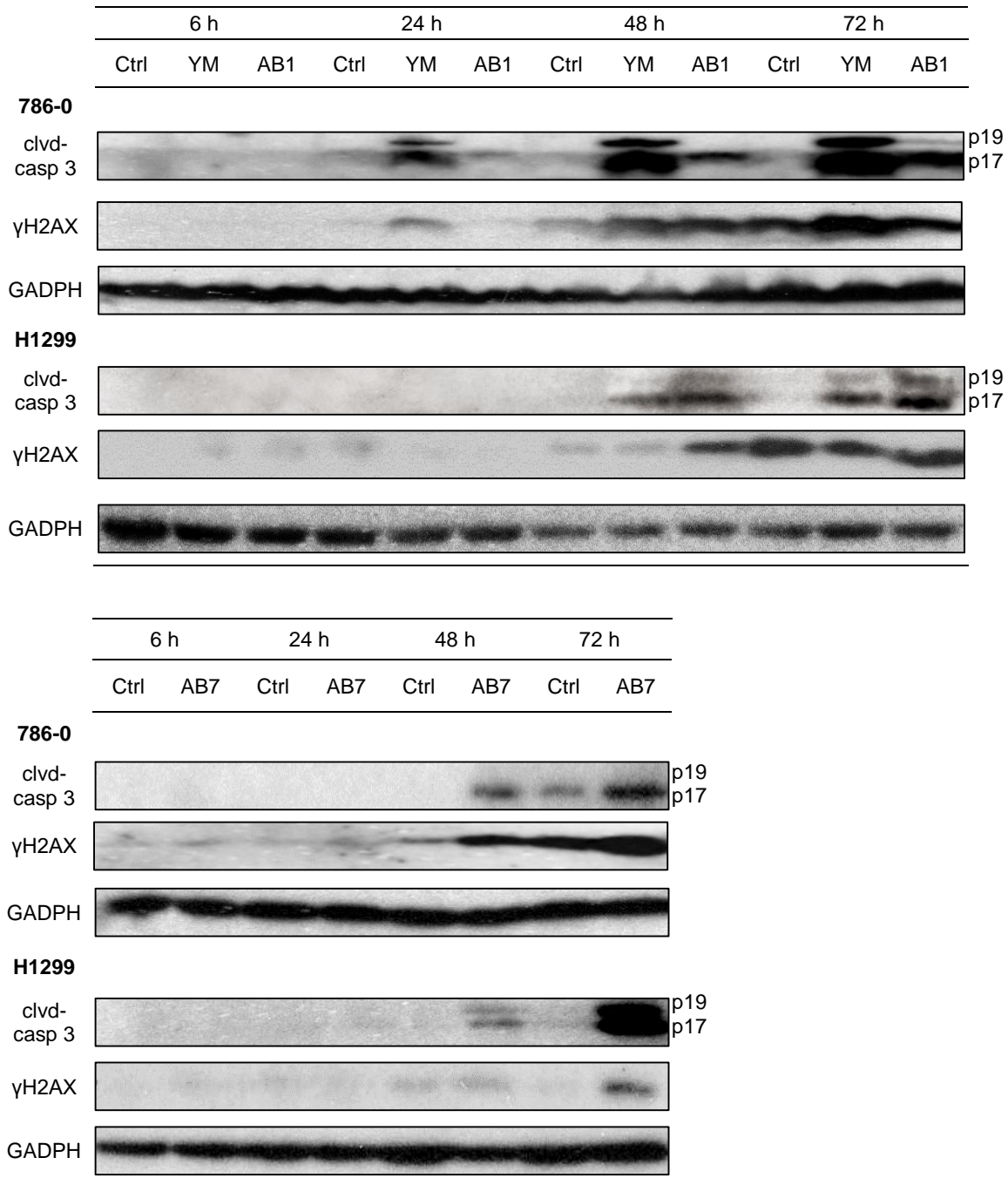
Figure 4.4. Levels of cleaved caspase 3 and γH2AX after 6, 12, 24 72 h treatment of RCC786-0 or H1299 with YM155, **AB1** or **AB7**. Concentrations used were 50 nM (YM155), 37.5 nM (**AB1**) and 30 nM (**AB7**) on 786-0 cells, and 37.5 nM (YM155, **AB1**), and 30 nM (**AB7**) on H1299 cells. The p19 fragment of cleaved caspase 3 is the precursor of p17.[193] GAPDH was used as loading control.

		RCC786-0 – 48 h						H1299 – 48 h					
		YM155			AB1			YM155			AB1		
	C	$\frac{1}{2}$x	1x	2x	$\frac{1}{2}$x	1x	2x	C	$\frac{1}{2}$x	1x	2x	$\frac{1}{2}$x	1x	2x

clvd-casp 3

γH2AX

GAPDH

p19
p17
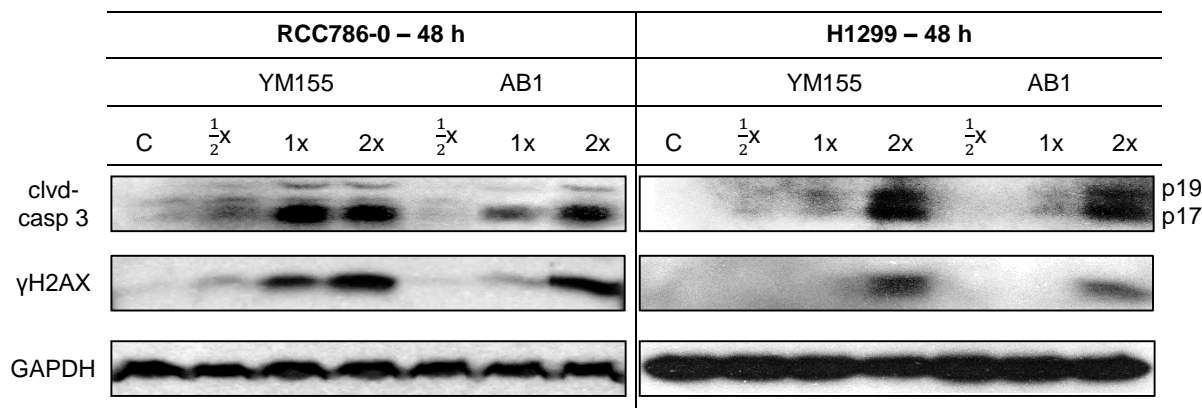
Figure 4.5. YM155 and **AB1** induced concentration dependent increases in γH2AX in RCC786-0 and H1299 cells. Cells were incubated with test compounds at 0.5x, 1x and 2x IC$_{50}$ for 48 h, following which γH2AX and cleaved caspase 3 (p17, p19) levels were probed by immunoblotting. The p19 fragment of cleaved caspase 3 is the precursor of p17. GADPH was used as loading control.

Next, RCC786-0 and H1299 cells were treated with different concentrations (0.5x, 1x, 2x IC$_{50}$) of YM155 and **AB1** at a fixed time point (48 h). Levels of γH2AX and cleaved caspase 3 were then determined. As seen from Figure 4.5, both compounds induced concentration-dependent increases in γH2AX and cleaved caspase 3.

Taken together, YM155, **AB1** and **AB7** induced time-dependent increases in γH2AX levels in both RCC786-0 and H1299 cells. These increases were aligned to increases in cleaved caspase 3 levels. Concentration dependent increases in these markers were also observed in YM155 and **AB1**-treated cells.

4.4   Discussion

Based on the in vitro ThO displacement assay, YM155 is a DNA intercalator. Its binding affinity to DNA is modest compared to doxorubicin. The modifications undertaken in the present series

of compounds failed to significantly improve intercalation although several analogs were found to be comparable or marginally more potent than YM155. The SAR identified the intact dioxonaphthoimidazolium scaffold as an essential feature for DNA intercalation but the relative importance of the different motifs in the scaffold could not be distinguished, as was possible for growth inhibition. Features that promoted intercalation were ring bearing side chains at N^1 and N^3. At N^3, azinylmethyl side chains were permissible. The regioisomeric bias against ortho-substituted azines that was prominently observed for growth inhibition was again apparent for DNA intercalation. At N^1, diverse cyclized moieties (benzyl, pyrazinylmethyl, tetrahydrofurfuryl) and N', N'-disubstituted aminoalkyl side chains which had adversely affected growth inhibition, were acceptable features for DNA intercalation. In fact, aside from the common requirement of an intact scaffold, there were few overlapping structural features for DNA intercalation and growth inhibition. Notably, there was a marked preference for cyclized or bulky substituents at N^1, C^2 and N^3 which was not permitted for growth inhibition. It is noted however that N^1, N^3-dimethyl substituted **AB7** was good for both activities.

In spite of the quinone presence in YM155, the present evidence does not support a strong redox cycling role for YM155. On the *in vitro* assay, YM155 was weaker than naphthoquinone and on the cell-based H_2DCF assay, it failed to generate free radicals under conditions that saw strong responses from naphthoquinone. Limited overlaps were observed in the SAR trends for redox cycling and growth inhibition. First, there is less certainty as to whether the intact scaffold is required for redox cycling or even if the presence of quinone will ensure redox cycling. Cases in point are **C1-2** (no benzene ring) and naphthoquinone (no imidazolium) which are good redox cyclers, and **C4-1** and **C4-2** which are not redox cyclers in spite of a quinone presence. Second, contrary to growth inhibitory requirements, ring bearing groups on N^1 or N^3 (but not small alkyl groups at the same positions) were generally well tolerated for redox cycling. Third,

N^3-azinylmethyl analogs with ortho-nitrogens were surprisingly good redox cyclers, in contrast to their poor growth inhibitory properties.

The question that needs to be addressed in this chapter is whether growth inhibition by functionalized dioxonaphthoimidazoliums and YM155 in particular, is due to DNA damage brought about by intercalation and redox cycling. The present evidence does not unequivocally support this hypothesis.

Firstly, there is limited overlap in the structural requirements for growth inhibition and DNA intercalation/redox cycling. The intact dioxonaphthoimidazolium scaffold is required for growth inhibition and DNA intercalation but is optional for redox cycling. Side chain requirements are also different as highlighted in the preceding paragraphs.

Secondly, YM155, **AB1**, **AB7** and **A3-3** did not generate free radicals on the cell based H$_2$DCF assay, at least not at the concentrations investigated with the sole exception of **C1-2**. YM155, **B1-3** and **C1-2** had comparable redox cycling EC$_{50}$ values (0.7 – 1.4 µM) but only **C1-2** was active on the cell based assay. This discrepancy between the *in vitro* and *in vivo* results is puzzling. A possible reason may be that YM155 and **B1-3** have lower IC$_{50}$ values where at those concentrations, the generation of ROS *in vivo* was insignificant, compared to the significantly higher IC$_{50}$ value (0.58 µM) of **C1-2**.

Third, although YM155 and some of its potent analogs (**AB1**, **AB7**) induced the formation of DNA damage biomarker γH2AX in treated cells, it was detected only after 24 h or longer which is inconsistent with the rapidity of the DNA damage response. There was also a close alignment in the appearance γH2AX and the apoptotic marker cleaved caspase 3. As γH2AX is also formed as a consequence of DNA fragmentation which occurs during apoptosis, one may

question if the detection of γH2AX observed here solely reflected direct DNA damage by the test compounds.

Lastly, a compound that induces DNA damage response or triggers redox cycling would discriminate poorly between malignant and non-malignant cells. Doxorubicin and naphthoquinone are cases in point. Doxorubicin acts primarily by DNA intercalation followed by inhibition of topoisomerase II, and to lesser extent, by generating ROS.[194] As DNA transcription and replication are essential processes in both malignant and non-malignant cells, doxorubicin has a narrow therapeutic window. Naphthoquinone is a redox cycler and the generation of ROS would affect both malignant and non-malignant cells.[195] In the present investigation, the average growth inhibitory IC_{50} values of doxorubicin and naphthoquinone were 103 nM and 6.3 µM (Table 4.3) respectively. Compared to their IC_{50} values on non-malignant IMR-90, they were only 2.4 – 2.6 times more potent on malignant cells. On the other hand, YM155 is more potent (average IC_{50} 34 nM) and more selective (selectivity ratio 9-fold) than doxorubicin and naphthoquinone. Furthermore, the preclinical and clinical experiences with YM155 have been positive. Taken together, this is not a profile one would expect from a compound that induces DNA damage.

Table 4.3. Growth inhibitory IC_{50} values of doxorubicin and naphthoquinone.[a]

	Growth inhibitory IC_{50}, µM				
Compound	RCC786-0	RCC4/VA	H1299	H1666	IMR-90
Doxorubicin	0.0915 ± 0.0135	0.131 ± 0.009	0.145 ± 0.011	0.0439 ± 0.0008	0.213 ± 0.027
Naphthoquinone	6.38 ± 0.13	5.51 ± 0.96	3.42 ± 0.56	9.78 ± 0.56	13.3 ± 2.0

[a] Evaluated by MTT assay, 72h incubation, 37°C, 5% CO_2. Mean ± SD for n = 3 determinations.

It was noted that there are several YM155 analogs (**A5-1**, **B3-X**, **B4-X**, **C1-2**) which are weaker growth inhibitors (0.58 – 8.8 µM), but are comparable or exceed YM155 in terms of DNA intercalation and redox cycling and have poor selectivity ratios (2 to 4-fold). **C1-2** was also active on the cell based H_2DCF assay. Taking this together with the above points, it is conceivable that DNA damage arising from intercalation and redox cycling contribute significantly to the mode of action of these significantly weaker compounds. On the other hand, YM155 and analogs that are more potent and exhibit greater selectivity may act by a mechanism/target that does not involve DNA damage.

4.5   Conclusion

YM155 and its dioxonaphthoimidazolium analogs were modest DNA intercalators, with limited potential as redox cyclers. Thus, their capacity to inflict direct DNA damage by these mechanisms should be reconsidered. While it would be remiss to disregard DNA as a target of YM155 and its potent analogs altogether, its involvement in growth inhibition may not be as significant as originally proposed.

4.6   Experimental

4.6.1   Materials

Media for RCC786-0 and H1299 cells and subculturing conditions were as described in Chapter 3. Herring sperm DNA was obtained from Promega Ptd. Ltd. (Madison, WI, USA). Doxorubicin, naphthoquinone, thiazole orange, phenol red sodium, dithiothreitol, horseradish peroxidase and Cellytic M® buffer were purchased from Sigma-Aldrich (St. Louis, MO, USA). 2', 7'-Dichlorodihydrofluorescein (H_2DCF) diacetate was purchased from Life Technologies Corporation (Carlsbad, CA, USA). Anti-cleaved caspase-3 and anti-γH2AX antibodies were obtained from Cell Signalling Technology Inc. (Danvers, MA, USA) and anti-GADPH antibody was from Santa Cruz Biotechnology Inc. (Santa Cruz, CA, USA). The microplate reader (Tecan

Infinite[TM] M200 Pro) was used to obtain readings. Dose response curves were plotted using GraphPad Prism 5 (San Diego, CA).

4.6.2   Fluorescent intercalator displacement assay

Previously reported methods were followed with modifications.[185, 186] To each well in a black 96-well plate was added 98.5 µL of BPE (biphosphate-phosphate-EDTA) buffer (comprising 6.0 mM Na_2HPO_4, 2.0 mM NaH_2PO_4, 1.0 mM Na_2EDTA; total Na^+ concentration 16.0 mM; pH 7.0) containing 2 mg/mL herring sperm DNA and 1 µL of 10 µM thiazole orange (ThO) in deionised water. The resulting mixture was incubated at room temperature (25°) for 5 min. 0.5 µL of compound (200-fold concentration in DMSO) was added, kept at room temperature for 8 minutes, with agitation (500 rpm on a plate shaker) and fluorescence read at $\lambda_{excitation}$ = 503 nm, $\lambda_{emission}$ = 536 nm on a microplate reader. DMSO per well was kept at 0.5% v/v. Test compound and doxorubicin (positive control) were tested over a range of concentrations in at least 3 separate experiments. The percentage of undisplaced thiazole orange at a specific concentration of test compound was determined from the expression:

% Undisplaced thiazole orange = $RFU_{compound}/RFU_{control}$ x 100%, where $RFU_{compound}$ = fluorescence of test compound and thiazole orange, and $RFU_{control}$ = fluorescence of thiazole orange without test compound. The DC_{50} of test compound (concentration to reduce basal fluorescence of thiazole orange (10 µM) by 50%) was determined by plotting % undisplaced thiazole orange against logarithmic concentration of test compound.

4.6.3   Phenol red-horseradish peroxidase redox cycling assay

Previously reported methods were followed with modifications.[187, 188] 2 µL test compound (200-fold concentration in DMSO), 18 µL Hank's Balanced Salt Solution (HBSS) and 40 µL

dithiothreitol (DTT) solution (2.5 mM in HBSS) were sequentially added to each well in a 96-well clear plate. The contents were shaken for 45 min at 600 rpm on a plate shaker, after which was immediately added 40 µL of horseradish peroxidase-phenol red solution (150 µg/mL horseradish peroxidase, 1 mM phenol red sodium in HBSS) and the plate shaken again for another 10 min at 600 rpm. 15 µL 1M NaOH was added to each well, agitated (1 min) and absorbance readings were read at 610nm on a microplate reader. DMSO content per well was kept at 1% v/v. Test compound and positive control naphthoquinone were tested over a range of concentrations. The absorbance at 610 nm was plotted against logarithmic concentration of test compound from which EC_{50} (concentration required to increase oxidized phenol red absorbance to 50% of maximum value) was determined.

4.6.4   Dichlorodihydrofluorescein (H$_2$DCF) diacetate assay

RCC786-0 and H1299 cells were seeded at 1.0 x 10^4 cells/well and 1.5 x 10^4 cells/well respectively in black-walled, clear-bottom 96-well cell culture plates and incubated for 24 h at 37°C, 5% CO_2 in 100 µL of media. 2 µL H$_2$DCF-diacetate in DMSO was then added to each well to give a final concentration of 20 µM and cells were incubated for another hour. The media was removed by aspiration and replaced by 100 µL of pre-warmed PBS containing test compound and 0.5% v/v of DMSO. After incubation for 2 h, plates were read on a microplate reader at $\lambda_{excitation}$ = 495 nm, $\lambda_{emission}$ = 526 nm. Test compounds were tested at concentrations corresponding to 1x, 2x, 5x and 10x cell-based IC_{50} and fluorescence at each concentration was expressed as fold-change of control fluorescence recorded in untreated cells.

4.6.5   Western blotting

RCC786-0 and H1299 cells were seeded at a cell density of 5.0 x 10^5 cells/plate in 100mm petri dishes (24 h, 37°C, 5% CO_2) containing 5 mL of media. The media was removed by aspiration and replaced by 10 mL of fresh media containing test compound and 0.5% v/v of DMSO. After

incubation for the indicated times (6, 24, 48 or 72 h), cells were harvested and lysed in Cellytic

M® buffer (Sigma-Aldrich, St. Louis, MO, USA). Protein content was assessed by Bradford

assay and subjected to SDS-PAGE. Cells were blocked in 5% non-fat milk and probed with anti-

cleaved caspase 3 or anti-γH2AX antibodies to determine protein levels. Anti-GADPH antibody

was used as a loading control.

Chapter 5: Effects of YM155 and selected analogs on the NF-κB pathway

5.1.   Overview of the NF-κB pathway

The nuclear factor-kappaB (NF-κB) pathway is widely associated with immune response[115], inflammation[196] and the pathogenesis of inflammatory diseases such as asthma, rheumatoid arthritis and inflammatory bowel disease[197]. More recently, it has been implicated in tumorigenesis and cancer.[116, 117] The nuclear factor-kappaB family of transcription factors comprises 5 members or subunits (p65/RelA, p105/50, p100/52, RelB, c-Rel) characterized by a Rel Homology Domain (RHD) which recognizes and binds to the NF-κB response elements (Figure 5.1).[198] RHD is also required for dimerization between NF-κB members and binding to the inhibitor of kappaB (IκB), a specific inhibitory factor that retains the NF-κB dimers in the cytoplasm.[199] p65, Rel-B and c-Rel possess a transactivation domain (TAD) which is absent in p100/52 and p105/50. TAD is required to activate transcription and hence, the upregulation of target genes. NF-κB heterodimers that have TAD in at least one monomeric unit would be able to activate transcription whereas homodimers made up of p50 or p52 which do not have TAD, are thought to suppress transcription.[200] p105 and p100 are precursors of p50 and p52 respectively. They contain ankyrin domains which mask the nuclear localization signals on the subunits and block the ability of dimers to bind to DNA.[201] Cleavage of the ankyrin repeats liberate p50 and p52 which can then translocate to the nucleus and bind to DNA.
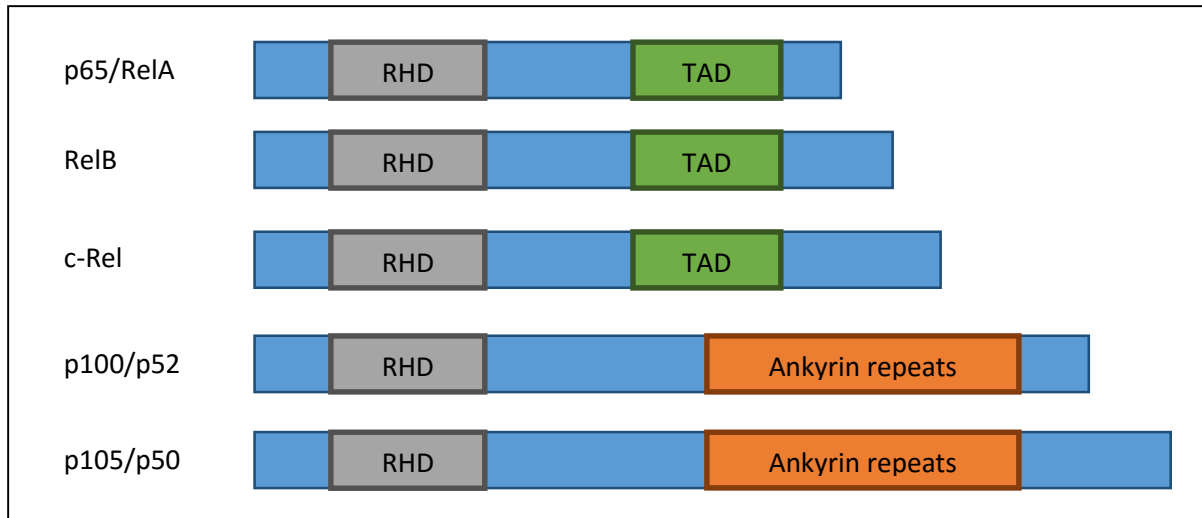
Figure 5.1. Members of the NF-κB family of transcription factors. Members contain a Rel homology domain (RHD) that is required for binding to the consensus sequence GGGPNNPyPyCC (where P is A/G, Py is C/T, and N is any base) on DNA. Only p65, RelB and c-Rel contain transactivation domains (TAD) which are necessary for upregulating NF-κB controlled genes. p52 and p50 are synthesized as the larger p100 and p105 precursor proteins. The ankyrin repeats are cleaved from the C-terminal to give p52 and p50.

There are three pathways which are well characterized in NF-κB signaling. The canonical pathway which was the first to be elucidated, is activated by a variety of cytokines, notably tumor necrosis factor-α (TNF-α). When TNF-α binds to its cognate receptor, various cytosolic proteins such as TRAF2 are recruited and activated.[200] Downstream transduction leads to the phosphorylation and activation of the inhibitor of IκB kinase (IKK) complex which consists of IKKα, IKKβ and IKKγ (NEMO). IκB, which binds to and prevents nuclear translocation of p65 by masking its nuclear localization signal, is then phosphorylated by the active IKK complex and subsequently marked for ubiquitination and proteasomal degradation. p65 is thus liberated and forms a dimer with p50 which translocates to the nucleus where it upregulates various target genes after further phosphorylation events and recruitment of other transcription factors. In contrast, p50 does not undergo a ligand stimulated activation but is constitutively activated

when the ankyrin domains are removed from its precursor p105. It is noteworthy that IκB is also phosphorylated by casein kinase 2 (CK2) besides the IKK complex, typically as a result of DNA damage induced by UV radiation or xenobiotics. This constitutes the atypical pathway.[202]

Figure 5.2. Activation of the NF-κB pathway. (A) In the canonical pathway, activation of the IKK complex leads to phosphorylation of IκB and its eventual proteosomal degradation. p65 is released, dimerizes with p50 and translocates to the nucleus, where it upregulates the transcription of genes with antiapoptotic and anti-inflammatory functions. (B) In the non-

canonical pathway, NIK activation is followed by activation of an IKKα homodimer which then phosphorylates p100 and release of p52 upon p100 cleavage. p52 heterodimerizes with RelB, translocates to the nucleus and upregulates genes responsible for lymphoid organogenesis and B-cell development. (C) The atypical pathway is triggered by DNA damage which activates p38 and CK2 sequentially, leading to phosphorylation of IκB in an IKK independent manner. The subsequent steps converge with the canonical pathway.

The non-canonical pathway involves RelB and p52, with lymphotoxin B receptor (LTBR), CD40 and receptor activator of nuclear factor kappa-B (RANK) as typical upstream receptors. Upon activation by cytokines such as lymphotoxin B and RANK ligand (RANKL), a phosphorylation cascade is triggered starting from NF-κB inducing kinase (NIK), then IKKα homodimer and finally p100 which is then cleaved to produce the active p52 subunit. p52 dimerizes with RelB to form a heterodimer which translocates to the nucleus and upregulates relevant genes. [203]

The non-canonical pathway has been implicated in lymphoid organogenesis and B-cell development and survival. It is also implicated in the carcinogenesis of certain lymphoid malignancies such as multiple myeloma.[203, 204] The canonical pathway has been extensively investigated over the past two decades for its role in inflammation and inflammatory diseases.[205-207] There is increasing evidence that the canonical pathway is constitutively activated in several cancers, [208, 209] although the mechanisms are not well elucidated. Many of the gene products regulated by the canonical pathway are involved in angiogenesis (VEGF)[210, 211], anti-apoptosis (survivin, XIAP, Bcl-2, Bcl-xl, Mcl1)[20, 212-215], metastasis (ICAM-1, VCAM-1)[208] and cell proliferation (cyclin D1)[216]. Some of these targets (survivin, Mcl1) are also affected by YM155.

The involvement of the NF-κB pathway in the tumorigenesis of RCC has been mentioned in Chapter 3. The p65 and p50 subunits have been shown to be overexpressed in several RCC cell lines.[202] In the clinical setting, NF-κB activity was first shown in 2003 to be upregulated in a small cohort of patients where it was noted that 69% of patients with metastatic disease presented with upregulated expression of p50 and p65, along with downregulated IκB.[217] Subsequent studies reported p65 overexpression in at least 70% of patient samples[218] while a meta-analysis revealed that the NF-κB pathway is upregulated in around 40% of RCC cases.[219] Upregulation of NF-κB is also associated with poor prognostic outcomes. The majority of ccRCCs are associated with mutations in the von Hippel Lindau (VHL) tumor suppressor gene. In the absence of a functional VHL, the NF-κB pathway is upregulated through the accumulation of HIF-1[220] and activation of the NF-κB agonist Card9 which is normally suppressed by VHL.[202] Studies have shown that the promoter region of the HIF-α gene contains an NF-κB binding sequence, and HIF-α levels increase when the canonical pathway is stimulated by TNF-α.[220, 221] Even in tumors with functional VHL, NF-κB signalling is constitutively activated.[202, 222] Thus, inhibiting the NF-κB pathway might be viewed as delivering a "one-two punch" on RCC: First by curtailing the production of pro-survival proteins controlled by p65, and secondly by disrupting HIF-induced angiogenesis.

Constitutive activation of the NF-κB pathway in NSCLC was reported earlier than RCC.[223] These and later studies found p50 overexpression in at least 80% of clinical samples.[224, 225] Activation of the NF-κB pathway was associated with poor prognosis and higher mortality, indicating its importance to the tumorigenic process.[226] Evidence from studies performed on NSCLC cell lines confirmed the overexpression of p65 and p50, and current evidence supports the view that the p50 plays a larger role in NSCLC.[227] Although commonly regarded as a repressor, the p50/p50 homodimer may activate transcription upon association with Bcl-3, a member of the IκB family.[228] This association was found to be potentially oncogenic in nasopharyngeal cancer. The

NF-κB pathway also crosstalks with the EGFR pathway and mTOR which is downstream of EGFR is able to phosphorylate IKK complexes, thereby activating the NF-κB pathway.[229] Therefore there is a sound rationale for targeting the NF-κB pathway in NSCLC.

Survivin overexpression has been shown to be a biological sequela of NF-κB activation in several malignancies. NF-κB inhibition in multiple myeloma cells downregulate survivin expression.[230] In adult T cell lymphoma, the viral protein Tax produced by its etiological agent human T lymphotropic virus 1 (HTLV-1) directly activates the survivin gene. An NF-κB binding site on the survivin promoter was required for Tax-induced survivin expression and deletion of this site resulted in a loss of Tax responsiveness.[212] Cross-talk between p53 and NF-κB was reported to modulate survivin expression.[231] In quiescent cells, p53 binds to the survivin promoter to inhibit transcription of the gene but under conditions of replication stress, p53 induces survivin transcription [45, 232, 233] by a mechanism that involves NF-κB. [44] In yet another study on animal xenografts bearing head and neck squamous cell carcinoma cells, the transcription factor inhibitor of differentiation (Id1) upregulated survivin via a NF-κB dependent mechanism.[234]

5.2. Objectives

The preceding discussion has highlighted the tumorigenic role of the NF-κB pathway and the causality between NF-κB signaling and survivin expression. Hence, it is of interest to determine if disruption of NF-κB signaling has a part to play in the suppression of survivin by YM155. As survivin is downstream of many signaling pathways that are constitutively activated in cancer cells, interception of an upstream target by YM155 would result in altered levels of survivin, and possibly other apoptotic proteins as well. Thus it is hypothesized that YM155 disrupts the NF-κB pathway and that this effect contributes to the suppression of survivin and by extension, the cell killing effects of YM155. To this end, the effects of YM155 and a selected analog **AB1** were

investigated on selected proteins and processes in the NF-κB pathway, namely the

phosphorylation of p50 and p65, binding of NF-κB dimers to their consensus elements and

expression of NF-κB controlled genes.

5.3. Results

5.3.1. YM155 and analogs induced apoptotic cell death in RCC786-0 and H1299 cells.

The apoptogenic effects of YM155 have been widely reported and in Chapter 4, it was shown

that its potent analogs (**AB1**, **AB7**) increased levels of the apoptotic protein marker, cleaved

caspase 3. To confirm that apoptosis is the primary mechanism of cell death induced by YM155

analogs, other approaches were employed to investigate this phenomenon.

First, a commercial multiplex assay (ApoTox-Glo™) was used to simultaneously monitor cell

viability, cytotoxicity and apoptotic events in RCC786-0 and H1299 cells treated with YM155,

AB1, **A4-1** and **B2-4**. The growth inhibitory activity of **AB1** was comparable to YM155 but **B2-4**

and **A4-1** were less potent. If these compounds also induced apoptosis, it would support the

notion that this mode of cell death is characteristic of the dioxonaphthoimidazolium scaffold and

applies to analogs with a broad range of potencies. The assay would also report on the

prevalence of necrotic vis-à-vis apoptotic cell death in treated cells.

YM155
IC_{50}(RCC786-0) 54 nM
IC_{50}(H1666) 14 nM

AB1
IC_{50}(RCC786-0) 34 nM
IC_{50}(H1666) 17 nM

A4-1
IC_{50}(RCC786-0) 2900 nM
IC_{50}(H1666) 2800 nM

B2-4
IC_{50}(RCC786-0) 420 nM
IC_{50}(H1666) 150 nM
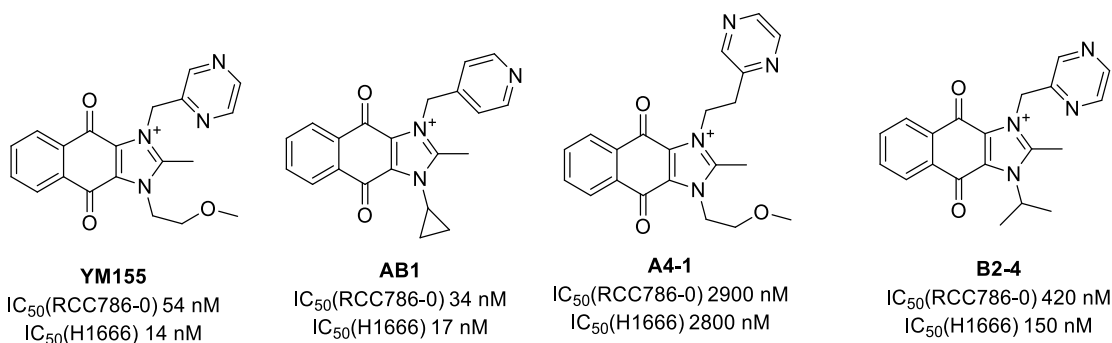
Second, fluorescence-activated cell sorting (FACS) analysis of treated cells double stained with

Annexin V-FITC (fluorescein isothiocyanate) conjugate and propidium iodide (PI) was

undertaken to determine the extent to which apoptosis and necrosis contribute to cell death. Only YM155 and **AB1** were investigated. Third, levels of anti- and pro-apoptotic proteins in treated cells were probed to confirm the occurrence of apoptosis.

5.3.1.1. Multiplex assay for apoptosis

Briefly, viability and cytotoxicity are monitored in the multiplex assay by the activities of two proteases ("live-cell" protease and "dead-cell" protease) on their respective peptide substrates. The substrate for the "live-cell" protease enters intact cells where it is cleaved by the live-cell protease to release a fluorophore which generates a fluorescence signal that is proportional to the number of live cells. When a cell undergoes necrosis, it loses its membrane integrity. Live-cell protease activity will cease and "dead-cell" proteases are released into the surrounding medium and act on a cell-impermeable substrate to generate a different fluorescent signal. If cell viability is found to decrease without a concurrent increase in necrosis (cytotoxicity), then apoptosis, not necrosis, is the major mechanism of cell death. Confirmation of apoptosis is provided by the 3rd component of the multiplex assay which detects the release of caspases 3 and 7. The caspases remove luciferin from a peptide substrate which then reacts with luciferase to generate a luminescence signal proportional to the amount of active caspases.

RCC786-0 and H1299 cells were incubated with YM155, **AB1**, **B2-4** and **AB1** at concentrations of 0.2x to 5x IC$_{50}$ for 48 h before being analyzed on the multiplex assay. The results on RCC786-0 and H1299 cells are given in Figures 5.3 and 5.4 respectively. The test compounds decreased viabilities on both cell lines in a dose dependent manner and 50% viability was observed at concentrations that approximated to IC$_{50}$ values determined on the MTT assay. On the other hand, dose-dependent increases in "dead-cell protease" activity which is a measure of necrosis/cytotoxicity were not consistently observed. Thus, decreases in cell viability were not accompanied by increases in necrotic cell death. On the other hand, dose dependent increases

in caspase activities (except at the highest concentration, possibly due to declining number of viable cells) were observed. These results support the notion that the loss in cell viability was largely due to caspase-mediated apoptosis with negligible contribution from necrotic cell death.

It should be mentioned that to quantify caspase activation, the presence of viable cells at each test concentration was taken into account. This was achieved by dividing the change in caspase induced increase in luminescence (relative to control) by the fluorescence reading attributed to the "live cell" protease (relative to control) to give the "normalized" caspase activation (caspase activity per viable cell) at each concentration.

RCC786-0
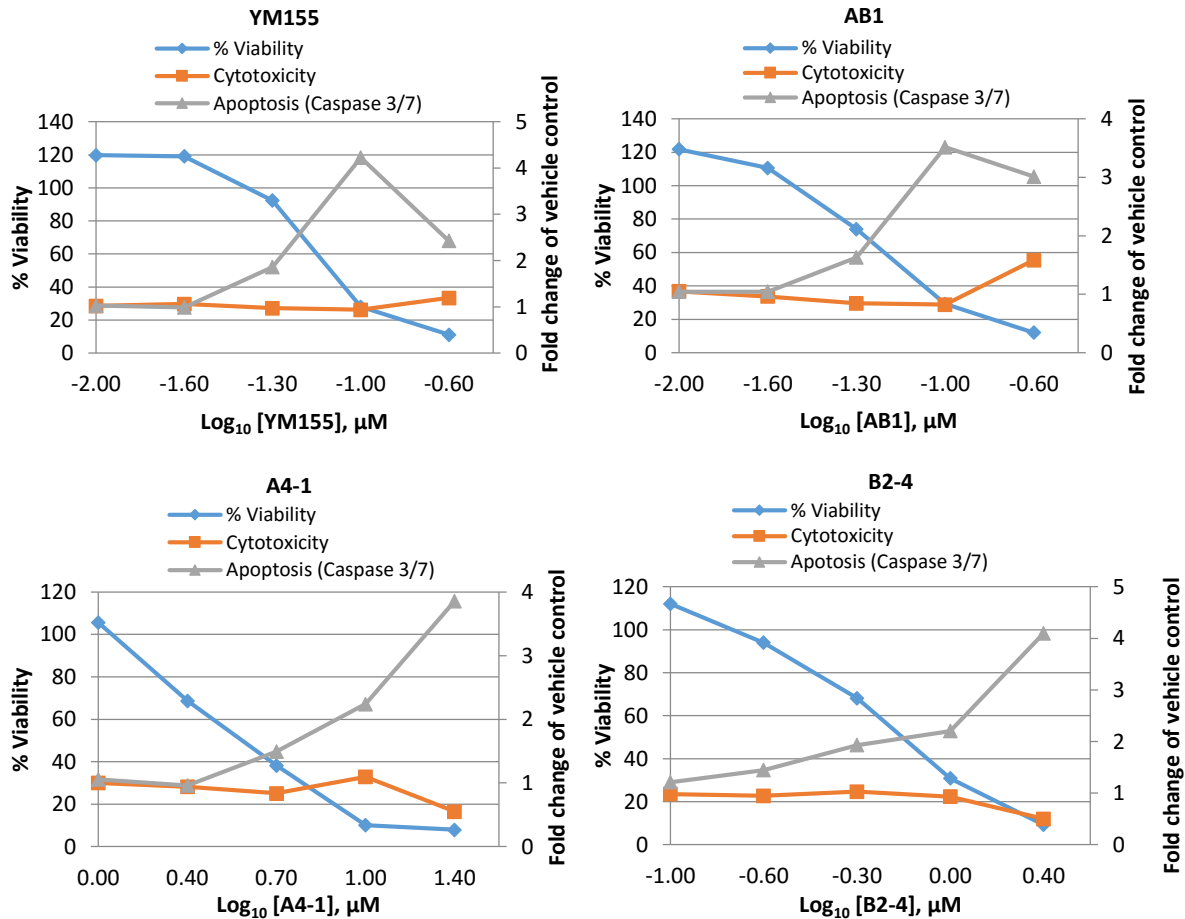
Figure 5.3. Evaluation of YM155, **AB1**, **A4-1** and **B2-4** on cell viability, cytotoxicity and caspases 3 and 7 activation using the multiplex Apotox-Glo™ assay. Compounds were incubated with RCC786-0 cells for 48 h at concentrations ranging from 0.2x to 5x IC$_{50}$ on RCC786-0. Y axis on left hand side monitors % viability while the right hand side axis monitors fold change in cytotoxicity or normalized caspase activation compared to untreated control cells. Normalized caspase activation is the caspase activity per viable cell.

H1299
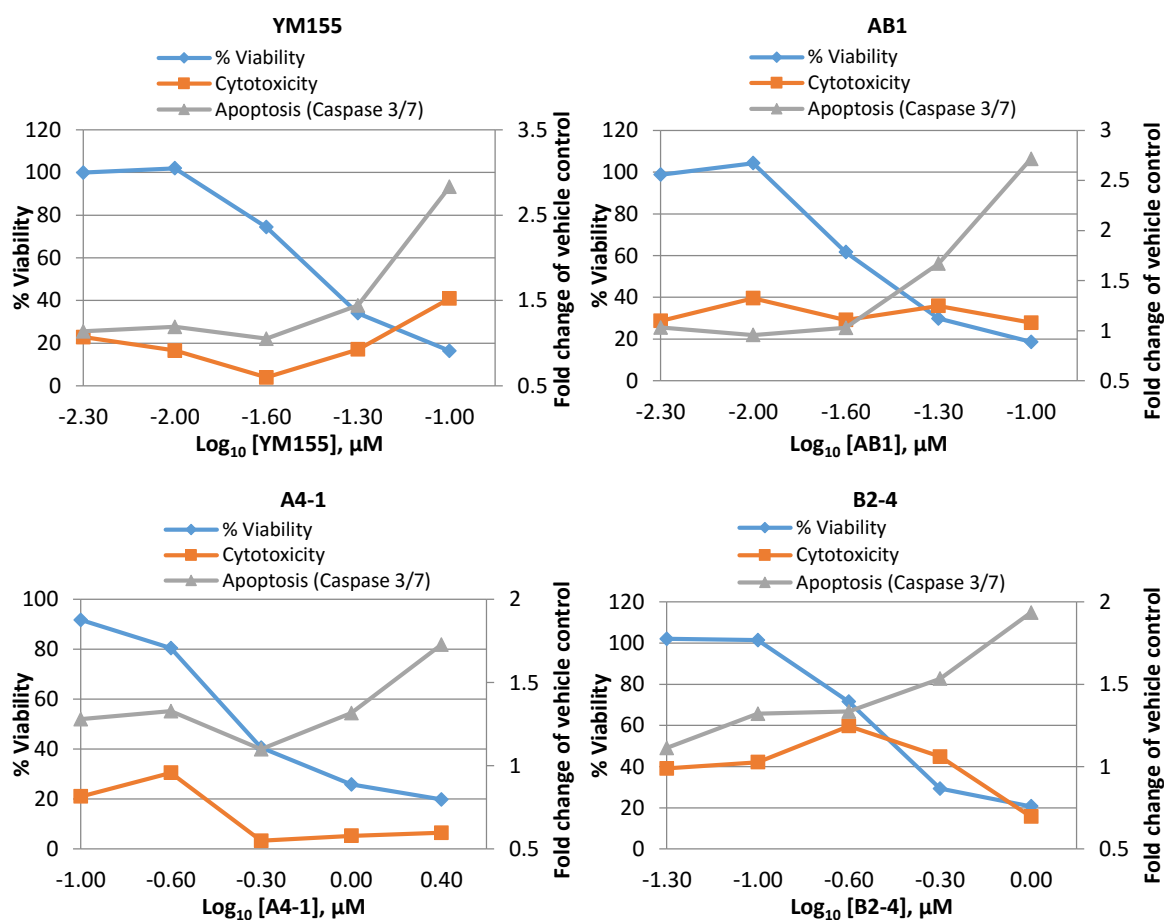
Figure 5.4. Evaluation of YM155, **AB1**, **A4-1** and **B2-4** on cell viability, cytotoxicity and caspases 3 and 7 activation using the multiplex Apotox-Glo™ assay. Compounds were incubated with H1299 cells for 48h at concentrations ranging from 0.2x to 5x IC$_{50}$ on H1299.

5.3.1.2. Annexin V-FITC/Propidium iodide (PI) assay

In the 2nd approach, cells were treated with varying concentrations of YM155 and **AB1** (0.5x, 1x, 2x or 5x IC_{50}) for 24 h or 48 h, double stained with Annexin V-FITC and PI, and subsequently analyzed by FACS. Briefly, the onset of apoptosis is characterized by translocation of phosphatidylserine from the inner to outer surfaces of cell membranes. Once positioned in the outer membrane, the phosphatidylserine residues bind to Annexin V and are detected by the fluorescence of FITC. On the other hand, PI which is a fluorescent DNA intercalator, is excluded from viable cells and only permeates membranes of cells in late apoptosis or necrosis.[235] Thus, apoptotic cells are positively stained by Annexin V but not PI (early apoptosis) or positively stained by both Annexin V and PI (late apoptosis). Necrotic cells are only stained by PI. The distribution of cells in the various phases under the different treatment conditions are shown in Figures 5.5 (RCC786-0) and 5.6 (H1299).

It can be seen that the apoptogenic effects of YM155 and **AB1** were both time and concentration dependent. Stronger and faster responses were elicited on RCC786-0 than H1299 cells suggesting differences in their susceptibilities to the test compounds. For instance, nearly 40% of RCC786-0 cells were found in the early and late apoptotic state after 48 h of exposure to the highest concentration (4x IC_{50}, 250 nM) of YM155 and **AB1**. In comparison, no more than 15% of H1299 cells were found to be apoptotic under similar conditions. Lastly, the compounds did not substantially increase the proportion of necrotic cells, except for YM155 and **AB1** on RCC786-0 cells at 48 h. Even then, the proportion of apoptotic cells exceeded that of necrotic cells for each treatment condition, indicating that apoptosis is the main driver of cell death by **AB1**.
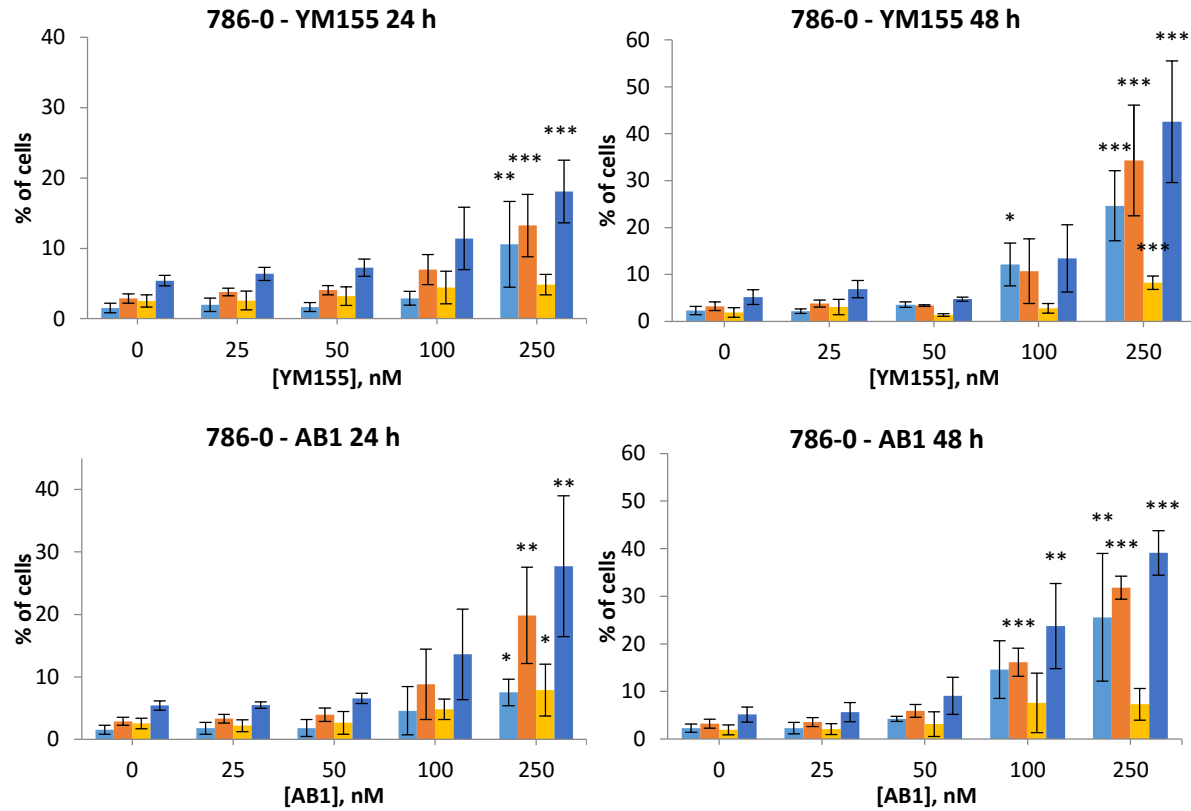
necrosis; **early apoptosis;** **late apoptosis;** **total apoptosis**

Figure 5.5. YM155 and **AB1** induce apoptosis in RCC786-0 cells. Percentage of cells undergoing necrosis and apoptosis when treated with different concentrations of YM155 or **AB1** at 24 and 48 h time points. Error bars represent the standard deviations of three separate experiments. * p < 0.05; ** p < 0.01; *** p < 0.001 (Tukey post-hoc test of respective populations of treated groups vs control).

necrosis; early apoptosis; late apoptosis; total apoptosis
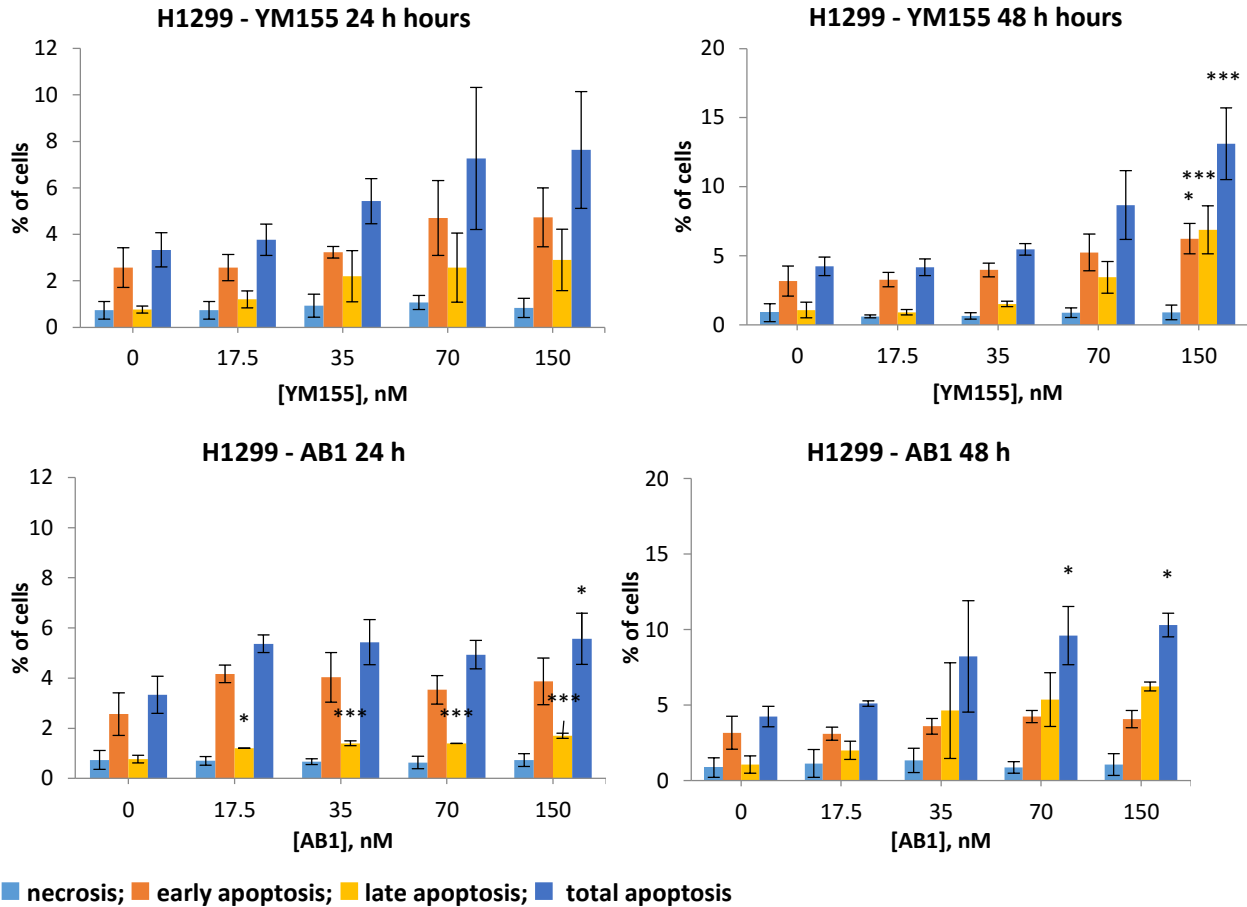
Figure 5.6. YM155 and **AB1** induce apoptosis in H1299 cells. Percentage of cells undergoing necrosis and apoptosis when treated with different concentrations of YM155 or **AB1** at 24 and 48 h time points. Error bars represent the standard deviations of three separate experiments. * p < 0.05; ** p < 0.01; *** p < 0.001 (Tukey post-hoc test of respective populations of treated groups vs control).
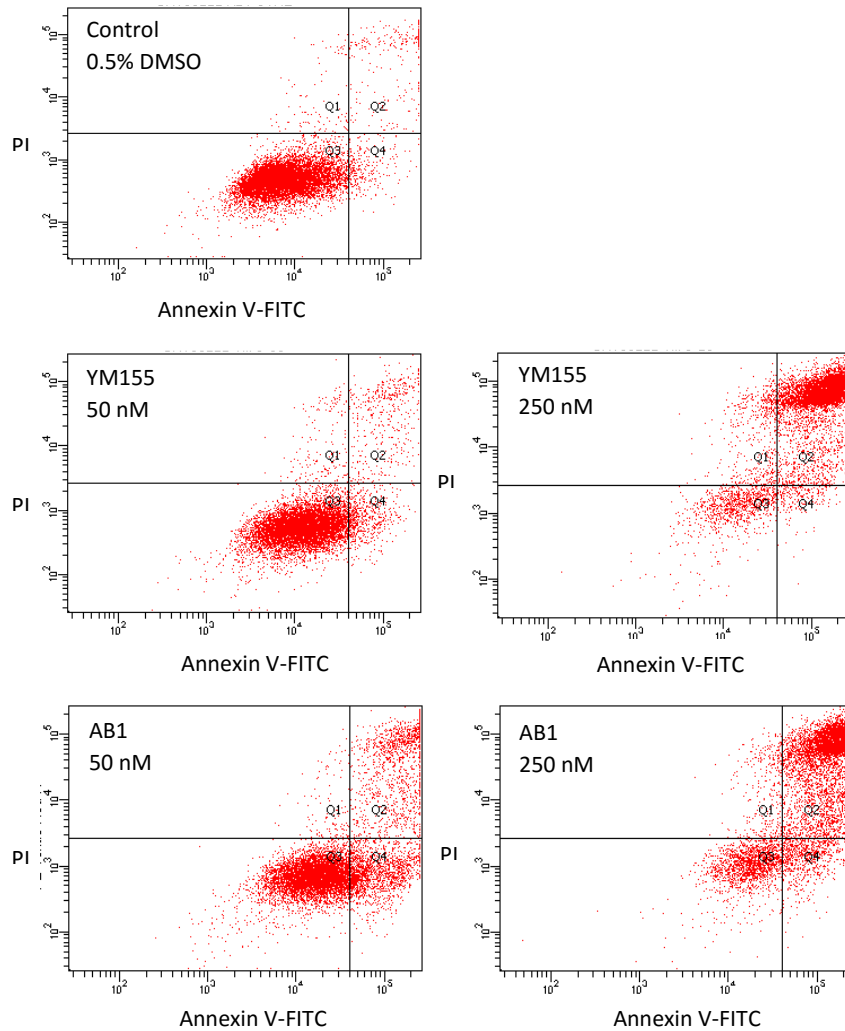
Figure 5.7. Dot plots of Annexin V-FITC fluorescence vs. PI fluorescence for vehicle control, YM155 or **AB1** treated RCC786-0 cells after 48 h incubation. Clockwise from the upper left quadrant of each plot: Q1 (necrotic cells), Q2 (late apoptotic cells), Q4 (early apoptotic cells) and Q3 (healthy cells).
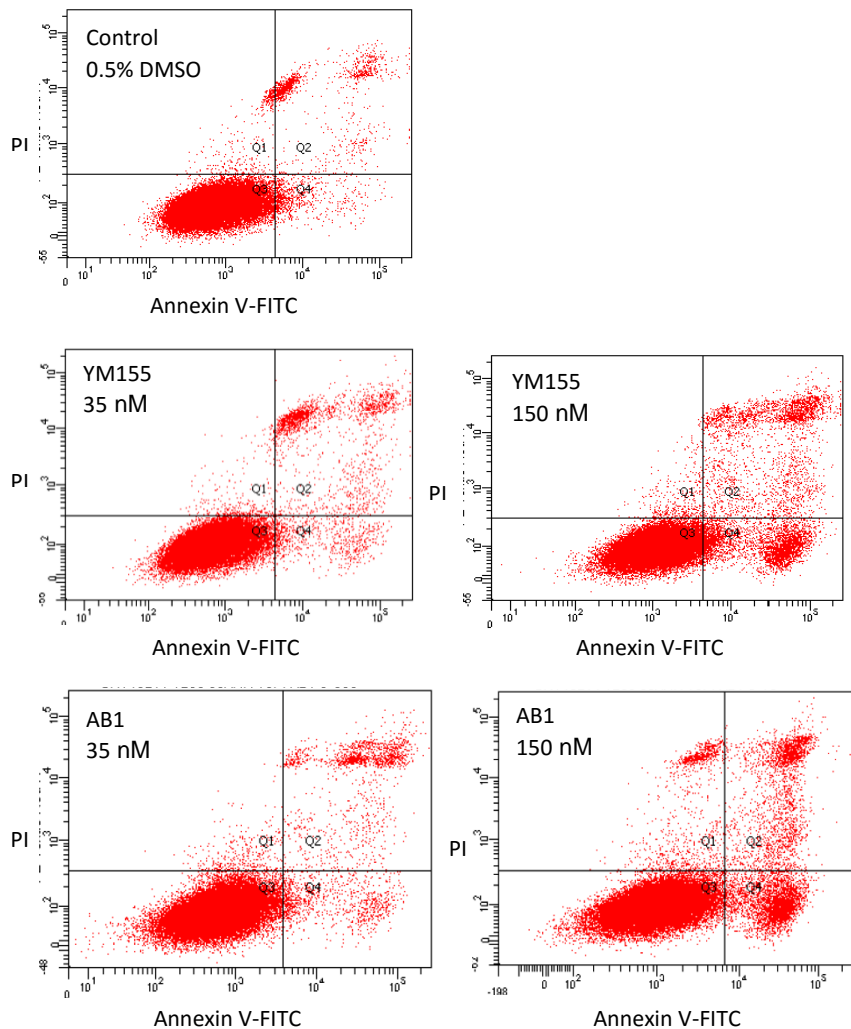
Figure 5.8. Dot plots of Annexin V-FITC fluorescence vs. PI fluorescence for vehicle control, YM155 or **AB1** treated H1299 cells after 48 h incubation. Clockwise from the upper left quadrant of each plot: Q1 (necrotic cells), Q2 (late apoptotic cells), Q4 (early apoptotic cells) and Q3 (healthy cells).

Figures 5.7 and Figure 5.8 depict the dot plots of Annexin V-FITC against PI fluorescence of treated RCC786-0 and H1299 respectively at the 48 h time point (dot plots at 24 h time point are provided in Appendix 2). These plots provide a "kinetic" aspect to the changing proportion of cells in various phases at different concentrations of YM155 and **AB1**. Low concentrations of YM155 and **AB1** caused cells to move towards early apoptosis (Q4) while higher concentrations

saw a progression towards the late stages of apoptosis (Q2). Noticeably, the proportion of necrotic cells (Q1) remained small.

5.3.1.3. Western Blotting

Lastly, levels of cleaved caspase 3, Bcl-2, Mcl1, BAX and survivin were monitored in H1299 and RCC786-0 cells treated at various time points and varying concentrations of YM155 and **AB1**. **AB7** was also investigated in some of these assays. It should be mentioned that γH2AX was monitored concurrently in these blots but are not shown here. As γH2AX levels were probed to assess strand breaks in DNA, they were discussed in Chapter 4 together with cleaved caspase 3. The latter is shown again in Figures 5.9, 5.10 and discussed in the following paragraph as it is an important marker of apoptosis.

Figure 5.9 shows time dependent changes (6, 24, 48, 72 h) in cleaved caspase 3 levels in cells treated with YM155, **AB1** and **AB7** at their respective IC_{50} concentrations. On RCC786-0 cells, cleaved caspase 3 levels were observed early (24 h) in YM155 treated cells but later (48 h) in **AB1** and **AB7** treated cells. However on treated H1299 cells, cleaved caspase 3 was consistently detected at the 48 h time point for all three compounds.

Figure 5.10 shows dose dependent increases in cleaved caspase 3 in cells treated with increasing amounts of YM155 or **AB1** at a fixed time point of 48 h. **AB7** was not investigated. Cleaved caspase 3 levels in both cell lines were detected at a lower concentration (0.5x IC_{50}) of YM155 as compared to **AB1** (IC_{50}). YM155 is likely more apoptogenic than **AB1**.

YM155 and **AB1** were also investigated for their effects on selected anti-apoptotic (survivin, Bcl-2, Mcl1) and pro-apoptotic (BAX) proteins. **AB7** was investigated on survivin only. As in the

case of cleaved caspase 3, the effects of varying incubation times and concentrations were explored.

	6 h			24 h			48 h			72 h		
	C	YM	AB1	C	YM	AB1	C	YM	AB1	C	YM	AB1

786-0

clvd-casp 3		p19
		p17

Bcl-2

Mcl1

BAX

survivin

GAPDH

H1299

clvd-casp 3		p19
		p17

Bcl-2

Mcl1

BAX

survivin

GAPDH
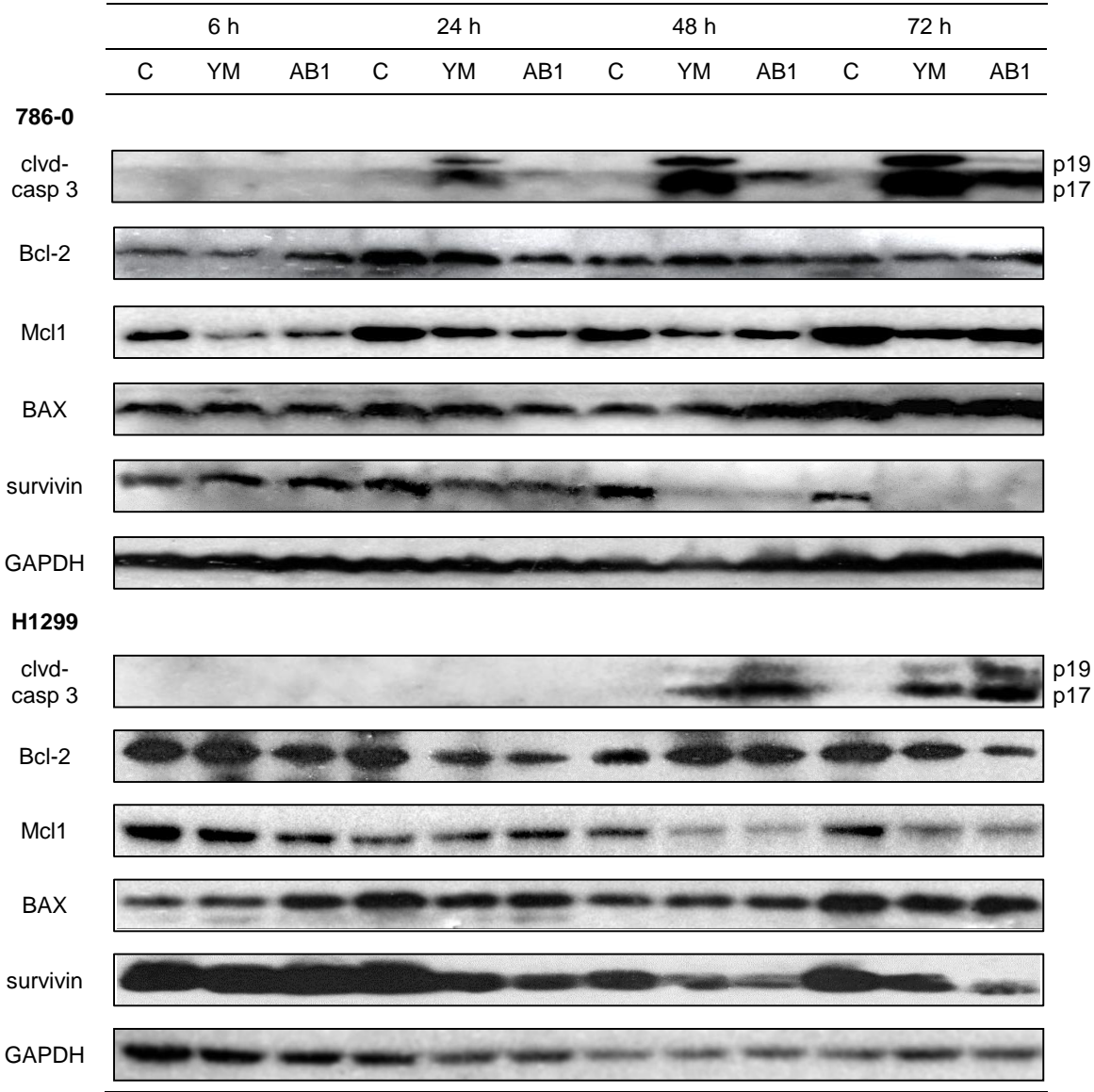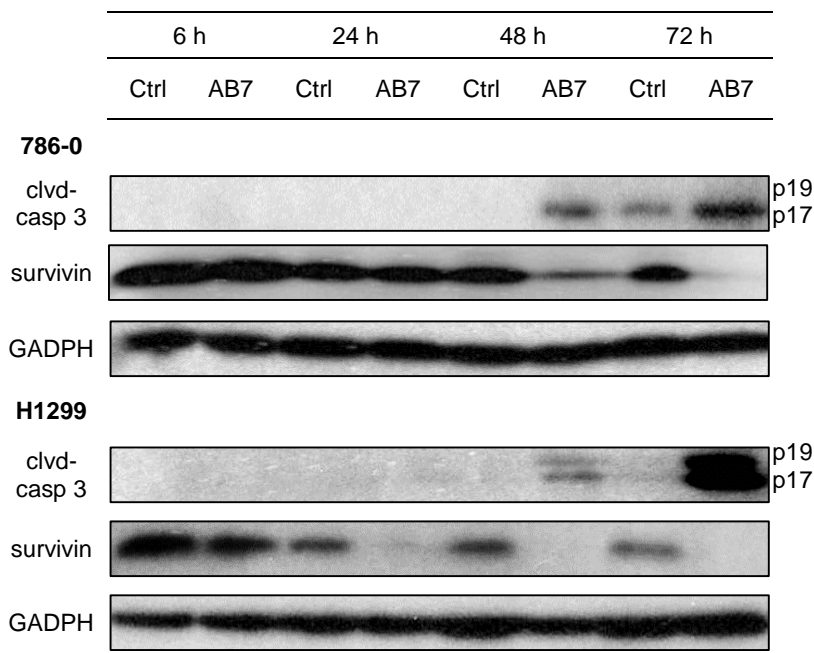
Figure 5.9. Levels of cleaved caspase 3 and other apoptosis-related proteins after 6, 24, 48, 72 h treatment of RCC786-0 or H1299 with YM155, **AB1** or **AB7.** Concentrations used were 50 nM (YM155), 37.5 nM (**AB1**) and 30 nM (**AB7**) on RCC786-0 cells, and 37.5 nM (YM155, **AB1**), and 30 nM (**AB7**) on H1299 cells. GAPDH was used as a loading control.

YM155, **AB1** and **AB7** reduced survivin levels in treated H1299 and RCC786-0 cells. The reductions increased with time and were observed earlier in H1299 cells (24 h) as compared to RCC786-0 cells (48 h). That **AB1** and **AB7** were comparable to YM155 in this regard suggest that side chain modifications at N^1 and N^3 do not affect survivin suppressant activity. YM155 and **AB1** also reduced levels of Mcl1 on both cell lines. The decreases were observed by 6 h in RCC786-0 cells but later (48 h) in H1299 cells. On the other hand, levels of Bcl-2 and BAX remained largely unchanged over time on both cell lines (Figure 5.9).
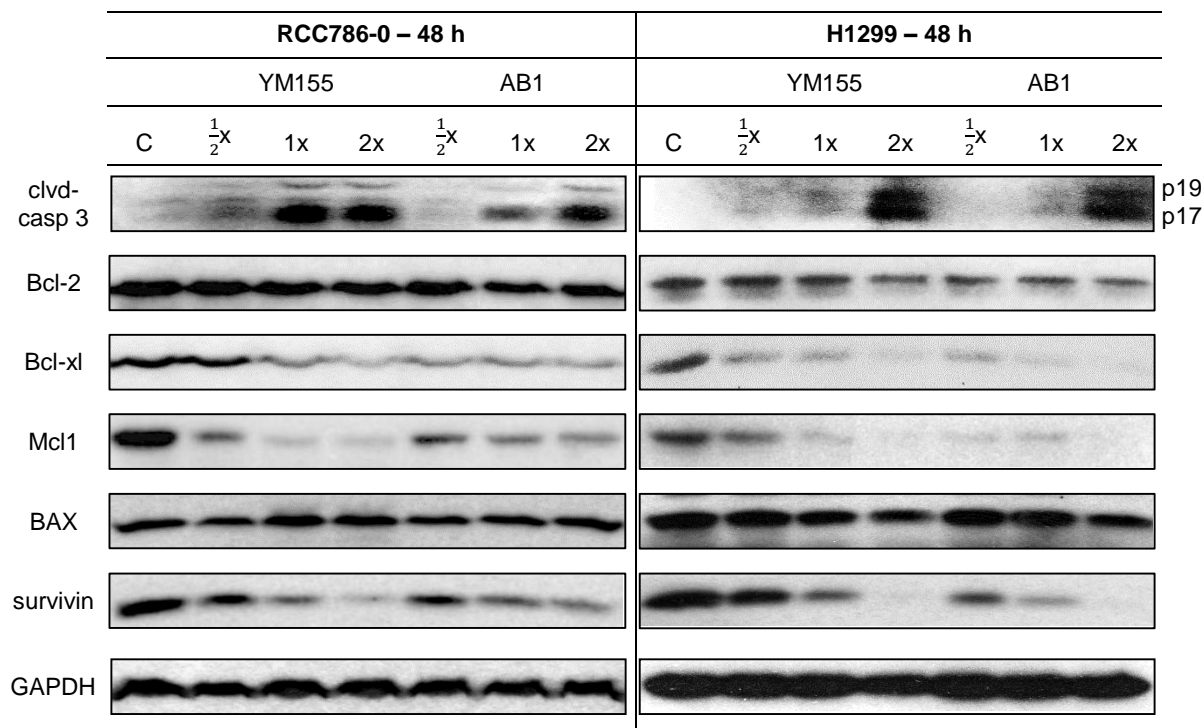
Figure 5.10. Levels of cleaved caspase 3 and other apoptosis-related proteins after 48 h treatment of RCC786-0 or H1299 with YM155 or **AB1** at 0.5x, 1x and 2x IC_{50} (as in Fig 5.9). GAPDH was used as a loading control.

As for YM155 and **AB1**-induced dose dependent changes in the levels of the afore-mentioned proteins, this was only observed for survivin and Mcl1, but not Bcl-2 and BAX (Figure 5.10). Another anti-apoptotic protein Bcl-xl was also probed and YM155 and **AB1** were found to induce dose dependent reductions as well. Based on the concentrations required to initiate reductions in survivin, Mcl1 and Bcl-xl, there are indications that H1299 cells were more susceptible to the test compounds and in particular **AB1**. For instance, **AB1** at 0.5x IC_{50} significantly reduced Mcl1 and Bcl-xl levels in H1299 but not RCC786-0 cells.

In summary, YM155 and **AB1** suppressed survivin, Mcl1 and Bcl-xl on both cell lines. BAX and Bcl-2 levels were not affected by these compounds. The suppression of Mcl1 and Bcl-xl by

YM155 and **AB1** is noteworthy because these proteins regulate apoptosis at the mitochondrial level which is an early event preceding caspase activation. The downregulation of Mcl1 by YM155 has been investigated in some detail and found to occur at the transcriptional level, independent of survivin expression and caspase activity.[49]

5.3.2. Silencing of p65 and p50 affected the viability of RCC786-0 and H1299 cells

Before investigating for effects of YM155 and **AB1** on the NF-κB pathway, it was necessary to assess the importance of this pathway for cell viability and survival. To this end, RCC786-0 and H1299 cells were transfected with p50 and p65 silencing RNAs (siRNA) at 10 nM and 50 nM. Viabilities were assessed after 48 h and 72 h by the MTT assay.

As seen from Figure 5.11, viability was significantly affected by the silencing of the p50 and p65 genes in RCC786-0 cells. The losses increased with time and concentration of the siRNA. On H1299 cells, silencing of the p65 gene caused smaller losses in viability. Even after 72 h, viability was reduced by only 20%, with limited evidence of dose or time dependency. In contrast, greater losses were observed when p50 was silenced. Thus, there is a strong cell line-specific effect with regard to the silencing of these NF-κB subunits and cell viabilities appear to be more greatly affected by the silencing of p50 as compared to p65.

Figure 5.11. (A) Silencing of p50 and p65 leads to loss of cell viability in both RCC786-0 and H1299 cells. Error bars represent the standard deviations of three separate experiments. * p < 0.05; ** p < 0.01; *** p < 0.001 (Tukey post-hoc test of respective populations of siRNA-treated groups vs control). (B) Western blotting showing successful silencing of p50 and p65 in H1299 and RCC786-0 cells 72 h post-transfection. p105 is the precursor form of p50 and is cleaved to give the latter. All siRNA were used at 50 nM for Western blotting. Negative control cells were treated with empty Lipofectamine 3000. Non-targeting siRNA treated cells were treated with siRNA not specific to any known sequences. GAPDH was used as loading control.

5.3.3. YM155 and **AB1** reduced the binding of p50 and p65 to their consensus elements in an in vitro assay.

NF-κB dimers (p50/p65, p50/p50) translocate from cytosol to nucleus where they bind to specific DNA sequences (consensus elements) on the κB sites to initiate gene transcription. To determine if YM155 and **AB1** interfere with the binding of NF-κB dimers to their consensus sequences, an enzyme-linked immunosorbent assay (ELISA) was carried out on a commercially purchased kit. Briefly, the kit comprises biotin-conjugated short oligonucleotide sequences (5'-GGGACTTTCC-3') corresponding to the NF-κB response elements which are immobilized onto 96-well plates coated with streptavidin. Wells are treated with nuclear lysates containing NF-κB units (p50/p65, p50/p50). These bind to the response elements and are detected by anti-p65 or anti-p50 primary antibodies and HRP-linked secondary antibodies. A substrate of HRP is then added which on cleavage, generates a chemiluminescent signal which is proportional to the extent to which the NF-κB dimers are bound to the consensus elements.
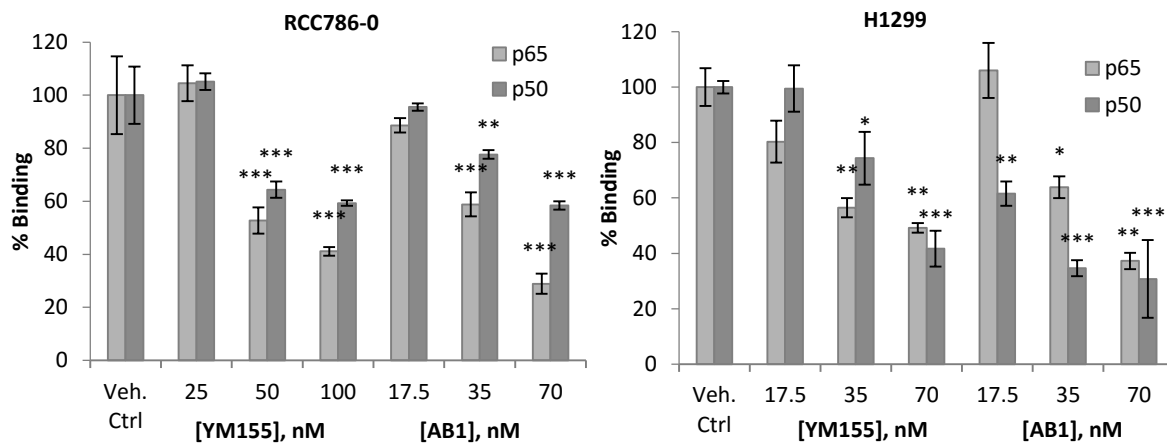
Figure 5.12. YM155 and **AB1** caused losses in the binding of p65 and p50 to the consensus NF-κB response elements. Cells were treated with 0.5x, 1x or 2x growth inhibitory IC_{50} of YM155 or **AB1** for 48 h, nuclear lysates were prepared and tested as described in text. Error bars represent the standard deviations of three separate experiments. Significant statistical difference from vehicle control is indicated as follows: * $p < 0.05$; ** $p < 0.01$; *** $p < 0.001$ (Tukey post-hoc test of respective populations of treated groups vs control).

As seen from Figure 5.12, YM155 and **AB1** reduced the binding of p50 and p65 to their consensus elements in RCC786-0 and H1299 cells. Both compounds caused comparable dose-dependent losses in p65 binding on both cell lines. YM155 also reduced p50 binding in a dose-dependent manner on both cell lines. The losses were broadly aligned to that observed for p65. Interestingly, **AB1** caused steeper losses in p50 binding in H1299 cells as compared to RCC786-0 cells. Notably, significant reductions (~40%) were observed at 0.5x IC_{50} (17.5 nM) of **AB1** in H1299 cells. This level of loss was elicited by 2x IC_{50} of **AB1** (70 nM) in RCC786-0 cells and 2x IC_{50} of YM155 (100 nM) in H1299 cells.

The experiments were repeated in the presence of TNF-α which serves to stimulate the NF-κB pathway.[236] Losses in p50 and p65 binding in YM155- and **AB1**-treated cells were again observed and were particularly pronounced in RCC786-0 cells where p50 and p65 binding were reduced to only 10% at 2x IC_{50} of YM155 and **AB1** (Figure 5.13). Interestingly, the dramatic reduction in p50 binding that was observed earlier in H1299 cells treated with 0.5x IC_{50} **AB1** was not evident in TNF-α stimulated cells.

These results come with the caveat that the diminished binding of p50 and p65 to their consensus sequences may be due to the downregulation of p65 and p50 protein expression by the test compounds. To explore this possibility, p65 and p50 levels in total cell lysates were investigated by Western blotting in the following section.
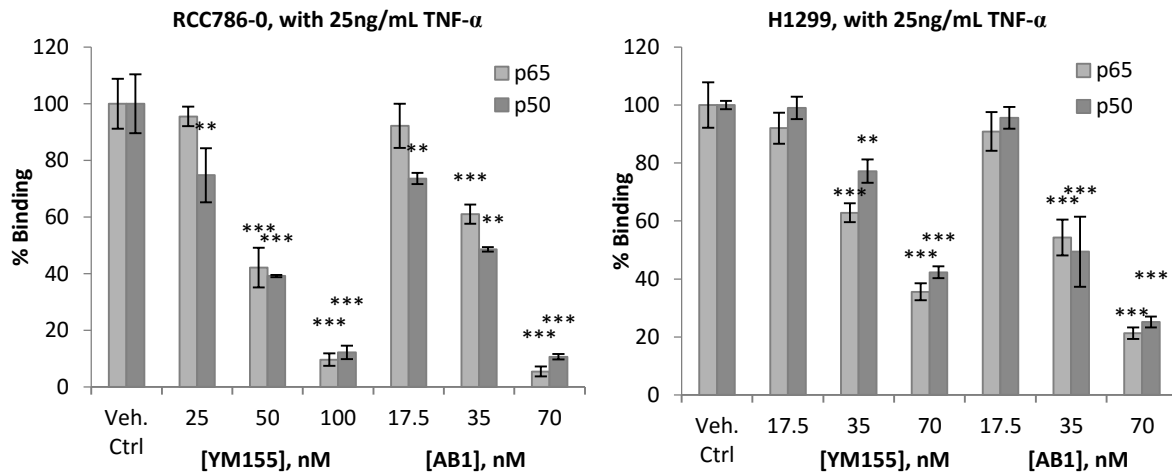
Figure 5.13. YM155 and **AB1** induced losses in binding of p65 and p50 to the consensus NF-κB response element DNA sequence. Cells were treated with 0.5x, 1x or 2x growth inhibitory IC$_{50}$ of YM155 or **AB1** for 48 h in the presence of 25 ng/mL TNF-α. Error bars represent the standard deviations of three separate experiments. Significant statistical difference from vehicle control is indicated as follows: * $p < 0.05$; ** $p < 0.01$; *** $p < 0.001$ (Tukey post-hoc test of respective populations of treated groups vs control).

5.3.4. YM155 and **AB1** inhibit phosphorylation of p50 in H1299 and RCC786-0 cells

RCC786-0 and H1299 cells were treated with a fixed concentration (IC$_{50}$) of YM155 and **AB1** at various time points (6, 24, 48, 72 h) after which lysates were prepared and probed for IκBα, p50, p65 and p105 by western blotting. As mentioned earlier, IκBα is a specific inhibitory factor that retains the NF-κB dimers in the cytoplasm and p105 is the precursor of p50. As seen from Figure 5.14, there was no change in the levels of IκBα, p50, p65 and p105 over time. Neither were there changes when cells were treated with increasing amounts (0.5x IC$_{50}$ to 2x IC$_{50}$) of YM155 and **AB1** for 48h (Figure 5.15).

p50 and p65 are converted to their functionally active states by phosphorylation. Phosphorylation of p65 at Ser536 controls its transcriptional activity while phosphorylation of

p50 at Ser337 regulates DNA binding.[237-239] Hence, levels of phospho-p65 and phospho-p50 were also monitored in treated cells over time (Figure 5.14) and at varying concentrations of YM155 and AB1 (Figure 5.15).
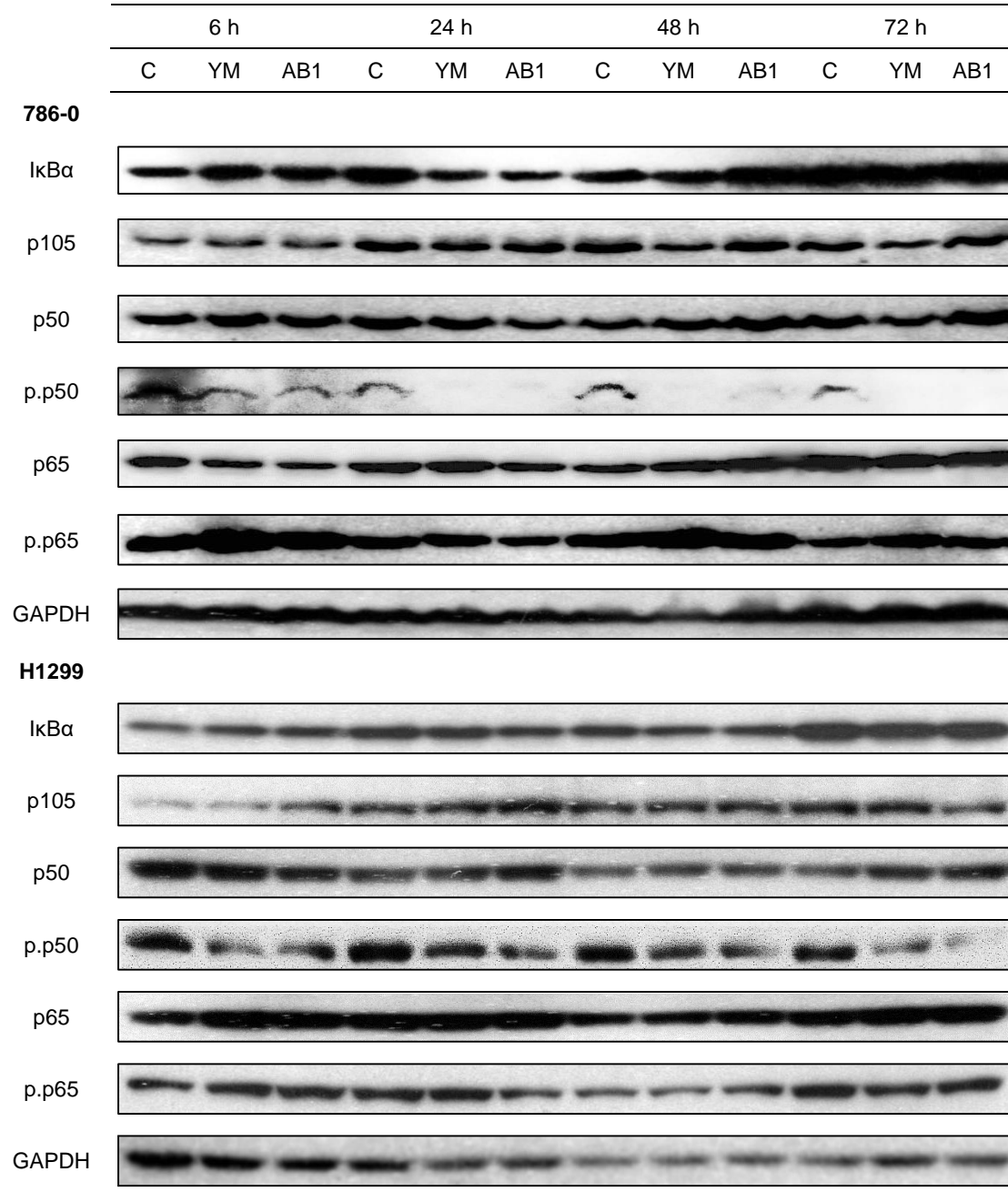
		6 h			24 h			48 h			72 h	
	C	YM	AB1	C	YM	AB1	C	YM	AB1	C	YM	AB1

786-0

IκBα

p105

p50

p.p50

p65

p.p65

GAPDH

H1299

IκBα

p105

p50

p.p50

p65

p.p65

GAPDH

Figure 5.14. Levels of IκBα, NF-κB subunits p50 (p105), p65 and their respective phosphorylated forms (p.p50, p.p65) after 6, 24, 48, 72 h treatment of RCC786-0 or H1299 with

108

YM155 or **AB1.** Concentrations used were 50 nM (YM155) or 37.5 nM (**AB1**) on 786-0 cells, and 37.5 nM (YM155, AB1) on H1299 cells. GAPDH was used as a loading control.

	RCC786-0 – 48h							H1299 – 48h						
		YM155			AB1				YM155			AB1		
	C	$\frac{1}{2}$x	1x	2x	$\frac{1}{2}$x	1x	2x	C	$\frac{1}{2}$x	1x	2x	$\frac{1}{2}$x	1x	2x
IκBα														
p105														
p50														
p.p50														
p65														
p.p65														
GAPDH														
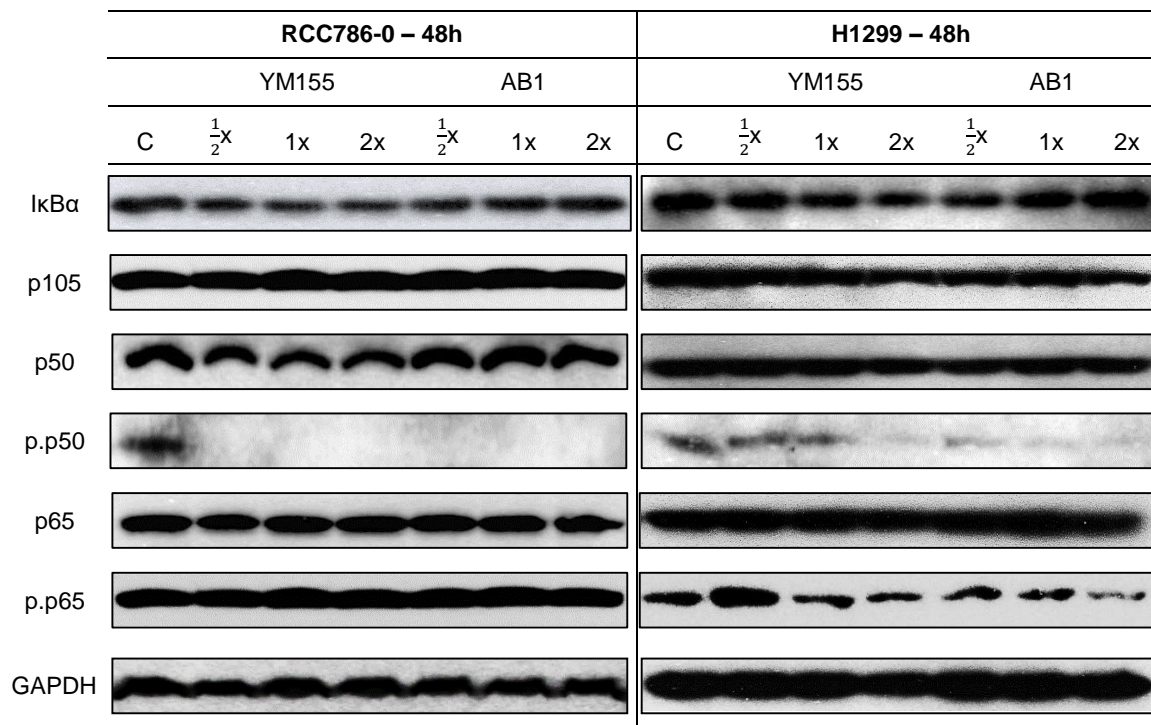
Figure 5.15. Levels of IκBα, NF-κB subunits p50 (p105), p65 and their respective phosphorylated forms (p.p50, p.p65) after 48 h treatment of RCC786-0 or H1299 with YM155 or **AB1** at 0.5x, 1x and 2x IC_{50} (as in Fig 5.14). GAPDH was used as a loading control.

Neither YM155 nor **AB1** reduced phospho-p65 levels in a time-dependent manner. Dose-wise, reductions in phospho-p65 levels were only noted in H1299 cells treated with higher concentrations (2x IC_{50}) of both compounds. This was not observed in RCC786-0 cells where phospho-p65 levels were unchanged.

In contrast, phospho-p50 levels were markedly reduced in YM155/**AB1**-treated cells. Decreases were more pronounced in RCC786-0 cells where hardly any phospho-p50 was detected after 24

h in the treated cells. It was again reinforced in the dose-dependent experiments where stronger responses were elicited from RCC786-0 cells as seen from the lower concentrations (1/2 x IC$_{50}$) of YM155 and **AB1** required to completely suppress phospho-p50 levels as compared to H1299 cells.

From these results, it is deduced that YM155 and **AB1** do not disrupt the expression of IκBα, p65, p50 and its precursor p105 in the NF-κB signalling pathway. That IκBα levels remained unchanged suggests that the NF-κB/IκB complex is not targeted. Rather the compounds intercepted the phosphorylation of p50 which is required for the binding of p50- containing dimers (p50/p65, p50/p50) to their consensus sequences in DNA. On the other hand, phosphorylation of p65 was not impeded by YM155 and **AB1**, pointing to selective targeting of the p50 subunit.

A caveat to these findings is that YM155 and **AB1** could have blocked the translocation of NF-κB dimers from the cytoplasm to the nucleus as this would also result in diminished levels of phospho-p50. To investigate this possibility, lysates from treated cells were separated into nuclear and cytoplasmic fractions and probed for phospho-p50 and phospho-p65 by western blotting.

5.3.5. YM155 and **AB1** selectively suppressed the phosphorylation of p50 in the nuclear
         compartment

Cytoplasmic and nuclear fractions prepared from H1299 and RCC786-0 cells treated with YM155 and **AB1** (IC$_{50}$, 48 h) were separately probed by western blotting for total and phosphorylated p65 and p50. As seen in Figure 5.16, p65 and p50 were found in the cytoplasmic and nuclear compartments of the treated cells and their levels were comparable to that of the untreated controls. Thus, YM155 and **AB1** did not perturb p50 or p65 levels in either

compartment and it is unlikely that they interfere with the translocation of NF-κB dimers

(p50/p65, p50/p50) from cytoplasm to nucleus.

	RCC786-0 – 48 h						H1299 – 48 h					
	Ctrl		YM155		AB1		Ctrl		YM155		AB1	
	cyt	nuc	cyt	nuc	cyt	nuc	cyt	nuc	cyt	nuc	cyt	nuc
p65												
p.p65												
p105												
p50												
p.p50												
lamin B												
α-tubulin												
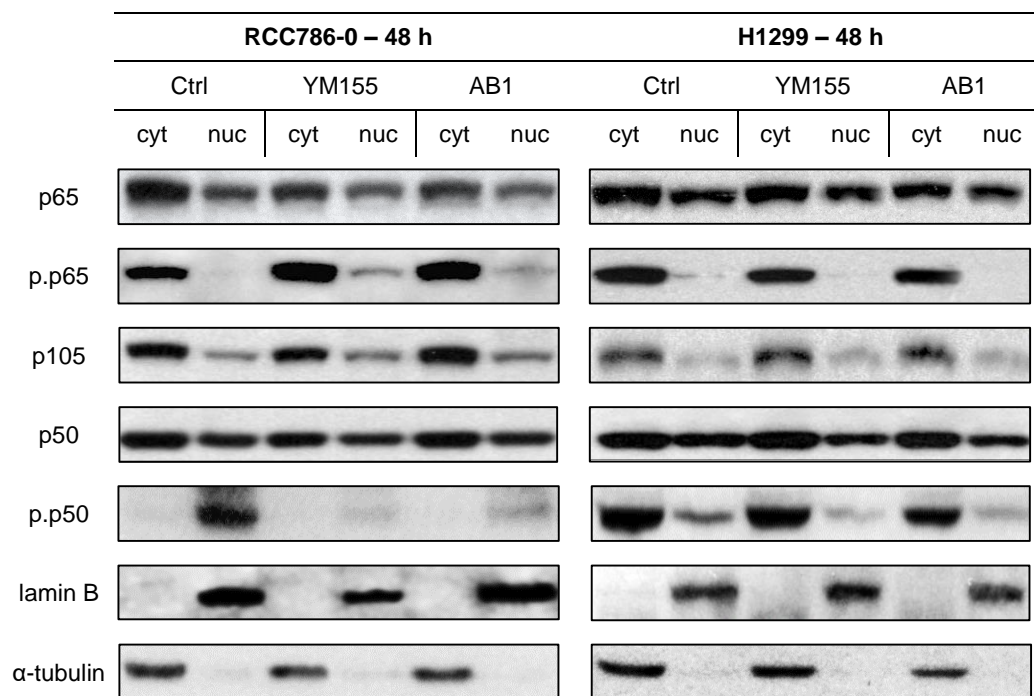
Figure 5.16. Cytoplasmic and nuclear levels of p105, p50, p65 and their phosphorylated forms

(p.p50 and p.p65) after 48 h treatment of RCC786-0 or H1299 with YM155 or **AB1** at ½ x, 1x

and 2x IC_{50} (as in Fig 5.14). Lamin B and α-tubulin were used as loading controls for the nuclear

and cytoplasmic fractions respectively.

Levels of p105, the precursor protein of p50, in the cytoplasm and nuclei of treated cells were

also examined. No change in p105 was observed in the cytoplasm of treated cells which was in

keeping with the unaltered cytoplasmic levels of p50. Although p105 is generally regarded to be

confined to the cytoplasm, traces of it were detected in the nuclei of control H1299 and

RCC786-0 cells, with slightly higher levels in RCC786-0 cells. In any case, p105 levels in the

cytosolic and nuclear fractions were unchanged in the presence of YM155 or **AB1** on both cell

lines.

Next, the distribution of phospho-p50 and phospho-p65 in the cytosol and nuclei of treated cells were examined (Figure 5.16). Phospho-p65 was almost entirely localized in the cytoplasm of untreated cells and the cytoplasmic levels were not reduced in the presence of YM155 or AB1. Curiously, both compounds induced a slight elevation in nuclear levels of phospho-p65 in RCC786-0 cells.

In contrast, phospho-p50 was detected in nuclear extracts of untreated RCC786-0 and H1299 cells. In RCC786-0 cells, phospho-p50 was exclusively localized in the nuclei whereas in H1299 cells it was found in both compartments, with higher levels in the cytoplasm. Exposure to YM155 or **AB1** resulted in significant reductions in nuclear phospho-p50 but minimal changes to cytoplasmic phospho-p50 levels. The reductions in nuclear phospho-p50 were particularly pronounced in RCC786-0 cells as compared to H1299 cells, which were aligned to the observations on the time- and concentration-dependent changes in total phospho-p50 levels.

In summary, the analyses of the cytoplasmic and nuclear contents of phosphorylated p65 and p50 support the notion that YM155 and **AB1** did not block the cytosol to nuclear translocation of NF-κB dimers. The present evidence points to suppressed phosphorylation of nuclear (but not cytoplasmic) p50 at serine 337.

5.3.6. YM155 and **AB1** reduce expression of NF-κB controlled genes

Since the NF-κB subunits act as transcription factors, it was of interest to determine if YM155 and **AB1** inhibited the transcription of NF-κB controlled gene. A luciferase reporter assay was employed in which GloResponse™ NF-κB-RE-*luc2P* HEK293 cells containing a stably transfected luciferase gene controlled by a minimal TATA box promoter with several NF-κB response elements were incubated with increasing amounts (1 – 10 nM) of YM155 and **AB1** for

48h. TNF-α was then added to stimulate the pathway. If transcription was interrupted, a diminished luminescent signal would be detected. Figure 5.17 shows that both compounds reduced NF-κB reporter activity in a dose dependent manner. At low concentrations (2.5 – 5 nM), **AB1** elicited greater reductions than YM155 but at the highest concentration (10 nM), both compounds reduced reporter activity to the same extent. Thus, YM155 and **AB1** attenuated NF-κB transcriptional activity and reduced the expression of NF-κB controlled genes.
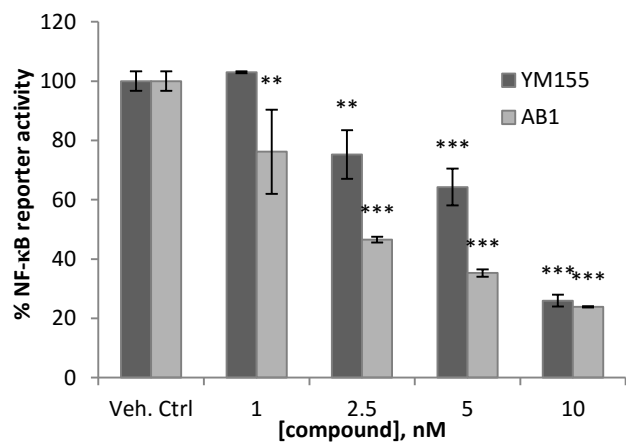
Figure 5.17. NF-κB reporter activity as assessed by HEK293 NF-κB-RE-luc2P cells. Cells were treated with 4 different concentrations of YM155 or **AB1** in addition to vehicle control and incubated for 48 h before assay. Error bars represent the standard deviations of three separate experiments. Significant statistical difference from vehicle control is represented by an asterisk (*) when $p < 0.05$, two asterisks (**) when $p < 0.01$ and three asterisks (***) when $p < 0.001$ (Tukey post-hoc test of respective populations of treated groups vs control).

5.4. Discussion

The objective of this chapter is to investigate if YM155 and a representative potent analog (**AB1**) disrupted the NF-κB pathway in a way that would contribute to the suppression of survivin. To this end, the investigations have revealed a hitherto unrecognized effect of YM155

on the phosphorylation of the p50 subunit of NF-κB. This property was also observed in **AB1**, suggesting that it is common to the functionalized dioxonaphthoimidazolium scaffold.

Both YM155 and **AB1** induced time- and dose-dependent reductions in total phospho-p50 extracted from treated H1299 and RCC786-0 cells. A closer analysis revealed that only the pool of phospho-p50 in the nuclear compartments of treated cells were diminished. Notably, cytoplasmic levels of phospho-p50 (when present) were minimally affected. Intriguingly, p50 levels in the cytosol and nuclei of treated cells were unchanged, implicating a specific effect on the phosphorylation of nuclear p50.

The effects of YM155 and **AB1** were conspicuously limited to the p50 subunit. Neither compound affected p65 or phospho-p65 levels in whole cell lysates nor the cytoplasmic/ nuclear compartments. The unaltered levels of p50 and p65 in the cytosolic and nuclear compartments of treated cells lend support to the notion that the nuclear translocation of the NF-κB dimers was not intercepted by YM155 or **AB1**.

Levels of the inhibitory protein IκBα were also unchanged in treated cells, indicating that the NF-κB/IκB complex and by extension, proteins that lie upstream of IκBα in the NF-κB signaling pathway, were not targeted by YM155 and **AB1**.

Phosphorylation on p50 on serine 337 has been found to be critical for DNA binding[237, 238, 240], and it is conceivable that the inhibition of p50 phosphorylation would compromise the functionality of the p50/p65 and p50/p50 dimers. Indeed, YM155 and **AB1** inhibited the binding of p50 and p65 to the κB consensus sequences and attenuated transcription in the luciferase reporter assay. This would imply a disruption in the transcriptional activities of the NF-κB subunits. Thus, genes activated by p50/p65 would be repressed while those repressed by

p50/p50 would be activated. YM155 and **AB1** were in effect "silencing" the NF-κB pathway and the consequences, as seen from the silencing experiments of p50 and p65 genes, was a significant loss in cell viability.

Notwithstanding, the question remains as to how YM155 and **AB1** suppressed the phosphorylation of p50. Various kinases have been proposed to effect phosphorylation of p50. Guan et al posited that a protein kinase A subunit was responsible for phosphorylating Ser 337 of p50[54] while others have proposed phosphorylation at alternative serine residues in p50 by a DNA-dependent protein kinase, which was necessary not only for DNA binding but transcriptional activity as well.[241] It is conceivable that YM155 and **AB1** inhibited the activities of these or other putative enzymes involved in p50 phosphorylation.

Another question that needs to be addressed relates to how disruption of p50 phosphorylation would affect survivin levels. The survivin gene is activated by many transcription factors, including NF-κB.[44, 45] Previous reports have highlighted that YM155 suppresses survivin by inhibiting the binding of transcription factors ILF3 and Sp1 to the survivin promoter. The present results would implicate NF-κB as another transcription factor that is intercepted by YM155 by inhibiting the phosphorylation of p50. Furthermore, it is tempting to speculate that survivin is not the only protein whose transcription is intercepted by YM155 and **AB1**. Levels of the anti-apoptotic proteins Mcl1 and Bcl-xl were also diminished by both compounds and their reductions could also be due to diminished transcription arising from disrupted p50 phosphorylation. There is literature support to show that Mcl1 and Bcl-xl are controlled in part by the NF-κB pathway.[215, 242]

5.5.   Conclusion

The findings in this chapter have shown that YM155 and **AB1** disrupted the phosphorylation of the p50 subunit which regulates the binding of NF-κB dimers to DNA and transcription of NF-κB controlled genes. These effects were observed in RCC786-0 and H1299 cells at concentrations that were relevant to growth inhibition. Both compounds suppressed phosphorylation of nuclear (not cytoplasmic) p50, obstructed the binding of p50 to its consensus sequence and reduced NF-κB reporter activity in luciferase transfected HEK293 cells. The interception of p50 phosphorylation could have disrupted the transcription of survivin, Mcl1 and Bcl-xl and led to apoptotic cell death. Together these results elucidate a novel mechanism that could account for the potent effects of these dioxonaphthoimidazolium analogs on cell viability.
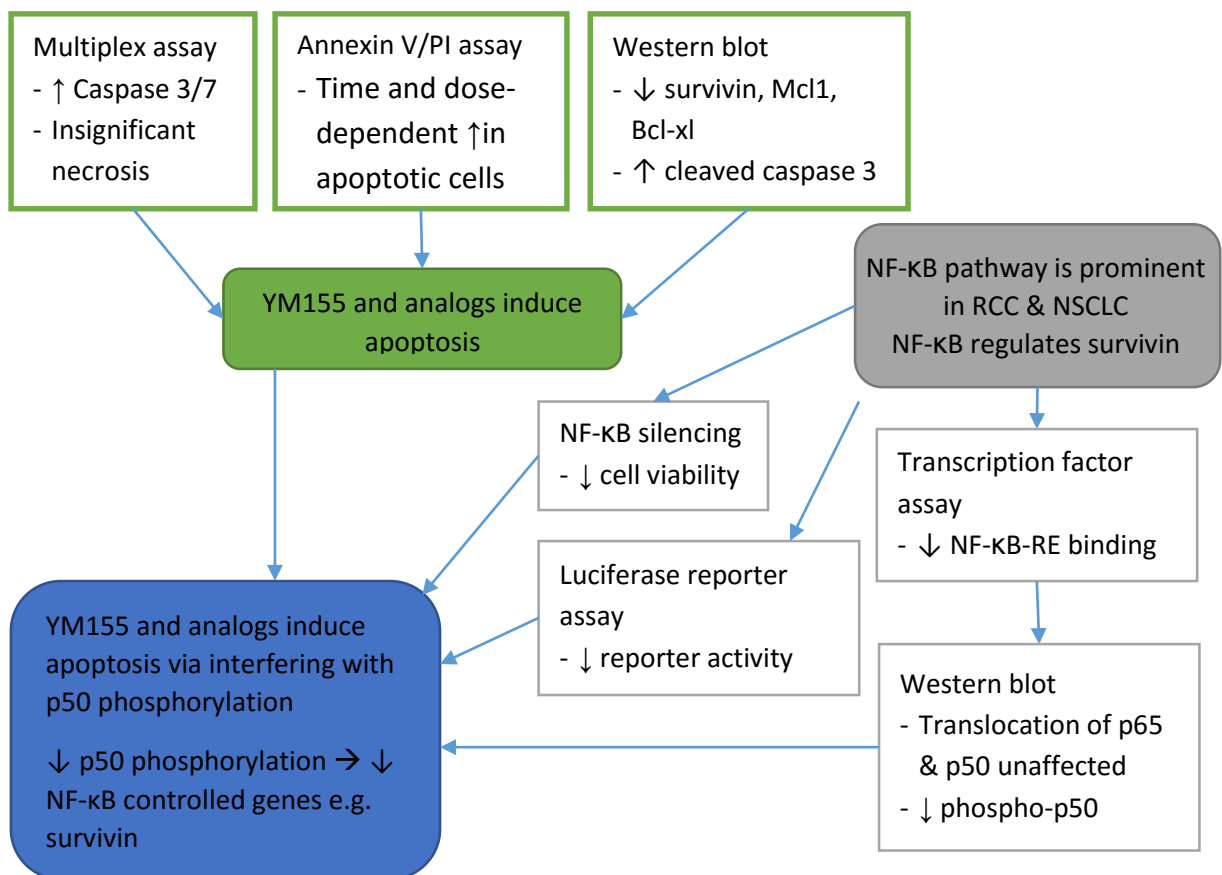
Figure 5.18. Summary of assays, results and conclusions for Chapter 5.

5.6. Experimental

5.6.1. General biology

Cell culture reagents were obtained from sources described in Chapter 3. GloResponse™ NF-κB–RE-*luc2P* HEK293 cells were obtained from Promega (Madison, WI, USA). They were grown in complete DMEM supplemented with 50 µg/mL hygromycin B (Sigma-Aldrich Co., St. Louis, MO, USA). Cells were sub-cultured at a ratio of 1:6 on reaching 90% confluence. Lipofectamine 3000®, TNF-α and ON-TARGETplus® non-targeting siRNAs were obtained from Life Technologies Inc (Carlsbad, CA, USA), Peprotech, (Rocky Hill, NJ, USA) and GE Dharmacon® (Little Chalfont, Buckinghamshire, UK) respectively. The Annexin V-FITC apoptosis detection kit and Cellytic M® buffer were from Sigma-Aldrich (St. Louis, MO, USA). The Pierce transcription factor assay kits for NF-κB p65/p50 and NE-PER® nuclear and cytoplasmic extraction reagents were from Thermo Scientific (Rockford, IL, USA). All antibodies were obtained from Cell Signalling Technology Inc. (Danvers, MA, USA) except for the anti-GADPH antibody which was purchased from Santa Cruz Biotechnology Inc. (Santa Cruz, CA, USA). p50 or p65 siRNA were also obtained from Santa Cruz. ONE-Glo™ Luciferase assay reagent was from Promega (Madison, WI, USA). A Tecan Infinite™ M200 Pro microplate reader was used to obtain fluorescence/luminescence readouts.

5.6.2. ApoTox-Glo™ assay

The commercially available Apotox-Glo™ assay kit was used for the simultaneous determination of compound-induced viability, necrosis and caspase activation in cells. The kit utilized two fluorescent substrates to simultaneously detect viable cells and dead cells and a luminogenic peptide substrate which when cleaved by caspases-3/7 produced a light signal that was indicative of apoptosis. RCC786-0 cells were seeded in black-walled clear-bottom 96-well plates at a density of 3.5×10^3 cells/well and incubated for 24 h at 37°C, 5% CO_2 in 100 µL of

media. The media was removed by aspiration and replaced with 100 µL of fresh media containing test compound and 0.5% v/v DMSO. Control wells comprised the same media without test compound. After incubation for 48 h, the assay was performed according to the manufacturer's instructions. Fluorescence and luminescence were read on a microplate reader and plots of viability, cytotoxicity and caspase activation versus concentration of test compound were generated. Caspase activation readings were normalized against fluorescence readings for viability at the same concentration of test compound in order to take into account cell viability.

5.6.3. Detection of apoptosis

RCC786-0 and H1299 cells were seeded in 6-well plates at a density of 2×10^5 cells/well in 1 mL of media. After 24 h at 37°C, 5% CO_2, the media was removed by aspiration and replaced with 2 mL media containing test compound and 0.5% v/v DMSO. Control wells contained untreated cells. Cells were incubated for another 24 or 48 h after which they were harvested, washed, and resuspended in an Eppendorf tube containing the supplied binding buffer (800 µL). The Annexin V-FITC conjugate and propidium iodide (PI) were added to the cell suspension following manufacturer's instructions, incubated for 10 min, filtered (61 µm filter) and assessed by flow cytometry on the BD LSRFortessa® Cell Analyzer (BD Biosciences, Franklin Lakes, NJ, USA). Results were analyzed on the FACSDiva Version 6.2 (BD Biosciences, Franklin Lakes, NJ, USA) software. Each test compound was evaluated at 5 concentrations with no less than three separate experiments.

5.6.4. p65 and p50 small-interfering RNA (siRNA) transfection

RCC786-0 and H1299 cells were seeded in 96-well plates at 3×10^3 cells/well (100 µL media) or 10mm plates (5×10^5 cells/plate, 5 mL media). After incubation for 24 h (37°C, 5% CO_2), the media was removed by aspiration and cells transfected with p50 or p65 siRNA using

Lipofectamine 3000® following manufacturer's instructions. ON-TARGETplus® non-targeting

siRNAs were used as a negative control. Transfected cells were subjected to either the MTT

assay or Western blotting after 48 or 72 h of incubation.

5.6.5. Transcription factor assay for p65 and p50

RCC786-0 and H1299 cells were seeded in 6-well plates at 2×10^4 cells/well in 1 mL of media.

After 24 h at 37°C, 5% CO_2, the media was removed by aspiration and replaced with 2mL

media containing test compound and 0.5% v/v DMSO with or without 25 ng/mL TNF-α. Control

wells contained untreated cells with or without 25 ng/mL TNF-α. Cells were incubated for

another 24 or 48 h, harvested and lysed with NE-PER® nuclear and cytoplasmic extraction

reagents to give nuclear and cytoplasmic fractions. Protein content of the nuclear fractions were

quantified by Bradford assay. The presence of active p65 or p50 in each fraction was

determined with the Pierce NF-κB p65 or p50 transcription factor assay kits.

5.6.6. Western blotting

RCC786-0 and H1299 cells were seeded at a cell density of 5×10^5 cells/plate in 100mm Petri

dishes (5 mL media per dish) for 24 h at 37°C, 5% CO_2. The media was then removed by

aspiration and replaced with 10 mL of fresh media containing test compound and 0.5% v/v of

DMSO. After incubation for a specified period (6, 24, 48, 72 h), cells were harvested and lysed

in Cellytic M® buffer or NE-PER® nuclear and cytoplasmic extraction reagents. Protein content

of lysates/extracts were assessed by Bradford assay and subjected to SDS-PAGE. After

transferring proteins to PVDF membranes, blocking was performed in 5% non-fat milk and

probed with various primary antibodies to determine protein levels. Anti-GAPDH antibody was

used as a loading control. Bands were visualized with Western Bright ECL substrate from

Advansta Inc. (Menlo Park, CA, USA).

5.6.7. NF-κB-RE *luc2p* reporter assay

GloResponse™ NF-κB-RE *luc2P* HEK293 cells were used to assess the effect of test compounds on NF-κB promoter activity. GloResponse™ HEK293 cells were seeded in white-walled 96-well plates at 3 x 10^4 cells/well in 100 μL of complete DMEM for 24 hours (37°C, 5% CO_2). The media in each well was removed and test compound (100 μL DMEM, 0.5% v/v DMSO) was added. After incubation for 48 h, TNF-α was added to give a final concentration of 20 ng/mL, and incubated for another 5 h. Subsequently, 100 μL of ONE-Glo™ Luciferase assay reagent was added, plates were agitated (350 rpm, 3 min), luminescence was read on a plate reader and normalized against viability at the same concentration of test compound to give % promoter activity of cells.

5.6.8. Statistical analysis

Data were expressed as mean ± standard deviation. One-way analysis of variance (ANOVA) with Tukey post-hoc tests were performed (IBM SPSS Statistics v19.0) for comparison of means and statistical difference. Level of significance was set at $p < 0.05$ unless indicated.

Chapter 6: SAR and mechanistic studies on YM155 as a stem cell clearing agent

6.1.   Introduction

Organ and tissue transplantations have saved millions of lives since their inception, and continue to do so each year especially for end-stage organ failure where they are the only treatment option.[243] Significant advances in surgical techniques and supportive care have propelled the field forward, but shortages in donated organs, a problem exacerbated by the aging population, is a pressing bottleneck. Patients who have received organs face the prospect of life-long immunosuppressant therapy to stave off organ rejection. Immunosuppressants like cyclosporine are associated with several toxicities and may increase the risk of cancers and infections.[244-246]

Regenerative medicine is a viable means of addressing the many limitations of organ transplantation. By growing fresh organs and tissues, the problem of organ shortage is alleviated. Immunocompatibility is further assured if the cells used in generating the desired organs and tissues are from the patient.[247] In this regard, the use of stem cells for regenerative medicine can be said to have revolutionized the field.

Stem cells exhibit the capacity for plasticity which under the correct stimuli, are able to differentiate into a variety of cell types. They also exhibit the ability for self-renewal, that is, replicating without loss of pluripotency.[247] Stem cells may be classified into three main types – embryonic stem (ES) cells, adult/somatic stem cells and induced pluripotent stem (iPS) cells. ES cells possess the greatest plasticity. They are arguably the best known and also the most controversial as they originate from the inner cell mass of the blastocyst.[248] Harvesting these cells invariably destroys the blastocyst, raising ethical objections as it is widely viewed as the start of "life".[249] Indeed, ethical issues concerning ES cells are the main impediment to their deployment in regenerative medicine. Adult stem cells are found in differentiated tissues and

can be used to regenerate these tissues. They are multipotent rather than pluripotent, which means that they can develop into some but not all cell types. This limits their utility in regenerative medicine since organs contains a wide range of cell types. Examples of adult stem cells are those found in the bone marrow which generate blood cells of various lineages,[250] and the stroma which are the source of cells (osteoblasts, chondrocytes, myocytes, adipocytes) in connective tissues.[251, 252] iPS cells were discovered in 2006-2007 when Takahashi and Yamanaka demonstrated that mice and human fibroblasts could be converted to a stem cell-like state by transfection of four transcription factors - Oct4, Sox2, Klf4 and c-Myc.[253, 254] Of these "Yamanaka factors", Klf4 and c-Myc are associated with cancer and indeed, a large proportion of the transformed cells eventually became malignant. Varying the "recipe", in particular replacing one or more of the four factors, particularly Klf4 and c-Myc, with other genes like Nanog, LIN28 provided a partial solution.[255] iPS cells differentiate into cells derived from all 3 germ layers in the embryo and are thus as pluripotent as ES cells. If the original pool of differentiated /somatic cells are derived from the patient, their conversion to iPS cells would overcome the ethical objections and problems with immune incompatibility which plague ES cells. Hence iPS cells are a promising alternative to ES cells for regenerative medicine.

However, one critical hurdle that limits the widespread adoption of stem cells in regenerative medicine is the need to completely eliminate remnant undifferentiated stem cells with teratoma (tumour)-forming potential within the regenerated tissues and organs. A study has shown that as few as ten thousand residual undifferentiated cells were sufficient to trigger tumour formation in immunodeficient mice.[70] Furthermore, many of the pluripotent transcription factors and iPSC reprogramming factors are oncogenes or closely associated with tumour formation.[69]

Consequently, to fully unleash the therapeutic potential of stem cells in the field of regenerative medicine, undifferentiated stem cells must be fully and specifically eradicated from their differentiated counterparts.

Various strategies have been proposed to achieve this end. The simplest would be to extend the time required for differentiation as this would reduce the number of undifferentiated cells. However this approach may be unsuitable for certain applications where the regenerated tissue needs to be transplanted within a certain time frame before over-maturation sets in.[256] Alternatively, monoclonal antibodies may be employed to target a specific antigen (such as podocalyxin-like protein 1, SSEA-4 or TRA-1-60) on the stem cell.[257, 258] When coupled with magnetic or fluorescence activated cell sorting, clearing efficiencies as high as 80% or more have been reported. However, this technique is not readily translated to the clinical setting since properly formed tissues and organs cannot be subjected to cell sorting without incurring considerable losses in viability.

Another approach involves the site specific insertion of a herpes simplex virus 1 thymidine kinase (HSV1-TK) suicide gene at the Oct4 locus of iPSC.[259] As the endogenous Oct4 promoter is only active in undifferentiated cells, the suicide gene will be exclusively propagated in these cells. They can then be selectively removed by an antiviral drug like ganciclovir. However, this approach would further complicate the genetic makeup of the ES cells and may indirectly increase the risk of malignancies.
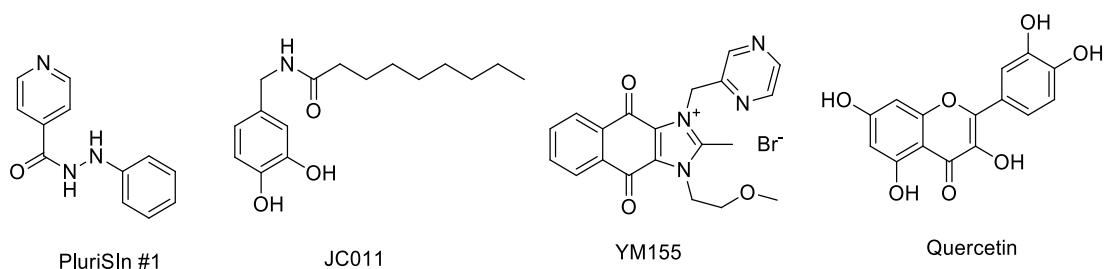
Figure 6.1. Small molecules with ability to clear remnant stem cells.

A relatively simple and cost effective method of eradicating remnant stem cells is the use of small molecules to specifically target rogue undifferentiated stem cells while sparing normal differentiated populations. Several have been reported in the literature (Figure 6.1). The oleate synthesis inhibitor PluriSIn #1 induced ER stress, attenuated protein synthesis and triggered apoptosis in iPSC.[260] Another compound JC011, a structural analog of capsaicin, selectively eliminated iPSC by up-regulating the ER stress response.[261] Lee et al identified quercetin and YM155 as inhibitors of iPSC-derived teratoma formation.[68] Both compounds targeted survivin, and their efficacies reflected the potential of exploiting the unique signature of pro- and anti-apoptotic gene expression in hESC as a means of eradicating teratomas. As mentioned earlier, stem cells express more pro-apoptotic genes than anti-apoptotic genes compared to their differentiated counterparts. Hence, the survival of stem cells is critically dependent on the few resident anti-apoptotic genes, which if inhibited would induce apoptosis of residual undifferentiated stem cells and hence reduce the likelihood of teratoma formation.

YM155 induced apoptosis in ES and iPS cells with an IC_{50} of around 5 nM and eliminated teratomas in animal models.[68] It is not known if YM155 inhibits the stem cell transcription factors responsible for triggering the differentiation process. If it does, it would abolish both the self-renewal and pluripotent characteristics of stem cells. In view of the findings in Chapter 5 where YM155 and **AB1** were found to disrupt the transcription of NF-κB controlled genes and possibly

that of anti-apoptotic proteins survivin, Mcl1 and Bcl-xl by blocking phosphorylation of p50, it is tempting to propose a similar action on the stem cell factors by these compounds.

6.2. Objectives

In this chapter, YM155 and its analogs are investigated for their effects on the viability of embryonal carcinoma (EC) cell lines NCCIT and NTERA-2 with the aim of establishing the SAR for growth inhibition on EC cells and drawing comparisons to the SAR deduced from RCC and NSCLC cells (Chapter 3). Overlapping structural requirements would hint at a similar mode of action by these compounds on these two cell types (stem cells and malignant cells). The 2nd objective is to investigate the effects of YM155 and selected analogs on various stem cell factors (Sox 2, Nanog, Oct4) that are important for maintaining stem cells (ES, EC and an iPS cell line) in their undifferentiated state. A reduction in the transcription or protein expression of Sox2, Nanog or Oct4 would indicate that YM155 and its analogs potentially promote the differentiation of stem cells which would in turn reduce the likelihood of the cells transforming to the malignant phenotype.

6.3. Results

6.3.1. Growth inhibitory activity of YM155 and analogs on EC cell lines

The growth inhibitory activities of YM155 and its analogs (Series A, B, C and AB) were evaluated on two embryonal carcinoma (EC) cell lines NCCIT and NTERA-2. ECs are a rare form of germ cell tumors. They are pluripotent and have similar genetic profiles as ES cells. EC cells are the malignant counterparts of ES cells and widely used as their substitutes.[262-264] They are particularly useful for screening purposes as their growth requirements are comparatively less demanding than those of ES and iPS cells. Table 6.1 lists the growth inhibitory IC_{50} values of YM155 and analogs on these cell lines and the non-malignant IMR-90 cells.

YM155 is more potent on the EC cells (IC_{50} 1.5 – 2.1 nM) than on RCC and NSCLC cells (14 –

54 nM). As for the YM155 analogs, the range of determinable IC_{50} values was 1.99 nM (**A3-3**) to

34.3 µM (**C4-2**) on NCCIT (median IC_{50} 24.2 nM) and 1.49 nM (YM155) to 28.9 µM (**C4-1**) on

NTERA-2 (median IC_{50} 13.8 nM). This translates to approximately 10^4 fold difference in potency,

exceeding that observed on RCC and NSCLC cells where there was only 10^3 fold difference (9

nM to 9 µM) but with higher median values (113 – 633 nM). IC_{50} values from NCCIT and

NTERA-2 were strongly correlated (Spearman correlation coefficient ρ = 0.973) (Table 6.2),

suggesting that the SAR deduced from NCCIT should apply to NTERA-2 and vice versa.

Significant correlations (ρ = 0.83 – 0.87) were also observed between IC_{50} values from EC and

malignant RCC and NSCLC cell lines. Thus, one would expect overlapping structural

requirements EC and malignant cells.

Table 6.1. Growth inhibitory IC_{50} values of YM155 and synthesized analogs on EC cell lines and

IMR-90.

Compound	Growth Inhibitory IC_{50}, nM[a]			Average selectivity ratio [b]
	NCCIT	NTERA-2	IMR-90	
YM155	2.09 ± 0.07	1.49 ± 0.08	247 ± 37	142
A1-1	43.7 ± 3.2	31.9 ± 3.9	1160 ± 70	31.4
A1-2	75.6 ± 11.8	30.8 ± 3.4	5270 ± 960	120
A1-3	53.6 ± 1.5	44.2 ± 7.3	1450 ± 50	29.9
A2-1	76.6 ± 8.6	71.6 ± 1.5	2010 ± 110	27.2
A3-1	19.7 ± 3.3	13.8 ± 1.0	2520 ± 110	155
A3-2	5.46 ± 0.32	3.79 ± 0.55	611 ± 44	137
A3-3	1.99 ± 0.26	1.55 ± 0.15	176 ± 9	101
A3-4	25.7 ± 4.7	9.36 ± 1.83	3180 ± 40	232
A3-5	2.23 ± 0.11	1.98 ± 0.40	205 ± 14	97.7
A3-6	6.22 ± 0.58	4.62 ± 0.22	276 ± 27	52.1
A3-7	5.51 ± 0.99	3.63 ± 0.43	187 ± 12	42.7

Compound	Growth Inhibitory IC$_{50}$, nM[a]			Average selectivity ratio [b]
	NCCIT	NTERA-2	IMR-90	
A3-8	20.6 ± 1.98	10.6 ± 0.8	2000 ± 130	143
A4-1	104 ± 8	52.0 ± 2.4	2810 ± 520	40.5
A5-1	2411 ± 175	2803 ± 506	8820 ± 1210	3.40
A6-1	17.8 ± 1.94	13.2 ± 0.9	743 ± 89	49.0
A6-2	26.2 ± 0.9	12.3 ± 1.6	345 ± 38	20.6
A6-3	22.2 ± 2.2	12.9 ± 1.5	1230 ± 130	75.4
A6-4	24.2 ± 3.5	16.4 ± 3	1720 ± 83	88.0
A6-5	60.3 ± 2.8	35.3 ± 5.9	3890 ± 290	87.3
A6-6	24.0 ± 0.6	12.0 ± 2.3	1160 ± 140	72.5
A6-7	45.1 ± 4.0	17.3 ± 1.0	2640 ± 540	106
A6-8	57.1 ± 7.0	23.2 ± 3.7	6790 ± 290	206
B1-1	25.6 ± 2.8	21.1 ± 3.3	2480 ± 320	107
B1-2	188 ± 9	56.4 ± 9.6	9890 ± 170	114
B1-3	21.9 ± 1.04	13.8 ± 0.7	1430 ± 260	84.5
B2-1	13.8 ± 1.8	7.62 ± 1.37	582 ± 89	59
B2-2	8.86 ± 0.85	3.63 ± 0.56	480 ± 22	93.2
B2-3	5.71 ± 0.82	3.45 ± 0.67	565 ± 27	131
B2-4	20.9 ± 2.1	13.5 ± 2.8	1420 ± 150	86.7
B2-5	4.88 ± 0.57	1.99 ± 0.30	213 ± 20	75.3
B2-6	10.2 ± 1.1	4.69 ± 0.26	1620 ± 140	252
B2-7	48.4 ± 1.4	31.4 ± 2.9	7970 ± 180	209
B2-8	158 ± 3	109 ± 23	6580 ± 180	50.6
B3-1	149 ± 5	105 ± 14	5610 ± 380	45.5
B3-2	59.1 ± 5.7	19.0 ± 1.8	3570 ± 710	124
B4-1	501 ± 90	512 ± 30	7420 ± 760	14.6
B4-2	1364 ± 71	919 ± 74	3730 ± 110	3.40
C1-1	34.8 ± 1.9	19.6 ± 2.0	1900 ± 110	75.8
C1-2	441 ± 32	318 ± 20	1360 ± 150	3.68
C2-1	>100 µM	>100 µM	>100 µM	-

Compound	Growth Inhibitory IC$_{50}$, nM[a]			Average selectivity ratio [b]
	NCCIT	NTERA-2	IMR-90	
C2-2	>100 µM	>100 µM	>100 µM	-
C2-3	>100 µM	>100 µM	>100 µM	-
C3-1	>100 µM	>100 µM	>100 µM	-
C3-2	>100 µM	>100 µM	>100 µM	-
C4-1	24000 ± 1000	28900 ± 3400	55400 ± 4600	2.11
C4-2	34300 ± 5700	8290 ± 1190	73000 ± 4500	5.47
AB1	2.46 ± 0.20	2.56 ± 0.25	287 ± 59	115
AB2	7.61 ± 1.03	4.44 ± 0.35	310 ± 51	55.3
AB3	40.5 ± 2.4	34.6 ± 0.8	649 ± 79	17.4
AB4	20.1 ± 2.1	15.2 ± 0.9	440 ± 7	25.4
AB5	10.4 ± 1.4	9.15 ± 0.92	484 ± 64	49.7
AB6	8.38 ± 0.54	5.72 ± 0.48	475 ± 91	69.9
AB7	24.2 ± 2.0	6.08 ± 0.60	159 ± 16	16.4

[a] Evaluated by MTT assay, 72 h incubation, 37ºC, 5% CO_2. Mean ± SD for n = 3 determinations;

[b] Mean of IC$_{50\ IMR-90}$ / IC$_{50\ EC\ cell\ line}$.

Table 6.2. Spearman correlation matrix of ρ values derived from IC$_{50}$ values of test compounds on EC (NCCIT, NTERA-2), ccRCC (RCC786-0, RCC4/VA) and NSCLC (H1299, H1666) cell lines.[a]

	NCCIT	NTERA-2	RCC786-0	RCC4/VA	H1299	H1666
NCCIT	1.000	0.973	0.854	0.827	0.855	0.903
NTERA-2	0.973	1.000	0.867	0.852	0.870	0.920
RCC786-0	0.854	0.867	1.000	0.950	0.942	0.965
RCC4/VA	0.827	0.852	0.950	1.000	0.924	0.919
H1299	0.855	0.870	0.942	0.924	1.000	0.950
H1666	0.903	0.920	0.965	0.919	0.950	1.000

[a] Only compounds with measurable IC$_{50}$ values were analysed.

In the following paragraphs, the SAR of YM155 was analyzed on NCCIT with a view of drawing comparisons with SAR deduced on H1666 cells.

Analysis of the series C compounds once again highlighted the importance of the quinone moiety. Analogs that retain the quinone moiety (**C2-1**, **C4-1**, **C4-2**) showed smaller losses in activity as compared to those without the quinone (**C2-X**, **C3-X**). The relative importance of the various features in the tricyclic scaffold were discernible. After the quinone, the next most important feature was the positive charge on the imidazolium N, followed by the distal benzene ring. This sequence was also observed for growth inhibitory activities. The C^2 ethyl homolog of YM155 (**C1-2**) showed diminished activity, similarly indicating limited tolerance for even a minor modification at the scaffold.

Quinone containing Series C compounds

| **C1-2** | **C4-1** | **C4-2** |
| IC_{50} 441 nM | IC_{50} 24000 nM | IC_{50} 34300 nM |
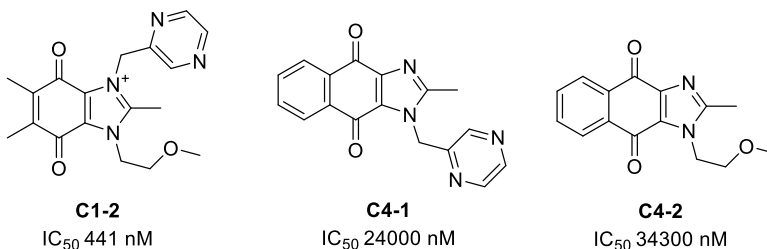
Non-quinone containing Series C compounds :IC50 > 100 µM

| **C2-1** | **C2-2** | **C2-3** | **C3-1** | **C3-2** |

| YM155 | C1-1 |
| IC_{50} 2.1 nM | IC_{50} 35 nM |
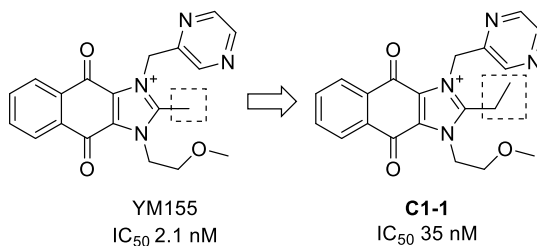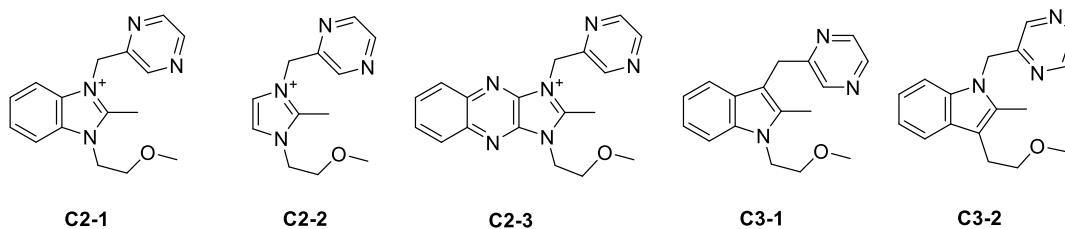
Analysis of the series A compounds revealed many overlapping structural requirements that were also critical for growth inhibition of H1666. These were:

(i) Maintaining a methylene linker between N^3 and the pyrazine ring as seen from the reduced activities of **A4-1** and **A5-1**. **A5-1** was in fact the least potent compound in Series A.

A4-1
IC_{50} 104 nM

A5-1
IC_{50} 2411 nM
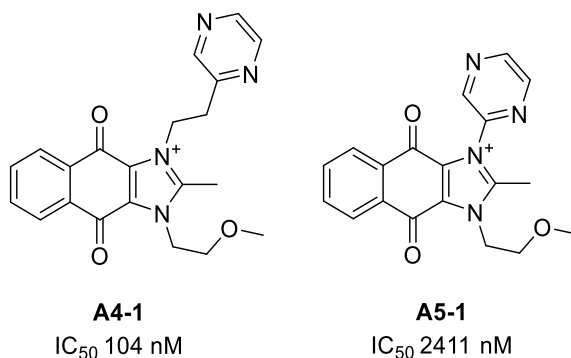
(ii) Preference for azinylmethyl moieties at N^3: Analogs with non-azinylmethyl residues (**A1-X**, **A2-1**) had poor activity.

Where R =

YM155
IC_{50} 2.1 nM

A1-1
IC_{50} 44 nM

A1-2
IC_{50} 76 nM

A1-3
IC_{50} 54 nM
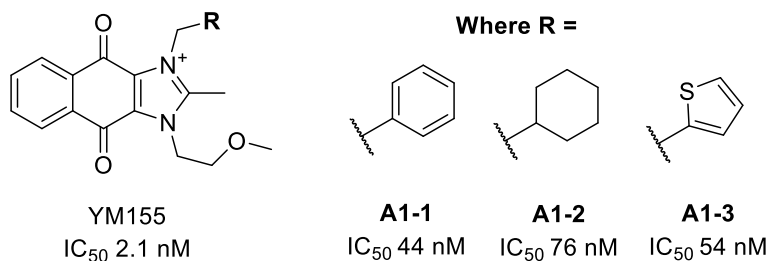
(iii) Regioisomeric bias against azines with ortho azomethine N atoms. The adverse effect of an ortho-N may be offset by the concurrent presence of meta or para N atoms as seen in **A3-5**.

where R =

YM155
IC_{50} 2.1 nM

A3-1
IC_{50} 20 nM

A3-2
IC_{50} 5.5 nM

A3-3
IC_{50} 2.0 nM

A3-4
IC_{50} 26 nM

A3-5
IC_{50} 2.2 nM

A3-6
IC_{50} 6.2 nM

130
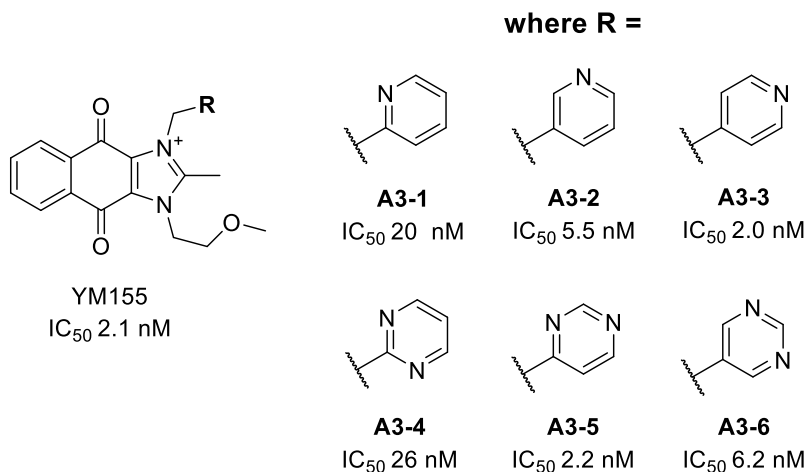
There were however noticeable differences in structural requirements. First, although alkyl substituents were permissible at N^3, structural preferences were less well defined. Thus IC_{50} values varied within a narrower range (26 – 60 nM) on NCCIT as compared to H1666 (29 – 280 nM) for the same set of **A6-X** analogs. Differences in growth inhibitory activities of analogs with methyl, ethyl, propyl and cyclopropyl at N^3 were not readily distinguished.

A6-2
IC_{50} 26 nM

A6-3
IC_{50} 22 nM

A6-4
IC_{50} 24 nM

A6-6
IC_{50} 24 nM
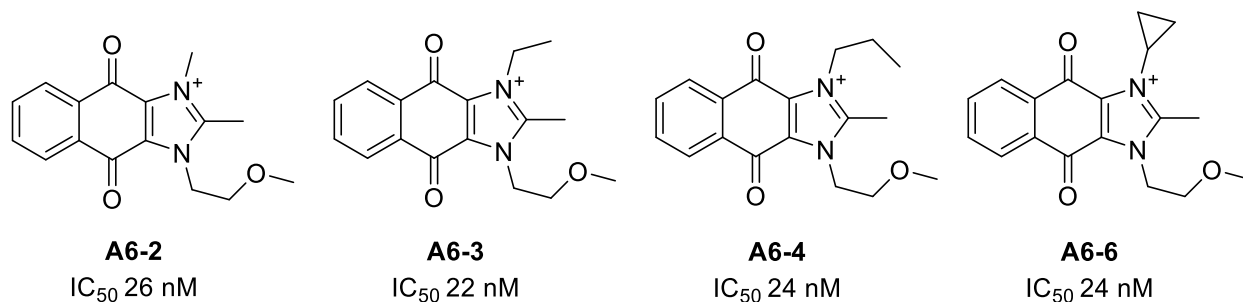
Second, the symmetrically substituted analog **A6-1** had surprisingly good activity. It was more potent than all the N^3-alkyl analogs on NCCIT and comparable to the most potent analog (**A6-6**) on NTERA-2. In contrast, it was significantly less potent than the N^3-alkyl analogs in H1666 and other malignant cells.

A6-1
$IC_{50 \text{ NCCIT}}$ 18 nM
$IC_{50 \text{ NTERA-2}}$ 13 nM
$IC_{50 \text{ H1666}}$ 73 nM

A6-6
$IC_{50 \text{ NCCIT}}$ 24 nM
$IC_{50 \text{ NTERA-2}}$ 12 nM
$IC_{50 \text{ H1666}}$ 56 nM
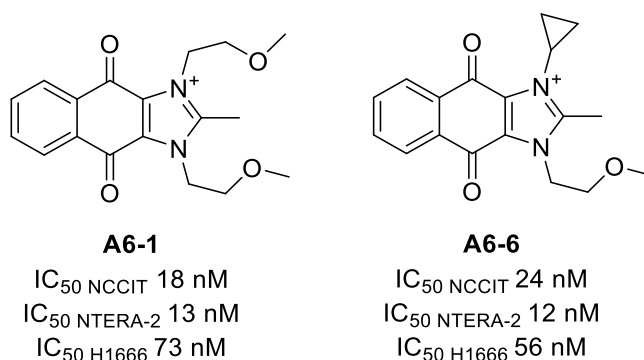
Several SAR similarities were also detected in series B. These were:

(i) Losses in activity when the 2'-methoxyethyl side chain at N^1 was modified by demethylation (**B1-1**), homologation (**B1-3**), cyclization (**B1-2**) or functionalized with substituted amino groups (**B4-X**).

where R =

YM155
IC$_{50}$ 2.1 nM

B1-1
IC$_{50}$ 26 nM

B1-2
IC$_{50}$ 190 nM

B1-3
IC$_{50}$ 22 nM

B4-1
IC$_{50}$ 500 nM

B4-2
IC$_{50}$ 1400 nM
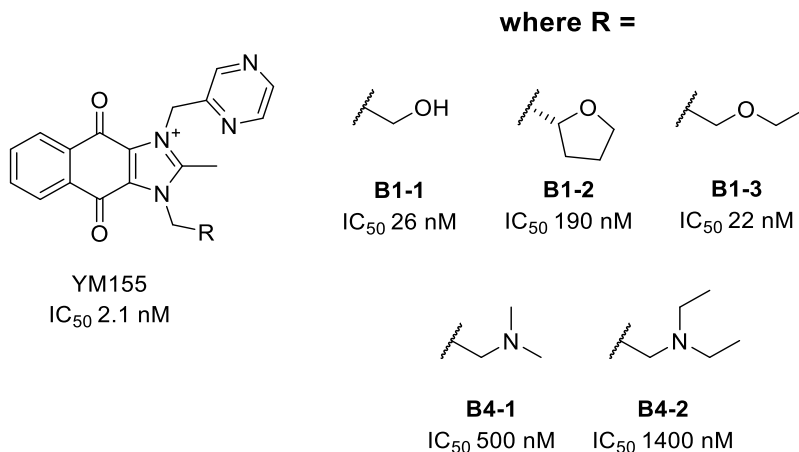
(ii) Poor tolerance for ring containing side chains at N^1 as seen from the diminished activities of **B1-2**, **B2-8**, **B3-1** and **B3-2**. Mention should be made of the anomalous activity of **B3-2** in that it was surprisingly potent on NTERA-2 (IC$_{50}$ 19 nM) and in fact, equipotent to the other symmetrically substituted analog **A6-1** (IC$_{50}$ 13 nM). This is contrary to the prevailing notion that ring bearing substituents were poorly tolerated on the scaffold and not observed on the RCC/NSCLC cells.

B1-2
IC$_{50}$ 190 nM

B2-8
IC$_{50}$ 160 nM

B3-1
IC$_{50}$ 150 nM

B3-2
IC$_{50}$ 59 nM
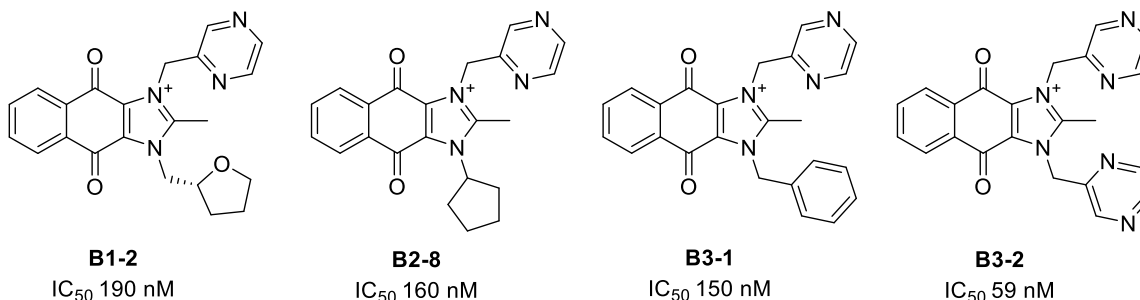
(iii) Analogs with N^1-alkyl groups were permissible. Potencies of N^1-alkyl analogs decreased in the order of cyclopropyl > propyl > ethyl > butyl > methyl > isopropyl > isobutyl, which broadly concurred with the sequence observed in H1666. The N^1-cyclopropyl analog (**B2-5**) was also the most potent on NTERA-2.
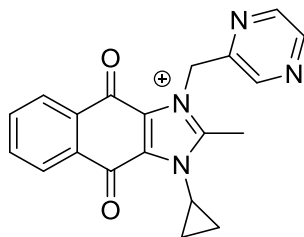
B2-5
IC$_{50 \text{ NCCIT}}$ 5 nM
IC$_{50 \text{ NTERA-2}}$ 2 nM

As for the series AB compounds, they were not as potent as anticipated in spite of bearing "optimal" substituents identified from series A (N^3) and series B (N^1). **AB1** was the most promising but no better than YM155 on the EC cells. In this series, analogs with pyridin-4'-ylmethyl at N^3 (**AB1**, **AB2**) were the most potent, followed by those with pyridin-3'-ylmethyl (**AB5**, **AB6**) and finally, pyrimidin-5'-ylmethyl (**AB3**, **AB4**). In contrast, the N^1 substituent (ethyl or cyclopropyl) had limited influence on activity. These findings were also observed on RCC and NSCLC cells. A notable difference was **AB7** which was only modestly potent on EC cells in spite of its outstanding activity on RCC and NSCLC cells.
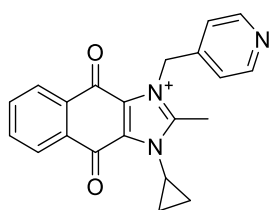
AB1
IC$_{50}$ 2.5 nM
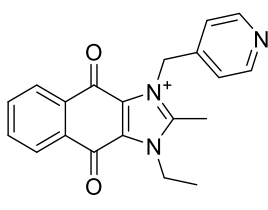
AB2
IC$_{50}$ 7.6 nM
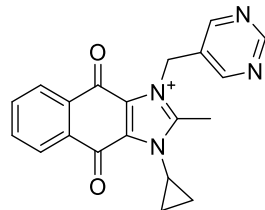
AB3
IC$_{50}$ 41 nM
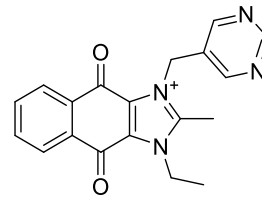
AB4
IC$_{50}$ 20 nM
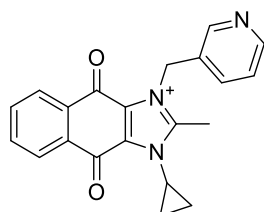
AB5
IC$_{50}$ 10 nM
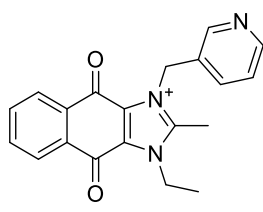
AB6
IC$_{50}$ 8.4 nM
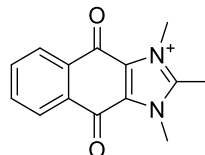
AB7
IC$_{50}$ 24 nM

Moving on to the selectivity of compounds, it is immediately apparent that YM155 and its analogs had excellent selective activities on the EC cells. Compared to non-malignant IMR-90 cells, YM155 was 142 times more potent on the EC cells. Selectivity ratios for its analogs were in the range of 2 (**C4-1**) to 250 (**B2-6**), a significant improvement over RCC/NSCLC cells where ratios were 1.5 to 19. Tellingly, potent analogs like **A3-3**, **A3-5**, **B2-5** and **AB1** had selectivity ratios exceeding 70 (in favor of EC cells) as compared to ratios of only 10 on RCC/NSCLC cells. Furthermore, some analogs (**A3-4**, **A6-8**, **B2-6, B2-7**) that had outstanding selectivities (≥ 200) on EC cells, had nanomolar potencies (IC_{50} 5 – 50 nM). While growth inhibitory activities were admittedly weaker than YM155 and its potent analogs, these compounds still merit attention in view of their strong selective activities.

Taken together, the SAR profiles of YM155 and its analogs on EC cells closely mirrored that observed on RCC/NSCLC cells. In both instances, the intact dioxonaphthoimidazolium scaffold was identified as a critical feature for activity whereas functionalization at N^1 and N^3 served mainly to fine-tune activity. However, even the most promising modifications resulted only in minor improvements in activity. Thus while several compounds could match YM155 in terms of potency, none could exceed it by 2-fold or more.

6.3.2. Growth inhibitory activity of YM155 and selected analogs on other stem cell lines

Having shown that YM155 and its analogs inhibited the viability of EC cells, a follow-up investigation was carried out on a human embryonic stem cell (hESC) H9 and an induced pluripotent stem cell line HCT-8 3.11. HCT-8 3.11 was derived from its non-stem cell malignant counterpart HCT-8, a colorectal carcinoma, through transfection of the Yamanaka factors (Sox2, Oct4, Klf4, c-Myc).[253, 254] The analogs selected for evaluation covered a range of potencies – **A3-3**, **AB1** (potent, IC_{50} 2 – 3 nM); **AB2**, **AB7** (moderately potent, IC_{50} 5 – 25 nM); **A2-1**, **B2-8**, **B3-1** (weakly potent, IC_{50} > 100 nM). The results are given in Table 6.3.

Table 6.3. Growth inhibitory IC$_{50}$ values of YM155 and 7 synthesized analogs on ES cell line H9, colorectal carcinoma cell line HCT-8, and iPS cell counterpart HCT-8 3.11.

Compounds	IC$_{50}$ (nM) [a]			
	H9 [b]	HCT-8 [c]	HCT-8 3.11 [c]	EC (NTERA-2/NCCIT) [d]
YM155	10.0 ± 1.6	21.8 ± 2.6	6.43 ± 0.97	1.5 / 2.1
A3-3	11.6 ± 1.6	11.8 ± 0.5	7.26 ± 1.32	1.6 / 2.0
A4-1	174 ± 7	1210 ± 152	215 ± 41	52 / 104
B2-8	156 ± 31	1250 ± 269	367 ± 71	110 / 160
B3-1	739 ± 148	2130 ± 367	604 ± 80	110 / 150
AB1	4.21 ± 0.49	15.4 ± 2.3	5.47 ± 0.80	2.5 / 2.6
AB2	4.31 ± 0.54	28.9 ± 1.7	7.66 ± 1.00	4.4 / 7.6
AB7	24.9 ± 0.2	32.9 ± 1.5	13.9 ± 1.5	6.1 / 24

[a] Determined by MTT assay after 24 h ([b]) or 72 h ([c]) incubation and presented as mean ±SD of n = 3 separate determinations. [d] IC$_{50}$ of EC cells were included for comparison.

A3-3   A4-1   B2-8   B3-1

AB1   AB2   AB7
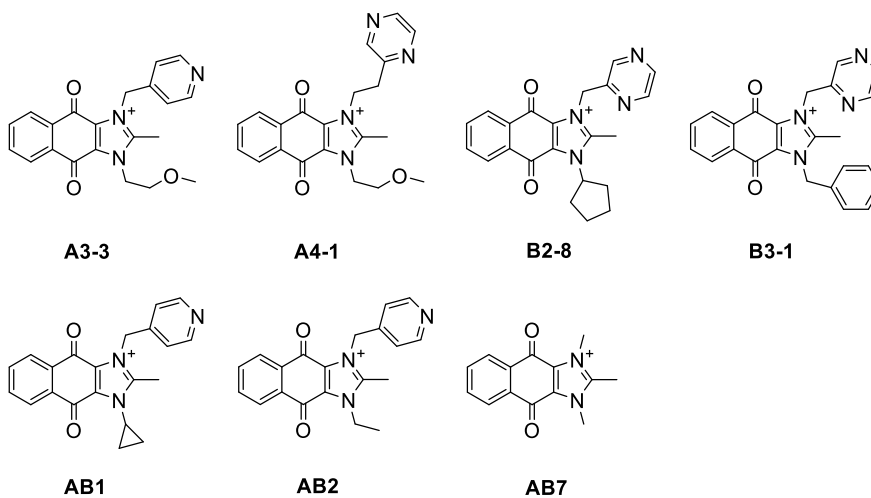
Growth inhibitory potencies on H9 were determined after 24 h incubation. In spite of the shorter incubation time, IC$_{50}$ values remained in the nanomolar range, although they were generally higher than those obtained on the EC cells. An exception was **AB2** which retained the same level of potency on both H9 and the EC cells. The rank order of potencies were broadly similar to that observed on the EC cells, but **AB1** and **AB2** were now the most potent analogs exceeding that of YM155 and **A3-3**.

The growth conditions of H9 were unlike those of HCT-8 3.11 and the EC cells in that mouse embryonic fibroblasts (MEF) were required as feeder cells. When a co-culture of untreated H9 and MEF cells was examined microscopically, the spindle-shaped MEF feeders and the colony forming H9 cells were readily distinguished (Figure 6.2, 1st column). When the H9 cells lost their viabilities, a "hollowing out" was observed as the colonies collapsed and the sharp boundaries of the colonies were lost. This was observed when H9 cells were treated with YM155 and **AB1** at 50 nM (Figure 6.2, 3rd column). Importantly, the MEF cells remained viable with no observable morphological changes. They retained their viabilities even at 10x IC_{50} of YM155 and **AB1**, thus confirming the selective activities of these compounds on the stem cells.

(A) YM155
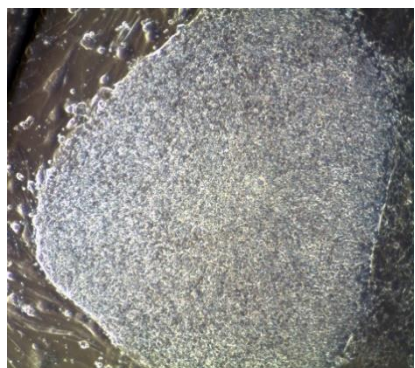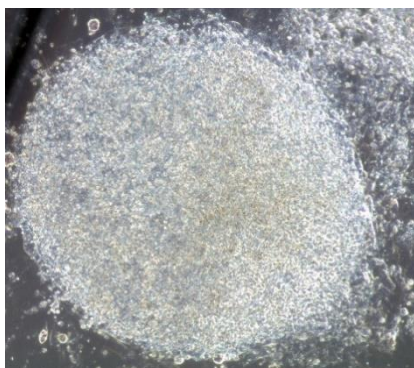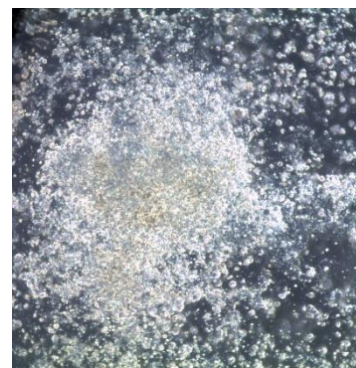
| 0.5% v/v DMSO | 5 nM | 50 nM |

(B) AB1

| 0.5% v/v DMSO | 5 nM | 50 nM |

136
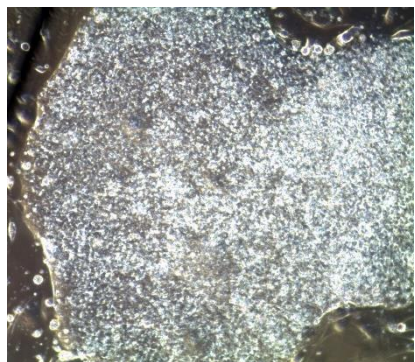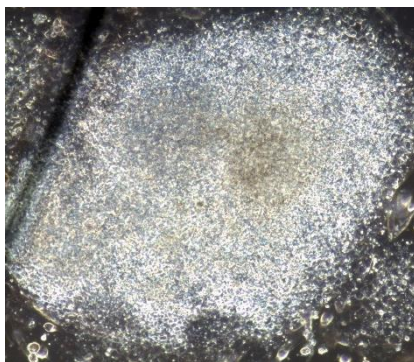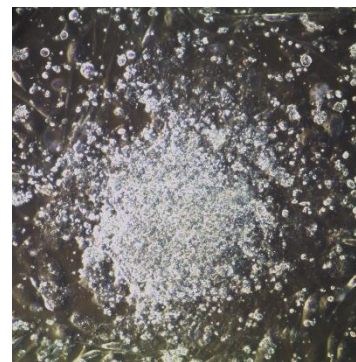
Figure 6.2. Morphology of H9-MEF cultures following 24 h treatment with 5 nM and 50 nM of (A) YM155 and (B) **AB1** in comparison with DMSO vehicle control. The characteristic clear demarcation of colonies' boundaries were lost as the concentration of YM155 and **AB1** increased. Eventually, the colonies collapsed, indicating loss of viability. A set of background control with only MEF showed negligible loss of viability for MEF (< 5%) under similar conditions (data not shown). Images presented are representative of the triplicates performed in the experiment.

The test compounds were also found to affect the viability of the iPSC HCT-8 3.11. YM155, **A3-3**, **AB1** and **AB2** were the most active (IC_{50} 5 – 8 nM) whereas **A4-1**, **B2-8**, **B3-1** were less active (IC_{50} 200 – 600 nM). Interestingly, growth potencies on HCT-8 3.11 exceeded that of HCT-8 by 1.5 – 5 fold, suggesting an increase in sensitivity of the transformed cells to growth inhibition.

6.3.3. Effects of YM155, **AB1** and **AB7** on the transcriptional activities of Sox2, Oct4, Nanog and p50 in NCCIT, H9, HCT-8 and HCT-8 3.11 cells.

Having shown that YM155 and **AB1** adversely affected viability of various stem cell types (EC, hESC, iPSC), experiments were planned to investigate their effects on the pluripotent markers that maintain stem cells in the undifferentiated state. The effects of YM155, **AB1** and **AB7** on the expression of mRNAs by Sox2, Oct4 and Nanog were monitored in treated NCCIT, H9, HCT-8 and HCT-8 3.11 cells. Of these markers, Sox2 and Oct4 are the most critical and essential.[265] Nanog, which is downstream of Sox2 and Oct4 is another important factor.[266]

The role of NF-κB signalling in maintaining pluripotency of iPSC was highlighted by Takase et al who showed that the pathway was upregulated in undifferentiated iPSC.[267] When suppressed with p65 siRNA, the expression of Oct4 and Nanog were found to be reduced. Furthermore,

Armstrong et al also showed that disrupting the NF-κB pathway in hESC led to downregulation of Sox2, Oct4 and Nanog.[268] In view of the effects of YM155 and **AB1** on the phosphorylation of p50 (Chapter 5), the expression of p50 mRNA was also monitored in treated cells.

Table 6.4. IC$_{50}$ values of YM155, **AB1** and **AB7** after 24 h treatment on NCCIT, H9, HCT-8 and HCT-8 3.11.

Compounds	IC$_{50}$ (nM) at 24 h			
	NCCIT	H9	HCT-8	HCT-8 3.11
YM155	10	10	55	15
AB1	30	4	45	20
AB7	150	25	145	40

The expression of mRNAs by Sox2, Oct4, Nanog and p50 were probed by qRT-PCR. Briefly, cells were incubated with a fixed concentration (IC$_{50}$ determined after 24 h incubation, Table 6.4) of the test compound for 12 h (NCCIT, H9, HCT-8, HCT-8 3.11) and 24 h (NCCIT, H9) after which, mRNAs were harvested and converted to cDNA for analysis by qRT-PCR. mRNA levels of the housekeeping gene GAPDH were used for normalization. The 24 h analysis was carried out on YM155 and AB1 treated cells only.

Figure 6.3 shows the fold change in mRNA expression of Sox2 in treated cells after an incubation period of 12 h and 24 h. At the 12 h time point, mRNA levels of Sox2 were significantly reduced in NCCIT cells treated with YM155, **AB1** and **AB7**. These reduction, particularly those induced by **AB1** and **AB7**, were more pronounced after 24 h. Time dependent reductions were also observed in H9 cells. At the 12 h time point, only YM155 reduced Sox2 mRNA levels but after 24 h, reductions were also observed in **AB7** treated cells but not in **AB1** treated cells. The delayed response elicited by **AB7** suggests that it is slower acting compared

to YM155. Likewise, **AB1** may be slow acting as well and requires a longer time period to produce significant Sox2 reductions in H9 cells.
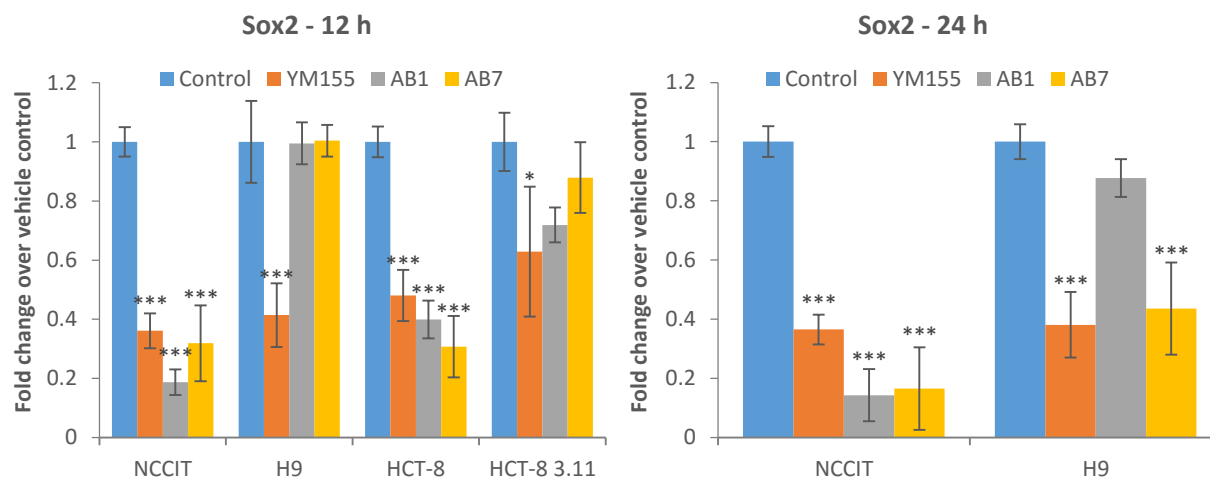
Figure 6.3. Expression levels of Sox2 mRNA following 12 or 24 h of treatment with YM155, **AB1** or **AB7** quantified by qRT-PCR. Bars represent the fold-change of cDNA normalized against GAPDH in the same sample. Error bars represent the standard deviations of three separate experiments. Significant statistical difference from vehicle control is represented by an asterisk (*) when $p<0.05$, two asterisks (**) when $p<0.01$ and three asterisks (***) when $p<0.001$ (Tukey post-hoc test of respective populations of treated groups vs control).

The transcriptional activity of the Sox2 gene was also reduced in treated HCT-8 at the 12 h time point. These reductions were almost comparable to those observed in treated NCCIT (12 h) but were less pronounced in HCT-8 3.11. Since a significant proportion of Sox2 expression in HCT-8 3.11 is due to a transfected gene, it is possible that the latter is not regulated in the same way as the native gene. The smaller reductions in HCT8 3.11 may well reflect the effects of the compounds on the non-transfected gene. Time dependency was not investigated in HCT-8 and HCT-8 3.11 cells.
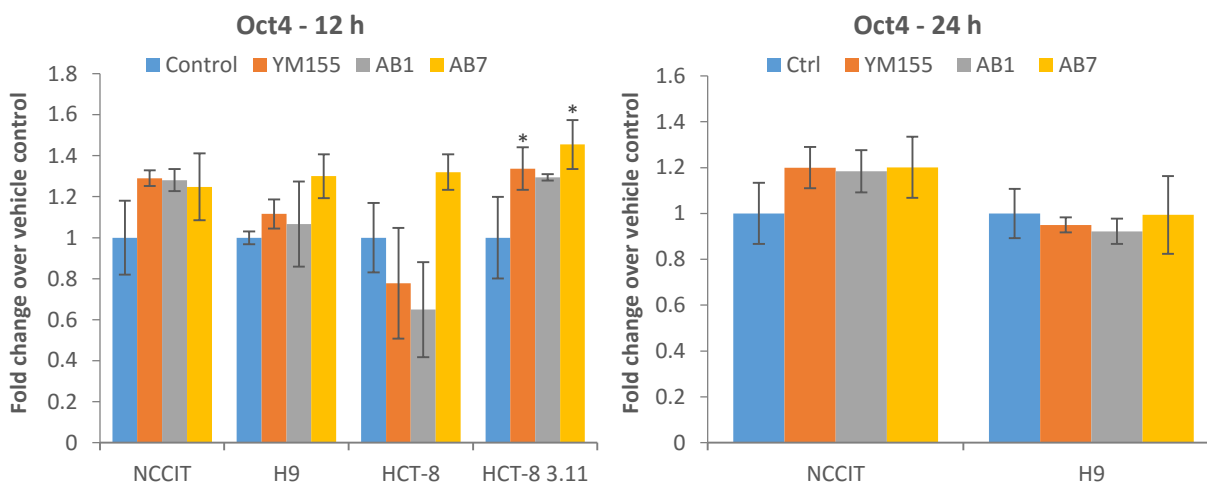
Figure 6.4. Expression levels of Oct4 mRNA following 12 or 24 h of treatment with YM155, **AB1** or **AB7** quantified by qRT-PCR. Bars represent the fold-change of cDNA normalized against GAPDH in the same sample. Error bars represent the standard deviations of three separate experiments. Significant statistical difference from vehicle control is represented by an asterisk (*) when $p<0.05$, two asterisks (**) when $p<0.01$ and three asterisks (***) when $p<0.001$ (Tukey post-hoc test of respective populations of treated groups vs control).

In the case of Oct4 (Figure 6.4), there was no discernible reduction in the mRNA levels across all the stem cell lines treated with the test compounds. Small increases were observed in treated HCT-8 3.11 cells. At 24 h Oct4 mRNA levels were similar to control in NCCIT and H9 cells.
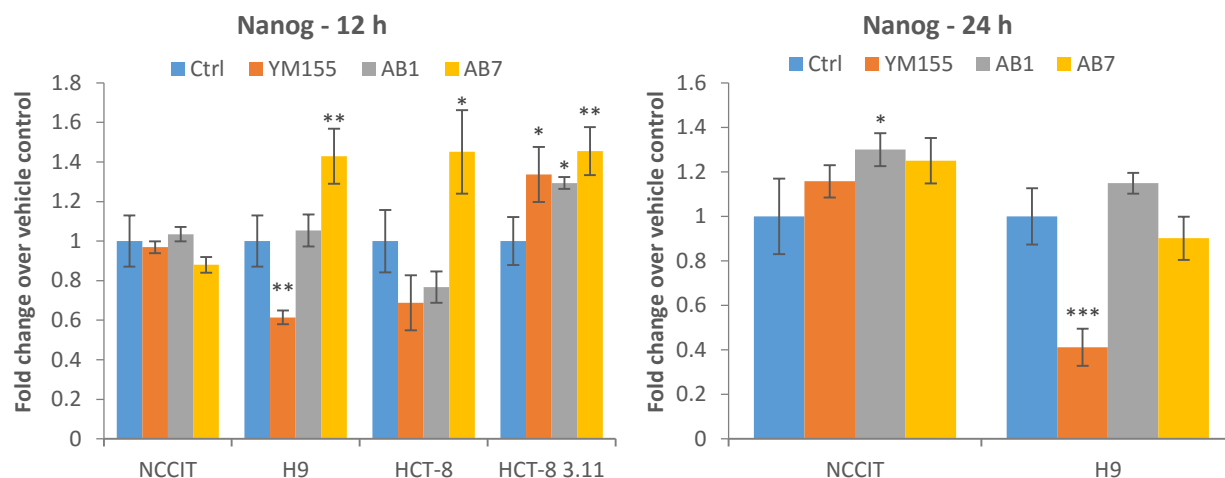
Figure 6.5. Expression levels of Nanog mRNA following 12 or 24 h of treatment with YM155, **AB1** or **AB7** quantified by qRT-PCR. Bars represent the fold-change of cDNA normalized against GAPDH in the same sample. Error bars represent the standard deviations of three separate experiments. Significant statistical difference from vehicle control is represented by an asterisk (*) when $p<0.05$, two asterisks (**) when $p<0.01$ and three asterisks (***) when $p<0.001$ (Tukey post-hoc test of respective populations of treated groups vs control).

The transcriptional activity of Nanog is reportedly moderated by Sox2 and Oct4 which lie upstream to it.[266] As Sox2 and Oct4 activities were affected differently by the test compounds on NCCIT, the effects on Nanog are not readily explained with the present data. It is however noteworthy that YM155 reduced Nanog mRNA levels in H9 cells at 12 h and this reduction was more pronounced at 24 h. The concurrent strong decreases in Sox2 mRNA may have a role in the decreases of Nanog. **AB1** and **AB7** did not affect Nanog mRNA levels even after 24 h, perhaps due to a slower mode of action.
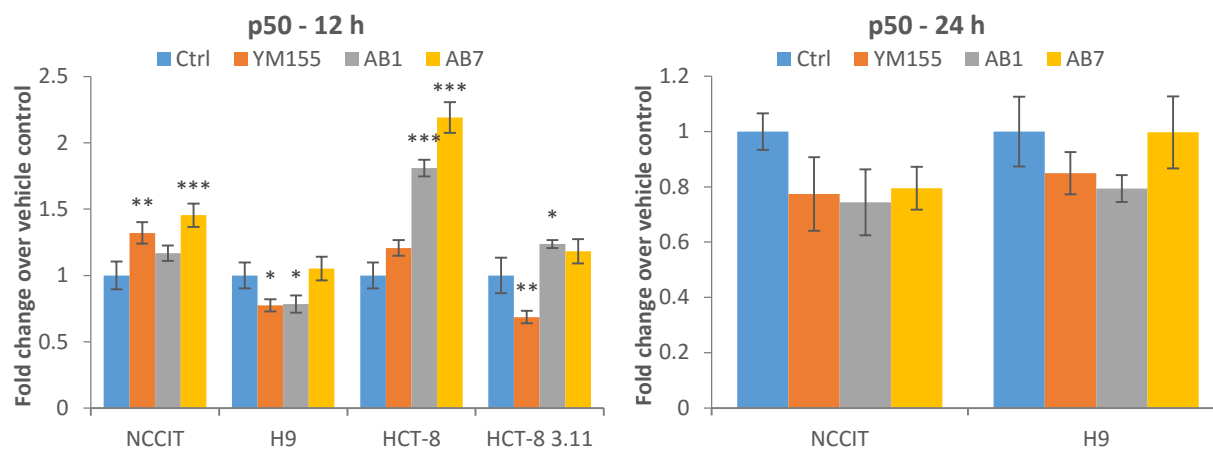
Figure 6.6. Expression levels of p50 mRNA following 12 or 24 h of treatment with YM155, **AB1** or **AB7** quantified by qRT-PCR. Bars represent the fold-change of cDNA normalized against GAPDH in the same sample. Error bars represent the standard deviations of three separate experiments. Significant statistical difference from vehicle control is represented by an asterisk (*) when $p<0.05$, two asterisks (**) when $p<0.01$ and three asterisks (***) when $p<0.001$ (Tukey post-hoc test of respective populations of treated groups vs control).

Figure 6.6 shows the fold change in mRNA expression of p50 in treated cells after an incubation period of 12 h and 24 h. Levels were elevated in treated NCCIT cells at the 12 h time point but decreased after 24 h. In H9, only YM155 and **AB1** slightly reduced p50 mRNA levels and likewise the effect was no longer apparent at 24 h. On HCT-8 cells, p50 mRNA levels were increased by all three compounds to varying extents, but they were reduced by YM155 and increased by **AB1** in HCT-8 3.11.

Taken together, this section has shown YM155, **AB1** and **AB7** have limited effects on the transcriptional activities of the genes that maintain stem cells in their undifferentiated state. Only Sox2 transcriptional activity was consistently reduced by YM155, **AB1** and **AB7** in NCCIT (12 and 24h) and to a lesser degree, in H9 (only after 24 h and for YM155, **AB7** only). At 12 h, Sox2

levels were significantly reduced by all three compounds in HCT-8 and to a lesser degree in its iPS counterpart HCT-8 3.11, possibly due to the additional control of Sox2 expression by the transfected promoter. Oct4 activity was conspicuously unaffected by the test compounds on all cell lines, barring a slight increase at 12 h in HCT-8 3.11. Nanog, which is under the control of Sox2 and Oct4 appeared to be modestly affected by changes in levels of the former two genes, except in H9 cells treated with YM155.

As for p50 transcriptional activity, no definitive changes were observed across all the treated stem cell lines. This was largely anticipated since the findings in Chapter 5 showed that the main effect of YM155 and **AB1** was on the phosphorylation of p50 and not on its levels per se.

6.3.4. Effects of YM155 and **AB1** on levels of Sox2, survivin, cleaved caspase 3, p100, p65, phospho-p65, p50 and phospho-p50 in NCCIT, HCT-8 and HCT-8 3.11 cells.

Having noted that YM155 and **AB1** reduced Sox2 mRNA levels, Western blotting was carried out to determine if it would lead to a downregulation of Sox2 protein levels. Survivin, cleaved caspase 3, NF-κB subunits p65 and p50 were also probed under similar conditions. Briefly, NCCIT, HCT-8 and HCT-8 3.11 were incubated with YM155 and **AB1** at their IC_{50} and 2x IC_{50} concentrations for 48 h. Lysates were then prepared and probed with the relevant antibodies.

As seen in Figure 6.7, YM155 diminished Sox2 levels in treated cells at both concentrations (IC_{50}, 2x IC_{50}). Sox2 levels were also decreased in **AB1** treated cells, with greater losses at 2 × IC_{50}. These changes were in keeping with the down-regulation of Sox2 transcription observed earlier.

Cleaved caspase 3 and survivin were probed for evidence of the apoptogenic effects of YM155 and **AB1** on the stated cells. This was duly observed as seen from the appearance of cleaved

caspase 3 and reduction in survivin levels in the treated cells. The changes were more pronounced at 2x IC_{50} of YM155 and **AB1**.

Figure 6.7 shows that p50 and p65 levels were unchanged in the treated cells. p105, a precursor of p50, was similarly unaltered. On the other hand, phospho-p50 was significantly reduced by both compounds whereas phospho-p65 was unchanged. These findings were similar to those observed in RCC and NSCLC cells.
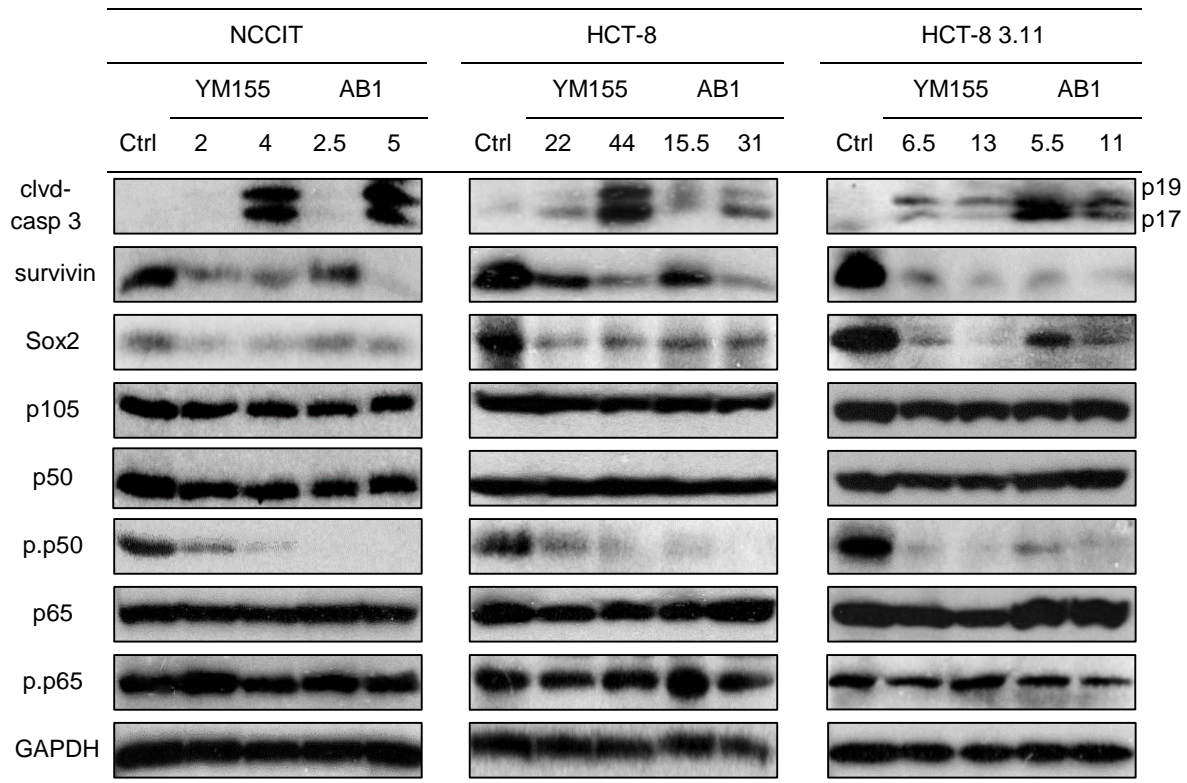
Figure 6.7. Cleaved caspase 3, survivin, Sox2 and NF-κB subunits p50, p65, p105 and their phosphorylated forms (p.p50, p.p65) levels in NCCIT, HCT-8 and HCT-8 3.11 after treatment with YM155 and **AB1** for 48 h. GAPDH was used as loading control.

6.4. Discussion

The main objectives of this chapter were to provide a better understanding of the effects on YM155 and its analogs on the viability and pluripotency of stem cells, namely to (i) establish the

SAR for growth inhibition of EC cells and to determine if these requirements coincided with those highlighted for malignant cells (Chapter 3) and (ii) determine if differentiation of stem cells would be intercepted by these compounds.

With regard to the 1st objective, it is abundantly clear that there were overlapping structural requirements for growth inhibition on the EC and malignant cells. Foremost was the importance of retaining an intact dioxonaphthoimidazolium scaffold. The contributions of the various components in the scaffold to activity were aligned to those observed earlier. At N^3, the pyrazinylmethyl side chain was preferentially replaced by isosteric azinylmethyl moieties and the regioisomeric bias against ortho substituted azines was again observed. At N^1, the most suitable replacement for the 2'-methoxyethyl side chain were short chain alkyl groups, with N^1-cyclopropyl the most favored. Lack of tolerance for bulky groups at N^1 and C^2 were again observed.

The most noticeable difference in structural requirements was the modest activity of **AB7** on EC cells, which stood in marked contrast to its highly ranked activity (twice more potent than YM155) on RCC/NSCLC cells. This may hint at a unique mode of action by **AB7** which is a minimally substituted dioxonaphthoimidazolium that is structurally different from YM155. Mention should also be made of the lesser contributions to activity when alkyl groups were introduced at N^1 or N^3, especially at N^3. These same modifications had a greater impact on RCC/NSCLC cells.

Aside from SAR considerations, the median IC_{50} values of YM155 and its analogs point to overall greater potency on EC cells as compared to RCC/NSCLC cells. This could have contributed to the greatly improved selective activities of these compounds on the EC cells. The spread of growth inhibitory IC_{50} values was also wider which may suggest that side chain

modifications were less well tolerated on EC cells and thus caused greater variations in activity. Tellingly, no analog that was more potent than YM155 on EC cells was identified from this exercise.

The growth inhibitory activities of YM155 and its potent analogs (**A3-3**, **AB1**, **AB2**, **AB7**) were not limited to EC cells but extended to H9 and HCT-8 3.11 cells. Nanomolar IC_{50} values were again observed. Selective activity was evident from the retention of viability in MEF cells in the co-culture with H9, as well as the higher IC_{50} values recorded for HCT-8 as compared to its induced pluripotent stem cell counterpart.

With regard to the 2nd objective, the results showed that YM155 and **AB1** blocked Sox2 expression in NCCIT and HCT-8 3.11 cells at both the gene and protein levels. The transcriptional activity of Sox2 was also reduced in H9 cells treated with YM155 and **AB1**. In contrast, the activities of Oct4 and Nanog were not consistently affected across the different stem cell types by YM155 and its analogs. As Sox2 is an important driver of the pluripotent state, the reduction in its activity would suggest that YM155 and **AB1** could potentially promote differentiation of stem cells.

Sox2 also protects cells from apoptosis and several studies have shown that in malignant cells, the anti-apoptotic properties of Sox2 was mediated (in part) by survivin.[269-271] Furthermore, survivin has been implicated in the maintenance of pluripotency.[65] The inter-related effects of Sox2 and survivin and concurrent declines in treated stem cells raises the possibility of another upstream event regulating the levels of Sox2 and hence, survivin.

NF-κB signalling is augmented in stem cells and is important for maintaining the self-renewing and pluripotent properties of these cells. Disrupting this pathway was reported to significantly

reduce Sox2, Nanog and Oct4 in ES and iPS cells as well as inducing differentiation.[267, 268] Survivin overexpression is also the result of NF-κB activation in several malignancies.[213] In the light of the present results which showed down-regulation of survivin, phospho-p50 and Sox2 in YM155 and **AB1**-treated stem cells (NCCIT, HCT-8 3.11), it is tempting to implicate a role for the NF-κB pathway in intercepting Sox2 expression and the suppression of survivin activity. The loss in p50 phosphorylation would disrupt gene transcription and if the affected gene products are involved in cell survival (like Sox2 and survivin), this would translate to an increased susceptibility to apoptotic cell death.

6.5. Conclusion

This chapter has provided insights into the potential of YM155 and its analogs as potent agents for the eradication of remnant stem cells from differentiated cell populations. They are well-positioned for this role because of their potent cell killing effects and their ability to promote cell differentiation. The first would markedly reduce residual stem cells while the second would further ensure their removal by promoting conversion to the differentiated state which would in turn lower the risk of reversion to the malignant phenotype.

6.6. Experimental

6.6.1. Cell lines and growth conditions

Human EC cells (NCCIT, NTERA-2) and human colorectal carcinoma HCT-8 cells were obtained from American Type Culture Collection (ATCC, USA). HCT-8 3.11, a pluripotent stem cell line induced from HCT-8, was a gift from Professor Wang Shu (Department of Biological Sciences, National University of Singapore). It was generated using a baculovirus vector to transfect Yamanaka factors into HCT-8.[254]

RPMI-1640 and DMEM were supplemented with 10% heat-inactivated FBS and 0.01% w/v penicillin G-streptomycin before culturing. NCCIT was maintained in RPMI-1640, while NTERA-2 and HCT-8 in DMEM. The media DMEM/F-12 (1:1) (Hyclone®, GE Healthcare, Buckinghamshire, UK) was supplemented with 1% FBS, 0.005% penicillin G-streptomycin, 5 mL of GlutaMax (Gibco®, Life Technologies Corporation, Carlsbad, CA, USA) and epidermal growth factor (Peprotech, Rocky Hill, NJ, USA) for the propagation of HCT-8 3.11.

Human embryonic stem (ES) cell H9 and mouse epithelial fibroblast (MEF) cells were gifts from Dr Chan Woon Khiong (Department of Biological Sciences, National University of Singapore) and originated from WiCell Research Institute Inc.(Madison, WI, USA). Passaging and maintenance of H9 cells was done by Ms Lam Kuen Kuen, Millie (Department of Biological Sciences, National University of Singapore). H9 cells were maintained in DMEM/F-12 (1:1) (Gibco®, Life Technologies Corporation, Carlsbad, CA, USA) prepared according to the following formulation:

Component	Volume	Final Concentration
DMEM/F12 (1:1)	40 mL	-
Knockout™ Serum Replacer	10 mL	20%
L-Glutamine (200 mM)	250 µL	1 mM
β-Mercaptoethanol (55 mM in PBS)	91 µL	0.1 mM
Non-essential Amino Acids 10 mM	500 µL	1x (0.1 mM)
Basic Fibroblast Growth Factor (FGF) Solution (25 µg/mL)	8 µL	4 ng/µl
Total volume	**50 mL**	-

Knockout™ Serum Replacer, L-glutamine, β-mercaptoethanol and non-essential amino acids solution were from Life Technologies Corporation. Basic fibroblast growth factor (FGF) was from Peprotech.

MEF cells were maintained in high glucose DMEM (Gibco®, Life Technologies Corporation, Carlsbad, CA, USA), supplemented with 10% FBS, 2 mM L-glutamine and 0.1 mM non-essential amino acids solution.

35mm culture dishes were coated with 1mL of 0.1% gelatin and incubated at 37°C for 1 h. 3.6 x 10^5 gamma-irradiated MEF cells were seeded onto each gelatin coated 35mm culture dish and incubated for 24 h for adherence. Thereafter, the MEF layer was washed once with PBS and ~100-120 H9 colonies suspended in H9 media were seeded. H9 media was changed daily and passaging was performed every 7 – 10 days depending on the size of colonies. During passaging, each large colony was carefully separated into 200 – 300 µm large pieces using a small scalpel. Roughly 100 – 120 pieces were then collected and seeded onto another 35mm culture dish previously seeded with MEF cells.

6.6.2. MTT assay

The MTT assay for NCCIT, NTERA-2, HCT-8 and HCT-8 3.11 was carried out as described in Chapter 3. The following cell densities were used: 3.0×10^3 cells/well (HCT-8, HCT-8 3.11), 4.0×10^3 cells/well (NTERA-2), 6.0×10^3 cells/well (NCCIT). Incubation with MTT was 2 h for the above cell lines.

For H9 cells, the above method was modified. MEF cells were seeded at a density of 5×10^4 cells/well on 24-well plates in MEF media and allowed to attach overnight at 37°C, 5% CO_2. Post attachment, MEF media was removed and H9 cells were seeded at 8×10^5 cells/well in 500 µL H9 media and incubated for 48 h. After the stated times, media was removed from each well by aspiration and replaced with 497.5 µL of media and 2.5 µL of test compound (prepared in DMSO stock solution at 200-fold higher concentration) and incubated for another 24 h. Compound-containing media was then removed and a 500 µL aliquot of 0.5 mg/mL MTT in

media was added per well and incubated for 2 h. The resulting formazan was dissolved in 250

µL DMSO and quantified at 570 nm on a microplate reader. It was necessary to correct for

changes in absorbance due to the presence of MEF cells, so wells with only MEF were set up

and treated with test compound as well. Absorbance from these wells were subtracted from

those containing H9 before calculating percentage viability. Percentage viability was determined

from the following expression

$$\text{Percentage viability} = \frac{A_\text{t} - A_\text{blank,t}}{A_\text{control} - A_\text{blank,control}} \times 100\%$$

Where A_t = Average of absorbance of compound-treated H9 + MEF cells
$A_\text{blank,t}$ = Average of absorbance of compound-treated MEF cells
A_control = Average of absorbance of untreated/control H9 + MEF cells
$A_\text{blank,control}$ = Average of absorbance of untreated/control MEF cells

6.6.3. qRT-PCR

NCCIT, H9, HCT-8 and HCT-8 3.11 were seeded at 8.0×10^5 cells/well into 6-well plates for 24

h followed by exposure to test compound for 12 or 24 h. RNA extraction was performed

following manufacturer's protocol (Qiagen RNeasy Mini Kit, Qiagen, Netherlands). RNA content

was quantified using a ND-1000 spectrophotometer (NanoDrop Technologies, USA). All

samples showed OD260/OD280 ratios between 1.73 and 2.11 with concentrations ranging from

~400 to ~1200 ng/µL. Results from an Agilent Bioanalyzer 2000 analysis showed that all

samples had RIN (RNA Integrity Number) of 9.4 – 10.

RNA (1.7 µg) was withdrawn from each sample for cDNA synthesis using Promega M-MLV

reverse transcriptase according to the recommended protocol (Promega, USA). Five primers,

namely Sox2, Nanog, Oct4, p50 and GAPDH, were ordered from AIT Biotech (Singapore)

based on sequences sourced from PrimerBank (Harvard Medical School, USA). PCR was

carried out in a volume of 20 µL using SYBR Green Dye on Applied Biosystem 7500 Fast Real

Time PCR system (Life Technologies, USA). Data analysis was performed using a comparative C_T (Threshold cycle) method and normalized to GAPDH expression levels.

6.6.4. Western blotting

Western blotting was performed in a similar manner as detailed in Chapter 4. Here, cell densities of 6.0×10^5 cells/100mm plate, 8.0×10^5 cells/100mm plate and 1.2×10^6 cells/100mm plate were used for NCCIT, HCT-8 and HCT-8 3.11 respectively. Anti-Sox2 antibodies were purchased from Santa Cruz Biotechnology Inc. (Santa Cruz, CA, USA).

6.6.5. Statistical analysis

Data were expressed as mean ± standard deviation. One-way analysis of variance (ANOVA) with Tukey post-hoc tests were performed (IBM SPSS Statistics v19.0) for comparison of means and statistical difference. Level of significance was set at $p < 0.05$ unless indicated.

Chapter 7: Conclusions and Future Work

The aim of this thesis is to test the hypothesis that a detailed understanding of the mode of action of YM155 would promote the development of dioxonaphthoimidazolium analogs as a promising class of potent anti-cancer therapeutics. To investigate this hypothesis, two broad approaches were followed. The first approach focused on preparing a library of YM155 analogs to query the structural requirements for growth inhibition. In spite of the advanced status of YM155 as a clinical candidate for cancer, surprisingly little is known of its structure-activity relationship (SAR). Without this information, developing more potent analogs would pose a formidable challenge. The second approach focused on investigating the mode of action of YM155. Various reports have questioned if the suppression of survivin is the sole and main effect of YM155-induced cytotoxicity. The consensus is that YM155 is a DNA intercalating agent and induces a DNA damage response that leads to apoptotic cell death. There is a sound structural basis to support this claim. The positively charged planar scaffold of YM155 would promote DNA intercalation while the embedded quinone in the scaffold would generate free radicals via redox cycling and initiate DNA strand breaks. The library of YM155 analogs would permit a detailed assessment of the SAR for DNA intercalation and redox cycling, with the premise that overlapping structural requirements with growth inhibition would support a prominent role for DNA damage in the antiproliferative activity of YM155.

In the first approach, a library of 53 compounds were synthesized to interrogate the structural requirements for growth inhibition on two different malignant cell types (RCC and NSCLC). The library was designed to probe the importance of the side chains at N^1 and N^3 (series A, B and AB) and the core scaffold (series C). Figure 7.1 summarizes the key SAR findings from this exercise.
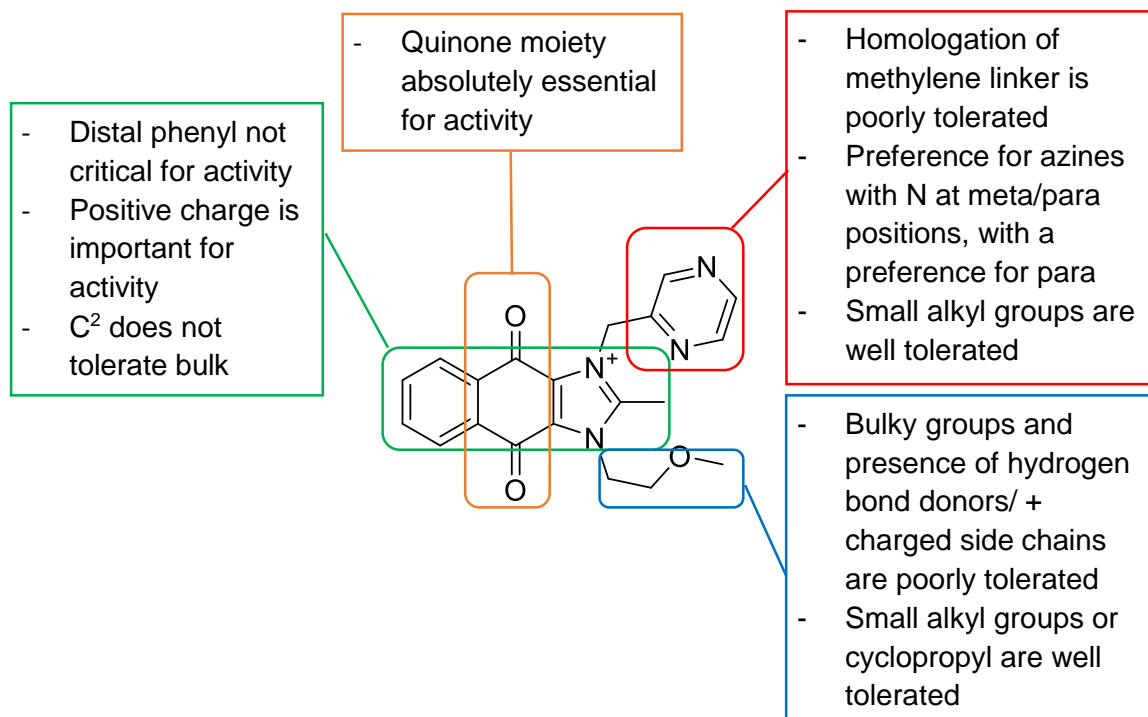
Figure 7.1. Summary of growth inhibitory structure-activity relationships of YM155

The intact scaffold was mandatory for potent activity (nanomolar to low micromolar IC_{50}) and dramatic losses were incurred when one or more rings were omitted from the tricyclic scaffold. In terms of relative contribution to activity, the quinone (ring B) was of foremost importance, followed by the imidazolium (ring C) and lastly the distal phenyl ring A. The side chains served to essentially fine-tune activity. Notwithstanding, specific structural requirements were evident, such as the regioisomeric preference of the N^3-azinylmethyl side chain, limited tolerance for bulky / ring bearing substituents at N^1, C^2 and N^3 and the favored presence of short, unbranched alkyl groups at N^1 or $N^{3.}$ The inclusion of methyl at N^1 and N^3 yielded the only analog (**AB7**) that was consistently more potent than YM155. Although the fold difference was slight (2-fold), **AB7** was unusually potent (IC_{50} 8.6 – 29 nM) with a selectivity against malignant cells (9.5-fold) that was comparable to YM155. More intriguing was its minimally substituted state which was in

sharp contrast to the polar, H- bonding side chains found in YM155 and the other members of the library.

YM155
IC_{50} 14 - 54 nM

AB7
IC_{50} 8.6 - 29 nM
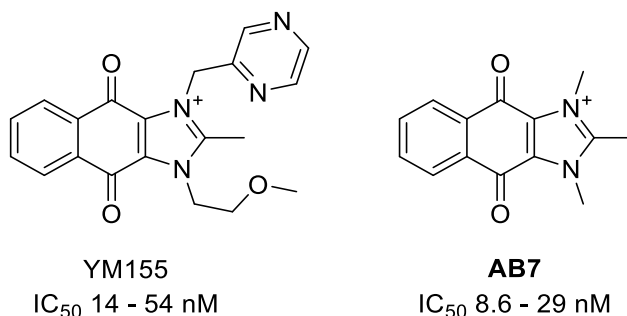
Following reports that YM155 inhibited the viability of stem cells[68], the synthesized compounds were evaluated on embryonic carcinoma (EC) cell lines, which are the malignant counterparts of embryonic stem (ES) cells. Nanomolar growth inhibitory potencies were found for YM155 and several analogs. SAR revealed the importance of the intact scaffold as before but there was less overlap in the structural requirements for the side chains. A notable difference was that analogs with short alkyl side chains at N^1 or N^3 were less effective on stem cells. Thus **AB7** had only modest growth inhibition. More striking was the significantly improved selectivity ratios associated with the EC cells. Potent analogs like YM155, **A3-3**, **A3-5** and **AB1** had ratios as high as 100 or more, as compared to narrower 10-fold selectivities observed for the same compounds on malignant cells. Growth inhibition was not limited to EC cells but extended to a human embryonic stem cell line (H9) and an induced pluripotent stem cell line (HCT-8 3.11). As only a few analogs were evaluated on these cell lines, no SAR could be deduced but observed trends point to similar requirements for the different stem cell types.

Taken together, functionalized dioxonaphthoimidazolium analogs displayed potent growth inhibitory activities against malignant and stem cells. Notwithstanding some differences in SAR, core features for activity remained the same, hinting at a possible shared mode of action. The potent and selective targeting of stem cells underscored the potential of this scaffold as stem

cell clearing agents. Several potent analogs (**A3-3**, **A3-5**, **AB1**, **AB2**, **AB7**) were identified, which depending on the cell line, were either equipotent or modestly more potent than YM155.
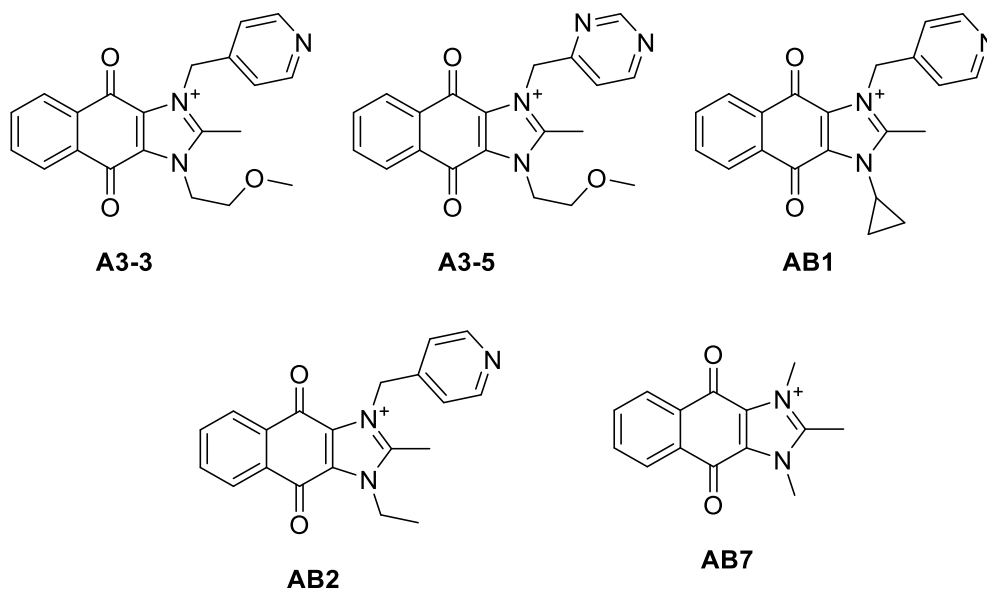
The thrust of the 2nd approach was to determine the role of the DNA damage in the mode of action of YM155. To this end, DNA intercalation and redox cycling properties of YM155 and its analogs were investigated by in vitro assays. The results showed that YM155 and its analogs were weak DNA intercalators, with limited potential as redox cyclers. Analysis of the structural requirements revealed a closer alignment between the SAR for DNA intercalation and growth inhibition. Notably the intact scaffold was mandatory for both activities although the relative importance of the individual rings could not be established for DNA intercalation. In the case of redox cycling, the scaffold was optional and intriguingly, even the presence of the quinone moiety did not always ensure measurable redox activity. Side chain requirements for intercalation and redox cycling also differed from that required for growth inhibition. Notably, ring bearing side chains at both N^1 and N^3 were preferred as opposed to smaller, non-ring groups at the same positions for growth inhibition. The regioisomeric preference associated with N^3-azinylmethyl side chains for growth inhibition was noticeably absent for redox cycling but still retained for intercalation. Alkyl groups at N^1 or N^3 which were acceptable modifications for

growth inhibition were not favored for either activity. **AB7** was a poor redox cycler but a more potent intercalator than YM155. Evidence from cell based assays showed that YM155 and several potent antiproliferative analogs (**AB1**, **AB7**) failed to generate significant amounts free radicals, indicating that redox cycling had a limited role in the mode of action of these compounds.

Notwithstanding these SAR deductions, YM155, **AB1** and **AB7** elevated levels of the DNA damage marker γH2AX in treated cells. However, these increases were not entirely compatible with the DNA damage response for several reasons. First, they were unusually delayed in terms of detection in treated cells and second, they were closely aligned to the appearance of the apoptotic marker protein cleaved caspase 3. This raises the possibility that the elevation of γH2AX is due to DNA fragmentation which accompanies apoptotic cell death. Future work should be directed towards determining the transcriptional profiles of RCC/NSCLC cells to determine if DNA repair genes are activated in the presence of YM155 or its analogs, as would be expected if the DNA damage response is a major contributor to cell death.

Taken together, the present findings have shown that the dioxonaphthoimidazolium analogs of YM155 were modest DNA intercalators with limited capacity to generate free radicals. Intercalation per se will not directly cause DNA damage but it will cause unwinding of the DNA helix which could render it susceptible to misreading, mutations and interference with transcription and replication. These events would in turn perturb gene products in several canonical pathways that are required for cell survival. Notwithstanding, the present results do not support a major role for the DNA damage response in the mode of action of the dioxonaphthoimidazoliums.

The NF-κB pathway was investigated as a possible target of YM155 in view of literature reports linking NF-κB activation to the overexpression of survivin in several malignancies. The corollary that suppression of survivin is due to inhibition of NF-κB signaling may thus hold true. Furthermore, anti-apoptotic proteins Mcl1 and Bcl-xl were downregulated in YM155 or **AB1**-treated RCC/NSCLC cells. The expression of these proteins are controlled in part by the NF-κB pathway.

A significant finding to emerge from these investigations was that YM155 and **AB1** induced time and dose dependent losses in phospho-p50 in RCC and NSCLC cell lines. These losses were confined to phospho-p50 in the nuclear compartment of treated cells. p50 levels and p65 in the cytosol and nuclei of treated cells were not affected. Neither were there any changes in the levels of phospho-p65 or IκBα in treated cells. Thus, YM155 and **AB1** did not inhibit the release of NF-κB dimers from the NF-κB/IκB complex and by extension, proteins that were upstream of IκBα in the signaling pathway. Neither did it inhibit the translocation of the NF-κB dimers from cytosol to nucleus.

Phosphorylation of p50 regulates the binding of NF-κB dimers to consensus DNA sequences on NF-κB response elements (κB sites). When impeded, this would attenuate the transcriptional activity of the NF-κB dimers and reduce the expression of NF-κB controlled genes. Indeed, both compounds suppressed NF-κB reporter activity in luciferase transfected HEK293 cells. In effect, the NF-κB pathway was inhibited by YM155 and **AB1**, and the consequence, as seen from the silencing experiments of the p50 gene, was a significant loss in cell viability. Interestingly, a specific loss in phospho-p50 with no change in p50, p65 or phospho-p65, was also observed in stem cells (NCCIT, HCT-8 3.11) that were treated with YM155 and **AB1**.

YM155 was reported to inhibit the self-renewal capacity of stem cells through its cell-killing effects. The present investigations have shown that YM155 also promoted the differentiation of stem cells through its inhibition of Sox2 (a Yamanaka transcription factor required for "stem cellness") at the mRNA and protein levels. By promoting their differentiation, YM155 will prevent transformation of the stem cells to the malignant phenotype. As these properties were also found for several of its analogs (**AB1**, **AB7**) at nanomolar concentrations, the dioxonaphthoimidazolium scaffold should be explored further as potential inhibitors of stem cell-derived teratomas in regenerative medicine.

There are still many unanswered questions in this thesis. One question pertains to **AB7** which is structurally the least similar to YM155 among the dioxonaphthoimidazolium analogs. In spite of its minimally substituted structure, **AB7** shared many of the properties of YM155 (DNA intercalation, suppression of survivin and p50 phosphorylation) and was modestly more potent than YM155 on malignant cells but not stem cells. A larger library of N^1, N^3-dialkyl substituted analogs may yet uncover more potent analogs, besides providing insight into the importance of the substitution motif.

A recent report proposed that the cytotoxic effects of YM155 was contingent on the expression and activity of a solute carrier SLC35F2 which is highly expressed in human cancers. Intriguingly, this may imply that the SAR deduced from the malignant cells is in fact the SAR for affinity to the solute carrier. If so, the anomalous activity of **AB7** on stem cells may reflect a weaker affinity to the resident solute carrier, which presumably is not identical to the one found in malignant cells. Screening the present library of compounds for binding affinity to the solute carrier would serve to address these issues. Specifically, it would be of interest to determine if the SAR derived for growth inhibition is correlated with that for the solute carrier.

Another question that requires clarification relates to the mechanism by which YM155 and **AB1** suppressed p50 phosphorylation. It would be of interest to determine if these compounds inhibit the kinase-mediated phosphorylation, and if so, the identity of the affected kinase. Screening YM155 and selected analogs on a kinome screen would provide some answers. Alternatively, transcriptome analyses of YM155/**AB-1** treated cells will disclose the global profile of targets affected by these compounds. Careful validation of the results would yield useful mechanistic clues.

The present data on stem cells has also opened up a new frontier for dioxonaphthoimidazoliums. Discovery that YM155 and AB1 specifically downregulate Sox2 hints at another pathway that these compounds may target. Interestingly, Sox2 levels in HCT-8 were also downregulated, highlighting a possible role of Sox2 in malignant cells. That p50 phosphorylation is also inhibited in stem cells may therefore imply a common mechanism of action of YM155 in both malignant and stem cells. What is required thus are knockdown studies of NF-κB subunits to examine if these affect Sox2 levels significantly, which will provide further evidence for a link between the NF-κB pathway and Sox2 as well as bringing forth the above pathway as a critical one in maintenance of stem cell pluripotency and viability.

This thesis has shown that YM155 and its analogs are suppressors of survivin and other anti-apoptotic proteins (Bcl-xl and Mcl1) and in stem cells, inhibitors of Sox2 transcription. Most significantly, they are also inhibitors of p50 phosphorylation. YM155 and its analogs are also able to intercalate DNA and redox cycle to a measurable degree, but these properties are unlikely to account for the major part of their mechanism of action. Instead, the present thesis suggests that YM155 and its analogs induce apoptosis in both malignant and stem cells through disruption of the NF-κB pathway. This disruption downregulates anti-apoptotic proteins, thereby tilting the balance of the cell towards apoptosis. In stem cells, an additional effect on

downregulation of Sox2 (which has also been found to be under NF-κB control) may also promote differentiation of pluripotent stem cells. As a final note, Sox2 downregulation was also observed in the colorectal carcinoma cell line HCT-8, highlighting a possible role of Sox2 in malignant cells that is also worthy of further investigations.

References

1. Altieri, D. C. Targeting survivin in cancer. *Cancer Lett* **2013,** 332, 225-228.

2. Deveraux, Q. L.; Reed, J. C. IAP family proteins--suppressors of apoptosis. *Genes Dev* **1999,** 13, 239-52.

3. Salvesen, G. S.; Duckett, C. S. IAP proteins: blocking the road to death's door. *Nat Rev Mol Cell Biol* **2002,** 3, 401-410.

4. Huang, Y.; Park, Y. C.; Rich, R. L.; Segal, D.; Myszka, D. G.; Wu, H. Structural basis of caspase inhibition by XIAP: differential roles of the linker versus the BIR domain. *Cell* **2001,** 104, 781-790.

5. Riedl, S. J.; Renatus, M.; Schwarzenbacher, R.; Zhou, Q.; Sun, C.; Fesik, S. W.; Liddington, R. C.; Salvesen, G. S. Structural basis for the inhibition of caspase-3 by XIAP. *Cell* **2001,** 104, 791-800.

6. Srinivasula, S. M.; Hegde, R.; Saleh, A.; Datta, P.; Shiozaki, E.; Chai, J.; Lee, R. A.; Robbins, P. D.; Fernandes-Alnemri, T.; Shi, Y.; Alnemri, E. S. A conserved XIAP-interaction motif in caspase-9 and Smac/DIABLO regulates caspase activity and apoptosis. *Nature* **2001,** 410, 112-116.

7. Tamm, I.; Wang, Y.; Sausville, E.; Scudiero, D. A.; Vigna, N.; Oltersdorf, T.; Reed, J. C. IAP-family protein survivin inhibits caspase activity and apoptosis induced by Fas (CD95), Bax, caspases, and anticancer drugs. *Cancer Res* **1998,** 58, 5315-5320.

8. Shin, S. J.; Sung, B. J.; Cho, Y. S.; Kim, H. J.; Ha, N. C.; Hwang, J. I.; Chung, C. W.; Jung, Y. K.; Oh, B. H. An anti-apoptotic protein human survivin is a direct inhibitor of caspase-3 and -7. *Biochemistry* **2001,** 40, 1117-1123.

9. Banks, D. P.; Plescia, J.; Altieri, D. C. Survivin does not inhibit caspase-3 activity. *Blood* **2000,** 96, 4002-4003.

10. Song, Z.; Yao, X.; Wu, M. Direct interaction between survivin and Smac/DIABLO is essential for the anti-apoptotic activity of survivin during taxol-induced apoptosis. *J Biol Chem* **2003,** 278, 23130-23140.

11. Oikawa, T.; Unno, Y.; Matsuno, K.; Sawada, J.-i.; Ogo, N.; Tanaka, K.; Asai, A. Identification of a small-molecule inhibitor of the interaction between Survivin and Smac/DIABLO. *Biochem Biophys Res Commun* **2010,** 393, 253-258.

12. Cheung, C. H. A.; Cheng, L. T.; Chang, K. Y.; Chen, H. H.; Chang, J. Y. Investigations of survivin: the past, present and future. *Front Biosci* **2011,** 16, 952-961.

13. Marusawa, H.; Matsuzawa, S.; Welsh, K.; Zou, H.; Armstrong, R.; Tamm, I.; Reed, J. C. HBXIP funcstions a a cofactor of survivin in apoptosis suppression. *EMBO J* **2003,** 22, 2729-2740.

14. Lens, S. M. A.; Vader, G.; Medema, R. H. The case for Survivin as mitotic regulator. *Curr Opin Cell Biol* **2006,** 18, 616-622.

15. Wheatley, S. P.; McNeish, I. A. Survivin: A Protein with Dual Roles in Mitosis and Apoptosis. *Int Rev Cytol* **2005,** 247, 35-88.

16. Altieri, D. C. The case for survivin as a regulator of microtubule dynamics and cell-death decisions. *Curr Opin Cell Biol* **2006,** 18, 609-615.

17. Grossman, D.; McNiff, J. M.; Li, F.; Altieri, D. C. Expression and targeting of the apoptosis inhibitor, survivin, in human melanoma. *J Invest Dermatol* **1999,** 113, 1076-1081.

18. Tu, S. P.; Jiang, X. H.; Lin, M. C. M.; Cui, J. T.; Yang, Y.; Lum, C. T.; Zou, B.; Zhu, Y. B.; Jiang, S. H.; Wong, W. M.; Chan, A. O. O.; Yuen, M. F.; Lam, S. K.; Kung, H. F.; Wong, B. C. Y. Suppression of survivin expression inhibits in vivo tumorigenicity and angiogenesis in gastric cancer. *Cancer Res* **2003,** 63, 7724-7732.

19. Ambrosini, G.; Adida, C.; Altieri, D. C. A novel anti-apoptosis gene, survivin, expressed in cancer and lymphoma. *Nat Med* **1997,** 3, 917-921.

20. Tracey, L.; Perez-Rosado, A.; Artiga, M. J.; Camacho, F. I.; Rodriguez, A.; Martinez, N.; Ruiz-Ballesteros, E.; Mollejo, M.; Martinez, B.; Cuadros, M.; Garcia, J. F.; Lawler, M.; Piris, M. A. Expression of the NF-kappaB targets BCL2 and BIRC5/Survivin characterizes small B-cell and aggressive B-cell lymphomas, respectively. *J Pathol* **2005,** 206, 123-134.

21. Markovic, O.; Marisavljevic, D.; Cemerikic-Martinovic, V.; Martinovic, T.; Filipovic, B.; Stanisavljevic, D.; Zivkovic, R.; Hajder, J.; Stanisavljevic, N.; Mihaljevic, B. Survivin expression in patients with newly diagnosed nodal diffuse large B cell lymphoma (DLBCL). *Med Oncol* **2012,** 29, 3515-3521.

22. Falleni, M.; Pellegrini, C.; Marchetti, A.; Oprandi, B.; Buttitta, F.; Barassi, F.; Santambrogio, L.; Coggi, G.; Bosari, S. Survivin gene expression in early-stage non-small cell lung cancer. *J Pathol* **2003,** 200, 620-626.

23. Zamparese, R.; Pannone, G.; Santoro, A.; Lo Muzio, L.; Corsi, F.; Pedicillo, M. C.; Scillitani, E. L.; Tortorella, S.; Staibano, S.; Piscuoglio, S.; Lo Russo, L.; Bufo, P. Survivin expression in renal cell carcinoma. *Cancer Invest* **2008,** 26, 929-935.

24. Byun, S.-S.; Yeo, W. G.; Lee, S. E.; Lee, E. Expression of survivin in renal cell carcinomas: Association with pathologic features and clinical outcome. *Urology* **2007,** 69, 34-37.

25. Church, D. N.; Talbot, D. C. Survivin in solid tumors: rationale for development of inhibitors. *Curr Oncol Rep* **2012,** 14, 120-128.

26. Gurbuxani, S.; Xu, Y.; Keerthivasan, G.; Wickrema, A.; Crispino, J. D. Differential requirements for survivin in hematopoietic cell development. *P Natl Acad Sci USA* **2005,** 102, 11480-11485.

27. Altieri, D. C. Survivin, cancer networks and pathway-directed drug discovery. *Nat Rev Cancer* **2008,** 8, 61-70.

28. Ryan, B. M.; O'Donovan, N.; Duffy, M. J. Survivin: a new target for anti-cancer therapy. *Cancer Treat Rev* **2009,** 35, 553-562.

29. Mita, A. C.; Mita, M. M.; Nawrocki, S. T.; Giles, F. J. Survivin: key regulator of mitosis and apoptosis and novel target for cancer therapeutics. *Clin Cancer Res* **2008,** 14, 5000-5005.

30. Ling, X.; Cao, S.; Cheng, Q.; Keefe, J. T.; Rustum, Y. M.; Li, F. A novel small molecule FL118 that selectively inhibits survivin, Mcl-1, XIAP and cIAP2 in a p53-independent manner, shows superior antitumor activity. *PLoS ONE* **2012,** 7, e45571.

31. Zhao, J.; Ling, X.; Cao, S.; Liu, X.; Wan, S.; Jiang, T.; Li, F. Antitumor activity of FL118, a survivin, Mcl-1, XIAP, and cIAP2 selective inhibitor, is highly dependent on its primary structure and steric configuration. *Mol Pharm* **2014,** 11, 457-467.

32. Eads, D.; Hansen, R. L.; Oyegunwa, A. O.; Cecil, C. E.; Culver, C. A.; Scholle, F.; Petty, I. T. D.; Laster, S. M. Terameprocol, a methylated derivative of nordihydroguaiaretic acid, inhibits production of prostaglandins and several key inflammatory cytokines and chemokines. *J Inflamm (Lond)* **2009,** 6.

33. Sun, Y.; Giacalone, N. J.; Lu, B. Terameprocol (tetra-O-methyl nordihydroguaiaretic acid), an inhibitor of Sp1-mediated survivin transcription, induces radiosensitization in non-small cell lung carcinoma. *J Thorac Oncol* **2011,** 6, 8-14.

34. Nakahara, T.; Takeuchi, M.; Kinoyama, I.; Minematsu, T.; Shirasuna, K.; Matsuhisa, A.; Kita, A.; Tominaga, F.; Yamanaka, K.; Kudoh, M.; Sasamata, M. YM155, a novel small-molecule survivin suppressant, induces regression of established human hormone-refractory prostate tumor xenografts. *Cancer Res* **2007,** 67, 8014-8021.

35. Nakahara, T.; Kita, A.; Yamanaka, K.; Mori, M.; Amino, N.; Takeuchi, M.; Tominaga, F.; Kinoyama, I.; Matsuhisa, A.; Kudoh, M.; Sasamata, M. Broad spectrum and potent antitumor activities of YM155, a novel small-molecule survivin suppressant, in a wide variety of human cancer cell lines and xenograft models. *Cancer Sci* **2011,** 102, 614-621.

36. Giaccone, G.; Zatloukal, P.; Roubec, J.; Floor, K.; Musil, J.; Kuta, M.; van Klaveren, R. J.; Chaudhary, S.; Gunther, A.; Shamsili, S. Multicenter phase II trial of YM155, a small-

molecule suppressor of survivin, in patients with advanced, refractory, non-small-cell lung cancer. *J Clin Oncol* **2009,** 27, 4481-4486.

37. Lewis, K. D.; Samlowski, W.; Ward, J.; Catlett, J.; Cranmer, L.; Kirkwood, J.; Lawson, D.; Whitman, E.; Gonzalez, R. A multi-center phase II evaluation of the small molecule survivin suppressor YM155 in patients with unresectable stage III or IV melanoma. *Invest New Drugs* **2011,** 29, 161-166.

38. Tolcher, A. W.; Quinn, D. I.; Ferrari, A.; Ahmann, F.; Giaccone, G.; Drake, T.; Keating, A.; de Bono, J. S. A phase II study of YM155, a novel small-molecule suppressor of survivin, in castration-resistant taxane-pretreated prostate cancer. *Ann Oncol* **2012,** 23, 968-973.

39. Clemens, M. R.; Gladkov, O. A.; Gartner, E.; Vladimirov, V.; Crown, J.; Steinberg, J.; Jie, F.; Keating, A. Phase II, multicenter, open-label, randomized study of YM155 plus docetaxel as first-line treatment in patients with HER2-negative metastatic breast cancer. *Breast Cancer Res Treat* **2015,** 149, 171-179.

40. Kudchadkar, R.; Ernst, S.; Chmielowski, B.; Redman, B. G.; Steinberg, J.; Keating, A.; Jie, F.; Chen, C.; Gonzalez, R.; Weber, J. A phase 2, multicenter, open-label study of sepantronium bromide (YM155) plus docetaxel in patients with stage III (unresectable) or stage IV melanoma. *Cancer Med* **2014**, epub ahead of print.

41. Nakamura, N.; Yamauchi, T.; Hiramoto, M.; Yuri, M.; Naito, M.; Takeuchi, M.; Yamanaka, K.; Kita, A.; Nakahara, T.; Kinoyama, I.; Matsuhisa, A.; Kaneko, N.; Koutoku, H.; Sasamata, M.; Yokota, H.; Kawabata, S.; Furiuchi, K. Interleukin enhancer-binding factor 3/NF110 is a target of YM155, a suppressant of survivin. *Mol Cell Proteomics* **2012,** 11, M111.013243.

42. Yamauchi, T.; Nakamura, N.; Hiramoto, M.; Yuri, M.; Yokoto, H.; Naitou, M.; Takeuchi, M.; Yamanaka, K.; Kita, A.; Nakahara, T.; Kinoyama, I.; Matsuhisa, A.; Kaneko, N.; Koutoku, H.; Sasamata, M.; Kobori, M.; Katou, M.; Tawara, S.; Kawabata, S.; Furuichi, K. Sepantronium Bromide (YM155) induces disruption of the ILF3/p54nrb complex, which is required for survivin expression. *Biochem Biophys Res Commun* **2012,** 425, 711-716.

43. Cheng, Q.; Ling, X.; Haller, A.; Nakahara, T.; Yamanaka, K.; Kita, A.; Koutoku, H.; Takeuchi, M.; Brattain, M. G.; Li, F. Suppression of survivin promoter activity by YM155 involves disruption of Sp1-DNA interaction in the survivin core promoter. *Int J Biochem Mol Biol* **2012,** 3, 179-197.

44. Schneider, G.; Krämer, O. H. NFκB/p53 crosstalk—a promising new therapeutic target. *Biochim Biophys Acta Rev Canc* **2011,** 1815, 90-103.

45. Schneider, G.; Henrich, A.; Greiner, G.; Wolf, V.; Lovas, A.; Wieczorek, M.; Wagner, T.; Reichardt, S.; von Werder, A.; Schmid, R. M.; Weih, F.; Heinzel, T.; Saur, D.; Kramer, O. H. Cross talk between stimulated NF-[kappa]B and the tumor suppressor p53. *Oncogene* **2010,** 29, 2795-2806.

46. Aggarwal, B. B.; Kunnumakkara, A. B.; Harikumar, K. B.; Gupta, S. R.; Tharakan, S. T.; Koca, C.; Dey, S.; Sung, B. Signal transducer and activator of transcription-3, inflammation, and cancer. *Ann N Y Acad Sci* **2009,** 1171, 59-76.

47. Czabotar, P. E.; Lessene, G.; Strasser, A.; Adams, J. M. Control of apoptosis by the BCL-2 protein family: implications for physiology and therapy. *Nat Rev Mol Cell Biol* **2014,** 15, 49-63.

48. Ola, M. S.; Nawaz, M.; Ahsan, H. Role of Bcl-2 family proteins and caspases in the regulation of apoptosis. *Mol Cell Biochem* **2011,** 351, 41-58.

49. Tang, H.; Shao, H.; Yu, C.; Hou, J. Mcl-1 downregulation by YM155 contributes to its synergistic anti-tumor activities with ABT-263. *Biochem Pharmacol* **2011,** 82, 1066-1072.

50. Jane, E. P.; Premkumar, D. R.; DiDomenico, J. D.; Hu, B.; Cheng, S. Y.; Pollack, I. F. YM-155 potentiates the effect of ABT-737 in malignant human glioma cells via survivin and Mcl-1 downregulation in an EGFR-dependent context. *Mol Cancer Ther* **2013,** 12, 326-338.

51. Na, Y. S.; Yang, S. J.; Kim, S. M.; Jung, K. A.; Moon, J. H.; Shin, J. S.; Yoon, D. H.; Hong, Y. S.; Ryu, M. H.; Lee, J. L.; Lee, J. S.; Kim, T. W. YM155 induces EGFR suppression in pancreatic cancer cells. *PLoS ONE* **2012,** 7, e38625.

52. Cheng, S. M.; Chang, Y. C.; Liu, C. Y.; Lee, J. Y.; Chan, H. H.; Kuo, C. W.; Lin, K. Y.; Tsai, S. L.; Chen, S. H.; Li, C. F.; Leung, E.; Kanwar, J. R.; Huang, C. C.; Chang, J. Y.; Cheung, C. H. YM155 down-regulates survivin and XIAP, modulates autophagy and induces autophagy-dependent DNA damage in breast cancer cells. *Br J Pharmacol* **2015,** 172, 214-234.

53. Dohi, T.; Okada, K.; Xia, F.; Wilford, C. E.; Samuel, T.; Welsh, K.; Marusawa, H.; Zou, H.; Armstrong, R.; Matsuzawa, S.; Salvesen, G. S.; Reed, J. C.; Altieri, D. C. An IAP-IAP complex inhibits apoptosis. *J Biol Chem* **2004,** 279, 34087-34090.

54. Tao, Y. F.; Lu, J.; Du, X. J.; Sun, L. C.; Zhao, X.; Peng, L.; Cao, L.; Xiao, P. F.; Pang, L.; Wu, D.; Wang, N.; Feng, X.; Li, Y. H.; Ni, J.; Wang, J.; Pan, J. Survivin selective inhibitor YM155 induce apoptosis in SK-NEP-1 Wilms tumor cells. *BMC Cancer* **2012,** 12, 619-632.

55. Glaros, T. G.; Stockwin, L. H.; Mullendore, M. E.; Smith, B.; Morrison, B. L.; Newton, D. L. The "survivin suppressants" NSC 80467 and YM155 induce a DNA damage response. *Cancer Chemother Pharmacol* **2012,** 70, 207-212.

56. Winter, G. E.; Radic, B.; Mayor-Ruiz, C.; Blomen, V. A.; Trefzer, C.; Kandasamy, R. K.; Huber, K. V. M.; Gridling, M.; Chen, D.; Klampfl, T.; Kralovics, R.; Kubicek, S.; Fernandez-Capetillo, O.; Brummelkamp, T. R.; Superti-Furga, G. The solute carrier SLC35F2 enables YM155-mediated DNA damage toxicity. *Nat Chem Biol* **2014,** 10, 768-773.

57. Bolton, J. L.; Trush, M. A.; Penning, T. M.; Dryhurst, G.; Monks, T. J. Role of quinones in toxicology. *Chem Res Toxicol* **2000,** 13, 135-160.

58. Vequaud, E.; Seveno, C.; Loussouarn, D.; Engelhart, L.; Campone, M.; Juin, P.; Barille-Nion, S. YM155 potently triggers cell death in breast cancer cells through an autophagy-NF-kB network. *Oncotarget* **2015,** 6, 13476-13486.

59. Minematsu, T.; Iwai, M.; Sugimoto, K.; Shirai, N.; Nakahara, T.; Usui, T.; Kamimura, H. Carrier-mediated uptake of 1-(2-methoxyethyl)-2-methyl-4,9-dioxo-3-(pyrazin-2-ylmethyl)-4,9-dihydro-1H-naphtho[2,3-d]imidazolium bromide (YM155 monobromide), a novel small-molecule survivin suppressant, into human solid tumor and lymphoma cells. *Drug Metab Disp* **2009,** 37, 619-628.

60. Minematsu, T.; Iwai, M.; Umehara, K.; Usui, T.; Kamimura, H. Characterization of human organic cation transporter 1 (OCT1/SLC22A1)- and OCT2 (SLC22A2)-mediated transport of 1-(2-methoxyethyl)-2-methyl-4,9-dioxo-3-(pyrazin-2-ylmethyl)- 4,9-dihydro-1H-naphtho[2,3-d]imidazolium bromide (YM155 monobromide), a novel small molecule survivin suppressant. *Drug Metab Disp* **2010,** 38, 1-4.

61. Iwai, M.; Minematsu, T.; Narikawa, S.; Usui, T.; Kamimura, H. Involvement of human organic cation transporter 1 in the hepatic uptake of 1-(2-methoxyethyl)-2-methyl-4,9-dioxo-3-(pyrazin-2-ylmethyl)-4,9-dihydro-1H-naphtho[2,3-d]imidazolium bromide (YM155 monobromide), a novel, small molecule survivin suppressant. *Drug Metab Disp* **2009,** 37, 1856-1863.

62. Fukuda, S.; Pelus, L. M. Survivin, a cancer target with an emerging role in normal adult tissues. *Mol Cancer Ther* **2006,** 5, 1087-1098.

63. Chiou, S. K.; Jones, M. K.; Tarnawski, A. S. Survivin - an anti-apoptosis protein: its biological roles and implications for cancer and beyond. *Med Sci Monit* **2003,** 9, Pi25-9.

64. Zwerts, F.; Lupu, F.; De Vriese, A.; Pollefeyt, S.; Moons, L.; Altura, R. A.; Jiang, Y.; Maxwell, P. H.; Hill, P.; Oh, H.; Rieker, C.; Collen, D.; Conway, S. J.; Conway, E. M. Lack

of endothelial cell survivin causes embryonic defects in angiogenesis, cardiogenesis, and neural tube closure. *Blood* **2007,** 109, 4742-4752.

65.   Mull, A. N.; Klar, A.; Navara, C. S. Differential localization and high expression of SURVIVIN splice variants in human embryonic stem cells but not in differentiated cells implicate a role for SURVIVIN in pluripotency. *Stem Cell Res* **2014,** 12, 539-549.

66.   Weikert, S.; Schrader, M.; Krause, H.; Schulze, W.; Muller, M.; Miller, K. The inhibitor of apoptosis (IAP) survivin is expressed in human testicular germ cell tumors and normal testes. *Cancer Lett* **2004,** 223, 331-337.

67.   Guvenc, H.; Pavlyukov, M. S.; Joshi, K.; Kurt, H.; Banasavadi-Siddegowda, Y. K.; Mao, P.; Hong, C.; Yamada, R.; Kwon, C. H.; Bhasin, D.; Chettiar, S.; Kitange, G.; Park, I. H.; Sarkaria, J. N.; Li, C.; Shakhparonov, M. I.; Nakano, I. Impairment of glioma stem cell survival and growth by a novel inhibitor for Survivin-Ran protein complex. *Clin Cancer Res* **2013,** 19, 631-642.

68.   Lee, M. O.; Moon, S. H.; Jeong, H. C.; Yi, J. Y.; Lee, T. H.; Shim, S. H.; Rhee, Y. H.; Lee, S. H.; Oh, S. J.; Lee, M. Y.; Han, M. J.; Cho, Y. S.; Chung, H. M.; Kim, K. S.; Cha, H. J. Inhibition of pluripotent stem cell-derived teratoma formation by small molecules. *P Natl Acad Sci USA* **2013,** 110, E3281-3290.

69.   Ben-David, U.; Benvenisty, N. The tumorigenicity of human embryonic and induced pluripotent stem cells. *Nat Rev Cancer* **2011,** 11, 268-277.

70.   Lee, A. S.; Tang, C.; Cao, F.; Xie, X.; van der Bogt, K.; Hwang, A.; Connolly, A. J.; Robbins, R. C.; Wu, J. C. Effects of cell number on teratoma formation by human embryonic stem cells. *Cell Cycle* **2009,** 8, 2608-2612.

71.   Baell, J.; Walters, M. A. Chemistry: Chemical con artists foil drug discovery. *Nature* **2014,** 513, 481-483.

72.   Matsuhisa, A.; Kinoyama, I.; Toyoshima, A.; Nakahara, T.; Takeuchi, M.; Okada, M. Fused imidazolium derivatives. May 11, 2004.

73.   Kuo, S.-C.; Ibuka, T.; Huang, L.-J.; Lien, J.-C.; Yean, S.-R.; Huang, S.-C.; Lednicer, D.; Morris-Natschke, S.; Lee, K.-H. Synthesis and cytotoxicity of 1,2-disubstituted naphth[2,3-d]imidazole-4,9-diones and related compounds. *J Med Chem* **1996,** 39, 1447-1451.

74.   Gopalan, B.; Narayanan, K.; Ke, Z.; Lu, T.; Zhang, Y.; Zhuo, L. Therapeutic effect of a multi-targeted imidazolium compound in hepatocellular carcinoma. *Biomaterials* **2014,** 35, 7479-7487.

75. Gopalan, B.; Ke, Z.; Zhang, C.; Kng, Y.; Suhaimi, N.-A. M.; Riduan, S. N.; Zhang, Y.; Zhuo, L. Metal-free imidazolium salts inhibit the growth of hepatocellular carcinoma in a mouse model. *Lab Invest* **2011,** 91, 744-751.

76. Pilarski, B. A new method for N-alkylation of imidazoles and benzimidazoles. *Liebigs Ann Chem* **1983,** 1983, 1078-1080.

77. Dupont, J.; Consorti, C. S.; Suarez, P. A. Z.; de Souza, R. F. Preparation of 1-butyl-3-methyl imidazolium-based room temperature ionic liquids. *Org Synth* **2002,** 79, 236.

78. Mahadevan, A.; Sard, H.; Gonzalez, M.; McKew, J. C. A general method for C3 reductive alkylation of indoles. *Tetrahedron Lett* **2003,** 44, 4589-4591.

79. Heaney, H.; Ley, S. V. N-alkylation of indole and pyrroles in dimethyl sulphoxide. *J Chem Soc, Perkin Trans 1* **1973**, 499-500.

80. Ljungberg, B.; Campbell, S. C.; Cho, H. Y.; Jacqmin, D.; Lee, J. E.; Weikert, S.; Kiemeney, L. A. The epidemiology of renal cell carcinoma. *Eur Urol* **2011,** 60, 615-621.

81. Cohen, H. T.; McGovern, F. J. Renal-cell carcinoma. *N Eng J Med* **2005,** 353, 2477-2490.

82. Rini, B. I.; Campbell, S. C.; Escudier, B. Renal cell carcinoma. *Lancet* **2009,** 373, 1119-1132.

83. Storkel, S.; Eble, J. N.; Adlakha, K.; Amin, M.; Blute, M. L.; Bostwick, D. G.; Darson, M.; Delahunt, B.; Iczkowski, K. Classification of renal cell carcinoma: Workgroup No. 1. Union Internationale Contre le Cancer (UICC) and the American Joint Committee on Cancer (AJCC). *Cancer* **1997,** 80, 987-989.

84. Motzer, R. J.; Bander, N. H.; Nanus, D. M. Renal-Cell Carcinoma. *N Eng J Med* **1996,** 335, 865-875.

85. Lam, J. S.; Shvarts, O.; Leppert, J. T.; Figlin, R. A.; Belldegrun, A. S. Renal cell carcinoma 2005: new frontiers in staging, prognostication and targeted molecular therapy. *J Urol* **2005,** 173, 1853-1862.

86. Gupta, K.; Miller, J. D.; Li, J. Z.; Russell, M. W.; Charbonneau, C. Epidemiologic and socioeconomic burden of metastatic renal cell carcinoma (mRCC): a literature review. *Cancer Treat Rev* **2008,** 34, 193-205.

87. Flanigan, R. C.; Campbell, S. C.; Clark, J. I.; Picken, M. M. Metastatic renal cell carcinoma. *Curr Treat Options Oncol* **2003,** 4, 385-390.

88. Onufrey, V.; Mohiuddin, M. Radiation therapy in the treatment of metastatic renal cell carcinoma. *Int J Radiat Oncol Biol Phys* **1985,** 11, 2007-2009.

89. Hartmann, J. T.; Bokemeyer, C. Chemotherapy for renal cell carcinoma. *Anticancer Res* **1999,** 19, 1541-1543.

90. Amato, R. J. Chemotherapy for renal cell carcinoma. *Seminars in oncology* **2000,** 27, 177-186.

91. Bharthuar, A. Metastatic renal cell carcinoma: Current scenario and future trends. *South Asian J Cancer* **2012,** 1, 30-35.

92. Maher, E. R.; Yates, J. R. W.; Harries, R.; Benjamin, C.; Harris, R.; Moore, A. T.; Ferguson-Smith, A. Clinical features and natural history of von Hippel-Lindau disease. *Q J Med* **1990,** 77, 1151-1163.

93. Alves, M. R.; Carneiro, F. C.; Lavorato-Rocha, A. M.; da Costa, W. H.; da Cunha, I. W.; de Cássio Zequi, S.; Guimaraes, G. C.; Soares, F. A.; Carraro, D. M.; Rocha, R. M. Mutational status of VHL gene and its clinical importance in renal clear cell carcinoma. *Virchows Archiv* **2014,** 465, 321-330.

94. Lessi, F.; Mazzanti, C.; Tomei, S.; Di Cristofano, C.; Minervini, A.; Menicagli, M.; Apollo, A.; Masieri, L.; Collecchi, P.; Minervini, R.; Carini, M.; Bevilacqua, G. VHL and HIF-1α: gene variations and prognosis in early-stage clear cell renal cell carcinoma. *Med Oncol* **2014,** 31, 1-7.

95. Raval, R. R.; Lau, K. W.; Tran, M. G.; Sowter, H. M.; Mandriota, S. J.; Li, J. L.; Pugh, C. W.; Maxwell, P. H.; Harris, A. L.; Ratcliffe, P. J. Contrasting properties of hypoxia-inducible factor 1 (HIF-1) and HIF-2 in von Hippel-Lindau-associated renal cell carcinoma. *Mol Cell Biol* **2005,** 25, 5675-5686.

96. Baldewijns, M. M.; van Vlodrop, I. J.; Vermeulen, P. B.; Soetekouw, P. M.; van Engeland, M.; de Bruine, A. P. VHL and HIF signalling in renal cell carcinogenesis. *J Pathol* **2010,** 221, 125-138.

97. Clark, P. E. The role of VHL in clear-cell renal cell carcinoma and its relation to targeted therapy. *Kidney Int* **2009,** 76, 939-945.

98. Masson, N.; Ratcliffe, P. J. HIF prolyl and asparaginyl hydroxylases in the biological response to intracellular O(2) levels. *J Cell Sci* **2003,** 116, 3041-3049.

99. Semenza, G. L. Hydroxylation of HIF-1: oxygen sensing at the molecular level. *Physiology (Bethesda)* **2004,** 19, 176-182.

100. Rathmell, W. K.; Wright, T. M.; Rini, B. I. Molecularly targeted therapy in renal cell carcinoma. *Expert Rev Anticancer Ther* **2005,** 5, 1031-1040.

101. Bindra, R. S.; Vasselli, J. R.; Stearman, R.; Linehan, W. M.; Klausner, R. D. VHL-mediated hypoxia regulation of cyclin D1 in renal carcinoma cells. *Cancer Res* **2002,** 62, 3014-3019.

102. Luu, V. D.; Boysen, G.; Struckmann, K.; Casagrande, S.; von Teichman, A.; Wild, P. J.; Sulser, T.; Schraml, P.; Moch, H. Loss of VHL and hypoxia provokes PAX2 up-regulation in clear cell renal cell carcinoma. *Clin Cancer Res* **2009,** 15, 3297-3304.

103. Yuen, J. S. P.; Cockman, M. E.; Sullivan, M.; Protheroe, A.; Turner, G. D. H.; Roberts, I. S.; Pugh, C. W.; Werner, H.; Macaulay, V. M. The VHL tumor suppressor inhibits expression of the IGF1R and its loss induces IGF1R upregulation in human clear cell renal carcinoma. *Nature* **2007,** 26, 6499-6508.

104. Bukowski, R. M.; Motzer, R. J.; Figlin, R. A. Renal cell carcinoma: molecular targets and clinical applications. In 2nd ed.; Humana Press: NY, 2009.

105. Yancopoulos, G. D.; Davis, S.; Gale, N. W.; Rudge, J. S.; Wiegand, S. J.; Holash, J. Vascular-specific growth factors and blood vessel formation. *Nature* **2000,** 407.

106. Hellstrom, M.; Kalen, M.; Lindahl, P.; Abramsson, A.; Betsholtz, C. Role of PDGF-B and PDGFR-beta in recruitment of vascular smooth muscle cells and pericytes during embryonic blood vessel formation in the mouse. *Development* **1999,** 126, 3047-3055.

107. Kondo, K.; Kaelin, W. G. The von Hippel-Lindau tumor suppressor gene. *Exp Cell Res* **2001,** 264, 117-125.

108. Arai, E.; Kanai, Y. Genetic and epigenetic alterations during renal carcinogenesis. *Int J Clin Exp Pathol* **2011,** 4, 58-73.

109. Slaton, J. W.; Inoue, K.; Perrotte, P.; El-Naggar, A. K.; Swanson, D. A.; Fidler, I. J.; Dinney, C. P. N. Expression levels of genes that regulate metastasis and angiogenesis correlate with advanced pathological stage of renal cell carcinoma. *Am J Pathol* **2001,** 158, 735-743.

110. Knaup, K. X.; Jozefowski, K.; Schmidt, R.; Bernhardt, W. M.; Weidemann, A.; Juergensen, J. S.; Warnecke, C.; Eckardt, K. U.; Wiesener, M. S. Mutual regulation of hypoxia-inducible factor and mammalian target of rapamycin as a function of oxygen availability. *Mol Cancer Res* **2009,** 7, 88-98.

111. The Cancer Genome Atlas Research, N. Comprehensive molecular characterization of clear cell renal cell carcinoma. *Nature* **2013,** 499, 43-49.

112. Wouters, B. G.; Koritzinsky, M. Hypoxia signalling through mTOR and the unfolded protein response in cancer. *Nat Rev Cancer* **2008,** 8, 851-864.

113. Ahn, K. S.; Aggarwal, B. B. Transcription factor NF-kappaB: a sensor for smoke and stress signals. *Ann N Y Acad Sci* **2005,** 1056, 218-233.

114. Moynagh, P. N. The NF-kB pathway. *J Cell Sci* **2005,** 118, 4389-4392.

115. Baeuerle, P. A.; Henkel, T. Function and activation of NF-kB in the immune system. *Annu Rev Immunol* **1994,** 12, 141-179.

116. Dolcet, X.; Llobet, D.; Pallares, J.; Matias-Guiu, X. NF-kB in development and progression of human cancer. *Virchows Archiv* **2005,** 446, 475-482.

117. Karin, M. NF-kB and cancer: mechanisms and targets. *Mol Carcinogenesis* **2006,** 45, 355-361.

118. van Uden, P.; Kenneth, N. S.; Rocha, S. Regulation of hypoxia-inducible factor-1alpha by NF-kappaB. *Biochem J* **2008,** 412, 477-484.

119. McDermott, D. F.; Rini, B. I. Immunotherapy for metastatic renal cell carcinoma. *BJU Int* **2007,** 99, 1282-1288.

120. Kapoor, A. K.; Hotte, S. J. Current status of cytokine therapy in management of patients with metastatic renal cell carcinoma. *Can Urol Assoc J* **2007,** 1, S28-S33.

121. Fyfe, G.; Fisher, R. I.; Rosenberg, S. A.; Sznol, M.; Parkinson, D. R.; Louie, A. C. Results of treatment of 255 patients with metastatic renal cell carcinoma who received high-dose recombinant interleukin-2 therapy. *J Clin Oncol* **1995,** 13, 688-696.

122. Yang, J. C.; Haworth, L.; Sherry, R. M.; Hwu, P.; Schwartzentruber, D. J.; Topalian, S. L.; Steinberg, S. M.; Chen, H. X.; Rosenberg, S. A. A Randomized Trial of Bevacizumab, an Anti–Vascular Endothelial Growth Factor Antibody, for Metastatic Renal Cancer. *N Eng J Med* **2003,** 349, 427-434.

123. Escudier, B.; Eisen, T.; Stadler, W. M.; Szczylik, C.; Oudard, S.; Siebels, M.; Negrier, S.; Chevreau, C.; Solska, E.; Desai, A. A.; Rolland, F.; Demkow, T.; Hutson, T. E.; Gore, M.; Freeman, S.; Schwartz, B.; Shan, M.; Simantov, R.; Bukowski, R. M. Sorafenib in Advanced Clear-Cell Renal-Cell Carcinoma. *N Eng J Med* **2007,** 356, 125-134.

124. Motzer, R. J.; Michaelson, M. D.; Redman, B. G.; Hudes, G. R.; Wilding, G.; Figlin, R. A.; Ginsberg, M. S.; Kim, S. T.; Baum, C. M.; DePrimo, S. E.; Li, J. Z.; Bello, C. L.; Theuer, C. P.; George, D. J.; Rini, B. I. Activity of SU11248, a multitargeted inhibitor of vascular endothelial growth factor receptor and platelet-derived growth factor receptor, in patients with metastatic renal cell carcinoma. *J Clin Oncol* **2006,** 24, 16-24.

125. Motzer, R. J.; Rini, B. I.; Bukowski, R. M.; Curti, B. D.; George, D. J.; Hudes, G. R.; Redman, B. G.; Margolin, K. A.; Merchan, J. R.; Wilding, G.; Ginsberg, M. S.; Bacik, J.; Kim, S. T.; Baum, C. M.; Michaelson, M. D. Sunitinib in patients with metastatic renal cell carcinoma. *JAMA* **2006,** 295, 2516-2524.

126. Motzer, R. J.; Hutson, T. E.; Cella, D.; Reeves, J.; Hawkins, R.; Guo, J.; Nathan, P.; Staehler, M.; de Souza, P.; Merchan, J. R.; Boleti, E.; Fife, K.; Jin, J.; Jones, R.; Uemura,

H.; De Giorgi, U.; Harmenberg, U.; Wang, J.; Sternberg, C. N.; Deen, K.; McCann, L.; Hackshaw, M. D.; Crescenzo, R.; Pandite, L. N.; Choueiri, T. K. Pazopanib versus sunitinib in metastatic renal-cell carcinoma. *N Eng J Med* **2013,** 369, 722-731.

127. Sternberg, C. N.; Davis, I. D.; Mardiak, J.; Szczylik, C.; Lee, E.; Wagstaff, J.; Barrios, C. H.; Salman, P.; Gladkov, O. A.; Kavina, A.; Zarba, J. J.; Chen, M.; McCann, L.; Pandite, L.; Roychowdhury, D. F.; Hawkins, R. E. Pazopanib in locally advanced or metastatic renal cell carcinoma: results of a randomized phase III trial. *J Clin Oncol* **2010,** 28, 1061-1068.

128. Rini, B. I.; Escudier, B.; Tomczak, P.; Kaprin, A.; Szczylik, C.; Hutson, T. E.; Michaelson, M. D.; Gorbunova, V. A.; Gore, M. E.; Rusakov, I. G.; Negrier, S.; Ou, Y. C.; Castellano, D.; Lim, H. Y.; Uemura, H.; Tarazi, J.; Cella, D.; Chen, C.; Rosbrook, B.; Kim, S.; Motzer, R. J. Comparative effectiveness of axitinib versus sorafenib in advanced renal cell carcinoma (AXIS): a randomised phase 3 trial. *Lancet* **2011,** 378, 1931-1939.

129. Hutson, T. E.; Lesovoy, V.; Al-Shukri, S.; Stus, V. P.; Lipatov, O. N.; Bair, A. H.; Rosbrook, B.; Chen, C.; Kim, S.; Vogelzang, N. J. Axitinib versus sorafenib as first-line therapy in patients with metastatic renal-cell carcinoma: a randomised open-label phase 3 trial. *Lancet Oncol* **2013,** 14, 1287-1294.

130. Escudier, B.; Gore, M. Axitinib for the management of metastatic renal cell carcinoma. *Drugs R D* **2011,** 11, 113-126.

131. Hudes, G.; Carducci, M.; Tomczak, P.; Dutcher, J.; Figlin, R.; Kapoor, A.; Staroslawska, E.; Sosman, J.; McDermott, D.; Bodrogi, I.; Kovacevic, Z.; Lesovoy, V.; Schmidt-Wolf, I. G. H.; Barbarash, O.; Gokmen, E.; O'Toole, T.; Lustgarten, S.; Moore, L.; Motzer, R. J. Temsirolimus, interferon alfa, or both for advanced renal-cell carcinoma. *N Eng J Med* **2007,** 356, 2271-2281.

132. Hutson, T. E.; Escudier, B.; Esteban, E.; Bjarnason, G. A.; Lim, H. Y.; Pittman, K. B.; Senico, P.; Niethammer, A.; Lu, D. R.; Hariharan, S.; Motzer, R. J. Randomized phase III trial of temsirolimus versus sorafenib as second-line therapy after sunitinib in patients with metastatic renal cell carcinoma. *J Clin Oncol* **2014,** 32, 760-767.

133. Motzer, R. J.; Escudier, B.; Oudard, S.; Hutson, T. E.; Porta, C.; Bracarda, S.; Grunwald, V.; Thompson, J. A.; Figlin, R. A.; Hollaender, N.; Kay, A.; Ravaud, A. Phase 3 trial of everolimus for metastatic renal cell carcinoma: final results and analysis of prognostic factors. *Cancer* **2010,** 116, 4256-4265.

134. Motzer, R. J.; Escudier, B.; Oudard, S.; Hutson, T. E.; Porta, C.; Bracarda, S.; Grunwald, V.; Thompson, J. A.; Figlin, R. A.; Hollaender, N.; Urbanowitz, G.; Berg, W. J.; Kay, A.;

Lebwohl, D.; Ravaud, A. Efficacy of everolimus in advanced renal cell carcinoma: a double-blind, randomised, placebo-controlled phase III trial. *Lancet* **2008,** 372, 449-456.

135. Abu-Hejleh, T.; Mezhir, J. J.; Goodheart, M. J.; Halfdanarson, T. R. Incidence and management of gastrointestinal perforation from bevacizumab in advanced cancers. *Curr Oncol Rep* **2012,** 14, 277-284.

136. Ovadia, D.; Esquenazi, Y.; Bucay, M.; Bachier, C. R. Association between takotsubo cardiomyopathy and axitinib: case report and review of the literature. *J Clin Oncol* **2015,** 33, e1-3.

137. Choueiri, T. K.; Je, Y.; Sonpavde, G.; Richards, C. J.; Galsky, M. D.; Nguyen, P. L.; Schutz, F.; Heng, D. Y.; Kaymakcalan, M. D. Incidence and risk of treatment-related mortality in cancer patients treated with the mammalian target of rapamycin inhibitors. *Ann Oncol* **2013,** 24, 2092-2097.

138. Gulland, A. *Global cancer prevalence is growing at "alarming pace," says WHO*. 2014; Vol. 348.

139. Boyle, P.; Levin, B. *World Cancer Report 2008*. World Health Organization: 2008; p 511.

140. Ramalingam, S.; Belani, C. Systemic chemotherapy for advanced non-small cell lung cancer: Recent advances and future directions. *The Oncologist* **2008,** 13, 5-13.

141. Slatore, C. G.; Gould, M. K.; Au, D. H.; Deffebach, M. E.; White, E. Lung cancer stage at diagnosis: Individual associations in the prospective VITamins and lifestyle (VITAL) cohort. *BMC Cancer* **2011,** 11, 228.

142. Molina, J. R.; Yang, P.; Cassivi, S. D.; Schild, S. E.; Adjei, A. A. Non-small cell lung cancer: epidemiology, risk factors, treatment, and survivorship. *Mayo clin proc* **2008,** 83, 584-594.

143. Stewart, D. J. Lung Cancer Resistance to Chemotherapy. In *Lung Cancer*, Stewart, D. J., Ed. Humana Press: 2010; pp 331-393.

144. Zhu, J.; Sharma, D. B.; Chen, A. B.; Johnson, B. E.; Weeks, J. C.; Schrag, D. Comparative effectiveness of three platinum-doublet chemotherapy regimens in elderly patients with advanced non–small cell lung cancer. *Cancer* **2013,** 119, 2048-2060.

145. Group, N. M.-A. C. Chemotherapy in addition to supportive care improves survival in advanced non-small-cell lung cancer: a systematic review and meta-analysis of individual patient data from 16 randomized controlled trials. *J Clin Oncol* **2008,** 26, 4617-4625.

146. da Cunha Santos, G.; Shepherd, F. A.; Tsao, M. S. EGFR mutations and lung cancer. *Annu Rev Pathol* **2011,** 6, 49-69.

147. Marchetti, A.; Martella, C.; Felicioni, L.; Barassi, F.; Salvatore, S.; Chella, A.; Camplese, P. P.; Iarussi, T.; Mucilli, F.; Mezzetti, A.; Cuccurullo, F.; Sacco, R.; Buttitta, F. EGFR mutations in non-small-cell lung cancer: analysis of a large series of cases and development of a rapid and sensitive method for diagnostic screening with potential implications on pharmacologic treatment. *J Clin Oncol* **2005,** 23, 857-865.

148. Mitsudomi, T. Molecular epidemiology of lung cancer and geographic variations with special reference to EGFR mutations. *Transl Lung Cancer Res* **2014,** 3, 205-211.

149. Wells, A. EGF receptor. *Int J Biochem Cell Biol* **1999,** 31, 637-643.

150. Linggi, B.; Carpenter, G. ErbB receptors: new insights on mechanisms and biology. *Trends Cell Biol* **2006,** 16, 649-656.

151. Yarden, Y.; Schlessinger, J. Epidermal growth factor induces rapid, reversible aggregation of the purified epidermal growth factor receptor. *Biochemistry* **1987,** 26, 1443-1451.

152. Jorissen, R. N.; Walker, F.; Pouliot, N.; Garrett, T. P. J.; Ward, C. W.; Burgess, A. W. Epidermal growth factor receptor: Mechanisms of activation and signalling. *Exp Cell Res* **2003,** 284, 31-53.

153. Schulze, W. X.; Deng, L.; Mann, M. Phosphotyrosine interactome of the ErbB-receptor kinase family. *Mol Syst Biol* **2005,** 1, 2005.0008-2005.0008.

154. Okutani, T.; Okabayashi, Y.; Kido, Y.; Sugimoto, Y.; Sakaguchi, K.; Matuoka, K.; Takenawa, T.; Kasuga, M. Grb2/Ash binds directly to tyrosines 1068 and 1086 and indirectly to tyrosine 1148 of activated human epidermal growth factor receptors in intact cells. *J Biol Chem* **1994,** 269, 31310-31314.

155. Margolis, B.; Skolnik, E. Y. Activation of Ras by receptor tyrosine kinases. *J Am Soc Nephrol* **1994,** 5, 1288-1299.

156. Chang, F.; Steelman, L. S.; Lee, J. T.; Shelton, J. G.; Navolanic, P. M.; Blalock, W. L.; Franklin, R. A.; McCubrey, J. A. Signal transduction mediated by the Ras/Raf/MEK/ERK pathway from cytokine receptors to transcription factors: potential targeting for therapeutic intervention. *Leukemia* **2003,** 17, 1263-1293.

157. Pelengaris, S.; Khan, M. The c-MYC oncoprotein as a treatment target in cancer and other disorders of cell growth. *Expert Opin Ther Targets* **2003,** 7, 623-642.

158. Harada, H.; Quearry, B.; Ruiz-Vela, A.; Korsmeyer, S. J. Survival factor-induced extracellular signal-regulated kinase phosphorylates BIM, inhibiting its association with BAX and proapoptotic activity. *P Natl Acad Sci USA* **2004,** 101, 15313-15317.

159. Zha, J.; Harada, H.; Yang, E.; Jockel, J.; Korsmeyer, S. J. Serine phosphorylation of death agonist BAD in response to survival factor results in binding to 14-3-3 not BCL-X(L). *Cell* **1996,** 87, 619-628.

160. Quesnelle, K. M.; Boehm, A. L.; Grandis, J. R. STAT-mediated EGFR signaling in cancer. *J Cell Biochem* **2007,** 102, 311-319.

161. Haura, E. B.; Turkson, J.; Jove, R. Mechanisms of disease: Insights into the emerging role of signal transducers and activators of transcription in cancer. *Nat Clin Pract Oncol* **2005,** 2, 315-324.

162. Leeman, R. J.; Lui, V. W.; Grandis, J. R. STAT3 as a therapeutic target in head and neck cancer. *Expert Opin Biol Ther* **2006,** 6, 231-241.

163. Sarbassov, D. D.; Guertin, D. A.; Ali, S. M.; Sabatini, D. M. Phosphorylation and regulation of Akt/PKB by the rictor-mTOR Complex. *Science* **2005,** 307, 1098-1101.

164. Song, G.; Ouyang, G.; Bao, S. The activation of Akt/PKB signaling pathway and cell survival. *J Cell Mol Med* **2005,** 9, 59-71.

165. Lynch, T. J.; Bell, D. W.; Sordella, R.; Gurubhagavatula, S.; Okimoto, R. A.; Brannigan, B. W.; Harris, P. L.; Haserlat, S. M.; Supko, J. G.; Haluska, F. G.; Louis, D. N.; Christiani, D. C.; Settleman, J.; Haber, D. A. Activating mutations in the epidermal growth factor receptor underlying responsiveness of non–small-cell lung cancer to gefitinib. *N Eng J Med* **2004,** 350, 2129-2139.

166. Pines, G.; Köstler, W. J.; Yarden, Y. Oncogenic mutant forms of EGFR: Lessons in signal transduction and targets for cancer therapy. *FEBS Lett* **2010,** 584, 2699-2706.

167. Miller, V. A.; Hirsh, V.; Cadranel, J.; Chen, Y.-M.; Park, K.; Kim, S.-W.; Zhou, C.; Su, W.-C.; Wang, M.; Sun, Y.; Heo, D. S.; Crino, L.; Tan, E.-H.; Chao, T.-Y.; Shahidi, M.; Cong, X. J.; Lorence, R. M.; Yang, J. C.-H. Afatinib versus placebo for patients with advanced, metastatic non-small-cell lung cancer after failure of erlotinib, gefitinib, or both, and one or two lines of chemotherapy (LUX-Lung 1): a phase 2b/3 randomised trial. *Lancet Oncol* **2012,** 13, 528-538.

168. Sandler, A.; Gray, R.; Perry, M. C.; Brahmer, J.; Schiller, J. H.; Dowlati, A.; Lilenbaum, R.; Johnson, D. H. Paclitaxel–Carboplatin alone or with Bevacizumab for non–small-cell lung cancer. *N Eng J Med* **2006,** 355, 2542-2550.

169. Reck, M.; von Pawel, J.; Zatloukal, P.; Ramlau, R.; Gorbounova, V.; Hirsh, V.; Leighl, N.; Mezger, J.; Archer, V.; Moore, N.; Manegold, C. Phase III trial of cisplatin plus gemcitabine with either placebo or bevacizumab as first-line therapy for nonsquamous non-small-cell lung cancer: AVAil. *J Clin Oncol* **2009,** 27, 1227-1234.

170. Garon, E. B.; Ciuleanu, T.-E.; Arrieta, O.; Prabhash, K.; Syrigos, K. N.; Goksel, T.; Park, K.; Gorbunova, V.; Kowalyszyn, R. D.; Pikiel, J.; Czyzewicz, G.; Orlov, S. V.; Lewanski, C. R.; Thomas, M.; Bidoli, P.; Dakhil, S.; Gans, S.; Kim, J.-H.; Grigorescu, A.; Karaseva, N.; Reck, M.; Cappuzzo, F.; Alexandris, E.; Sashegyi, A.; Yurasov, S.; Pérol, M. Ramucirumab plus docetaxel versus placebo plus docetaxel for second-line treatment of stage IV non-small-cell lung cancer after disease progression on platinum-based therapy (REVEL): a multicentre, double-blind, randomised phase 3 trial. *Lancet* **2014,** 384, 665-673.

171. Inoue, A.; Kobayashi, K.; Maemondo, M.; Sugawara, S.; Oizumi, S.; Isobe, H.; Gemma, A.; Harada, M.; Yoshizawa, H.; Kinoshita, I.; Fujita, Y.; Okinaga, S.; Hirano, H.; Yoshimori, K.; Harada, T.; Saijo, Y.; Hagiwara, K.; Morita, S.; Nukiwa, T. Updated overall survival results from a randomized phase III trial comparing gefitinib with carboplatin-paclitaxel for chemo-naive non-small cell lung cancer with sensitive EGFR gene mutations (NEJ002). *Ann Oncol* **2013,** 24, 54-59.

172. Kim, E. S.; Hirsh, V.; Mok, T.; Socinski, M. A.; Gervais, R.; Wu, Y. L.; Li, L. Y.; Watkins, C. L.; Sellers, M. V.; Lowe, E. S.; Sun, Y.; Liao, M. L.; Osterlind, K.; Reck, M.; Armour, A. A.; Shepherd, F. A.; Lippman, S. M.; Douillard, J. Y. Gefitinib versus docetaxel in previously treated non-small-cell lung cancer (INTEREST): a randomised phase III trial. *Lancet* **2008,** 372, 1809-1818.

173. Thatcher, N.; Chang, A.; Parikh, P.; Rodrigues Pereira, J.; Ciuleanu, T.; von Pawel, J.; Thongprasert, S.; Tan, E. H.; Pemberton, K.; Archer, V.; Carroll, K. Gefitinib plus best supportive care in previously treated patients with refractory advanced non-small-cell lung cancer: results from a randomised, placebo-controlled, multicentre study (Iressa Survival Evaluation in Lung Cancer). *Lancet* **2005,** 366, 1527-1537.

174. Mok, T. S.; Wu, Y.-L.; Thongprasert, S.; Yang, C.-H.; Chu, D.-T.; Saijo, N.; Sunpaweravong, P.; Han, B.; Margono, B.; Ichinose, Y.; Nishiwaki, Y.; Ohe, Y.; Yang, J.-J.; Chewaskulyong, B.; Jiang, H.; Duffield, E. L.; Watkins, C. L.; Armour, A. A.; Fukuoka, M. Gefitinib or carboplatin–paclitaxel in pulmonary adenocarcinoma. *N Eng J Med* **2009,** 361, 947-957.

175. Shepherd, F. A.; Rodrigues Pereira, J.; Ciuleanu, T.; Tan, E. H.; Hirsh, V.; Thongprasert, S.; Campos, D.; Maoleekoonpiroj, S.; Smylie, M.; Martins, R.; van Kooten, M.; Dediu, M.; Findlay, B.; Tu, D.; Johnston, D.; Bezjak, A.; Clark, G.; Santabarbara, P.; Seymour, L. Erlotinib in previously treated non-small-cell lung cancer. *N Eng J Med* **2005,** 353, 123-132.

176. Rosell, R.; Moran, T.; Queralt, C.; Porta, R.; Cardenal, F.; Camps, C.; Majem, M.; Lopez-Vivanco, G.; Isla, D.; Provencio, M.; Insa, A.; Massuti, B.; Gonzalez-Larriba, J. L.; Paz-Ares, L.; Bover, I.; Garcia-Campelo, R.; Moreno, M. A.; Catot, S.; Rolfo, C.; Reguart, N.; Palmero, R.; Sánchez, J. M.; Bastus, R.; Mayo, C.; Bertran-Alamillo, J.; Molina, M. A.; Sanchez, J. J.; Taron, M. Screening for Epidermal Growth Factor Receptor Mutations in Lung Cancer. *N Eng J Med* **2009,** 361, 958-967.

177. Sequist, L. V.; Yang, J. C.; Yamamoto, N.; O'Byrne, K.; Hirsh, V.; Mok, T.; Geater, S. L.; Orlov, S.; Tsai, C. M.; Boyer, M.; Su, W. C.; Bennouna, J.; Kato, T.; Gorbunova, V.; Lee, K. H.; Shah, R.; Massey, D.; Zazulina, V.; Shahidi, M.; Schuler, M. Phase III study of afatinib or cisplatin plus pemetrexed in patients with metastatic lung adenocarcinoma with EGFR mutations. *J Clin Oncol* **2013,** 31, 3327-3334.

178. Waring, M. J. Complex formation between ethidium bromide and nucleic acids. *J Mol Biol* **1965,** 13, 269-282.

179. Gurova, K. New hopes from old drugs: revisiting DNA-binding small molecules as anticancer agents. *Future Oncol* **2009,** 5, 1685.

180. Silverman, R. B.; Holladay, M. W. Chapter 6 - DNA-Interactive Agents. In *The Organic Chemistry of Drug Design and Drug Action (Third Edition)*, Silverman, R. B.; Holladay, M. W., Eds. Academic Press: Boston (USA), 2014; pp 275-331.

181. Kalgutkar, A. S.; Gardner, I.; Obach, R. S.; Shaffer, C. L.; Callegari, E.; Henne, K. R.; Mutlib, A. E.; Dalvie, D. K.; Lee, J. S.; Nakai, Y.; O'Donnell, J. P.; Boer, J.; Harriman, S. P. A comprehensive listing of bioactivation pathways of organic functional groups. *Curr Drug Metab* **2005,** 6, 161-225.

182. Sawahata, T.; Neal, R. A. Biotransformation of phenol to hydroquinone and catechol by rat liver microsomes. *Mol Pharmacol* **1983,** 23, 453-460.

183. Gant, T. W.; Ramakrishna Rao, D. N.; Mason, R. P.; Cohen, G. M. Redox cycling and sulphydryl arylation; Their relative importance in the mechanism of quinone cytotoxicity to isolated hepatocytes. *Chem Biol Interact* **1988,** 65, 157-173.

184. Halliwell, B.; Cross, C. E. Oxygen-derived species: their relation to human disease and environmental stress. *Environ Health Perspect* **1994,** 102, 5-12.

185. Tse, W. C.; Boger, D. L. A fluorescent intercalator displacement assay for establishing DNA binding selectivity and affinity. *Acc Chem Res* **2004,** 37, 61-69.

186. Boger, D. L.; Tse, W. C. Thiazole orange as the fluorescent intercalator in a high resolution fid assay for determining DNA binding affinity and sequence selectivity of small molecules. *Bioorg Med Chem* **2001,** 9, 2511-2518.

187. Soares, K. M.; Blackmon, N.; Shun, T. Y.; Shinde, S. N.; Takyi, H. K.; Wipf, P.; Lazo, J. S.; Johnston, P. A. Profiling the NIH Small Molecule Repository for compounds that generate H2O2 by redox cycling in reducing environments. *Assay Drug Dev Technol* **2010,** 8, 152-174.

188. Johnston, P. A.; Soares, K. M.; Shinde, S. N.; Foster, C. A.; Shun, T. Y.; Takyi, H. K.; Wipf, P.; Lazo, J. S. Development of a 384-well colorimetric assay to quantify hydrogen peroxide generated by the redox cycling of compounds in the presence of reducing agents. *Assay Drug Dev Technol* **2008,** 6, 505-518.

189. Rosenkranz, A. R.; Schmaldienst, S.; Stuhlmeier, K. M.; Chen, W.; Knapp, W.; Zlabinger, G. J. A microplate assay for the detection of oxidative products using 2′,7′-dichlorofluorescin-diacetate. *J Immunol Methods* **1992,** 156, 39-45.

190. Wang, H.; Joseph, J. A. Quantifying cellular oxidative stress by dichlorofluorescein assay using microplate reader. *Free Radic Biol Med* **1999,** 27, 612-616.

191. Bonner, W. M.; Redon, C. E.; Dickey, J. S.; Nakamura, A. J.; Sedelnikova, O. A.; Solier, S.; Pommier, Y. [gamma]H2AX and cancer. *Nat Rev Cancer* **2008,** 8, 957-967.

192. Huang, X.; Halicka, H. D.; Darzynkiewicz, Z. Detection of Histone H2AX Phosphorylation on Ser-139 as an Indicator of DNA Damage (DNA Double-Strand Breaks). *Curr Protoc Cytometry* **2001,** 30, 7.27.1-7.27-7.

193. Kavanagh, E.; Rodhe, J.; Burguillos, M. A.; Venero, J. L.; Joseph, B. Regulation of caspase-3 processing by cIAP2 controls the switch between pro-inflammatory activation and cell death in microglia. *Cell Death Dis* **2014,** 5, e1565.

194. Lyu, Y. L.; Kerrigan, J. E.; Lin, C.-P.; Azarova, A. M.; Tsai, Y.-C.; Ban, Y.; Liu, L. F. Topoisomerase IIB-mediated DNA double-strand breaks: implications in doxorubicin cardiotoxicity and prevention by dexrazoxane. *Cancer Res* **2007,** 67, 8839-8846.

195. Brunmark, A.; Cadenas, E. Redox and addition chemistry of quinoid compounds and its biological implications. *Free Radical Biology and Medicine* **1989,** 7, 435-477.

196. Barnes, P. J. Nuclear factor-kB. *Int J Biochem Cell Biol* **1997,** 29, 867-870.

197. Atreya, I.; Atreya, R.; Neurath, M. F. NF-kappaB in inflammatory bowel disease. *J Intern Med* **2008,** 263, 591-596.

198. Wolberger, C. Combinatorial transcription factors. *Curr Opin Genet Dev* **1998,** 8, 552-559.

199. Verma, I. M.; Stevenson, J. K.; Schwarz, E. M.; Van Antwerp, D.; Miyamoto, S. Rel/NF-kappa B/I kappa B family: intimate tales of association and dissociation. *Genes Dev* **1995,** 9, 2723-35.

200. Hayden, M. S.; Ghosh, S. Shared principles in NF-kB signalling. *Cell* **2008,** 132, 344-362.

201. Baldassarre, F.; Mallardo, M.; Mezza, E.; Scala, G.; Quinto, I. Regulation of NF-kappa B through the nuclear processing of p105 (NF-kappa B1) in Epstein-Barr virus-immortalized B cell lines. *J Biol Chem* **1995,** 270, 31244-31248.

202. Morais, C.; Gobe, G.; Johnson, D. W.; Healy, H. The emerging role of nuclear factor kappa B in renal cell carcinoma. *Int J Biochem Cell Biol* **2011,** 43, 1537-1549.

203. Sun, S. C. Non-canonical NF-kB signaling pathway. *Cell Res* **2011,** 21, 71-85.

204. Keats, J. J.; Fonseca, R.; Chesi, M.; Schop, R.; Baker, A.; Chng, W.-J.; Van Wier, S.; Tiedemann, R.; Shi, C.-X.; Sebag, M.; Braggio, E.; Henry, T.; Zhu, Y.-X.; Fogle, H.; Price-Troska, T.; Ahmann, G.; Mancini, C.; Brents, L. A.; Kumar, S.; Greipp, P.; Dispenzieri, A.; Bryant, B.; Mulligan, G.; Bruhn, L.; Barrett, M.; Valdez, R.; Trent, J.; Stewart, A. K.; Carpten, J.; Bergsagel, P. L. Promiscuous mutations activate the noncanonical NF-κB pathway in multiple myeloma. *Cancer Cell* **2007,** 12, 131-144.

205. Monaco, C.; Andreakos, E.; Kiriakidis, S.; Mauri, C.; Bicknell, C.; Foxwell, B.; Cheshire, N.; Paleolog, E.; Feldmann, M. Canonical pathway of nuclear factor κB activation selectively regulates proinflammatory and prothrombotic responses in human atherosclerosis. *P Natl Acad Sci USA* **2004,** 101, 5634-5639.

206. Marok, R.; Winyard, P. G.; Coumbe, A.; Kus, M. L.; Gaffney, K.; Blades, S.; Mapp, P. I.; Morris, C. J.; Blake, D. R.; Kaltschmidt, C.; Baeuerle, P. A. Activation of the transcription factor nuclear factor-kappaB in human inflamed synovial tissue. *Arthritis Rheum* **1996,** 39, 583-591.

207. Lappas, M.; Yee, K.; Permezel, M.; Rice, G. E. Sulfasalazine and BAY 11-7082 interfere with the nuclear factor-kappa B and I kappa B kinase pathway to regulate the release of proinflammatory cytokines from human adipose tissue and skeletal muscle in vitro. *Endocrinology* **2006,** 146, 1491-1497.

208. Sethi, G.; Sung, B.; Aggarwal, B. B. Nuclear factor-kB activation: from bench to bedside. *Exp Biol Med (Maywood)* **2008,** 233, 21-31.

209. Garg, A.; Aggarwal, B. B. Nuclear transcription factor-kappaB as a target for cancer drug development. *Leukemia* **2002,** 16, 1053-1068.

210. Shibata, A.; Nagaya, T.; Imai, T.; Funahashi, H.; Nakao, A.; Seo, H. Inhibition of NF-kappaB activity decreases the VEGF mRNA expression in MDA-MB-231 breast cancer cells. *Breast Cancer Res Treat* **2002,** 73, 237-243.

211. Zhang, J.; Peng, B. In vitro angiogenesis and expression of nuclear factor kappaB and VEGF in high and low metastasis cell lines of salivary gland adenoid cystic carcinoma. *BMC Cancer* **2007,** 7, 95-101.

212. Kawakami, H.; Tomita, M.; Matsuda, T.; Ohta, T.; Tanaka, Y.; Fujii, M.; Hatano, M.; Tokuhisa, T.; Mori, N. Transcriptional activation of survivin through the NF-kB pathway by human T-cell leukemia virus type I Tax. *Int J Cancer* **2005,** 115, 967-974.

213. Li, W.; Wang, H.; Kuang, C. Y.; Zhu, J. K.; Yu, Y.; Liu, J.; Huang, L. An essential role for the Id1/PI3K/Akt/NFkB/survivin signalling pathway in promoting the proliferation of endothelial progenitor cells in vitro. *Mol Cell Biochem* **2012,** 363, 135-145.

214. Stehlik, C.; de Martin, R.; Kumabashi, I.; Schmid, J. A.; Binder, B. R.; Lipp, J. Nuclear factor (NF)-kappaB-regulated X-chromosome-linked IAP gene expression protects endothelial cells from tumor necrosis factor alpha-induced apoptosis. *J Exp Med* **1998,** 188, 211-216.

215. Chen, C.; Edelstein, L. C.; Gelinas, C. The Rel/NF-κB family directly activates expression of the apoptosis inhibitor Bcl-xL. *Mol Cell Biol* **2000,** 20, 2687-2695.

216. Guttridge, D. C.; Albanese, C.; Reuther, J. Y.; Pestell, R. G.; Baldwin, A. S. J. NF-kappaB controls cell growth and differentiation through transcriptional regulation of cyclin D1. *Mol Cell Biol* **1999,** 19, 5785-5799.

217. Oya, M.; Takayanagi, A.; Horiguchi, A.; Mizuno, R.; Ohtsubo, M.; Marumo, K.; Shimizu, N.; Murai, M. Increased nuclear factor-kappa B activation is related to the tumor development of renal cell carcinoma. *Carcinogenesis* **2003,** 24, 377-384.

218. Matusan-Ilijas, K.; Damante, G.; Fabbro, D.; Dordevic, G.; Hadzisejdic, I.; Grahovac, M.; Maric, I.; Spanjol, J.; Grahovac, B.; Jonjic, N.; Lucin, K. Osteopontin expression correlates with nuclear factor-kappaB activation and apoptosis downregulation in clear cell renal cell carcinoma. *Pathol Res Pract* **2011,** 207, 104-110.

219. Peri, S.; Devarajan, K.; Yang, D.-H.; Knudson, A. G.; Balachandran, S. Meta-Analysis Identifies NF-κB as a Therapeutic Target in Renal Cancer. *PLoS ONE* **2013,** 8, e76746.

220. Gorlach, A.; Bonello, S. The cross-talk between NF-κB and HIF-1: further evidence for a significant liaison. *Biochem J* **2008,** 412, e17-e19.

221. van Uden, P., Kenneth, N. S., Rocha, S. Regulation of hypoxia-inducible factor-1alpha by NF-kappaB. *Biochem. J.* **2008,** 412, 477-484.

222. Sourbier, C.; Danilin, S.; Lindner, V.; Steger, J.; Rothhut, S.; Meyer, N.; Jacqmin, D.; Helwig, J.; Lang, H.; Massfelder, T. Targeting the nuclear factor-kB rescue pathway has promising future in human renal cell carcinoma therapy. *Cancer Res* **2007,** 67, 11668-11676.

223. Rayet, B.; Gelinas, C. Aberrant rel/nfkb genes and activity in human cancer. *Oncogene* **1999,** 18, 6938-6947.

224. Zhang, Z.; Ma, J.; Li, N.; Sun, N.; Wang, C. Expression of nuclear factor-kappaB and its clinical significance in nonsmall-cell lung cancer. *Ann Thorac Surg* **2006,** 82, 243-248.

225. Tang, X.; Liu, D.; Shishodia, S.; Ozburn, N.; Behrens, C.; Lee, J. J.; Hong, W. K.; Aggarwal, B. B.; Wistuba, II. Nuclear factor-kappaB (NF-kappaB) is frequently expressed in lung cancer and preneoplastic lesions. *Cancer* **2006,** 107, 2637-2646.

226. Zhang, D.; Jin, X.; Wang, F.; Wang, S.; Deng, C.; Gao, Z.; Guo, C. Combined prognostic value of both RelA and IkappaB-alpha expression in human non-small cell lung cancer. *Ann Surg Oncol* **2007,** 14, 3581-3592.

227. Mukhopadhyay, T.; Roth, J. A.; Maxwell, S. A. Altered expression of the p50 subunit of the NF-kappa B transcription factor complex in non-small cell lung carcinoma. *Oncogene* **1995,** 11, 999-1003.

228. Thornburg, N. J.; Pathmanathan, R.; Raab-Traub, N. Activation of nuclear factor-kappaB p50 homodimer/Bcl-3 complexes in nasopharyngeal carcinoma. *Cancer Res* **2003,** 63, 8293-8301.

229. Dan, H. C.; Cooper, M. J.; Cogswell, P. C.; Duncan, J. A.; Ting, J. P.; Baldwin, A. S. Akt-dependent regulation of NF-{kappa}B is controlled by mTOR and Raptor in association with IKK. *Genes Dev* **2008,** 22, 1490-1500.

230. Ni, H.; Zhao, W.; Kong, X.; Li, H.; Ouyang, J. NF-Kappa B modulation is involved in celastrol induced human multiple myeloma cell apoptosis. *PLoS ONE* **2014,** 9, e95846.

231. Rauch, A.; Hennig, D.; Schäfer, C.; Wirth, M.; Marx, C.; Heinzel, T.; Schneider, G.; Krämer, O. H. Survivin and YM155: How faithful is the liaison? *Biochim Biophys Acta* **2014,** 1845, 202-220.

232. Hoffman, W. H.; Biade, S.; Zilfou, J. T.; Chen, J.; Murphy, M. Transcriptional repression of the anti-apoptotic survivin gene by wild type p53. *J Biol Chem* **2002,** 277, 3247-3257.

233. Mirza, A.; McGuirk, M.; Hockenberry, T. N.; Wu, Q.; Ashar, H.; Black, S.; Wen, S. F.; Wang, L.; Kirschmeier, P.; Bishop, W. R.; Nielsen, L. L.; Pickett, C. B.; Liu, S. Human survivin is negatively regulated by wild-type p53 and participates in p53-dependent apoptotic pathway. *Oncogene* **2002,** 21, 2613-2622.

234. Lin, J.; Guan, Z.; Wang, C.; Feng, L.; Zheng, Y.; Caicedo, E.; Bearth, E.; Peng, J. R.; Gaffney, P.; Ondrey, F. G. Inhibitor of differentiation 1 contributes to head and neck squamous cell carcinoma survival via the NF-kappaB/survivin and phosphoinositide 3-kinase/Akt signaling pathways. *Clin Cancer Res* **2010,** 16, 77-87.

235. Vermes, I.; Haanen, C.; Steffens-Nakken, H.; Reutellingsperger, C. A novel assay for apoptosis flow cytometric detection of phosphatidylserine expression on early apoptotic cells using fluorescein labelled annexin V. *J Immunol Methods* **1995,** 184, 39-51.

236. Wajant, H.; Pfizenmaier, K.; Scheurich, P. Tumor necrosis factor signaling. *Cell Death Differ* **2003,** 10, 45-65.

237. Guan, H.; Hou, S.; Ricciardi, R. P. DNA binding of repressor nuclear factor-kB p50/p50 depends on phosphorylation of Ser337 by the protein kinase A catalytic subunit. *J Biol Chem* **2005,** 280, 9957-9962.

238. Hou, S.; Guan, H.; Ricciardi, R. P. Phosphorylation of serine 337 of NF-kB p50 is critical for DNA binding. *J Biol Chem* **2003,** 278, 45994-45998.

239. Karin, M.; Ben-Neriah, Y. Phosphorylation meets ubiquitination: the control of NF-kB activity. *Ann Rev Immunol* **2000,** 18, 621-663.

240. Li, C. C.; Dai, R. M.; Chen, E.; Longo, D. L. Phosphorylation of NF-KB1-p50 is involved in NF-kappa B activation and stable DNA binding. *J Biol Chem* **1994,** 269, 30089-30092.

241. Ju, J.; Naura, A. S.; Errami, Y.; Zerfaoui, M.; Kim, H.; Kim, J. G.; Abd Elmageed, Z. Y.; Abdel-Mageed, A. B.; Giardina, C.; Beg, A. A.; Smulson, M. E.; Boulares, A. H. Phosphorylation of p50 NF-kappaB at a single serine residue by DNA-dependent protein kinase is critical for VCAM-1 expression upon TNF treatment. *J Biol Chem* **2010,** 285, 41152-41160.

242. Liu, H.; Yang, J.; Yuan, Y.; Xia, Z.; Chen, M.; Xie, L.; Ma, X.; Wang, J.; Ouyang, S.; Wu, Q.; Yu, F.; Zhou, X.; Yang, Y.; Cao, Y.; Hu, J.; Yin, B. Regulation of Mcl-1 by constitutive activation of NF-kappaB contributes to cell viability in human esophageal squamous cell carcinoma cells. *BMC Cancer* **2014,** 14, 98.

243. Watson, C. J.; Dark, J. H. Organ transplantation: historical perspective and current practice. *Br J Anaesth* **2012,** 108 Suppl 1, i29-42.

244. Euvrard, S.; Kanitakis, J.; Claudy, A. Skin Cancers after Organ Transplantation. *N Eng J Med* **2003,** 348, 1681-1691.

245. Glover, M. T.; Deeks, J. J.; Raftery, M. J.; Cunningham, J.; Leigh, I. M. Immunosuppression and risk of non-melanoma skin cancer in renal transplant recipients. *Lancet* **1997,** 349, 398.

246. Colonna, J. O.; Ii; Winston, D. J.; Brill, J. E.; et al. Infectious complications in liver transplantation. *Arch Surg* **1988,** 123, 360-364.

247. Atala, A. Regenerative medicine strategies. *J Pediatr Surg* **2011,** 47, 17-28.

248. Thomson, J. A.; Itskovitz-Eldor, J.; Shapiro, S. S.; Waknitz, M. A.; Swiergiel, J. J.; Marshall, V. S.; Jones, J. M. Embryonic Stem Cell Lines Derived from Human Blastocysts. *Science* **1998,** 282, 1145-1147.

249. Baldwin, T. Morality and human embryo research. Introduction to the Talking Point on morality and human embryo research. *EMBO Reports* **2009,** 10, 299-300.

250. Gunsilius, E.; Gastl, G.; Petzer, A. L. Hematopoietic stem cells. *Biomed Pharmacother* **2001,** 55, 186-194.

251. Oreffo, R. O. C.; Cooper, C.; Mason, C.; Clements, M. Mesenchymal stem cells. *Stem Cell Reviews* **2005,** 1, 169-178.

252. Pittenger, M. F.; Mackay, A. M.; Beck, S. C.; Jaiswal, R. K.; Douglas, R.; Mosca, J. D.; Moorman, M. A.; Simonetti, D. W.; Craig, S.; Marshak, D. R. Multilineage potential of adult human mesenchymal stem cells. *Science* **1999,** 284, 143-147.

253. Takahashi, K.; Yamanaka, S. Induction of pluripotent stem cells from mouse embryonic and adult fibroblast cultures by defined factors. *Cell* **2006,** 126, 663-676.

254. Takahashi, K.; Tanabe, K.; Ohnuki, M.; Narita, M.; Ichisaka, T.; Tomoda, K.; Yamanaka, S. Induction of pluripotent stem cells from adult human fibroblasts by defined factors. *Cell* **2007,** 131, 861-872.

255. Yu, J.; Vodyanik, M. A.; Smuga-Otto, K.; Antosiewicz-Bourget, J.; Frane, J. L.; Tian, S.; Nie, J.; Jonsdottir, G. A.; Ruotti, V.; Stewart, R.; Slukvin, I. I.; Thomson, J. A. Induced pluripotent stem cell lines derived from human somatic cells. *Science* **2007,** 318, 1917-1920.

256. Li, J. Y.; Christophersen, N. S.; Hall, V.; Soulet, D.; Brundin, P. Critical issues of clinical human embryonic stem cell therapy for brain repair. *Trends Neurosci* **2008,** 31, 146-153.

257. Choo, A. B.; Tan, H. L.; Ang, S. N.; Fong, W. J.; Chin, A.; Lo, J.; Zheng, L.; Hentze, H.; Philp, R. J.; Oh, S. K.; Yap, M. Selection against undifferentiated human embryonic stem cells by a cytotoxic antibody recognizing podocalyxin-like protein-1. *Stem Cells* **2008,** 26, 1454-1463.

258. Fong, C. Y.; Peh, G. S.; Gauthaman, K.; Bongso, A. Separation of SSEA-4 and TRA-1-60 labelled undifferentiated human embryonic stem cells from a heterogeneous cell population using magnetic-activated cell sorting (MACS) and fluorescence-activated cell sorting (FACS). *Stem Cell Reviews* **2009,** 5, 72-80.

259. Naujok, O.; Kaldrack, J.; Taivankhuu, T.; Jorns, A.; Lenzen, S. Selective removal of undifferentiated embryonic stem cells from differentiation cultures through HSV1 thymidine kinase and ganciclovir treatment. *Stem Cell Reviews* **2010,** 6, 450-461.

260. Ben-David, U.; Gan, Q. F.; Golan-Lev, T.; Arora, P.; Yanuka, O.; Oren, Y. S.; Leikin-Frenkel, A.; Graf, M.; Garippa, R.; Boehringer, M.; Gromo, G.; Benvenisty, N. Selective elimination of human pluripotent stem cells by an oleate synthesis inhibitor discovered in a high-throughput screen. *Cell Stem Cell* **2013,** 12, 167-179.

261. Richards, M.; Phoon, C. W.; Goh, G. T. W.; Seng, E. K.; Guo, X. M.; Tan, C. M. F.; Chan, W.-K.; Lee, J. M. K. A new class of pluripotent stem cell cytotoxic small molecules. *PLoS ONE* **2014,** 9, e85039.

262. Andrews, P. W.; Matin, M. M.; Bahrami, A. R.; Damjanov, I.; Gokhale, P.; Draper, J. S. Embryonic stem (ES) cells and embryonal carcinoma (EC) cells: opposite sides of the same coin. *Biochem Soc Trans* **2005,** 33, 1526-1530.

263. Przyborski, S. A.; Christie, V. B.; Hayman, M. W.; Stewart, R.; Horrocks, G. M. Human embryonal carcinoma stem cells: models of embryonic development in humans. *Stem Cells Dev* **2004,** 13, 400-8.

264. Sperger, J. M.; Chen, X.; Draper, J. S.; Antosiewicz, J. E.; Chon, C. H.; Jones, S. B.; Brooks, J. D.; Andrews, P. W.; Brown, P. O.; Thomson, J. A. Gene expression patterns in human embryonic stem cells and human pluripotent germ cell tumors. *P Natl Acad Sci USA* **2003,** 100, 13350-13355.

265. Huangfu, D.; Osafune, K.; Maehr, R.; Guo, W.; Eijkelenboom, A.; Chen, S.; Muhlestein, W.; Melton, D. A. Induction of pluripotent stem cells from primary human fibroblasts with only Oct4 and Sox2. *Nat Biotech* **2008,** 26, 1269-1275.

266. Rodda, D. J.; Chew, J. L.; Lim, L. H.; Loh, Y. H.; Wang, B.; Ng, H. H.; Robson, P. Transcriptional regulation of nanog by OCT4 and SOX2. *J Biol Chem* **2005,** 280, 24731-24737.

267. Takase, O.; Yoshikawa, M.; Idei, M.; Hirahashi, J.; Fujita, T.; Takato, T.; Isagawa, T.; Nagae, G.; Suemori, H.; Aburatani, H.; Hishikawa, K. The role of NF-κB signaling in the maintenance of pluripotency of human induced pluripotent stem cells. *PLoS ONE* **2013,** 8, e56399.

268. Armstrong, L.; Hughes, O.; Yung, S.; Hyslop, L.; Stewart, R.; Wappler, I.; Peters, H.; Walter, T.; Stojkovic, P.; Evans, J.; Stojkovic, M.; Lako, M. The role of PI3K/AKT, MAPK/ERK and NFkappabeta signalling in the maintenance of human embryonic stem cell pluripotency and viability highlighted by transcriptional profiling and functional analysis. *Hum Mol Genet* **2006,** 15, 1894-1913.

269. Chen, S.; Li, X.; Lu, D.; Xu, Y.; Mou, W.; Wang, L.; Chen, Y.; Liu, Y.; Li, X.; Li, L. Y.; Liu, L.; Stupack, D.; Reisfeld, R. A.; Xiang, R.; Li, N. SOX2 regulates apoptosis through

MAP4K4-survivin signaling pathway in human lung cancer cells. *Carcinogenesis* **2014,** 35, 613-623.

270. Feng, R.; Zhou, S.; Liu, Y.; Song, D.; Luan, Z.; Dai, X.; Li, Y.; Tang, N.; Wen, J.; Li, L. Sox2 protects neural stem cells from apoptosis via up-regulating survivin expression. *Biochem J* **2013,** 450, 459-468.

271. Lin, F.; Lin, P.; Zhao, D.; Chen, Y.; Xiao, L.; Qin, W.; Li, D.; Chen, H.; Zhao, B.; Zou, H.; Zheng, X.; Yu, X. Sox2 targets cyclinE, p27 and survivin to regulate androgen-independent human prostate cancer cell proliferation and apoptosis. *Cell Prolif* **2012,** 45, 207-216.